MODERN SEDIMENTATION IN THE NORTHERN BARENTS SEA: INPUT, DISPERSAL AND DEPOSITION OF SUSPENDED SEDIMENTS FROM GLACIAL MELTWATER

by

STEPHANIE LOUISE PFIRMAN

B.A. 1974 Colgate University

SUBMITTED IN PARTIAL FULFILLMENT

OF THE REQUIREMENTS FOR THE DEGREE OF

DOCTOR OF PHILOSOPHY

at the

MASSACHUSETTS INSTITUTE OF TECHNOLOGY

and the

WOODS HOLE OCEANOGRAPHIC INSTITUTION

August, 1984

Signature of Author _____
Joint Program in Oceanography, Massachusetts Institute of Technology/Woods Hole Oceanographic Institution and Department of Earth, Atmospheric and Planetary Sciences, Massachusetts Institute of Technology, August, 1984.

Certified by _____
John D. Milliman
Thesis Supervisor

Accepted by _____
Chairman, Joint Committee for Marine Geology and Geophysics, Massachusetts Institute of Technology/Woods Hole Oceanographic Institution

MODERN SEDIMENTATION IN THE NORTHERN BARENTS SEA: INPUT, DISPERSAL, AND DEPOSITION OF SUSPENDED SEDIMENTS FROM GLACIAL MELTWATER

by

STEPHANIE LOUISE PFIRMAN

Submitted to the Department of Earth and Planetary Sciences
on August 3, 1984 in partial fulfillment of the
requirements for the degree of
Doctor of Philosophy

ABSTRACT

The modern depositional environment of the northern epicontinental Barents Sea varies from proximal to distal glaciomarine. The regional surface sediment distribution is controlled by erosion of shallow banks of the Pleistocene glaciated surface, with the fine material deposited in the deep basins. Near-bottom nepheloid layers are often observed indicating that fine grained sediments are being transported under present conditions. Minor additional sediment is supplied by iceberg rafting englacial material and sea-ice containing aeolian, resuspended, and beach sediments.

Glacial flour is supplied by several large stable meltwater outflow locations along the ice front. Because the water is fresh and nearly the same temperature as the ambient coastal water, it is bouyant. Although the traction load deposits as the meltwater plume rises to the sea surface, sand (as well as finer material) may be suspended. This material deposits from suspension at some distance from the discharge location (dependent on both the sediment settling velocity and the velocity of the ambient coastal water, resulting in well-sorted deposits near the outflow location). Most of the sediment in suspension is observed to deposit within a 5km radius of the outflow location, and suspended matter samples obtained 18km offshore were at background levels. However, meltwater plumes can often be observed in the surface water (in satellite photographs) at distances of 30km downstream, indicating transport of glacial sediments along the ice front.

Near the Nordaustlandet glacier front surface sediments are disturbed by glaciers advances and retreats which mechanically rework the sediment surface . The southwestern portion of the glacier front, Brasvellbreen, surged 18km between 1936 and 1938. An end moraine was deposited at the maximum extent of the surge. The ice then stagnated and disintegrated through calving. At present on the eastern portion of the Brasvellbreen ice front is active with frequent small (less than 50m) glacier advances and retreats. Evidence for this is shown by the minor ridge and swale moraines in this eastern area.

ACKNOWLEDGEMENTS

I thank my advisor John Milliman for his support and encouragement, my thesis defense chairman Elazar Uchupi, and my thesis committee members Ed Boyle, Mike McCartney, Keith Stolzenbach, and Brian Tucholke for their advice and guidance. The manuscripts benefitted by early reviews from David Aubrey, John Milliman, Paul Speer, and Stephen Swift (WHOI), Anders Solheim (from the Norwegian Polar Research Institute (NPRI) in Oslo, Norway), and Tore Vorren (from the Tromso, Norway Insitute for Geological Research).

The NPRI analyzed surface sediment texture, Tor Gammelsrod at the Geophyscial Institute in Bergen and Harald Loeng at the Institute for Marine Research in Bergen provided hydrographic information, and δO^{18} analyses were carried out in Richard Fairbanks' lab at Lamont-Doherty Geological Observatory. I thank Tom Keffer for PLOT5, Sharon Downey for measuring grain sizes of suspended sediments, Beecher Wooding for x-ray diffraction analysis of surface sediments, and Nancy Murphy, Donna Carson, and Stefan Masse for drafting most of the figures. Margaret Goud, John Collins, Barbara Braatz, Carol Eberhard, Curtiss Thompson, Bradford Butman and Cheryl Ann Hannan gave me a great deal of encouragement during the course of my research.

The Office of Naval Research supported my thesis research. The cooperative study was originally promoted by Anders Elverhoi at the NPRI and could not have been completed without ship time and logistical support from the NPRI. The captain, Terje Langvik, and the

crew of the R/V Lance, from which most research was carried out, greatly aided data collection by intrepidly navigating in treacherous sea-ice and uncharted waters. Travel funds were provided by the Norwegian Marshall Fund for Scientific Research and the Woods Hole Oceanographic Institution (WHOI) Education Department.

TABLE OF CONTENTS

INTRODUCTION

Glacigenic sediments occur in all geologic eras, except for the Mesozoic (Hambrey and Harland 1981). Although they are of minor volumetric importance, glacial deposits have been used to reconstruct former ice sheets, often implying dramatic climactic variations (Denton and Hughes 1981, Elverhoi in press). The terrestrial glacial sedimentary environment has been extensively investigated, especially the till deposits (Goldthwait 1971), and recently more emphasis has been placed on the glaciomarine environment (Molnia 1983). A prerequisite for a better understanding of ancient environments is thorough knowledge of modern glacial environments. Comparison of ancient glacial sediments with modern tidewater glacier analogs is necessary to understand their environmental significance.

Large areas of the northern continental shelves have been subjected to glacier erosion and deposition during the late Cenozoic (figure 1; Anderson et al. 1983). In many areas glaciers terminated in the open ocean either as tidewater glacier fronts or ice shelves (Rust and Romanelli 1975, Denton and Hughes 1981). Maximum sedimentary input to the open ocean occurred during retreat of these glaciers across the continental shelves (Flint 1971). Sediment eroded by continental ice sheets was transported to the open marine environment in ice push ridges, englacial material in icebergs, and basal meltwater. Recent observations of subpolar glaciers indicate

Figure 1. Proposed limits of late Wisconsin glaciation showing large extent of northern hemisphere influenced by glaciers (Denton and Hughes 1981, p.viii).

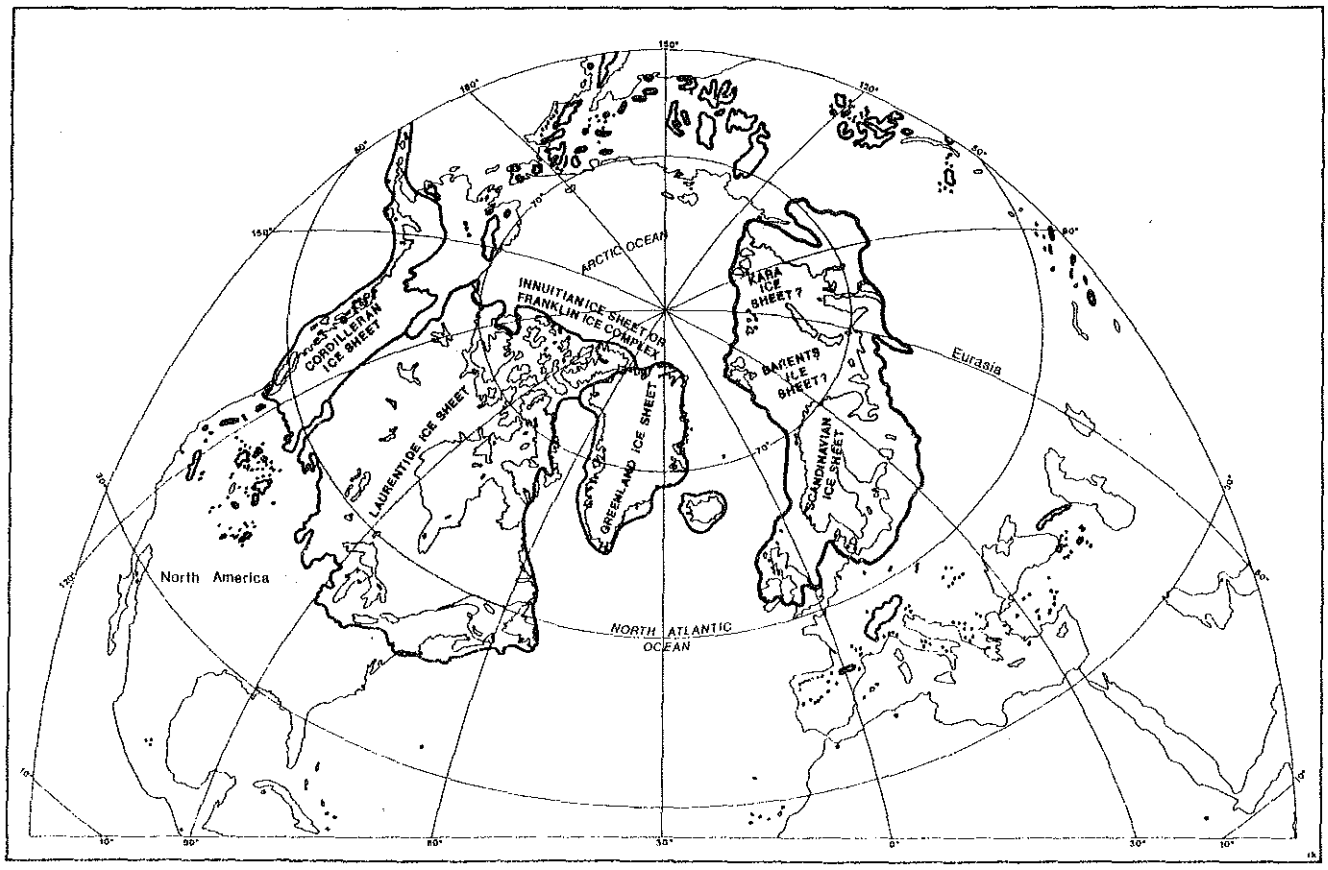

Schematic diagram of Northern Hemisphere ice sheets. Possible ice shelves not shown.

Figure 1

that perhaps 90% of glacially eroded material is transported to the ice front by meltwater (figure 2; Hagen et al. 1983). Glacial theory suggests that the most stable discharge mechanism for this meltwater is through large drainage networks culminating in a limited number of major meltwater outlets (Shreve 1972), analysis of late Quaternary deposits now exposed on land also indicate the presence of numerous meltwater channels deposited above basal till (Rust and Romanelli 1975). Thus input, dispersal, and deposition of suspended sediment from submarine meltwater plumes will determine the regional sedimentary impact of open-marine glacier systems analogous to Pleistocene continental shelf deglaciation conditions.

Previous work on glacier sediment input to the ocean has concentrated on subaerial meltwater streams (Syvitski et al. in prep.), fjord tidewater glacier systems (Powell 1980 and 1983), and the ice shelves of Antarctica (Anderson 1983). The Antarctic environment represents a situation where meltwater is generally absent, sedimentation is presently dominated by mass wasting and biogeneous deposition, and the continental margin is deep, steep, and the shelf dips landward in contrast to other formerly glaciated margins (Molnia 1983). Fjord-glacier systems of Alaska, Canada, and Norway represent waning stages of glaciation with glaciers depositing sediment in coastal embayments (Elverhoi, in press). Some aspects of sedimentation from glacial meltwater in these restricted environments may also be applied to the open-marine environment. Sediment transport via meltwater is greatest during the summer ablation season and minimal during the winter (Collins 1979, Farrow et al. 1983).

Figure 2. Tidewater glacier front sedimentary features (Edwards 1978, p.423).

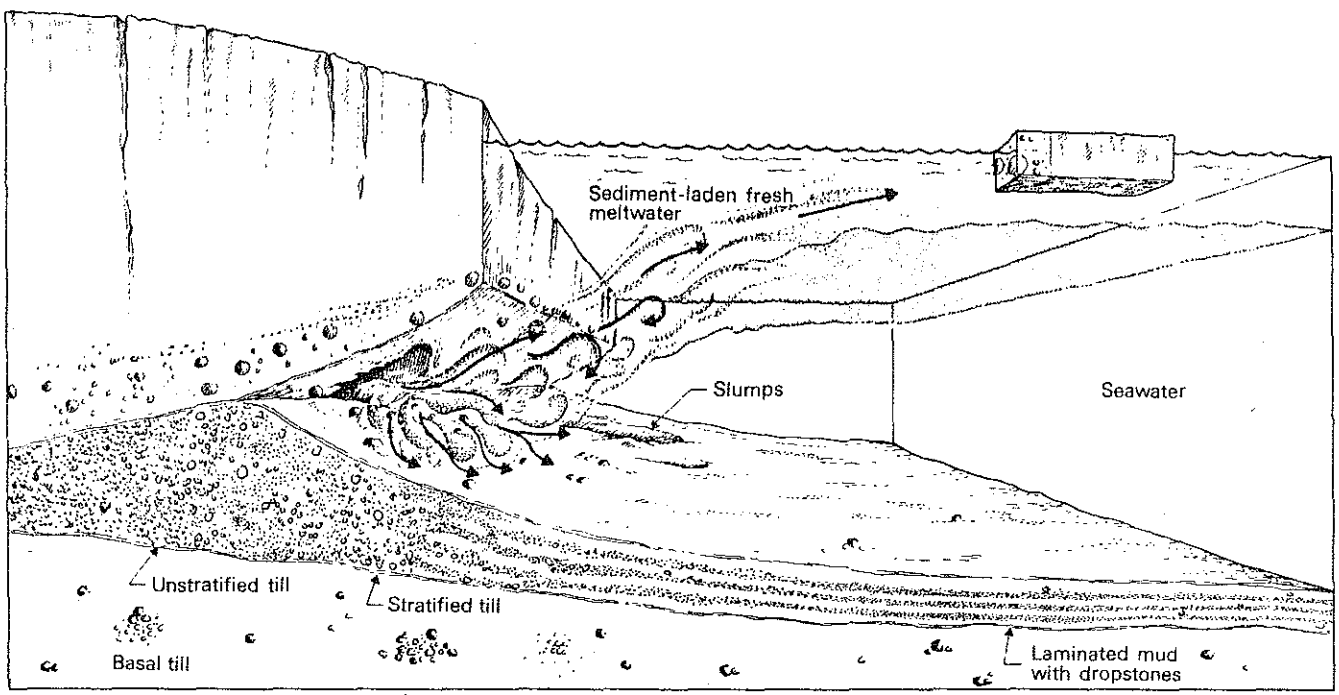
Sediment-laden fresh meltwater
Slumps
Seawater
Unstratified till
Stratified till
Basal till
Laminated mud with dropstones

Figure 2

Suspended sediment concentrations are highest in the first large summer discharges as winter erosional products are winnowed by subglacial streams (Collins 1979) but will only occasionally be high enough (greater than 38,000mg/1) to cause underflows in the marine environment (Powell 1980, Hoskin and Burrell 1972). Discharge of these meltwater streams into the ocean may occur at the base of the glacier (Edwards 1978) if the glacier is not extensively fractured or is actively retreating (Weertman 1972). The tunnel may migrate to sea level due to intrusion of salt water at the glacier terminus (Elverhoi et al. 1980). Deposition of fine-grained suspended sediment in the ice-proximal marine environment is enhanced by biologic scavaging and consequent fecal pellet production (Syvitski 1980, Syvitski and Murray 1981).

A number of questions unresolved by previous studies of glacier - ocean environments are: How will meltwater plumes disperse in the open marine environment? Where will various grain-sizes of sediment discharged in meltwater be deposited? What sedimentation rates may be expected? This study investigates these questions through comparison of the proximal tidewater glacier zone of the Nordaustlandet ice dome with regional depositional patterns of the recently glaciated Barents Sea. The Nordaustlandet region is a better analog for Pleistocene deglaciation conditions than previously studied fjord-tidewater glaciers because the glacier meltwater is discharged directly into the marine environment. Analysis of surface sediment characteristics,

circulation patterns, and suspended sediment distribution permit modelling of the input, dispersal, and deposition of suspended sediment from glacier meltwater plumes.

The thesis consists of four papers: 1) water mass analysis of the northern Barents Sea, 2) regional surface sediment response to the hydrographic regime, 3) recent glacial history and sea floor morphology of the western Nordaustlandet ice dome, and 4) analysis of processes controlling deposition of glacial sediment from glacier meltwater plumes discharged from Nordaustlandet. The first paper discusses the hydrographic regime through analysis of water mass distribution. Water mass transport directions and regions of intensified bottom currents are delineated. Regional circulation is dominated by a cyclonic gyre in the northern Barents Sea. Shallow, cold, and sea-ice bearing Arctic water flows southwest into the Barents Sea from the Arctic and Kara Seas. Warm Atlantic water enters the southern Barents Sea, meeting the Arctic water at the Polar Front (approximately 74°N). North of the Polar Front the water column is stratified with a surface low density layer of sea-ice meltwater at 0-30m, cold Arctic water at 30-150m, warm Atlantic water at 150-250m, and cooled Atlantic water in some basins deeper than 250m. Transport of modified Atlantic water into both the Norwegian-Greenland Sea and the Arctic Ocean may contribute to deep water formation.

The second paper discusses the surface sediment texture in relation to the bottom nepheloid layer distribution, near-bottom circulation, and ice rafting and gouging effects. Fine sediment is

winnowed from banks shallower than 200m (leaving a sandy-gravelly lag) by a combination of waves and tides superimposed on mean currents. Near-bottom nepheloid layers indicate that winnowing is a modern process and is associated with regions of current shear indicated by hydrographic profiles. Resuspended fine-grained sediment is observed to be transported via bottom nepheloid layers to deep basins. Mean currents may be locally strong enough to form sediment waves in one narrow strait at 250m water depth.

The third paper discusses the recent glacial history and sea floor morphology near Brasvellbreen, the westernmost sector of the Nordaustlandet ice dome. Brasvellbreen surged 18km from 1936-1938; this is the largest surge in recorded history (Paterson 1969). It subsequently retreated 0.5-2.0km and reached its present position in 1958; providing a unique opportunity to observe a recently glaciated sea floor. Sea floor affected by the surge is limited to a 5km zone seaward of the present glacier front. It consists of a till ridge, subparallel to the present front, and a network pattern of abandoned crevasse fills. This sea floor morphology is only 20 years old and shows no signs of recent modification except for occasional ice gouges, clean cobble pavement, and arcuate ridges in close proximity to the present-day glacier front (due to ice push or solifluction). Sedimentation during the surge occurred all along the glacier margin.

The fourth paper examines the recent input, dispersal and deposition of suspended sediment from two major meltwater plumes presently draining most of the Nordaustlandet ice dome; the plume

located just east of Brasvellbreen is discussed in the most detail, because sea-ice limited sampling to this region. These two meltwater plumes have been active at least since 1976, when the first Landsat satellite images were obtained. These images together with suspended sediment information show that the plumes are generally advected westward along the ice front. The plumes are seasonally variable, with sediment discharge reaching the sea surface only during July and August. Width of the plumes remains relatively constant (2.5km) downstream, suspended matter profiles are vertically homogenous, and concentration decreases offshore. Bounds on sediment and meltwater input may be obtained from downstream concentrations and dispersal patterns. Sediment suspended in meltwater is both predicted and observed to be deposited within a narrow (2.5km) ice-proximal zone. Deposition of material greater than 100μm generally occurs within 1km of the exit point, while fine material (less than 16um) can be transported great distances in a coastal current if not agglomerated by some means. Sea-floor depocenters are sensitive to the grain size distribution of the source, although surface sediment lithology, texture, and deposition rate are complicated due to the recent glacier surge when meltwater may have been discharged along the entire glacier base. Surface sediments greater than 40 km away appear unaffected by sediment input from the present-day Nordaustlandet glacier.

REFERENCES

Anderson, J.B., C. Brake, E. Domack, N. Meyers, R. Wright (1983) Development of a polar glacial-marine sedimentation model from Antarctic Quaternary deposits and glaciological information. in Molnia, B.F. (ed.) Glacial Marine Sedimentation. Plenum Press p.233-264.

Collins, D.N. (1979) Sediment concentration in meltwater as an indicator of erosion processes beneath an alpine glacier. J. Glaciol. 23:247-257.

Denton, G.H. and and T.J. Hughes (1981) The Last Great Ice Sheets. John Wiley and Sons.

Edwards, M.B. (1978) Glacial Environments. in Reading, H.G.(ed.) Sedimentary Environments and Facies. Elsevier. p416-438.

Elverhoi, A. (in press) Glacigenic and associated marine sediments in the Weddell Sea, fjords of Spitsbergen, and the Barents Sea: a review. Mar. Geol.

Elverhoi, A., O. Liestol, J. Nagy (1980) Glacial erosion, sedimentation, and microfauna in the inner part of Kongsfjorden, Spitsbergen. Nor. Polarinst. Skr. 172:33-58.

Farrow, G.E., J.P.M. Syvitski, V. Tunnicliffe (1983) Suspended particulate loading on the macrobenthos in a high turbid fjord: Knoght Inlet, British Columbia. Can. J. Fish. Aquat. Sci. 40 (suppl. 1):273-288.

Flint, R.F. (1971) Glacial and Quaternary Geology. John Wiley and Sons, Inc., New York. 892pp.

Goldthwait, R.P. (1971) Till: A Symposium. Ohio State University Press. 402pp.

Hagen, J.D., B. Wold, O. Liestol, C. Ostrem, J.L. Sollid (1983) Subglacial process at Bondhusbreen, South Norway: Some preliminary results. Ann. Glaciol. 4:000-000.

Hambrey, M.J. and W.B. Harland (1981) Summary of Earth's pre-Pleistocene glacial record. In: M.J. Hambrey and W.B. Warland (Eds.) Earth's pre-Pleistocene Glacial Record. Cambridge University Press, Cambridge. 943-954.

Hoskin, C.M. and D.C. Burrell (1972) Sediment transport and accumulation in a fjord basin; Glacier Bay, Alaska. J. Geol. 80:539-551.

Jones, G.A. and W.F. Ruddiman (1982) Assessing the global meltwater spike. Quaternary Res. 17:148-172.

Molnia, B.F. (1983) Subarctic glacial-marine sedimentation: a model. in Molnia, B.F. (ed.) Glacial Marine Sedimentation. Plenum Press p.95-144.

Molnia, B.F. (1983) Glacial Marine Sedimentation. Plenum Press 844pp.

Paterson, W.S.B. (1969) The Physics of Glaciers. Pergamon Press 250pp.

Powell, R. (1980) Holocene glacimarine sediment deposition by tidewater glaciers in Glacier Bay, Alaska. Ohio State Univ. Ph.D. thesis 420pp.

Powell, R. (1983) Glacial-marine sedimentation and processes and lithofacies of temperate tidewater glaciers, Glacier Bay, Alaska. in Molnia, B.F. (ed.) Glacial Marine Sedimentation. Plenum Press p.221-232.

Rust, B.R. and R. Romanelli (1975) Late Quaternary subaqueous outwash deposits near Ottawa, Canada. in Jopling, A.V. and B.C. McDonald Glaciofluvial and Glaciolacustrine Sedimentation. Soc. Econ. Pal. Min. 23:177-192.

Shreve R.L. (1972) Movement of water in glaciers. J. Glaciol. 11:205-214.

Syvitski, J.P.M. (1980) Flocculation, agglomeration, and zooplankton pellitization of suspended sediment in a fjord receiving glacial meltwater. in Fjord Oceanography. p615-623.

Syvitski, J.P.M. and J.W. Murray (1981) Particle interaction in fjord suspended sediment. Mar. Geol. 39:215-242.

Syvitski, J.P.M., K.W. Asprey, D.A. Clattenburg (in prep.) The prodelta environment: Suspended particle dynamics.

Weertman, J. (1972) General theory of water flow at the base of a glacier or ice sheet. Rev. Geophys. Space Phys. 10:287-333.

CHAPTER 1

Water masses of the northern Barents Sea

Stephanie L. Pfirman
Woods Hole Oceanographic Institution
Woods Hole, Massachusetts

ABSTRACT

The water column of the Barents Sea north of the Polar Front is stratified in the summer and consists of surface water (0-10m), Arctic Water (30-150m), Atlantic Water (150-250m), and Cold Deep Water (greater than 250m). Both Atlantic and Arctic Water have northern and southern sources. Mixing relationships between these water masses vary in different basins and are largely bathymetrically controlled. In the summer of 1981, northern sources for both Arctic and Atlantic Water were fresher than southern sources. If these observations are representative of summertime conditions, Atlantic Water which enters the Barents Sea from the north during the summer cannot provide a salt source for Arctic deep water. Southern Atlantic Water is shown to be extensively modified as it passes over shallow sills, and it could be a source for Arctic deep water.

INTRODUCTION

Formation of dense water in the Barents Sea has been speculated on for many years (Nansen 1915). This shallow sea was thought to be an ideal location for cooling of Atlantic Water, thereby forming dense bottom water and perhaps contributing to the deep water of the Arctic Ocean and the Norwegian-Greenland seas (Aagaard 1981; Swift et al. 1983, Midtun, in prep.). The location and the processes of formation of high-latitude deep water are important as they determine the circulation and nutrient distribution of most of the other world oceans. Although detailed descriptions of the hydrography have previously been reported (e.g. Tantsiura 1959, Novitskiy 1961), the data bases are not presented and results are difficult to evaluate. These studies are important to recognize however, because similar conclusions are reached in this study of the summertime temperature, salinity, and density of the major water masses in the northern Barents Sea. Modification and transport of the various water masses are also discussed, although data from the winter are not available. Data presented in this paper are limited to hydrographic observations obtained in the late summer when the northern Barents Sea is free from sea-ice.

The epicontinental Barents Sea is bounded by the Scandinavian Peninsula to the south, the Svalbard Archipelago to the west, and Franz Josef Land and Novaya Zemlya to the east (figure 1). It is continuous with the Norwegian Sea in the west, the Arctic Ocean to the north, and the Kara Sea to the east. Currents in this shallow sea are

Figure 1. Bathymetric map compiled by Solheim (1982). Box encloses study area shown in subsequent figures.

Explantion of Norwegian terminology: renna = trough

banken = bank

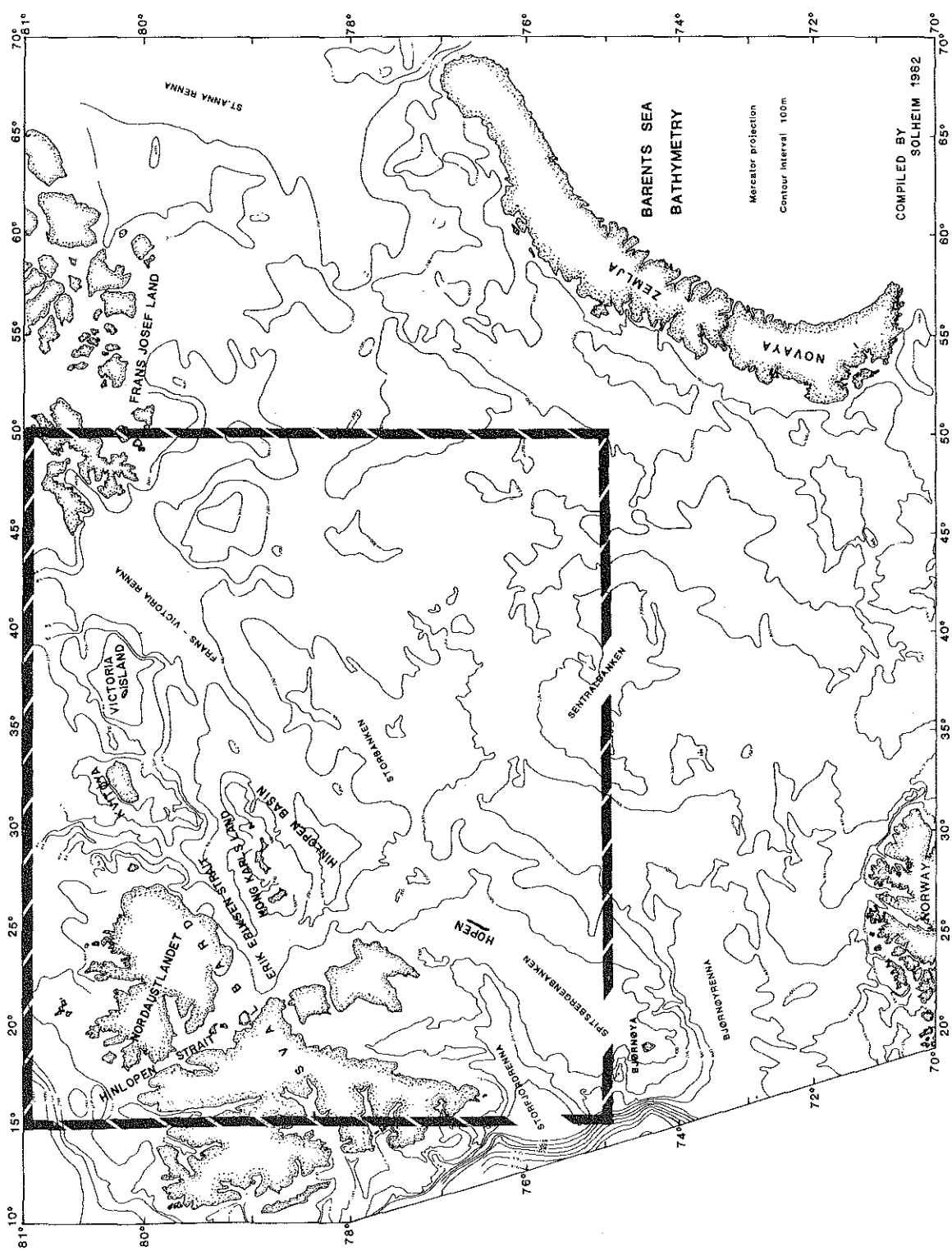
BARENTS SEA
BATHYMETRY
Mercator projection
Contour interval 100m
COMPILED BY
SOLHEIM 1982
ST.ANNA RENNA
FRANS JOSEF LAND
ZEMLJA
NOVAYA
FRANS - VICTORIA RENNA
VICTORIA ISLAND
NORDAUSTLANDET
HINLOPEN STRAIT
ERIK EDLSEN-STRAIT
KONG KARL'S LAND
HINLOPEN BASIN
STORBANKEN
SENTRALBANKEN
HOPEN
SPITSBERGENBANKEN
STORFJORDRENNA
BJØRNØYA
BJØRNØYTRENNA
NORWAY

Figure 1

Figure 2. General circulation map adapted by Loeng (1979) from Tantsiura (1959). Solid arrows denote warm water, broken arrows denote cold water. Heavy line indicates Polar Front. Labelled currents are:

1. West Spitsbergen Current
2. North Cape Current
3. South Cape Current
4. Persey Current
5. Hopen-Byornoya Current
6. East Spitsbergen Current
7. Arctic Atlantic Current
8. Novaya Zemlya Current

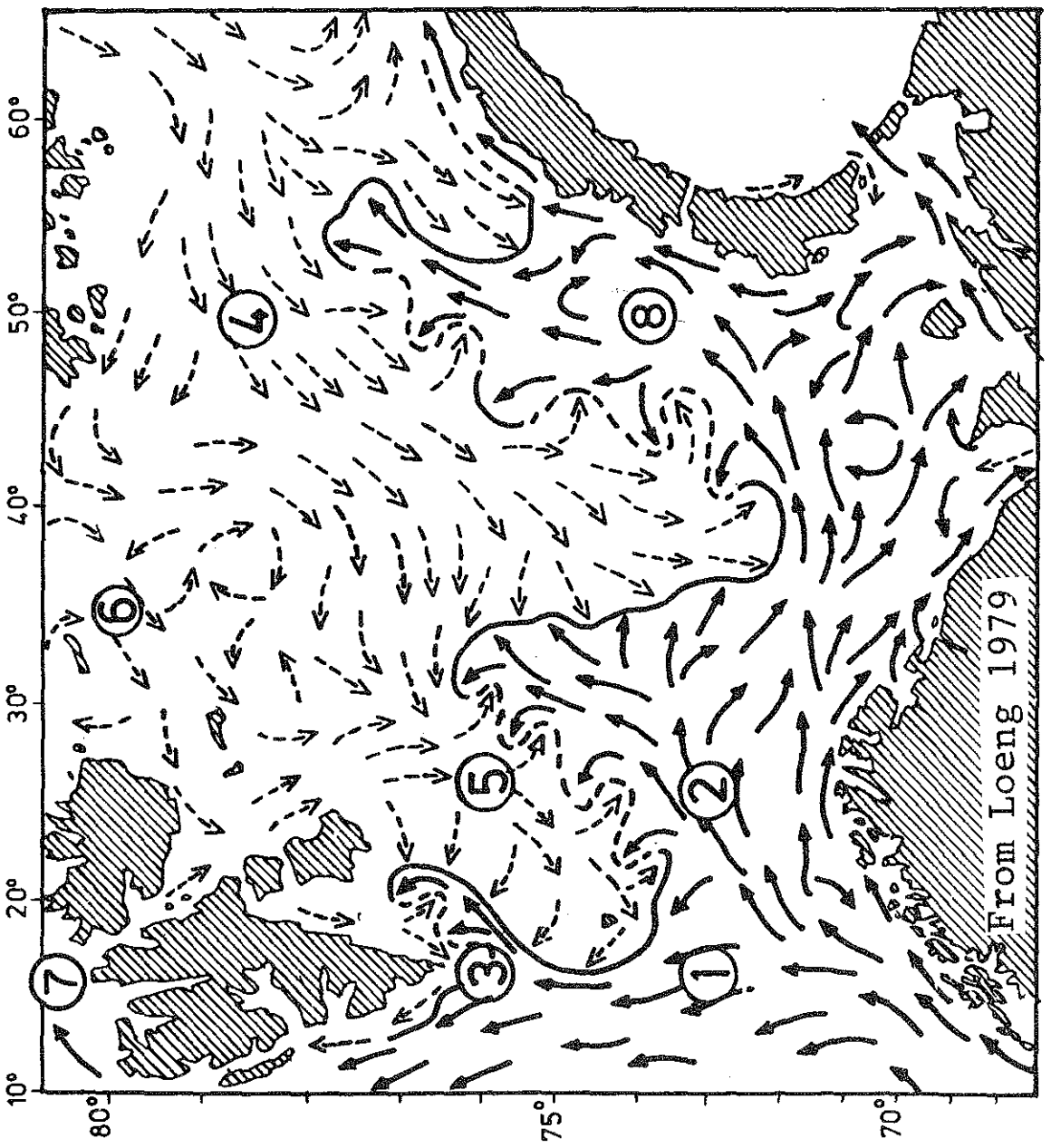

Figure 2

influenced by sea-floor topography and this results in a complex circulation pattern (figure 2). Accurate and detailed bathymetric information is therefore crucial to interpretation of the hydrography, but large regions unfortunately are still not well surveyed. Average water depth is 250m, and a series of northeast-southwest trending basins and sills are defined by the 200m isobath.

Hopen-Bjornoya Trough between Spitsbergenbanken and northern Norway is the major deep-water (greater than 300m) connection of the Barents Sea with the Norwegian-Greenland Sea (figure 1). This Trough shoals to the north and east. The major deep-water connection to the Arctic Ocean is Frans Josef-Victoria Trough between Victoria Island and Frans Josef Land. Bathymetry of this Trough is not well known, but depths exceed 300m. Straits to the west between the northern islands probably have sill depths near 250m. The sill depth between the Barents and Kara seas is about 250m. Both Hinlopen Strait to the west of Nordaustlandet, and Storfjord Trough to the west of Spitsbergenbanken have sill depths less than 150m and are therefore unimportant for deep water exchange.

Shallow water flow is affected by the numerous islands and shallow banks. Shallow banks which are especially important are Spitsbergenbanken, Storbanken, and Sentralbanken, because they are centrally located in the Barents Sea. Spitsbergenbanken is the shallowest, locally less than 50m, while Sentralbanken is the deepest, averaging 200m.

Hydrography

The Barents Sea hydrography is dominated by two water masses, Atlantic Water and Arctic Water. Atlantic Water may be further subdivided into northern and southern components, both derived from branches of the Norwegian Current (figure 2). Northern north Atlantic Water (henceforth known as Northern Atlantic Water or NAtW) flows along the west coast of Spitsbergen as the West Spitsbergen Current. Once it enters the Arctic Ocean it continues eastward along the northern slope and enters into the Barents Sea between Nordaustlandet and Franz Josef Land (Mosby 1938). Southern north Atlantic Water (henceforth known as Southern Atlantic Water or SAtW) splits off from the North Cape Current along northern Norway, and flows up Hopen - Bjornoya Trough and splits again in the vicinity of Sentralbanken. The branch west of Sentralbanken continues northward, and the branch to the south of Sentralbanken is called the Novaya Zemlya Current (figure 2). Both NAtW and SAtW are identified as being warm, greater than 0°C, and saline, greater than 34.7°/$_{oo}$ (figure 3). Southern Atlantic Water nearly fills the entire water column in the southern Barents Sea. Northern Atlantic Water is usually identified as a subsurface maximum in temperature at 200-250m in the northern Barents Sea.

The second major water mass, Arctic Water (also called winter water and polar water), is colder than -1.0°C with salinities of 34.2-34.5°/$_{oo}$. This near-freezing water mass originates from a deep convection layer developed during sea-ice formation at the sea surface

in the Arctic Ocean, the Barents Sea, and the Kara Sea (Ellertson et al. 1981). Arctic Water occurs in the Barents Sea from 30-100m water depth (figure 3). The boundary between this cold water and warm Atlantic Water to the south is a strong temperature gradient known as the Polar Front (figure 2). The surface expression of this front is located above the 100m isobath north of Hopen - Bjornoya Trough (Johannessen and Foster 1978).

The East Spitsbergen and Persey currents transport cold Arctic Water into the Barents Sea west and south of Franz Josef Land (figure 2, Tantsiura 1959, Novitskiy 1961). These cold, westerly flowing currents from the north oppose the warm easterly flowing North Cape Current in the south, resulting in a well-documented cyclonic circulation over the northern Barents Sea.

Cold Deep Water often occurs below warmer Atlantic Water and has approximately the same salinity (greater than $34.7°/_{oo}$). This water mass may form by cooling Atlantic Water near shallow banks (Tantsiura 1959, Loeng 1980) or may be due to modification of Arctic Water by brine rejection during sea-ice formation (Midtun, in prep.). Distribution of this dense water mass is patchy, with large seasonal and annual variations (Tantsiura 1959, and Loeng 1980).

Surface water forms during the summer as sea ice melts and retreats. Surface water is identified as a layer well mixed in both temperature and salinity from 0-10m, above a strong pycnocline (figure 3). Away from sea-ice, the surface layer rapidly warms by radiation during the summer (Loeng 1980). This further increases the density contrast with underlying water, placing a low-density lid over the

Figure 3. Station cast (A) and temperature - salinity plot (B) for station 187 (position indicated by large dot in figure 4). Station is located north of the Polar Front in Hinlopen Basin.

Abbreviations: TEM = temperature°C

STH = σ_t

SAL = Salinity°/$_{oo}$

σ_t is contoured on the temperature - salinity plot

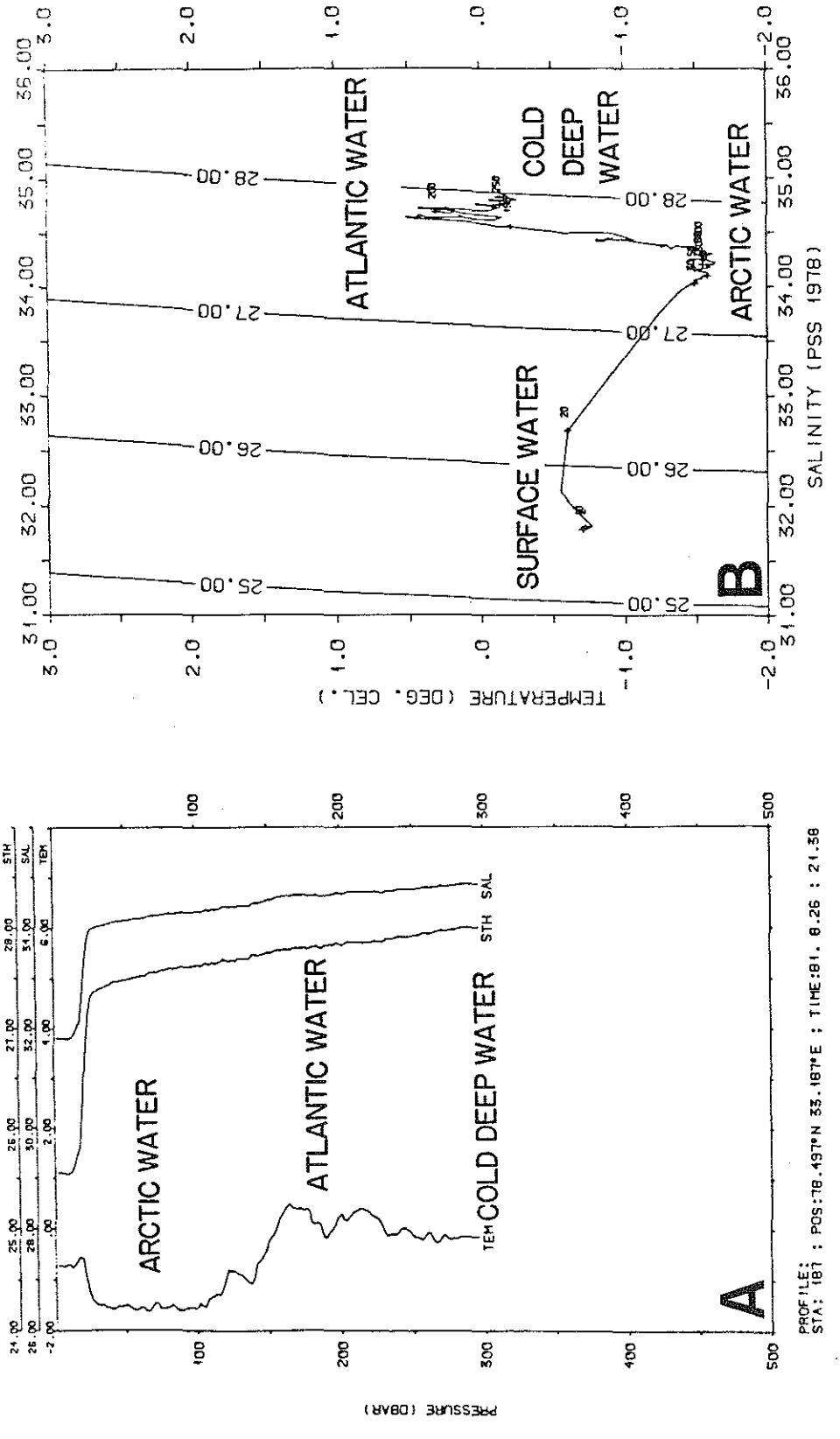
ARCTIC WATER
ATLANTIC WATER
COLD DEEP WATER
TEM
STH
SAL
A
PRESSURE (DBAR)
PROFILE:
STA: 181 : POS:78.497°N 53.187°E : TIME:81. 8.26 : 21.38
ATLANTIC WATER
COLD DEEP WATER
SURFACE WATER
ARCTIC WATER
B
TEMPERATURE (DEG. CEL.)
SALINITY (PSS 1978)

Figure 3

Barents Sea. The surface water becomes depleted in nutrients during late summer months (Mosby 1938, and Loeng 1980).

METHODS

Atlantic, Arctic, and Cold Deep Water masses were defined on the basis of temperature extrema, and the salinity, density, and depth to these temperature extrema were mapped for hydrographic data obtained in late summer, 1981. This method of following water masses is called the core method (Sverdrup et al. 1942 p.166 (discussion of Wüst 1935)), and was first used in the Barents Sea by Mosby (1938). It was used here, instead of more conventional plots on density or depth surfaces, because the water masses are rapidly modified in temperature and salinity (and therefore in density) as they flow through the Barents Sea. A north-south section (figure 4b) shows well defined cores based on temperature, and to a lesser extent on salinity. At these temperatures, density is almost entirely dependent on salinity.

Two problems plague formulation of water-mass distribution maps: low sampling density and lack of syncronism in measurements. The sampling problem exists in station location, spacing, and measurement frequency. The summer, 1981, data set is the most complete, but data from 1973-1982 are also used for comparison of specific locations and annual variations. All data (except 1980, 1981 and 1982 to the north of Kong Karls Land) were obtained by the Institute of Marine Research in Bergen, and they are only reported at standard depths (0, 5, 10,

Figure 4A. Station location map for 1981, the 200m isobath is contoured. Small dots indicate hydrographic stations taken by the R/V Lance in August 1981. All other stations were obtained by the Marine Research Institute in Bergen. Large dot indicates station 187 shown in figure 3. Numbered stations indicate locations of δO^{18} samples discussed in text.

B. North-south temperature, salinity, and density transects along 37°E, shown to the left by heavy line. Abbreviations for water masses are discussed in the text.

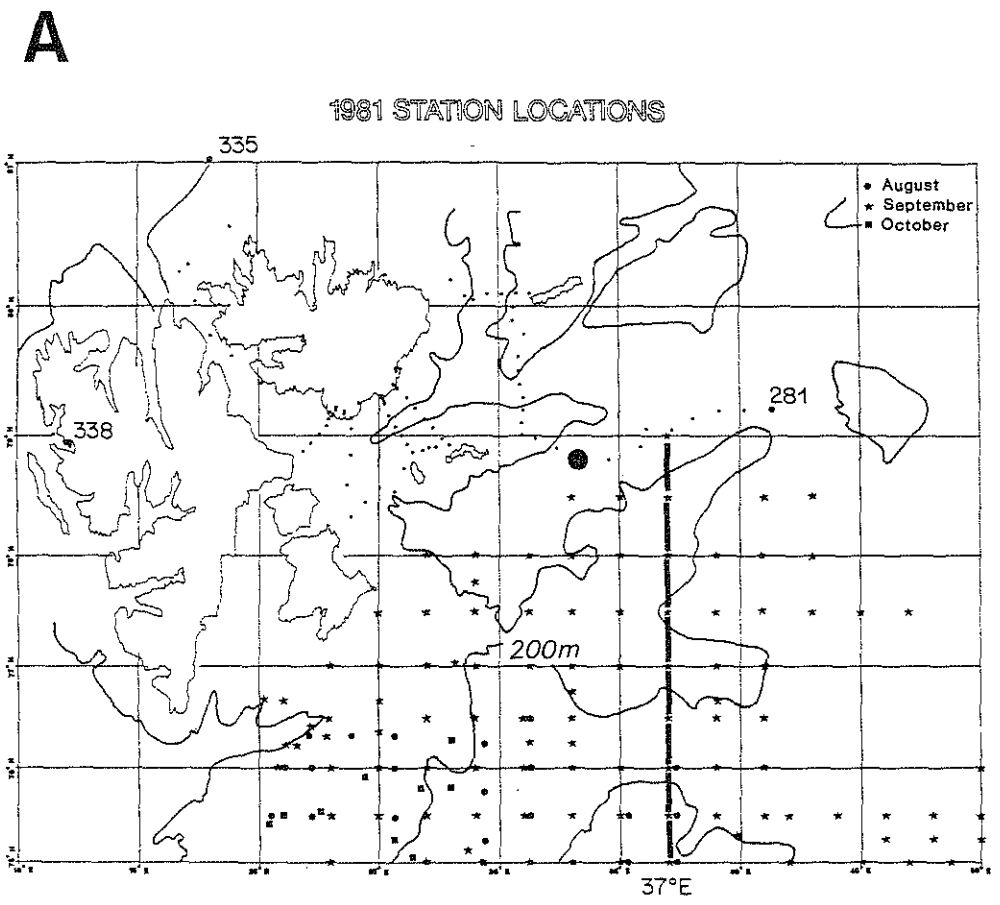
A
1981 STATION LOCATIONS
335
338
281
200m
37°E
August
September
October

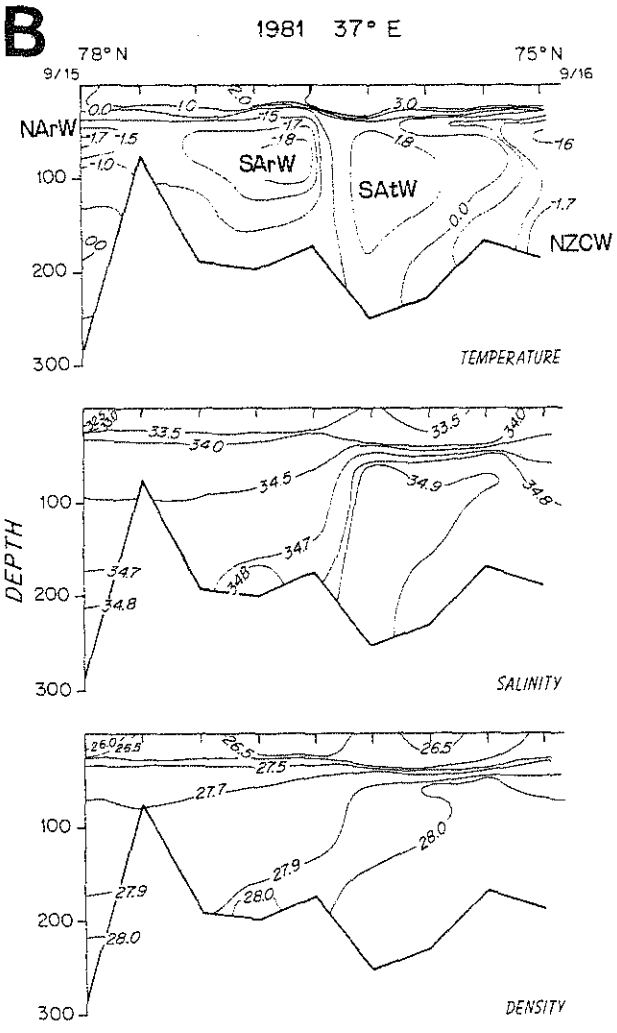
B
1981 37° E
78° N
75° N
9/15
9/16
NArW
SArW
SAtW
NZCW
TEMPERATURE
SALINITY
DENSITY
DEPTH
100
200
300

Figure 4

20, 30, 40, 50, 75, 100, 125, 150, 200, 250, 300, 350, 400m). Thus the most extreme values for the core often were not reported. However, since the core layers are generally vertically homogeneous over at least 50m, this sampling interval is close enough to show general patterns in temperature and salinity (figure 3). Since bathymetry is variable and water mass distribution appears to be largely controlled by bathymetry (Loeng 1980) the most extreme value of the water mass may not be sampled. For the 1981 data set this was not a major problem because spatial sampling density was extensive, except in narrow northern straits.

Finally, since hydrographic stations are not synoptic, and this is a very shallow sea, large changes can occur in surface water properties within a few months (Mosby 1938, and Loeng 1980). Waters below the surface layer in the region near the Polar Front, however, show only small variations over several weeks to a month in the summer (Loeng 1980). Most stations for this study were taken in August and September, 1981, and are considered to be synoptic.

H_2O^{18} samples were obtained at 61 stations in 1982 to examine water mass source and mixing relationships (appendix A). Eight stations were analyzed relative to Standard Mean Ocean Water (SMOW) (Broecker 1974, p. 145). Atlantic Water has a value of $0.42°/_{oo}$, and is isotopically the heaviest water mass in the Barents Sea. δO^{18} will be depleted by precipitation (δO^{18} of $-10.88°/_{oo}$) and glacier run-off (δO^{18} of $-14.28°/_{oo}$) in surface samples (appendix A), but formation or melting of sea ice will

not appreciably change the δO^{18} value. Evaporation enriches surface water in the isotopically heavy δO^{18}.

Volume transport (V_t) and geostrophic velocities (u_g) were calculated assuming a level of no motion at 125m, for hydrographic stations obtained south of Kong Karls Land in 1981.

$$u_g = (\Delta Dg)/(2\Omega \sin\phi\ \Delta x)$$

where: ΔD = dynamic height (referenced to 125m)
g = acceleration due to gravity
Ω = rotation of the earth
ϕ = latitude
Δx = distance between stations

$$V_t = u_g S \Delta x$$

where: S = water depth over which velocity is calculated.

A reference level of 125m was chosen because it is located between the cores of Arctic and Atlantic Water and because it yielded transport directions and velocities consistent with current meter observations (Loeng 1980), water mass distribution, and heat balances in this study. Results are sensitive to the reference level (Sverdrup et al. 1942 pp.390-395) and must be interpreted with care. Similar results were obtained by Novitskiy (1961) with a 200m reference level in deep basins, and a shallower (150-100m) reference level over banks.

RESULTS AND ANALYSIS

Water Mass Distribution

Surface Water: Surface water temperature generally decreases northward, from 5°C in the south to less than -1.0°C in the north (figure 5). The less regular surface salinity contours show a northward decrease, from 34.0°/$_{oo}$ in the south to less than

Figure 5. Water mass properties of the upper 100m:

A. Surface water temperature, late summer 1981

B. Surface water salinity

C. Arctic Water temperature

D. Arctic Water salinity

Hatched areas indicate regions where Arctic Water was not observed, either because of shallow water depth or because of the Polar Front.

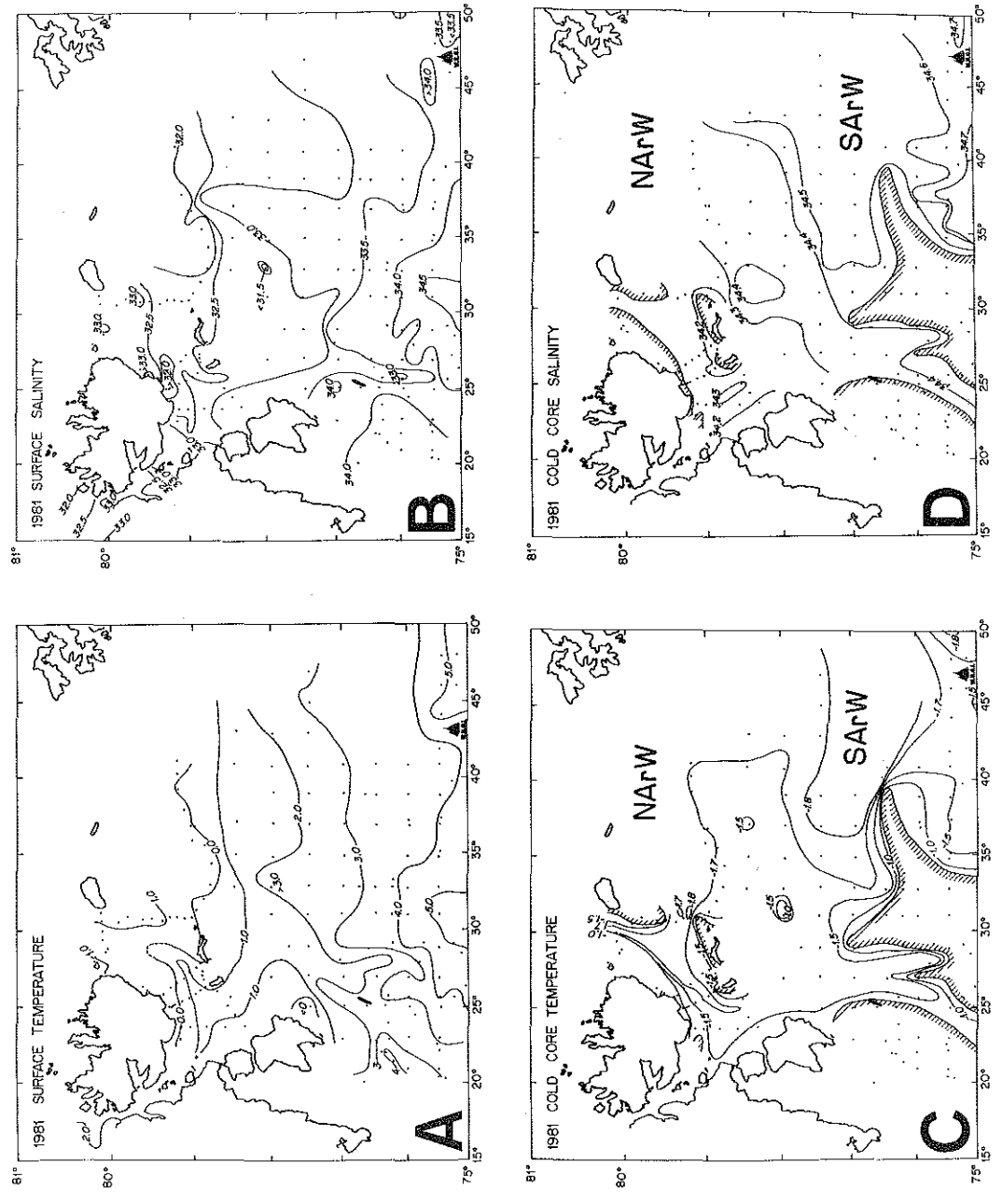
1981 SURFACE TEMPERATURE
A
1981 SURFACE SALINITY
B
1981 COLD CORE TEMPERATURE
NArW
SArW
C
1981 COLD CORE SALINITY
NArW
SArW
D

Figure 5

32.0°/$_{oo}$ near Kong Karls Land, with a corresponding density decrease from greater than 27.0 to less than 26.0σ_t.

Surface water in ice-free areas north of the Polar Front usually has a thermocline as well as a halocline at 10m. In ice-covered areas the gradient exists only in salinity and not in temperature (Loeng 1980). Because at these temperatures and salinities the density of sea water is dependent almost entirely on salinity, there is always a well developed pycnocline at 10-30m, defined by 27.0σ_t (appendix A). This pycnocline decouples the surface from the underlying water (Loeng 1980). Although the surface layer undergoes large changes in temperature due to solar radiation or sea-ice formation, these changes are not observed below the surface on the time scale of weeks (Loeng 1980).

The northward decrease in summer surface temperature results from a longer period of ice cover and therefore a shorter exposure to solar radiation in northern regions (Loeng 1980). The corresponding decrease in salinity may be attributed to the proximity of the sea ice and more recent melting. Deviations from this general pattern include a tongue of colder water extending southward along the east side of Spitsbergenbanken, which is probably a surface expression of the southward flowing Hopen-Bjornoya Current (figure 2).

The surface expression of the Polar Front is seen as a sharp increase in temperature (to 5.0°C) and salinity (to greater than 34.0°/$_{oo}$) in the southern part of the survey area (figure 5). Note that Atlantic Water influence is also seen in Storfjord Trough, where some of the West Spitsbergen Current has split off to the east.

Spitsbergenbanken, on the other hand, has lower salinity; shallow waters over the bank are well mixed in both temperature and salinity.

Arctic Water: Vertical profiles of temperature, salinity, and density (figure 3), show a layer of cold Arctic Water water (colder than 0°C, fresher than 34.7°/$_{oo}$, and denser than 27.6σ_t) located beneath the surface layer. Minimum temperatures in the Arctic Water typically occur near 75m water depth, but vary between 40 and 150m. Temperature-salinity (T-S) plots show that the Arctic Water mass is bounded by the freezing line over a broad range of salinity even in late summer (figure 6). Spatially, the temperature minimum and associated salinity have several well-defined features (figure 5). The cold core, by definition, is not common south of the Polar Front (figures 4 and 5). The tongue-like features in the Polar Front are caused by Atlantic Water extending over sills between banks. Arctic Water does not occur over very shallow banks or along coasts.

Northern Arctic Water (NArW) in the vicinity of the northern islands is colder than -1.7°C, with salinities of 34.2 to 34.3°/$_{oo}$. Stations are too infrequent to describe the distribution in detail, but the minimum temperatures appear centered over the deepest portion of the straits. A well-defined core of southern Arctic Water (SArW) occurs near Storbanken and has the most extreme water mass properties, colder than -1.8°C and saltier than 34.5°/$_{oo}$. This cold, saline water may be the westward expression of the Persey Current (figure 2). This current has been described as flowing out of the Arctic Ocean via the Kara Sea and entering the Barents Sea to the south of

Figure 6. Compilation of temperature - salinity relationships from core data. Contours are lines of constant σ_t.

Northern Arctic Water	NArW
Southern Arctic Water	SArW
Northern Atlantic Water	NAtW
Southern Atlantic Water	SAtW
Novaya Zemlya Cold Water	NZDW
Cold Deep water	CDW
Norwegian Sea Deep Water	star
Greenland Sea Deep Water	diamond
Arctic Ocean Deep Water	dot

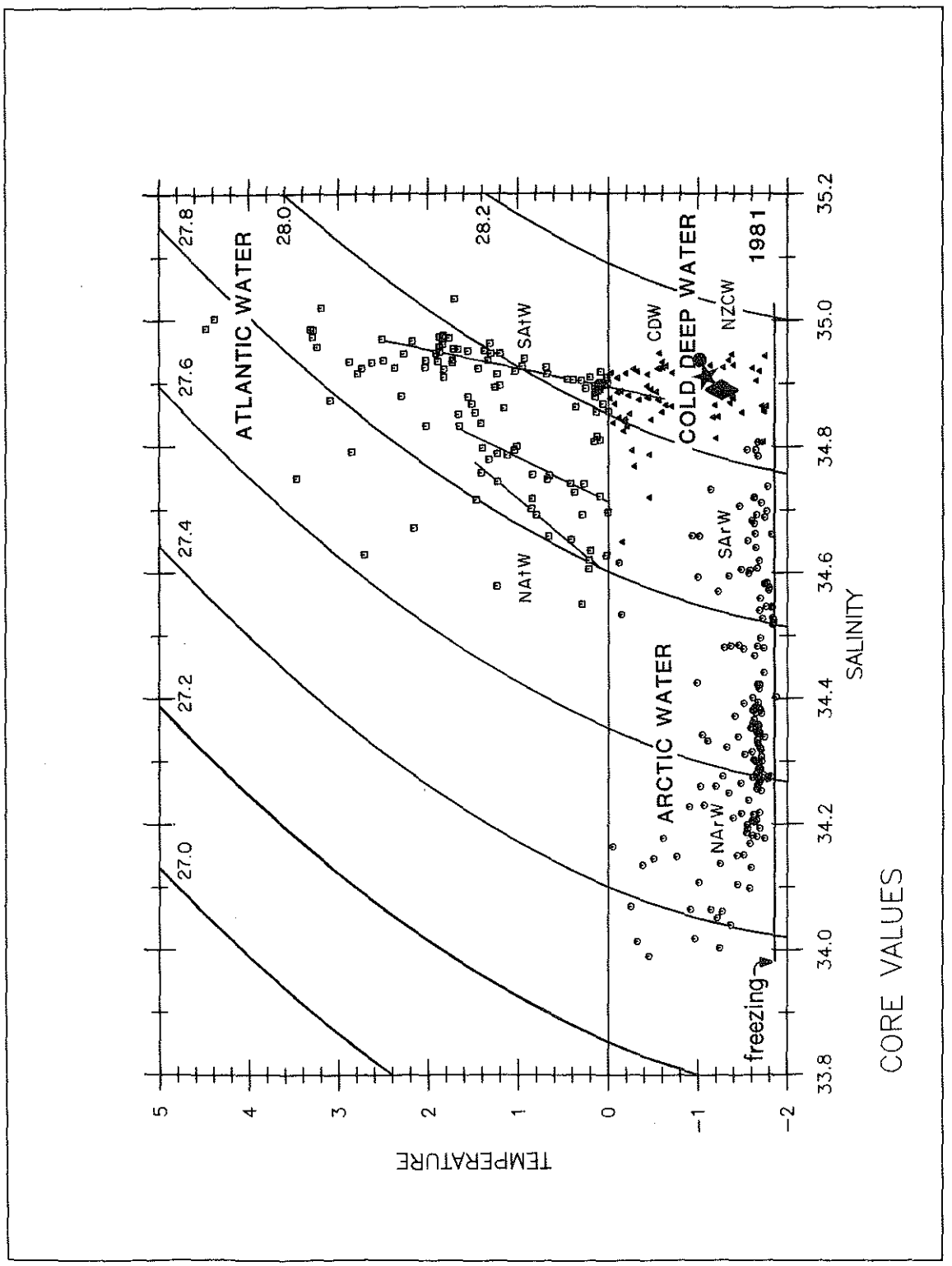
ATLANTIC WATER
ARCTIC WATER
COLD DEEP WATER
1981
CORE VALUES
NArW
SArW
NAtW
SAtW
CDW
NZCW
freezing
27.0
27.2
27.4
27.6
27.8
28.0
28.2
TEMPERATURE
SALINITY
5
4
3
2
1
0
−1
−2
33.8
34.0
34.2
34.4
34.6
34.8
35.0
35.2

Figure 6

Franz Josef Land, where it mixes with Atlantic Water (Novitskiy, 1960, and Tantsiura, 1959). However, eastern station locations in this study are too infrequent to determine the source. SArW is distinguished from NArW by higher salinity and lower temperature.

NArW and SArW merge west of Storbanken, where they also mix with slightly warmer surface water. The result is -1.5°C and 34.3°/$_{oo}$ water which forms the core of the Hopen-Bjornoya Current along the east side of Spitsbergenbanken. The Hopen-Bjornoya Current is observed as a tongue of cold water along the east flank of Spitsbergenbanken. A southward increase in salinity is observed, from 34.3 to 34.4°/$_{oo}$. A small offshoot of cold water projects eastward and occurs along a slight ridge of the 100m bathymetric contour at 76°N (figure 5). This small tongue was also observed in 1978, 1980, and 1982.

Atlantic water: Large areas of the Barents Sea do not contain the warm core of Atlantic Water (greater than 0°C and 34.7°/$_{oo}$). Atlantic Water is present in Storfjord Trough and the deep basins of the Barents Sea (figure 7). Northern and southern sources for Atlantic Water are evident in temperature distributions. Southern Atlantic Water (SAtW) was slightly more saline (34.9°/$_{oo}$) than northern Atlantic Water (NAtW - 34.8°/$_{oo}$) in the summer of 1981 (figures 6 and 7). Maximum temperature of the southern Atlantic Water core decreases northward, and maximum temperatures of the northern Atlantic Water are between 1.0 and 1.5°C. This pattern of core distribution is remarkably similar from year to year (figure 8)

Figure 7. Atlantic Water properties. Hatched areas indicate regions where Atlantic Water was not observed.

A. depth

B. temperature

C. salinity

D. density

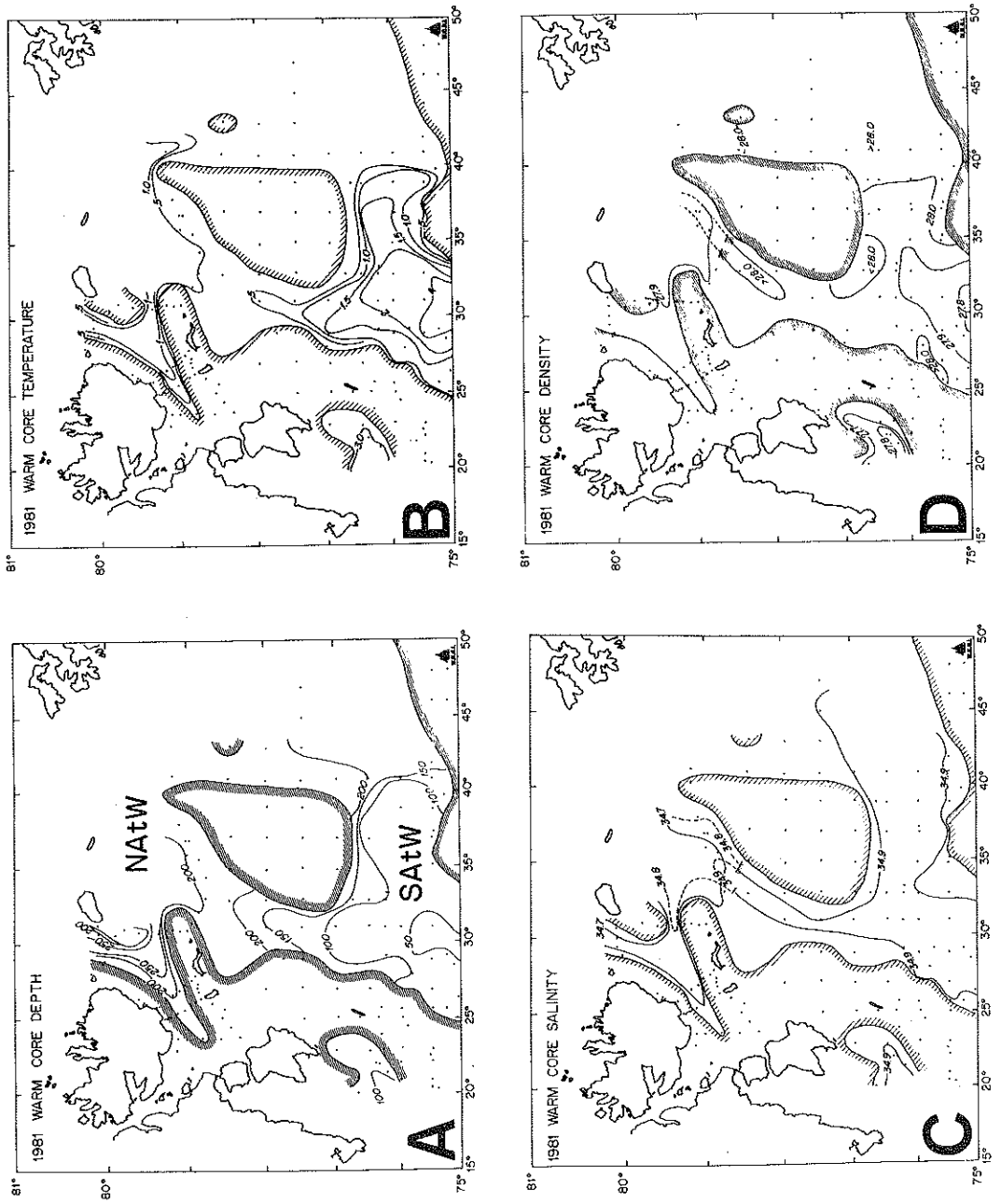
1981 WARM CORE DEPTH
NAtW
SAtW
A
1981 WARM CORE TEMPERATURE
B
1981 WARM CORE SALINITY
C
1981 WARM CORE DENSITY
D

Figure 7

although this may be fortuitous because Novitskiy (1961) discusses large annual variations. On the other hand, variations observed in Atlantic Water properties for 1978, 1980, 1981, and 1982 (figure 8) may reflect differing station locations, rather than changes in distribution of Atlantic Water. NAtW appears to be limited to depths greater than 150m, while the depth to the core of SAtW increases from 50m to greater than 200m moving northward from the Polar Front.

The major source for SAtW is the North Cape Current which enters the Barents Sea via Hopen - Bjornoya Trough. Spitsbergenbanken is too shallow for Atlantic Water to enter the Barents Sea from Storfjord Trough. SAtW splits south of Storbanken and flows north and east over sills. The maximum temperature of the core decreases during passage over the sills, but the core maintains a salinity close to 34.9°/$_{oo}$ and increases in density and depth (figure 7). In the T-S plot (figure 6), this is seen as an almost vertical line from the Atlantic source water of the North Cape and West Spitsbergen Currents, at 2°C and 35.0°/$_{oo}$.

It is not clear where NAtW enters the Barents Sea between the northern islands, since the straits have not all been sampled in one year since Mosby (1938). NAtW occurs in all northern basins deeper than 250m (figures 7 and 8). Mosby (1938) found the highest temperature and salinity water in Franz Josef - Victoria Trough. Since this strait is the deepest and the widest access to the Arctic Ocean, it is plausible that NAtW enters the Barents Sea through Frans Josef - Victoria Trough and flows south and west in the basins near Kong Karls Land. The strait between Kvitoya and Victoria islands may

Figure 8. Atlantic Water maximum temperatures for:

A.1978,

B.1980,

C.1981, and

D.1982. All data for 1978, and data south of 79°N for 1981 and 1982 courtesy of the Institute for Marine Research of Bergen, Norway.

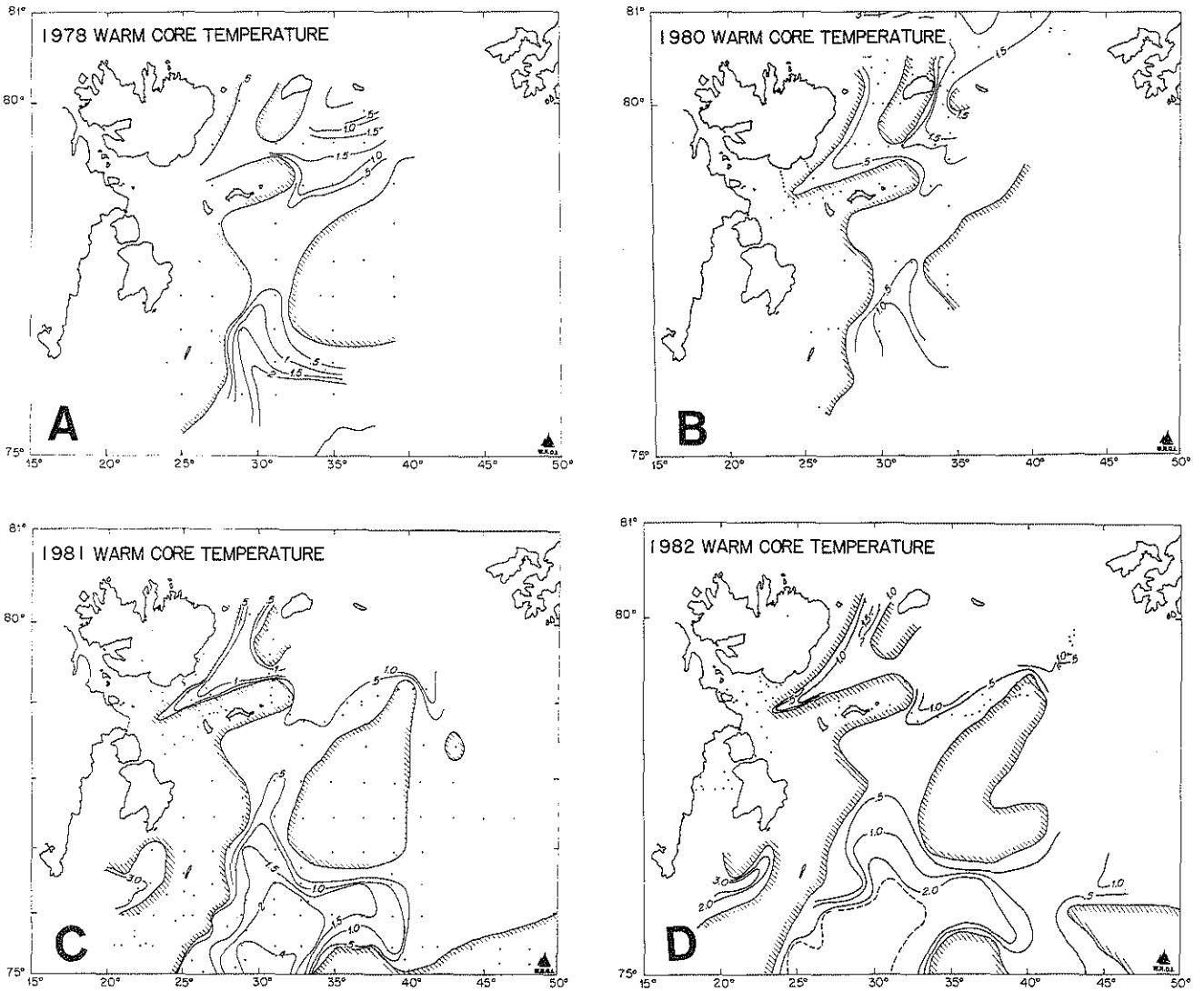
1978 WARM CORE TEMPERATURE
A
1980 WARM CORE TEMPERATURE
B
1981 WARM CORE TEMPERATURE
C
1982 WARM CORE TEMPERATURE
D
81°
80°
75°
15°
20°
25°
30°
35°
40°
45°
50°

Figure 8

be connected to Franz Josef - Victoria Trough and also could be a conduit for NAtW (see figure 1). Bathymetry is not well known in this region.

NAtW and SAtW merge in the vicinity of Kong Karls Land. Since NAtW is less saline (at least in 1981), it is also less dense, occuring above SAtW where both water masses are present. The fate of the SAtW to the north of Storbanken is difficult to determine with the station locations obtained thus far. The temperature maximum of SAtW occurs at approximately the 250m isobath (figure 7) along the western flank of Storbanken, indicating northerly flow. It is obvious that it does not flow around Storbanken, because it is not seen on the eastern side. Modified SAtW may continue to flow northward, possibly through Franz Josef - Victoria Trough and into the Arctic Ocean.

Cold Deep Water: Cold Deep Water, colder than 0°C and saltier than $34.7^{\circ}/_{\circ\circ}$ has a limited distribution and is the densest water mass in the Barents Sea (greater than 28.0 σ_t, figure 9). It can be divided into two different types on the basis of temperature (figure 6). Novaya Zemlya cold water (NZCW - colder than -1.0°C) is located in the southeastern portion of the study area north of Novaya Zemlya and has T-S properties similar to deep water of the Norwegian-Greenland Sea and the Arctic Ocean (figure 6 and Swift et al. (1983)). Cold Deep Water (CDW: -1.0°C to 0.0°C) occurs beneath SAtW west of Sentralbanken and Storbanken and appears to be slightly colder but otherwise similar to this warmer water mass (figure 9). Depth to the western cold water mass is variable, from less than 100m

to greater than 300m along the east slope of Spitsbergenbanken (figure 9). Salinity is generally around 34.9°/$_{oo}$, but is less north of Storbanken.

Regions where CDW is shallowest and densest (figure 9) are where Atlantic Water meets Arctic Water along the Polar Front, and the Atlantic core starts to sink beneath the Arctic Water. Atlantic Water could be cooled in this region by air-sea interaction because the surface layer is thin here, by melting sea-ice, or by double diffusion with the overlying and interleaving cold fresh Arctic Water. A portion of this CDW in Hopen-Bjornoya Trough (figure 9) may flow south into the Norwegian-Greenland Sea, contributing dense salty water (Swift et al., 1983). CDW formed from southern Atlantic Water by cooling over Storbanken sill can be traced along the western flank of Storbanken, but stations do not extend far enough north to see if it exits the Barents Sea through Frans Josef - Victoria Trough.

δO^{18} measurements obtained in 1982 north of Storbanken indicate that CDW below Atlantic Water may have δO^{18} values similar to the Atlantic Water core (figure 10). Formation probably occurs by cooling Atlantic Water, rather than by modification of δO^{18}- depleted surface water. In contrast, deep cold water in the Arctic Basin to the north has depleted δO^{18} relative to the warm Atlantic core; this indicates a different source (possibly modified surface water) for this deep water mass (figure 10). However, both deep water samples were obtained in the transition zone between the core of warm Atlantic Water and the core of Cold Deep Water (figure 10), so they may not be representative of the extreme Cold Deep Water properties.

Figure 9. Cold Deep Water properties. Hatched areas indicate regions where Cold Deep Water was not observed.

A. depth

B. temperature

C. salinity

D. depth

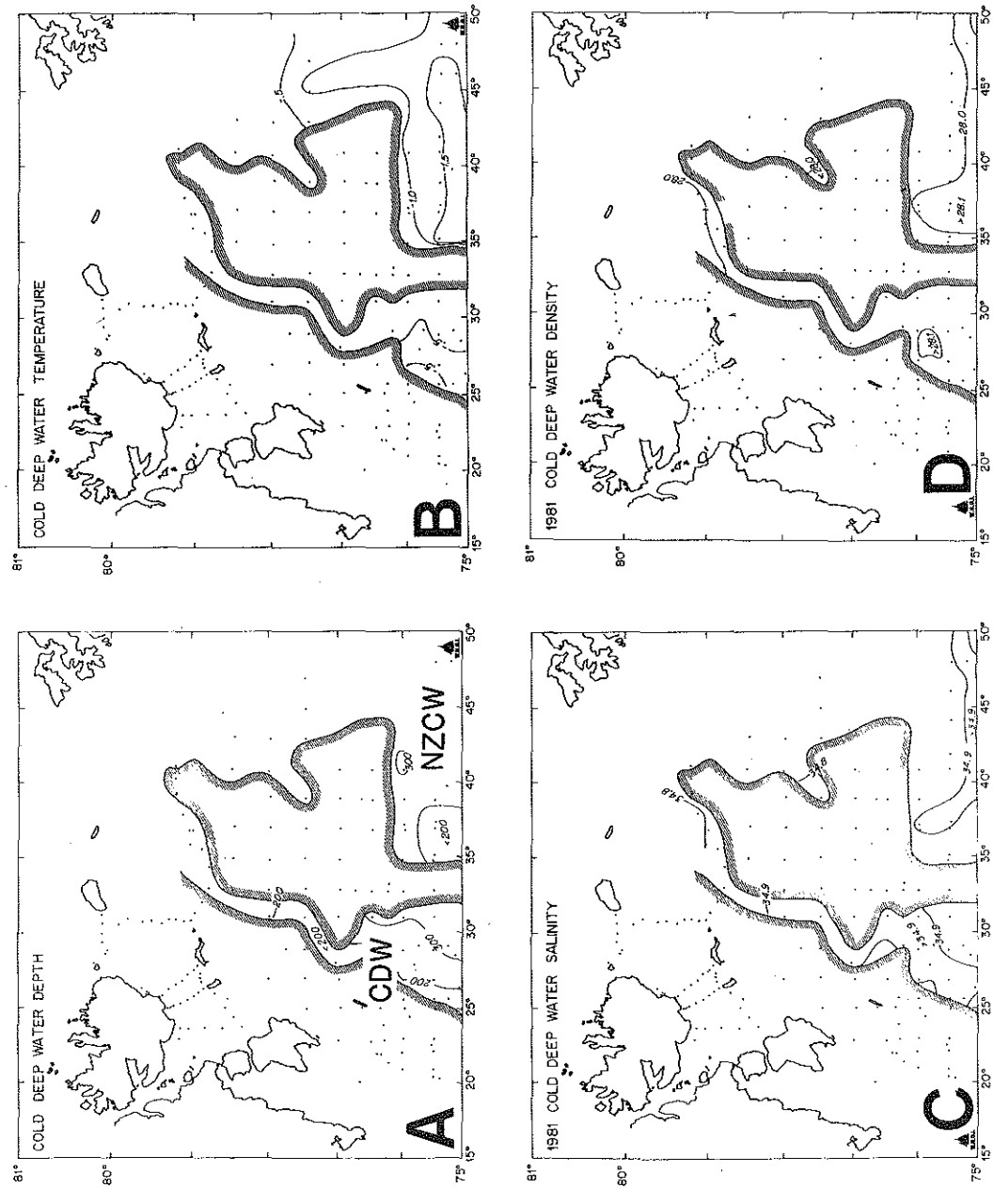
COLD DEEP WATER DEPTH
CDW
NZCW
A
COLD DEEP WATER TEMPERATURE
B
1981 COLD DEEP WATER SALINITY
C
1981 COLD DEEP WATER DENSITY
D

Figure 9

Figure 10. δO^{18} examples for 1982.

A. temperature vs. salinity for stations dicussed in the text. T-S properties of samples for δO^{18} marked with symbols.

B. δO^{18} vs. salinity

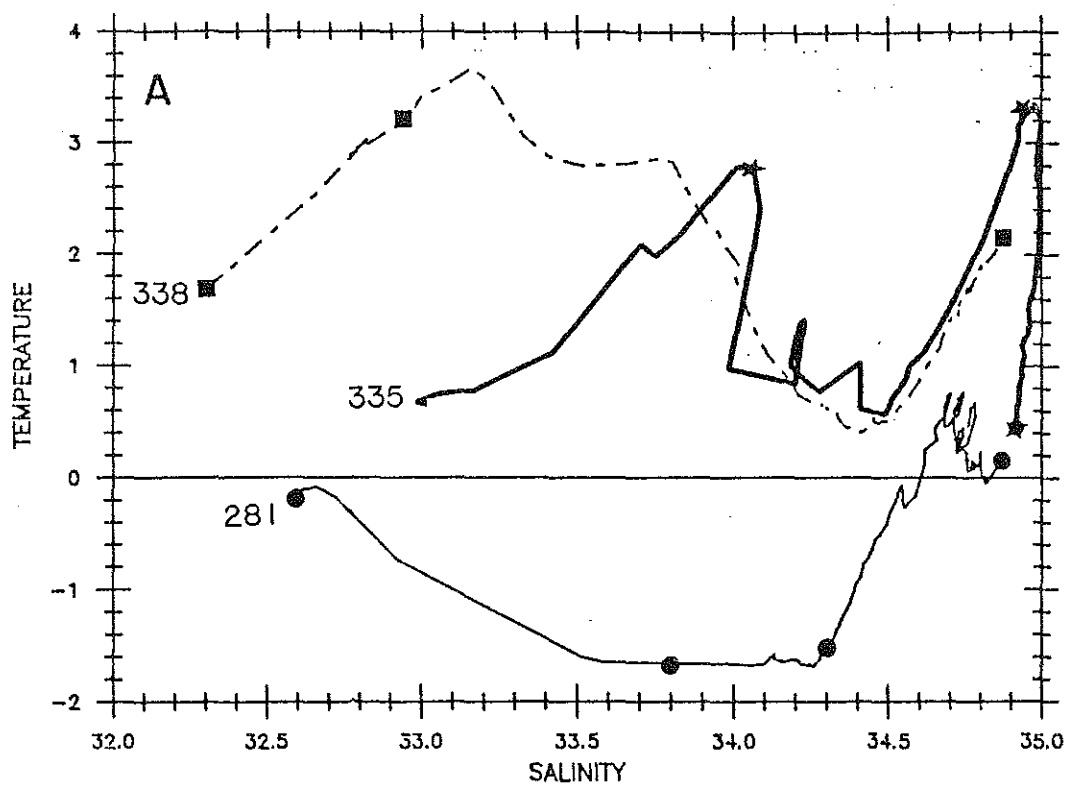
A
TEMPERATURE
SALINITY
338
335
281
4
3
2
1
0
-1
-2
32.0
32.5
33.0
33.5
34.0
34.5
35.0

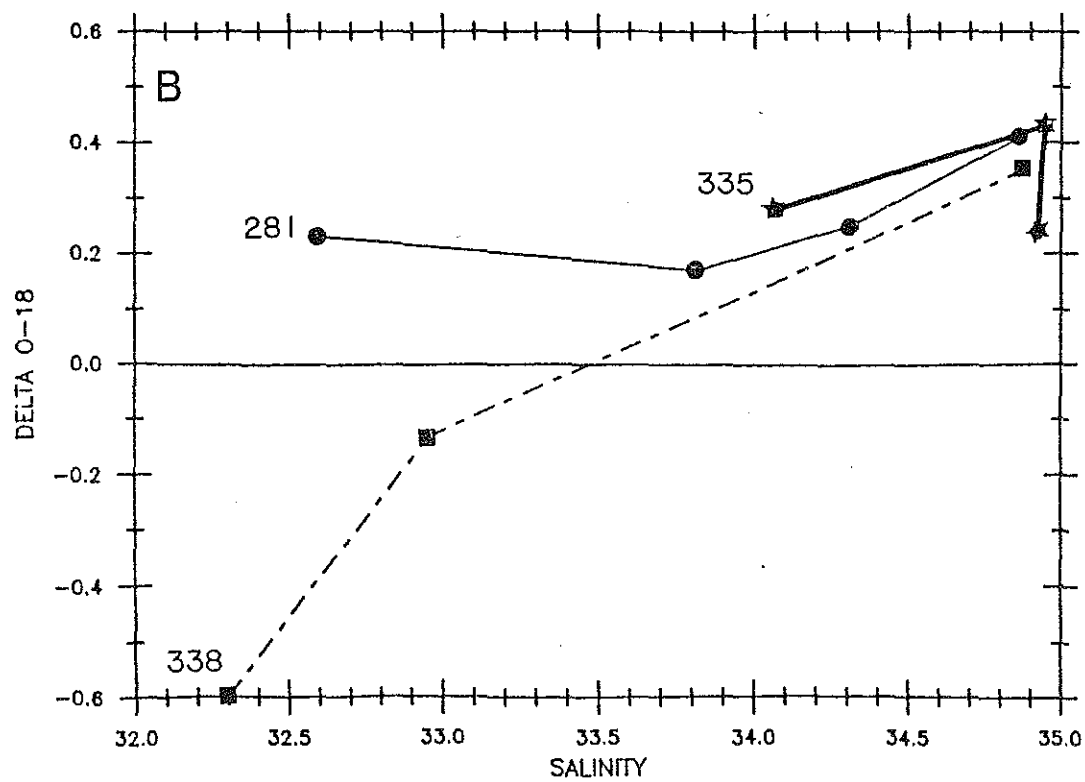
B
DELTA O-18
SALINITY
335
281
338
0.6
0.4
0.2
0.0
-0.2
-0.4
-0.6
32.0
32.5
33.0
33.5
34.0
34.5
35.0

Figure 10

Cold Deep Water is the densest water mass in the northern Barents Sea; the Institute of Marine Research data show a density exceeding $28.3\sigma_t$ in 1973. Because it is the bottom water mass in the northern Barents Sea, it receives regenerated nutrients diffusing from the sediments. Ellertsen et al. (1981) have measured silicate values of 6-7μM in the bottom waters south of Storbanken sill. Its properties seem to be determined by modification of Atlantic Water as it passes over the Storbanken sill and is therefore it is probably very sensitve to climatic variations. This cooled, dense Atlantic Water could therefore have a large impact on Arctic deep water if formed in large enough quantities.

NZCW observed in the southeastern portion of the Barents Sea, north of Novaya Zemlya, is near the freezing point (figure 6) and is the densest water mass in the study area (figure 9). This water mass may form by cooling Atlantic Water of the Novaya Zemlya Current along the bank north of Novaya Zemlya (Novitskiy 1961, Loeng 1980), or by brine rejection during sea-ice formation in the surface waters (Midtun, in prep.). Since winter data are difficult to obtain, the origin cannot be resolved at present. δO^{18} measurements could resolve this question but are not available; if NZCW forms by surface processes (such as sea-ice formation) it should be depleted in δO^{18} relative to Atlantic Water. NZCW appears to collect in small basins in the southeastern Barents Sea and has been observed flowing eastward into the Kara Sea (Midtun, in prep.) (figure 9). Recent bathymetric data indicate a deep conduit to Frans Josef - Victoria Trough in the northern Barents Sea (figure 1). NZCW could overflow if enough was formed in the winter, possibly passing through Frans Josef - Victoria Trough to the Arctic Ocean.

Both cold water masses are very dense (greater than $28.0\sigma_t$) and probably form during the winter. Late summer observations are likely to underestimate their importance.

Volume Transport

Volume transport, based on reference level at 125m, shows circulation patterns consistent with core analysis (figure 11 and chapter 2). NArW sources contribute $0.45 \times 10^6 m^3/sec$ ($10^6 m^3/sec$ = 1 Sverdrup (Sv)) to the Hopen-Bjornoya Current, and SArW sources contribute 0.65 Sv. Some of this cold water is appears to be lost through entrainment along the Polar Front, and 0.9 Sv exits from the study area along the east slope of Spitsbergenbanken with geostrophic velocities exceeding 30cm/sec (chapter 2). Approximately 0.5 Sv of CDW may be transported southwest in northern Hopen-Bjornoya Trough (also along the eastern slope of Spitsbergenbanken) continuing into the Norwegian - Greenland Sea (figure 11). Calculated geostrophic velocities of this southerly slope current locally exceed 10cm/sec (chapter 2). SAtW splits approximately in half, with 0.4 Sv of SAtW and CDW flowing north on either side of Storbanken (figure 11). Some fraction of this modified southern Atlantic Water reaches Frans Josef - Victoria Trough. Rudels (in prep.) estimates that 0.4 Sv of SAtW and CDW may exit the Barents Sea between Nordaustlandet and Frans Josef Land, while Aagaard and Greisman (1975) estimated 0.7sv. Mixing with NAtW in Frans Josef - Victoria Trough may alter the properties of

Figure 11. Schematic representation of Arctic and Atlantic Water transport paths based on water mass analysis and volume transports calculated with a reference level at 125m. Water mass abbreviations same as figure 6.

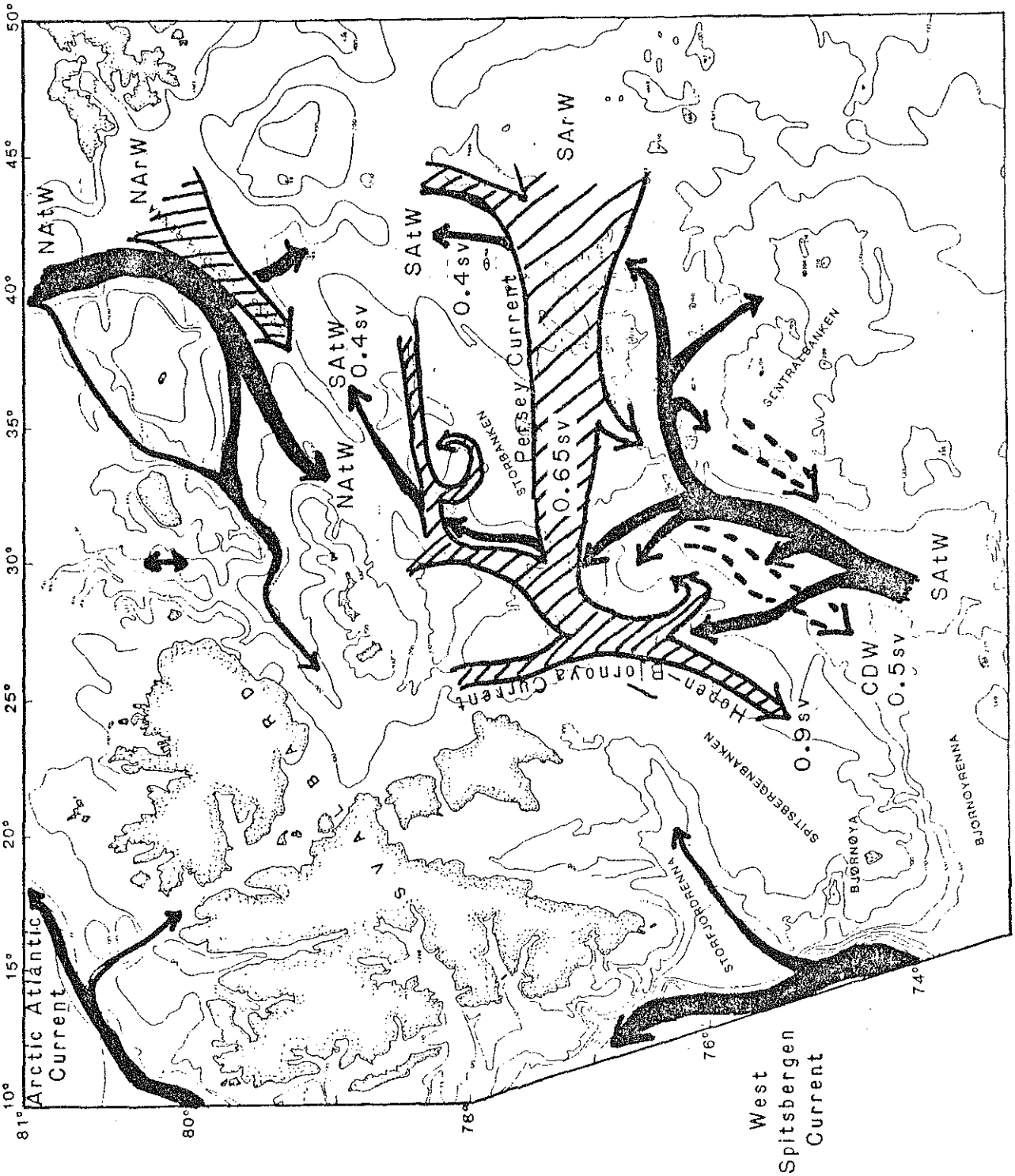
Arctic Atlantic Current
NAtW
NArW
SAtW
0.4sv
NAtW
SAtW
0.4sv
SArW
Storbanken
Persey Current
0.65sv
Hopen-Bjornoya Current
0.9sv
CDW
0.5sv
SAtW
Spitsbergenbanken
Sentralbanken
Bjornoya
Bjornoyrenna
Storfjordrenna
West Spitsbergen Current
81°
80°
78°
76°
74°
10°
15°
20°
25°
30°
35°
40°
45°
50°

Figure 11

the SAtW-CDW before it exits the northern Barents Sea. Mosby (1938) found Frans Josef - Victoria Trough was filled with NAtW with no Cold Deep Water near the bottom, indicating that CDW did not exit to the north through this strait in 1931.

Based on these volume transport and geostrophic velocity estimates, a heat balance may be constructed. As SAtW is transported north, it loses heat to the atmosphere south of the Polar Front. North of the Polar Front it loses heat to the overlying Arctic Water of the Persey Current. Maximum values for heat loss may be obtained by assuming the temperature extreme mapped in the water mass analysis occurs over 100m (Δz) for Atlantic Water, and 75m for Arctic Water (figure 3).

If SAtW decreases in temperature (ΔT) from 3.0°C to 1.5°C (figures 7 and 8) over a distance (Δx) of 200km, with an average velocity (u) of 7cm/sec (chapter 2), 220 Watts/m^2 will be released:

$$\text{Heat exchange} = (u\Delta T\Delta z C_p \rho)/\Delta x$$

where: C_p = heat capacity
ρ = water density

Previous estimates of heat loss to the atmosphere in this region range from 75 Watts/m^2 (Rudels, in prep.) to 100 Watts/m^2 (Bunker and Worthington 1976). The excess heat loss calculated here (approximately 100 Watts) is partly because the temperature extreme was used rather than the average temperature, partly because heat in the Polar Front region also goes into melting sea ice, and partly because the Atlantic Water actually forms a gyre in northern Hopen - Bjornoya Trough; so 200km may be an underestimate of the distance over which heat is lost.

North of the Polar Front, SAtW is overridden by SArW of the Persey Current. This cold water mass gains heat from the underlying SAtW, increasing in temperature from -1.8 to -1.5°C (figure 5), while SAtW cools another degree to 0.5°C (figure 7). These transformations occur over approximately 200km (figures 7 and 8). If the velocity of Arctic Water in the Persey Current is assumed to be 30cm/sec (chapter 2) while SAtW continues northward at 7cm/sec, heat gained by the Arctic Water and heat lost by the Atlantic Water balance at approximately 40 Watts/m^2 over a 40km zone west of Storbanken. At a transport rate of 7cm/sec, Atlantic Water will take approximately 2 months to travel the 400km through this transformation region.

DISCUSSION

Formation of dense bottom water in the Barents Sea could occur by cooling of saline Atlantic Water, or by increasing salinity of cold surface or Arctic Water through brine rejection during sea-ice formation. In late summer, 1981, the densest water mass in the Barents Sea was NZCW, with temperature - salinity properties similar to Norwegian-Greenland Sea and Arctic Ocean deep water. Regional distribution of this water mass is not well surveyed in this study, but the dense water appears to be confined to a basin north of Novaya Zemlya during the summer of 1981 (figure 9). Tantsiura (1959) identified this region north of Novaya Zemlya as a location where deep

convection is important in the Barents Sea, but the origin of NZCW is not known. If formed in large quantities, this dense water mass may overflow the small basins and perhaps affect the surrounding seas (Midtun, in prep.).

Slightly less dense CDW occurs along the eastern slope of Spitsbergenbanken (figure 9). Based on a reference level at 125m, CDW is transported to the southwest. Formation occurs in the region of the Polar Front, and must be due to cooling of Atlantic Water since this is not a region where sea-ice forms in large quantities.

Transport of modified Atlantic Water through the Barents Sea into the Arctic Ocean has been called upon as a possible salt source for Arctic deep water (Swift et al. 1983). This modified Atlantic Water may either be SAtW and CDW from a branch of the North Cape Current, or NAtW from the Arctic Atlantic current which recirculates near the northern islands (figure 11). In 1981, northern sources were fresher than southern sources; no matter how much the northern Atlantic Water was cooled in the Barents Sea, it would still be too fresh to form dense bottom water like that found in the Arctic Ocean (figure 6). The salinity difference between NAtW and SAtW could arise from mixing of NAtW with NArW (figure 5). NArW is less saline than SArW because it mixes with northern surface water, which receives fresh water from sea-ice melting. SArW mixes with saline surface Atlantic Water along the Polar Front (figures 5 and 7). Alternatively, NAtW may be fresher initially as it comes through Frans Josef - Victoria Trough. The core of Atlantic Water may have sunk below the sill depth to the north, so that water entering the northern Barents Sea is less extreme than that of the Arctic Basin. NAtW may also have been fresher in 1981 because variations in Atlantic Water properties occur through time (Blindheim

and Loeng 1981), and NAtW may be of a different vintage than SAtW since it has travelled around the Svalbard Archipelago. If differences in salinity are due to mixing with Arctic Water, then northern Atlantic Water should always be fresher, and therefore less likely as a deep water source. If the variations are due to initial variations in Atlantic Water, then modification of water from the Arctic Atlantic current in the northern Barents Sea could also produce deep water.

CONCLUSIONS

The most important deep water conduits between the northern Barents Sea and the surrounding seas are Franz Josef - Victoria Trough, Frans-Josef - Novaya Zemlya Strait and Hopen-Bjornoya Trough, while Sentralbanken, Storbanken and Spitsbergenbanken severely constrain both deep and shallow water flow in the southern regions.

Water column properties observed in late summer north of the Polar Front (approximately 74°N) in the Barents Sea are stratified; a layer of surface water is underlain by Arctic Water, which is in turn underlain by Atlantic Water (see figure 3). Below Atlantic Water, temperature usually decreases again, indicating Cold Deep Water overlying the sea floor. In the southern reaches of Franz Josef Trough, Atlantic Water from both northern and southern sources occurs (figure 11). To the south, near the Polar Front, Atlantic and Arctic Water interleave; Atlantic Water may mix with surface water above and

Arctic Water below instead of the more common situation where it mixes with the Arctic Water above and the Cold Deep Water below.

Arctic and Atlantic Water-mass cores, based on temperature extrema mapped in the northern Barents Sea, show distinctive temperature - salinity relationships in the various basins. Transport paths suggested by core analysis are consistent with circulation patterns indicated by volume transport calculations with an intermediate level of no motion (see also Tantsiura, 1959, Novitskiy 1960). Transport calculated with a level of no motion at 125m suggests 0.8 Sv of modified southern Atlantic Water flows northward into Frans-Victoria Trough, 0.9 Sv of Arctic Water flows southward as the Hopen-Bjornoya Current, and 0.5 Sv of cold modified Atlantic Water flows south along the deep eastern flank of Spitsbergenbanken. Northern Atlantic and Arctic Water were fresher than southern sources in the summer of 1981, although northern Atlantic Water ultimately comes from the same source as southern Atlantic Water - the Norwegian Current.

Formation of Novaya Zemlya cold water, with water-mass properties similar to Norwegian Sea Deep water and Arctic Deep water, apparently occurs by modification of southern Atlantic Water north of Novaya Zemlya. This dense water flows both northward and eastward, affecting the surrounding seas. Major outstanding problems are: 1) where and when does the modified Atlantic Water exit the Barents Sea, and 2) what happens in the winter, i.e. how much of the hydrography observed in the summer is a remnant from winter conditions, and how representative is the summer of 1981?

Acknowledgements

Tor Gammelsrod, Mike McCartney, and Bert Rudels are acknowledged for critical reviews of the manuscript. Tor Gammelsrod at the Geophysics Department of the University of Bergen processed the hydrographic data obtained in the northern Barents Sea in 1981 and 1982; Harald Loeng at the Institute for Marine Research in Bergen Norway provided most of the hydrographic data used in the southern portion of the study. Analysis of δO^{18} in water samples was done at Richard Fairbanks' laboratory at Lamont-Doherty Geological Observatory. Support for this research came from ONR contract N00014-01-C-009, with travel support from the Norwegian Marshall Fund. The Norwegian Polar Research Institute provided ship time and logistical support.

REFERENCES

Aagaard, K. (1981) On the deep circulation of the Arctic Ocean. Deep-Sea Research. 28A:251-268.

Aagaard, K. and P. Greisman (1975) Toward new mass and heat budgets for the Arctic Ocean. J. Geophys. Res. 80:3821-3827.

Blindheim, J. and H. Loeng (1981) Variability of Atlantic influence in the Norwegian and Barents Seas. Fisk. Dir. Skr. Ser. HavUnders. 17:161-189.

Broecker, W.S. (1974) Chemical Oceanography Harcourt Brace Jovanovich, Inc. 214pp.

Bunker, A.F. and L.V. Worthington (1976) Energy exchange charts of the North Atlantic Ocean. Bull. Amer. Meteor. Soc. 57:670-678.

Ellertsen, B., H.Loeng, F.Rey, S.Tjelmeland (1981) The feeding conditions ofcapelin during summer: Field observations in 1979 and 1980. Fisken Hav. 1981(3):1-68. in Norwegian.

Johannessen, O.M. and L.A. Foster (1978) A note on the topographically controlled oceanic Polar Front in the Barents Sea. J.G.R. 83(C9):4567-4571.

Loeng, H. (1979) A review of the sea ice conditions of the Barents Sea and the area west of Spitsbergen. Fisken Hav. 1979(2):29-75. in Norwegian.

Loeng, H. (1980) Physical oceanographic investigations in central parts of the Barents Sea, July 1978. Fisken Hav. 1980(3):29-60. in Norwegian.

Midtun, L. (in prep.) Formation of heavy bottom water in the Barents Sea.

Mosby, H. (1938) Svalbard Waters. Geofysiske Publikasjoner. 12(4):1-85.

Nansen, F. (1915) Spitsbergen Waters: Oceanographic obervations during the cruise of the "Veslemoy" to Spitsbergen in 1912. Vid. Selsk. Skr. I Matem-Naturv. Kl. 1915 no.2 Kristiana.

Novitskiy, V.P.(1961) Permanent currents of the Northern Barents Sea. Trudy Gosudarstvennogo Okeanograficheskogo Tnstituda. 64:1-32 Leningrad. (Translated by U.S.N.O. 1967)

Rudels, B. (in prep.) On the heat, mass salt balance of the Polar Ocean.

Solheim, A. (1982) Bathymetric map of the northwestern Barents Sea. unpub. NPRI document.

Sverdrup, H.U., M.W. Johnson, R.H. Fleming (1942) The Oceans: Their Physics, Chemistry, and General Biology. Prentice Hall, Inc. 1087pp.

Swift, J.H., T. Takahashi, H.D. Livingston (1983) The contributioon of the Greenland and Barents Sea to the deep water of the Arctic Ocean. J.G.R. 88(c10):5981-5986.

Tantsiura, A.I. (1959) On the currents of the Barents Sea. Transactins of the Polar Scientific Research Institute of Marine Fisheries and Oceanography - N.M. Knipovic (PINRO) 11:35-53 (in Russian, translated to English by the Norwegian Polar Research Institute 1983.)

Wüst, G. (1935) Die Stratosphare. Deutsche Atlantische Exped. Meteor 1925-1927, Wiss. Erg., Bd. 6, 1 Teil, 2 Lief, 288pp.

CHAPTER 2

Surface Sediment Response to Hydrographic Regime: the northern Barents Sea

Stephanie L. Pfirman
Woods Hole Oceanographic Institution
Woods Hole, Massachusetts

ABSTRACT

Modern surface sedimentation in the northern Barents Sea results from reworking of late Weichselian (Wisconsin) basal tills and glaciomarine sediments. At water depths less than 100m, bottom sediments are gouged by icebergs, causing a rough surface texture, and winnowed by near-bottom currents from wind-driven waves, creating a coarse lag deposit. Between 100 and 200m, occasional storm-generated waves and tidal currents superimposed on mean currents winnow fine-grained material from surface sediments. Mean currents are intensified in narrow straits and along the peripheries of basins, resulting in a near-bottom nepheloid layer that is associated with sea-floor winnowing or non-deposition of surface sediments. These suspended sediments are advected downstream with the mean currents and also down slope in bottom nepheloid layers. Deposition of resuspended fine-grained sediments generally occurs in the interiors of the numerous basins within this shallow epicontinental sea.

INTRODUCTION

The modern epicontinental Barents Sea spans a range of sedimentary environments, from glacial-marine in the north to year round ice-free conditions in the south (figure 1). The sea floor morphology of the Barents Sea is presently characterized by northeast-southwest trending basins and shallow banks which are best delineated by the 200m bathymetric contour (figure 1). Basins are seldom deeper than 300m, and the banks are typically 50-150m deep. Because there is only a thin cover of unconsolidated sediments (Elverhoi and Solheim 1983a), the bathymetry is an expression of the topography of the underlying bedrock which was subaerially eroded before glaciation during the late Pliocene and Pleistocene (Emelyanov et al. 1971, Solheim and Kristoffersen 1983, Vorren and Kristoffersen, in prep.).

Previous studies of Barents Sea sediments have concentrated primarily on the extent and type of Pleistocene glacial deposits (Klenova 1960, Dibner 1970, Emelyanov et al. 1971, Wright 1974, Grosswald 1980, Elverhoi and Solheim 1983). These authors have concluded that modern sedimentation is due to winnowing of fines from shallow banks and their subsequent redeposition in deep basins. This conclusion is based on observations that bank sediments are coarse and basin sediments are fine-grained, with the textural change occurring near 200m water depth (figure 2). Lithology of the coarse fraction of bank sediments in the Barents Sea reflects the composition of the underlying bedrock, while the mineralogy of the silt and clay sized

Figure 1. Bathymetry (Solheim 1984); maximum (heavy wavy line) and minimum (light wavy line) sea ice extent March 1975-1981, maximum (heavy dashed line) sea ice extent September 1977-1981; minimum for September is north of the study area (from Vinje 1984).

Stars indicate locations of current meter arrays discussed in the text.

Arrows point to locations of side-scan sonar profiles shown in figures 5 and 13.

Explanation of Norwegian terminology: renna = trough

banken = bank

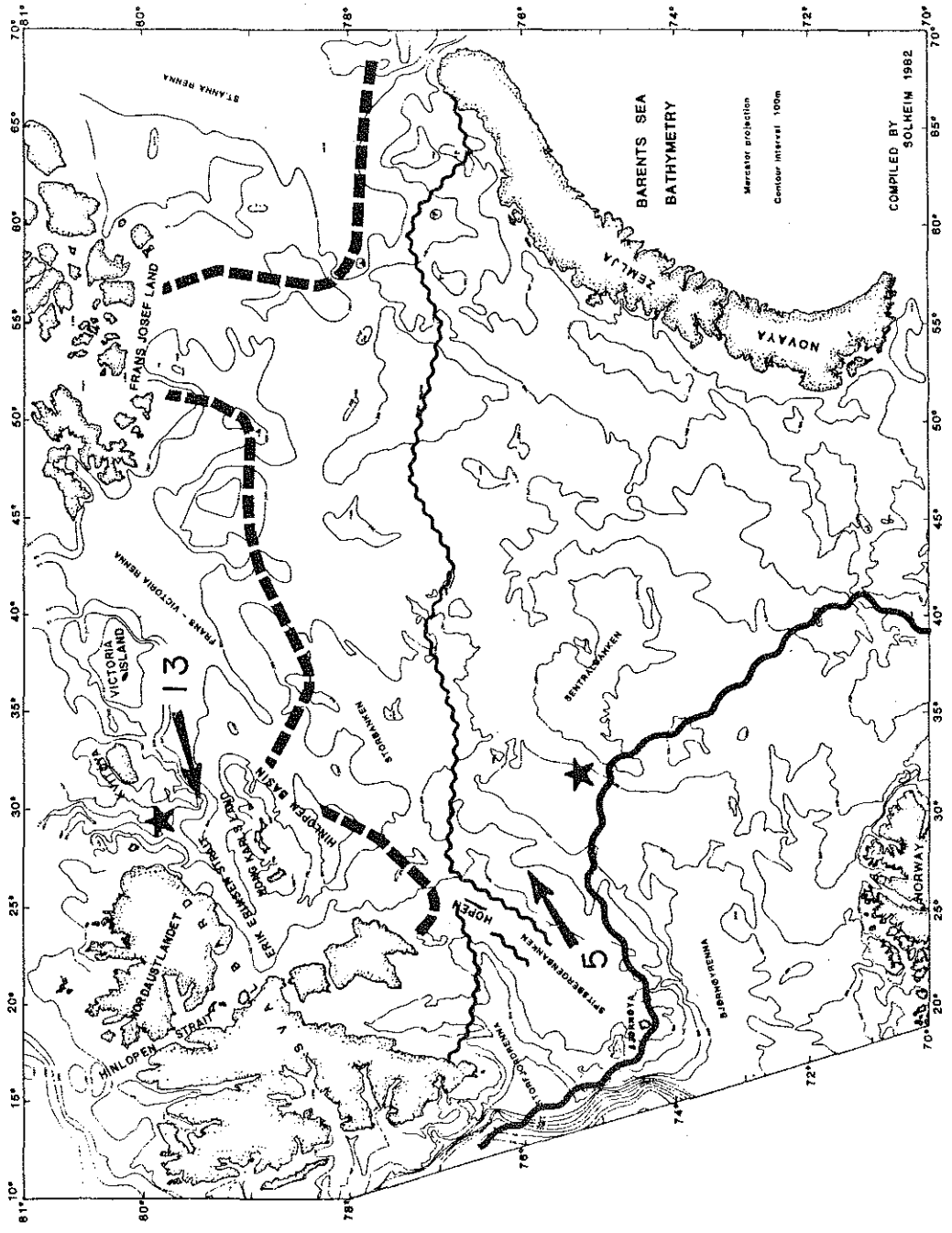
BARENTS SEA
BATHYMETRY
Mercator projection
Contour interval 100m
COMPILED BY
SOLHEIM 1982
FRANS JOSEF LAND
ST.ANNA RENNA
VICTORIA ISLAND
NORDAUSTLANDET
HINLOPEN STRAIT
ERIK EDLANDER STRAIT
MOHN KARL JENSEN
HINLOPEN BASIN
FRANS - VICTORIA RENNA
STORBANKEN
SENTRALBANKEN
SPITSBERGENBANKEN
HOPEN
BJØRNØYRENNA
NOVAYA ZEMLJA
NORWAY
13
5

Figure 1

Figure 2. Surface sediment map (adapted from from Elverhoi and Solheim 1983a):

Horizontal pattern	Sandy mud
Dot pattern	Sandy gravelly mud
Open circle pattern	Muddy sand and gravel
Gravel pattern	Gravel, gravelly sand, sandy gravel and sand

Surface sediment samples with greater than 2% gravel marked with open hexagon, samples with greater than 10% sand (calculated from gravel-free sediment) marked with an asterisk, (fine-grained samples shown by dot). Regions deeper than 200m with coarse surface sediment discussed in the text (A, B, C, D, E).

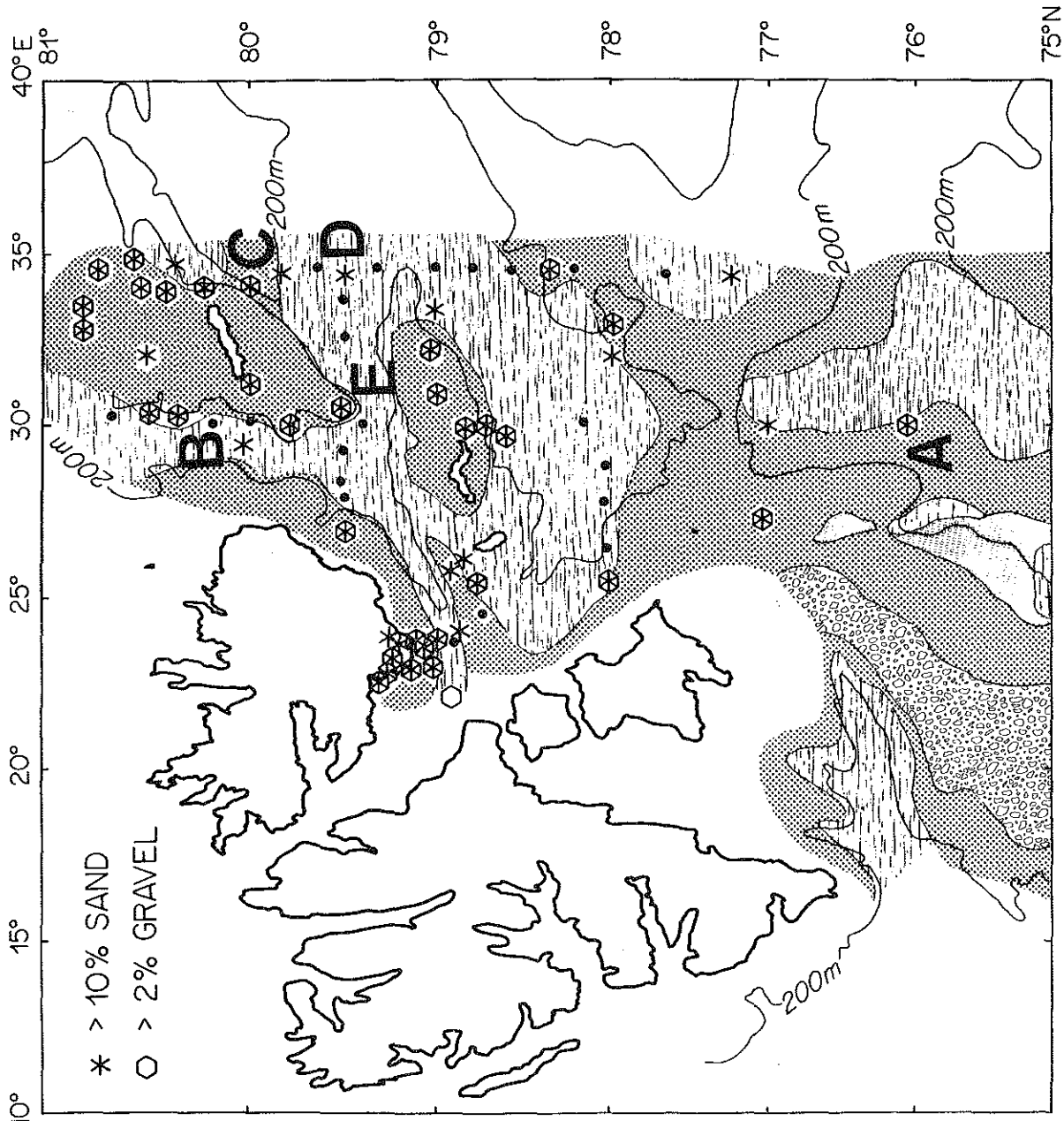
40°E
81°
80°
79°
78°
77°
76°
75°N
10°
15°
20°
25°
30°
35°
200m
A
B
C
D
E
* > 10% SAND
○ > 2% GRAVEL

Figure 2

material reflects a different bedrock source, indicating that significant transport has occurred (Wright 1974). Surface sediment texture along the northeastern coast of Norway similarly has been attributed to winnowing and redeposition of glacial sediments by a combination of mean currents and bottom currents driven by wind waves, internal waves, tides (e.g. Vorren at al. 1978, Holtedahl 1981, Holtedahl and Bjerkli 1982, Vorren et al. 1983).

The objective of this paper is to explain the distribution of surface sediment texture of the northern Barents Sea; data on hydrography, suspended sediment distribution, and ice rafting is used to determine the relative importance of primary deposition and redistribution processes. The distribution of Holocene sediments results from reworking of late Wisconsin glaciomarine sediments by wind generated waves and permanent currents. The modern sedimentary environment of the northern Barents Sea is a useful analog for interpretation of post-glacial sediment distribution of lower latitude continental shelves such as the Gulf of Maine and the Labrador and Alaskan shelves.

Geologic Setting:

The extent of the last glaciation in the Barents Sea is controversial (e.g. Grosswald 1980, Denton and Hughes 1980, Boulton et al. 1982). According to Solheim and Kristoffersen (in press), the Barents Sea probably was glaciated several times during the late Cenozoic. Data on glacial rebound from Kong Karls Land imply that at least the northern part of the Barents Sea was glaciated during late

Wisconsin (Salvigson 1981). Recent marine geological data indicate an extensive ice sheet in the Barents Sea during the late Wisconsin (Elverhoi and Solheim 1983a, Vorren and Kristoffersen, in prep.). Evidence for a Barents Sea ice sheet includes a blue-gray basal till which occurs above bedrock over much of the Barents Sea (Dibner 1970, Elverhoi and Solheim 1983a). The thickness of this unit is not well known in the northern Barents Sea. Basal till has not been found on banks shallower than 100m, perhaps due to post-depositional erosion. Seismic investigations indicate that the basal till is probably less than 5m thick in water depths less than 300m and is less than 15m thick in deeper basins (Elverhoi and Solheim 1983a). Sediment cores which could more precisely determine the thickness of the unit are difficult to obtain; the till contains a large amount of gravel and is so stiff and overconsolidated that it is difficult to sample.

The last deglaciation of the Barents Sea probably occurred in stages. Two steps in the deglaciation have been reconstructed from ice-marginal end moraines and glaciomarine sediments at 250-300m and 150-200m water depths (Elverhoi and Solheim 1983a). Glaciomarine deposits are thickest (15-20m) in water depths greater than 300m, and are only 1-3m thick in shallower water. They are soft, gray, have a cold water foraminiferal fauna, and have a large number of dropstones. On high resolution seismic profiles the surface of the late Wisconsin glaciomarine and till sequences is rough, perhaps partly due to ice gouging (Elverhoi and Solheim 1983a). Iceberg plough marks are observed at water depths to 250m on side-scan sonar records (Solheim in press). The icebergs which reworked these

sediments must have had a draft of 300-350m since raised shorelines (Salvigsen 1981) indicate that much of the Barents Sea was 50-100m deeper when these sediments were deposited (approximately 10,000yrBP, Elverhoi and Solheim 1983a). The disintegrating Barents ice sheet may have been the source for the large icebergs.

Sedimentary processes were radically altered during the early Holocene. Water depth decreased rapidly due to post-glacial isostatic rebound (Salvigsen 1981), while iceberg activity decreased with disappearance of the large ice sheet. Circulation was altered as northward migration of the Polar Front replaced cold Arctic water with warm, saline Atlantic water (Ruddiman and McIntyre 1973, Kellog 1976, Vorren et al. 1978, Forsberg 1983). Olive-green Holocene sediments began to be deposited in deep basins (figure 2) around 10,000yrBP in response to these environmental changes (Vorren et al. 1978, Holtedahl and Bjerkli 1982). Holocene sediments are 0.1 to 1.0m thick in deep basins, have a warmer water fauna, contain occasional dropstones (especially in the northern Barents Sea) and are in gradational contact with underlying glaciomarine sediments (Elverhoi and Solheim 1983). Sedimentation rates average 3-5cm/1000yr (Klenova 1960, Elverhoi and Solheim 1983a). If the only significant source for these recent deposits is reworking of shallow water sediments as suggested by Klenova (1960), Emelyanov et al. (1971), Wright (1974), Elverhoi and Solheim (1983a), and Forsberg (1983), then large quantities of fine-grained material must have been redistributed in the modern Barents Sea.

MATERIALS AND METHODS

Surface sediment distribution discussed in this paper is based on textural analysis of 80 large diameter (11cm) gravity cores and a surface sediment map compiled by Elverhoi and Solheim (1983b) (figure 2). Their data set for the map includes surface sediment samples and seismic profiles collected on our cruises to the Barents Sea in 1980-1983. Core tops were sampled in order to get 100g of sediment, excluding stones. In very stoney areas this necessitated sampling the upper 5cm, but usually the upper 3cm sufficed. Samples were separated into gravel (greater than 2mm), sand (2mm-0.063mm), and silt plus clay (less than .063mm) (appendix B). Side-scan sonar profiles (Klein 50kHz towfish, 600m swath width) coupled with 3.5kHz profiling provided local information on sea-floor morphology and sediment type (figure 1). Analysis of these sonographs is discussed more fully by Solheim and Pfirman (in press, chapter 3) and Solheim (in prep.).

Near-bottom suspended sediment distribution was mapped from 161 transmissometer profiles obtained in 1980, 1981, and 1982. A Montedero-Whitney TMU sensor was used to measure light transmission (white light source, one meter folded path length), light scattering, water temperature, and pressure. Measurements of water turbidity generally show a near-surface maximum, a subsurface minimum and a near-bottom increase in suspended particles (figure 3). The near-surface maximum is usually caused by biologic material (appendix C). Only the bottom nepheloid layer consisting of suspended mineral grains and some biologic material is discussed in this study. Water

Figure 3. Profile of excess turbidity showing high near-surface concentrations of suspended material due to biologic activity, a clear water minimum near 150m, and a deep water increase in suspended material (bottom nepheloid layer).

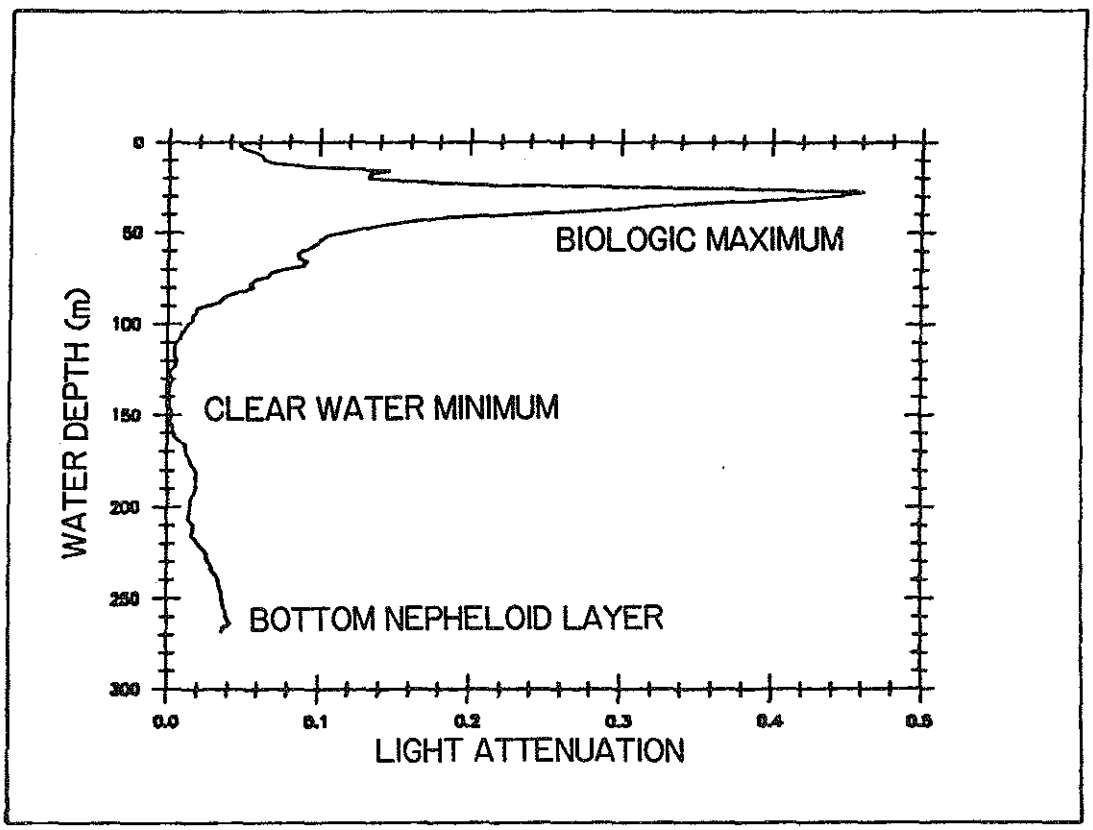
WATER DEPTH (m)
0
50
100
150
200
250
300
0.0
0.1
0.2
0.3
0.4
0.5
LIGHT ATTENUATION
BIOLOGIC MAXIMUM
CLEAR WATER MINIMUM
BOTTOM NEPHELOID LAYER

Figure 3

samples were obtained from 115 stations at 3 or 4 depths (often including surface, biologic maximum at 20-30m, clear water depth, 10 meters above bottom, and 1 meter above bottom). The water samples were filtered on paired 0.45μm Millipore filters. Turbidity measurements were calibrated by the deep-water suspended sediment concentrations from filtered water samples, and they are reported in concentration units (mg/l) (appendix C). Because of instrument drift, light scattering for all three years is reported relative to the clear-water value for that particular station, and it thus represents local "excess turbidity" (appendix C). Excess turbidity yields a qualitative understanding of the strength of the local near-bottom nepheloid layer, assuming that all particles in suspension are mineralogic and have similar grain size (Moody and Butman in prep., Baker and Lavelle in press, appendix C). Although an integrated value for the whole bottom layer (e.g., Eittreim et al. 1976) might be more meaningful, this was not calculated here; the station profile often stopped short of the sea floor and thus did not sample the entire bottom nepheloid layer. For the same reason, excess turbidity values probably underestimate near-bottom suspended sediments.

Information on modern circulation and current shear is required in order to relate the near-bottom suspended sediment distibution to the modern hydrographic regime. Most of the regional suspended matter data was collected in 1980 when the conductivity sensor failed on the Montedero-Whitney unit. Salinity, and therefore density and geostrophic shear, could not be calculated for this data. However, hydrographic data were collected by the Institute for Marine Research

in Bergen in the same region in 1981. Since the temperature distribution for 1981 is similar to that observed in 1980 (chapter 1), the 1981 data were used for analysis of current shear in the study area. Geostrophic velocity calculations are based on a reference level at 125m and dynamic height calculated from the density distribution (chapter 1).

Surface marine observations of wave periods and height for sea and swell in the Barents Sea were obtained from the National Climatic Center in order to estimate the effect of sea-surface conditions on sea-floor reworking. The data base includes observations from 1860 to 1974. Data is presented in raw numbers of observations over a 10° longitude by 5° latitude region for four quadrants of the Barents Sea (Marsden squares 286 (20-30°E) and 285 (30-40°E)).

RESULTS AND ANALYSIS

Surface sediment texture is generally coarse-grained in water depths less than 200m and fine-grained in deeper basins (figure 2). This basic pattern is examined first to determine which processes cause the apparent depth-dependence of modern depositional patterns. This is followed by a discussion of the origin of local deposits of coarse sediments in deep basins.

Shallow-water deposits

Seventy-five percent of the 32 surface sediment samples below

200m water depth have less than 1% gravel (figures 2 and 4). The proportion of sand (calculated from gravel-free sediment) similarly decreases with depth. All 24 stations shallower than 125m have greater than 10% sand and 60% of stations deeper than 200m have less than 10% sand (figure 4). The surface-sediment textural discontinuity may occur because coarse sediments are presently deposited above 200m or because fine sediments are deposited below 200m. Potential origins of coarse sediment textures are deposition from ice rafting, iceberg turbation of the surface layer (by mixing up deeper coarse material), or winnowing of fines from surface sediments. Possible recent sources for fine sediments are rivers and glaciers, or sediments resuspended and transported from other surface sediments.

Ice rafting:

Ice rafting must occur preferentially above 200m to cause the textual discontinuity, however there is no reason for deposition of ice-rafted material to be depth-dependent. Sea-ice transport in the Barents Sea is mainly from northeast to southwest via the East Spitsbergen and Persey Currents (Vinje 1984). The maximum southward extent of modern sea-ice occurs in March and the minimum in September (figure 1, Vinje 1984). Coarse beach sediments, shells, and windblown material are observed in samples melted from dirty sea-ice. Coastal material incorporated in sea-ice indicates that it was fast-ice, and is probably from the shores of the Svalbard Archipelago and the Siberian islands. If ice-rafting by sea-ice is important, deposition should occur to some degree over the entire northern Barents Sea since

Figure 4. Surface sediment texture plotted vs. station water depth. Small A, B, C, D, E's represent samples obtained from locations marked in figure 2.

A. Scatter plot of weight percent gravel vs. water depth for surface sediment samples.

B. Scatter plot of weight percent sand (calculated on a gravel-free basis) vs. water depth for surface sediment samples.

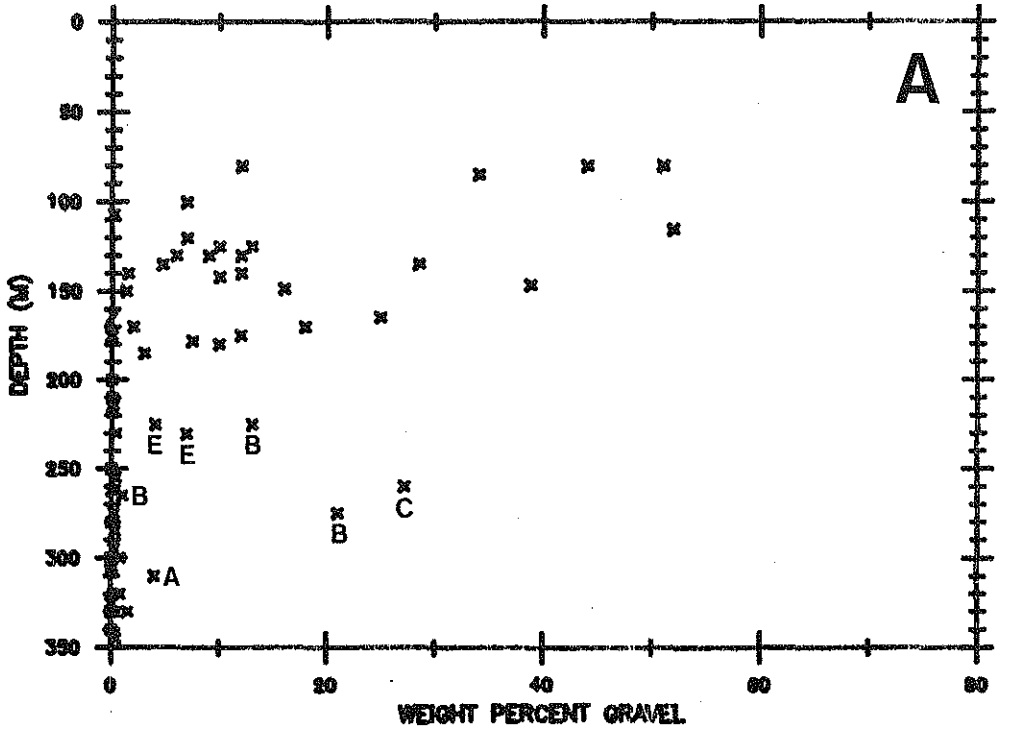

SURFACE SEDIMENTS

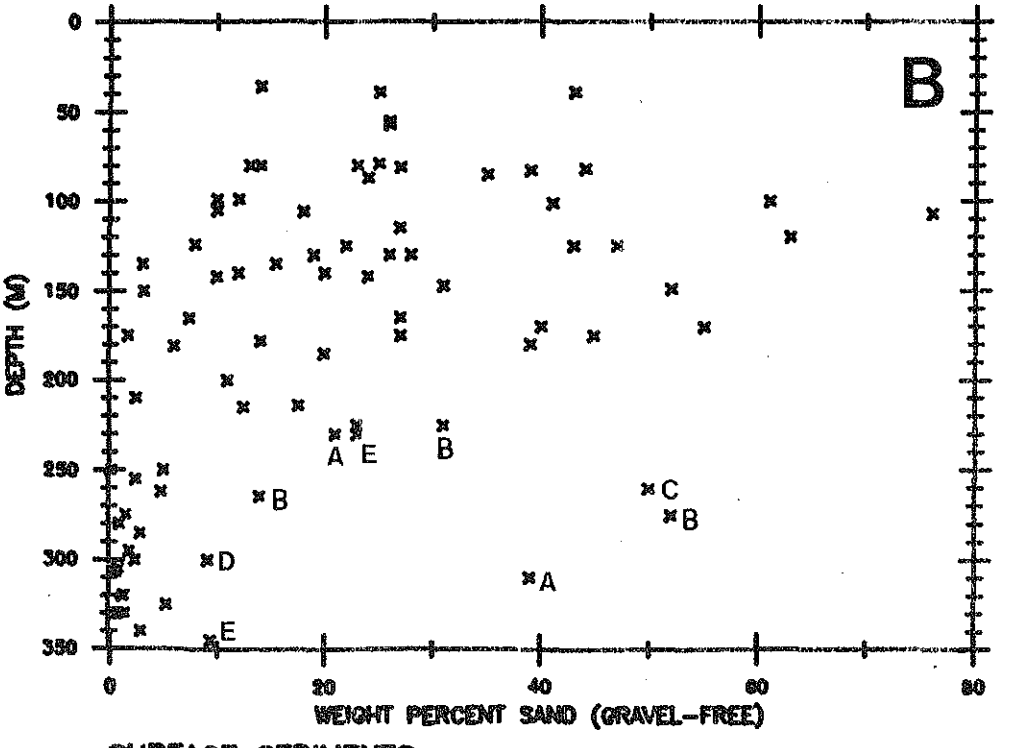

SURFACE SEDIMENTS

Figure 4

it is covered by sea-ice during the winter (figure 1). However, sediments in deep northern basins (close to island sources) have low contents of sand and gravel, indicating that sediments rafted by sea-ice either are diluted by rapidly accumulating deep basin sediments or are not significant. Since sedimentation rates are only a few cm/1000yr (Klenova at al. 1960, Elverhoi and Solheim 1983a), ice rafting does not appear to be a reasonable mechanism for deposition of coarse material in shallow regions of the Barents Sea (see also Emelyanov et al. 1971, Forsberg 1983).

Ice gouging:

If surface sediments are reworked by icebergs down to 200m surface sediment texture could be coarsened because: 1) resuspension of fine sediments into the water column enhances redistribution of surface sediments by bottom currents; 2) bottom roughness increases, thus increasing bottom-current shear stress and encouraging winnowing; and 3) homogenization of the surface layer forms an iceberg turbate (Vorren et al. 1978) with a different character than originally deposited. Eroded plough marks are observed on the sea-floor up to 250m on side-scan profiles (figure 5 and Solheim in press) and possibly extend to deeper water depths. However, these gouges are thought to be ancient because only 120m thick icebergs are presently available in the Barents Sea (Elverhoi and Solheim 1983a). Recent iceberg ploughing of the upper 5m of the sea floor is extensive in the Barents Sea in water depths less than 100m (chapter 3, Solheim in prep.). Reworking of the sea-floor by modern ice gouging may explain

Figure 5A. Side-scan sonar sonographs (50kHz towfish, 600m swath width, orthogonally rectified) obtained near Polar Front, east side of Spitsbergen Bank. Profile shows difference in acoustic reflectivity between winnowed plough mark berms (dark) and probably finer material (light) infilling the ice gouges.

B. 3.5kHz profile. Surface relief is presently less than 3m over the reworked ice gouges (see figure 1 for location).

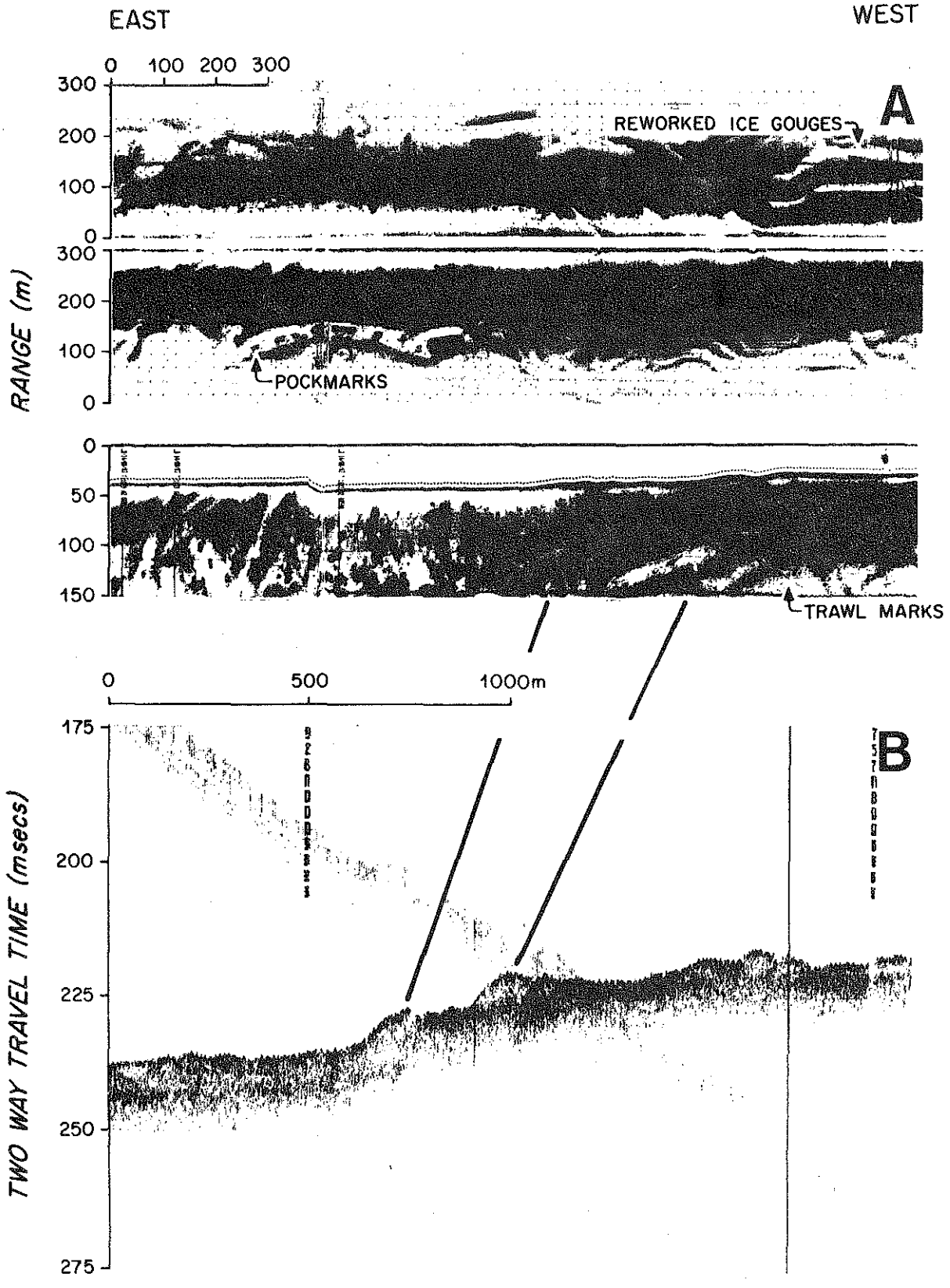
EAST
WEST
0 100 200 300
300
200
100
0
REWORKED ICE GOUGES
A
RANGE (m)
POCKMARKS
0
50
100
150
TRAWL MARKS
0 500 1000m
175
200
225
250
275
TWO WAY TRAVEL TIME (msecs)
B

Figure 5

the coarse sediments occurring above 110m, but does not explain the textural change at 200m.

Sediment redistribution:

Winnowing of fine-grained sediments from shallow banks by bottom currents appears the most likely explanation for the surface sediment texture of the Barents Sea. This winnowing could have occurred when the surface sediments were initially exposed to marine conditions as the Barents Ice Sheet disintegrated. Since detailed wave, tide, and current information are not available for this region, the driving mechanism for the bottom currents cannot be precisely stated. Erosion of bottom sediments depends on bottom shear stress, size and cohesiveness of the bottom sediments, bed roughness, and biologic activity in the surface sediments. Sediment transport depends on the duration, speed, and direction of the erosional event. Conditions required for erosion of non-cohesive sediments finer than 63μm under oscillating and steady currents are fairly well defined (e.g. Madsen and Grant 1976) and are used in this study to determine where reworking of the sea-floor by waves and currents is likely to occur. Ice gouging causes large variations in the sea floor roughness, but bed roughness is considered here to be of the same order as the sediment grains because bottom photographs generally show a smooth sea-floor with no bedforms.

Location and velocity of permanent currents is based on the late summer water-mass distribution and calculations of current shear for 1981 (chapter 1). In general, northern Barents Sea circulation is in

the form of a cyclonic gyre (figure 6). The water mass structure is dominated by warm deep Atlantic water flowing north and east and cold shallow Arctic water flowing to the south and west; the region of intersection is called the Polar Front. Atlantic water enters the southern Barents Sea through the Barents Trough and flows northeastward at 10cm/sec (figure 7 and Ellertsen et al. 1981) along the west side of Storbanken, possibly exiting the Barents Sea west of Frans Josef Land (figure 6). Atlantic water also enters the Barents Sea between the northern islands, from a branch of the Arctic extension of the West Spitsbergen current (figure 6). Cold, southeasterly flowing Arctic water intersects the east Spitsbergen coast south of Kong Karls Land. Here it forms a well developed southerly current, the Hopen-Bjornoya Current, which has surface velocities of several knots along the eastern and southern flanks of Spitsbergenbanken (figures 7, 8 and 9, Novitskiy 1961). Cooling of Atlantic water east of Spitsbergenbanken results in formation of a cold deep water mass (chapter 1) which flows southward with an estimated velocity of 15cm/sec along the deep eastern slope of Spitsbergenbanken (figures 7 and 8).

For a steady current, velocity at 1m above bottom (U_{1m}) must be 42cm/sec for resuspension of less than 63μm sediments in the absence of bedforms (23cm/sec for a physical roughness of 3cm - Butman and Moody 1984):

$$u_{1m} = (u^*/k) \ln (z/z_o)$$

where: u_* = shear velocity
k = von Karmen's constant (0.4)
z = distance above bottom (=1m)
z_o = roughness length scale (taken here to be proportional to the grain diameter (d(cm)): $z_o = d/30$)

Figure 6. Cartoon of circulation based on water mass distribution analysis and volume transport calculated with a reference level at 125m (chapter 1). At = Atlantic water
Ar = Arctic water

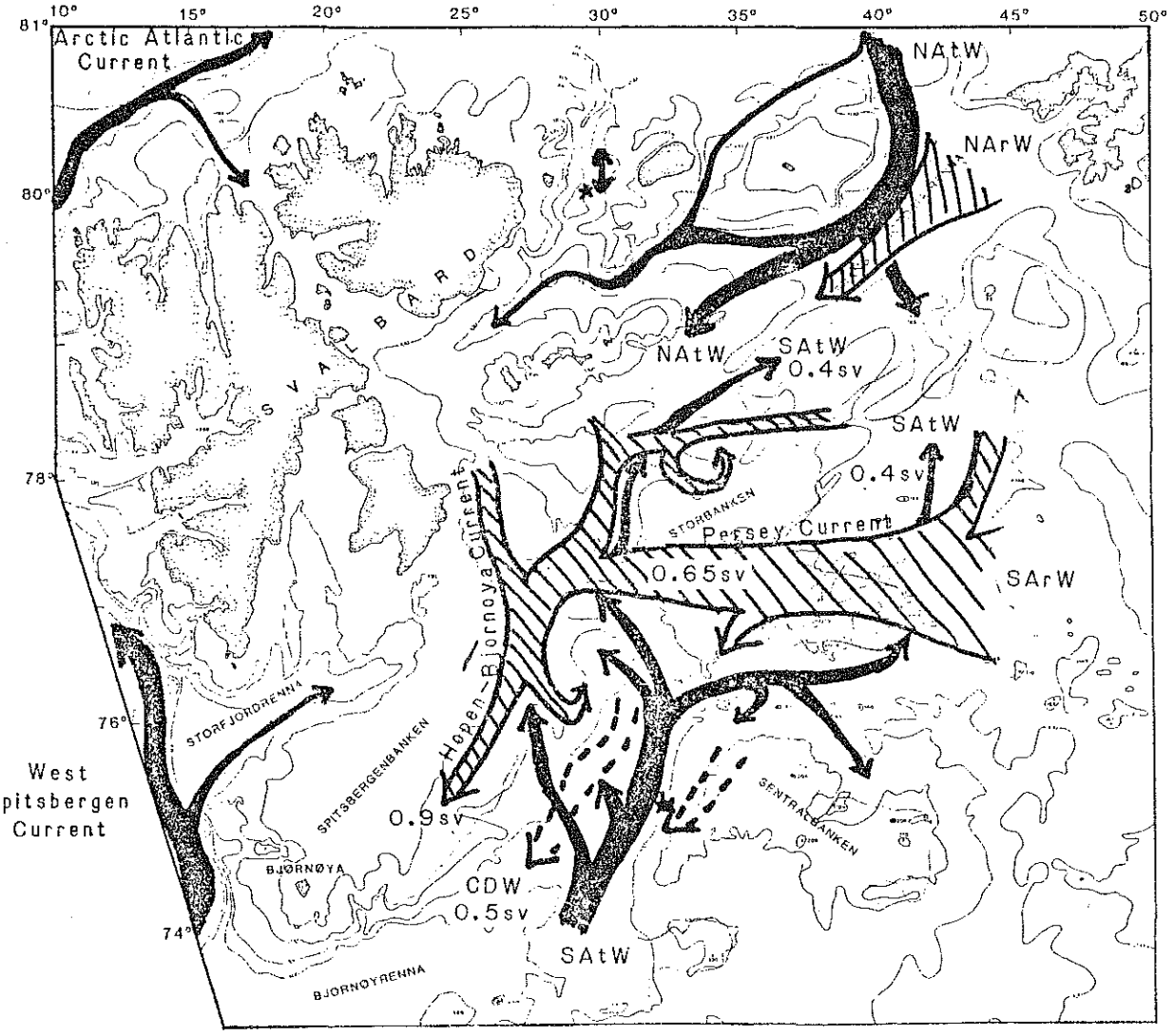
10°
15°
20°
25°
30°
35°
40°
45°
50°
81°
80°
78°
76°
74°
Arctic Atlantic Current
NAtW
NArW
SVALBARD
NAtW
SAtW
0.4sv
SAtW
0.4sv
STORBANKEN
Persey Current
0.65sv
SArW
Hopen-Bjornoya Current
West Spitsbergen Current
STORFJORDRENNA
SPITSBERGENBANKEN
0.9sv
BJØRNØYA
CDW
0.5sv
SENTRALBANKEN
SAtW
BJORNØYRENNA

Figure 6

Figure 7. Temperature (A) and geostrophic velocity (B) calculated for hydrographic transect at 75° 30'N. Hydrographic data courtesy of the Institute for Marine Research in Bergen, Norway. Negative values of velocity indicate southward direction.

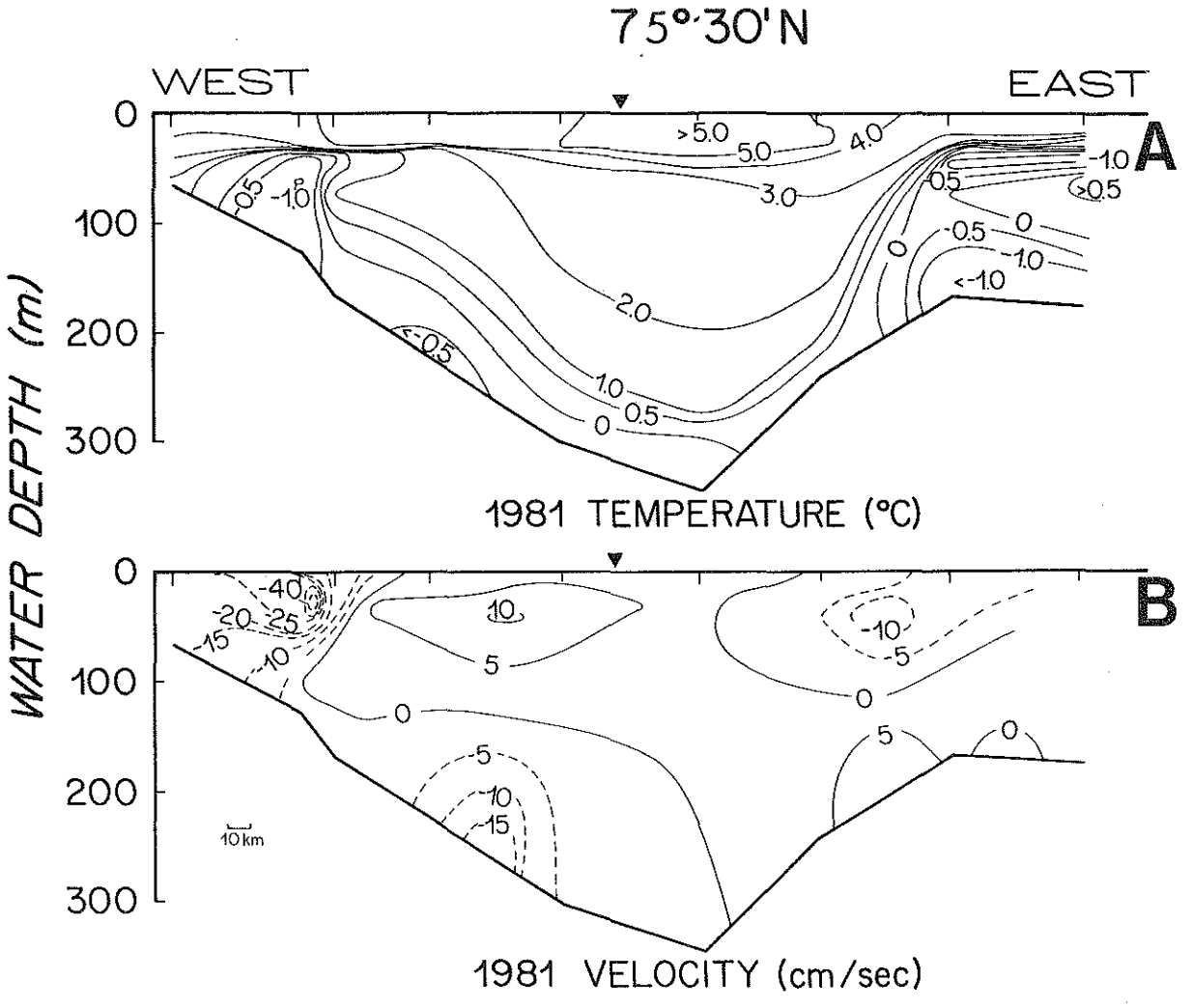
75°30'N
WEST
EAST
WATER DEPTH (m)
0
100
200
300
>5.0
5.0
4.0
3.0
2.0
1.0
0.5
0
-0.5
-1.0
<-1.0
<-0.5
>0.5
A
1981 TEMPERATURE (°C)
-40
-20
-25
-15
-10
-5
10
5
-10
B
10 km
1981 VELOCITY (cm/sec)

Figure 7

Figure 8. Water column observations obtained at 77°N.

A. Suspended matter observations obtained in 1980. Contours are of near-bottom excess turbidity and numbers in italics are measured SPM concentrations.

B. Water temperature (1980).

C. Temperature (light dotted lines) and geostrophic velocity (heavy dashed and solid lines) calculated for hydrographic transect (1981) from data courtesy of the Institute for Marine Research in Bergen, Norway. Negative values of velocity indicate southward direction.

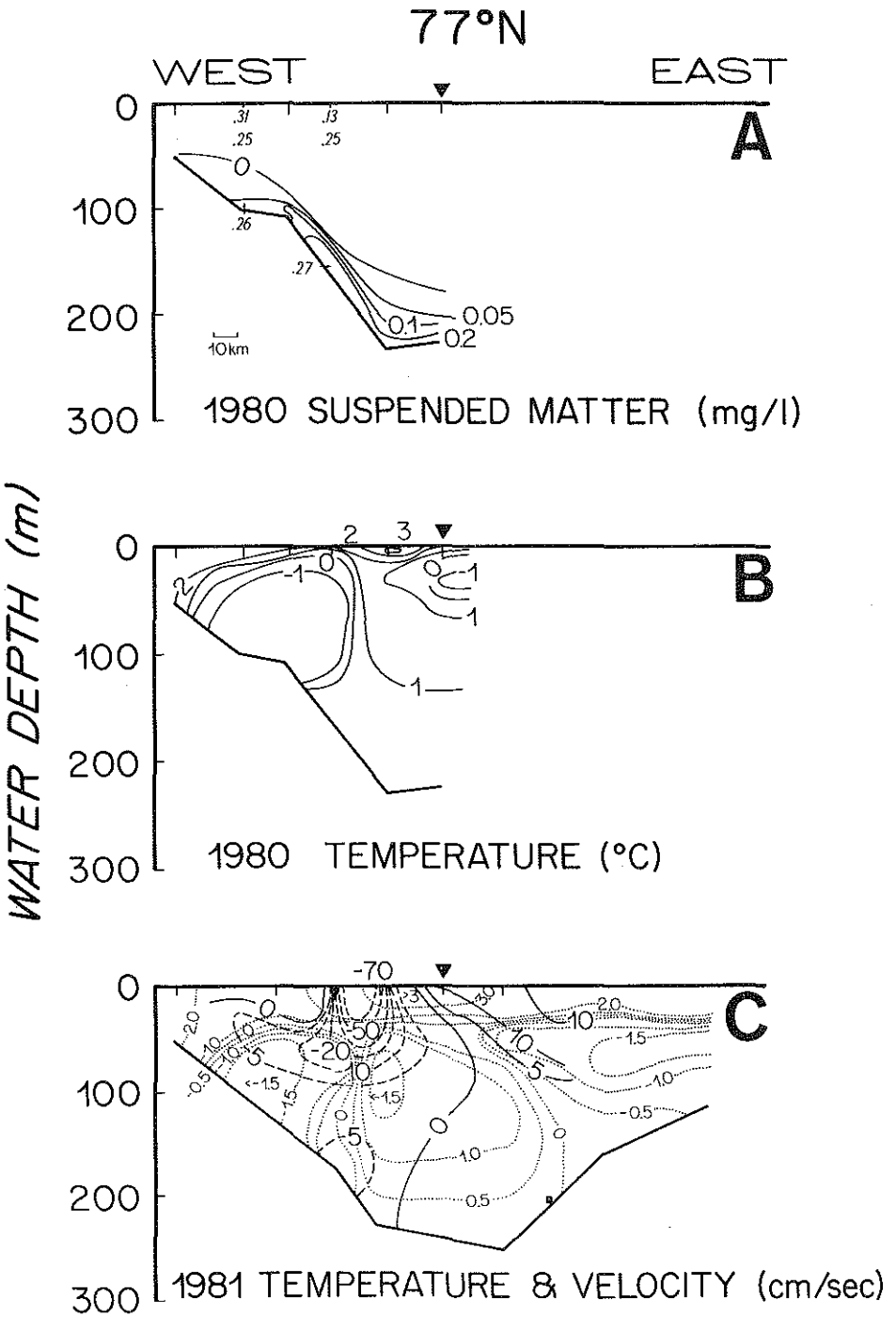
77°N
WEST
EAST
A
0
100
200
300
.31
.25
.13
.25
0
.26
.27
0.1
0.05
0.2
10km
1980 SUSPENDED MATTER (mg/l)
WATER DEPTH (m)
B
2
3
-1
0
1
1980 TEMPERATURE (°C)
-70
C
-50
-20
10
5
1.0
0.5
1981 TEMPERATURE & VELOCITY (cm/sec)

Figure 8

Figure 9. Water column observations obtained at 78°N (for details on data presentation see caption for figure 8)

A. Near-bottom excess turbidity and SPM concentration (1980).

B. Temperature (1980).

C. Temperature and geostrophic velocity calculated for hydrographic transect (1981) at same latitude from data courtesy of the Institute for Marine Research in Bergen, Norway. Negative values of velocity indicate southward current direction.

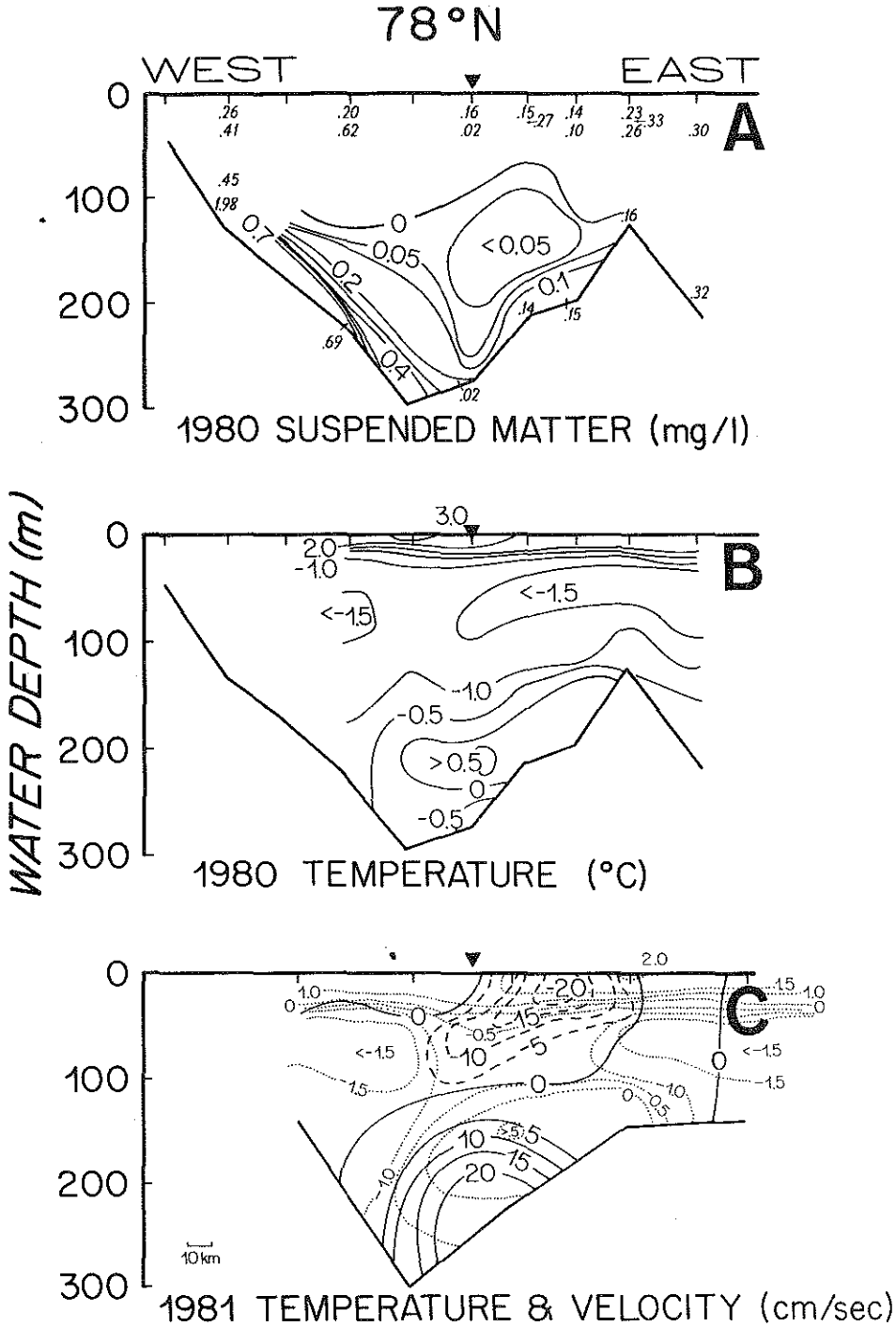
78°N
WEST
EAST
A
0
100
200
300
.26 .41
.20 .62
.16 .02
.15 .27
.14 .10
.23 .26
.33 .30
.45 .98
0.7
0
0.05
<0.05
0.2
0.1
.16
.14
.15
.32
.69
0.4
.02
1980 SUSPENDED MATTER (mg/l)
WATER DEPTH (m)
B
3.0
2.0
-1.0
<-1.5
<-1.5
-1.0
-0.5
>0.5
0
-0.5
1980 TEMPERATURE (°C)
C
2.0
1.0
0
-20
-15
-10
-5
-0.5
0
<-1.5
1.5
0
0.5
1.0
10
5
15
20
10km
1981 TEMPERATURE & VELOCITY (cm/sec)

Figure 9

However, the potential for sediment reworking may be substantially modified by biologic activity (either enhancing or inhibiting erosion). In addition, larger scale surface roughness (such as iceberg gouges and dropstones) increases the potential for local erosion of surface sediments. In situ flume experiments have shown that sediments are eroded at U_{1m} of 7.5 - 22 cm/sec (Young and Southard 1978). Geostrophic shear calculations suggest a range of velocity for mean currents from 5-15cm/sec. Therefore mean velocities of permanent currents may be high enough to resuspend fine-grained sediment. The Hopen-Bjornoya Current which has velocities exceeding 40cm/sec (figures 7 and 8). This current could easily resuspend and transport sediments southwards along eastern Spitsbergenbanken.

Tidal currents in the Barents Sea are thought to have higher velocites than permanent currents (other than the Hopen-Bjornoya Current, Tantsiura 1959). However, only two vertical current meters arrays have been deployed in the northern Barents Sea which have records suitable for analysis of tidal currents. Both current meters arrays are located in deep basins (northern array - 255m water depth (Aagaard et al. 1984), southern array - 308m water depth (Ellertsen et al. 1981, located on figure 1) and both recorded velocities greater than 15cm/sec in the upper 75m (Ellertsen et al. 1981, Aagaard et al. 1984). Tidal current velocity decreases with depth; the current meter located 5m above bottom recorded velocities of less than 7cm/sec at the northern current meter (Aagaard et al. 1984) and 10-15cm/sec at the southern current meter (Ellertsen et al. 1981). These near-bottom velocities may be high enough to resuspend the less than 63μm fraction. Although no current meter data exist over the shallow banks, it is probable that tidal currents are strong enough to resuspend shallow water sediments (based on the velocity structure of the two current meter arrays).

Surface waves generated by storms can cause resuspension of bottom sediments with much lower velocities since they cause oscillitory near-bottom flows (Madsen and Grant 1976). Orbital velocity decreases with depth and is linearly related to the amplitude and period of the surface wave. In order to determine the near-bottom velocity (U_{bm}) and the maximum excursion amplitude under a wave (A_{bm}) at a certain water depth (h), the wave period (T), length (L), and amplitude (a) must be known.

$$U_{bm} = A_{bm}\omega = a\omega/(\sinh(k*h)$$

where: $k=2\pi/L$

$L=1.56*T^2$ (deep water waves)

$\omega=2\pi/T$

These values may then be used to determine the wave Reynolds number (R_e), the wave friction factor (f_w), and therefore the bottom shear stress (τ_{bm}) and the bottom shear velocity (u^*):

$$f_w=2/(R_e)^{1/2} \text{ (for low } R_e)$$
$$R_e=U_{bm}A_{bm}/\nu$$
$$\tau_{bm}= 1/2\ \rho f_w U_{bm}^2$$
$$u^* = (\tau_{bm}/\rho)$$

These equations can be rearranged to solve for the the wave amplitude in terms of the wave height, period, and the shear velocity:

$$a = (u^*/\nu^{1/2})\sinh(kh) \ / \ \omega^2$$

This equation can be used to determine the critical wave necessary to resuspend surface sediments at various water depths (figure 10) since a bottom shear velocity of 1.3cm/s for oscillating flow is required to erode less than 125μm sediment (assuming cohesionless sediment, surface roughness on the order of the grain diameter, and no superimposed mean flow: Madsen and Grant 1976, Butman and Moody 1984).

Figure 10. Surface marine observations for the Barents Sea. The number of observations from 1860-1974 is contoured for wave amplitude and period. Superimposed on these contours are lines of the critical wave required to erode 63μm material on a flat bed in the absence of of a mean current at water depths labelled in the upper left quadrant

A. Sea

B. Swell

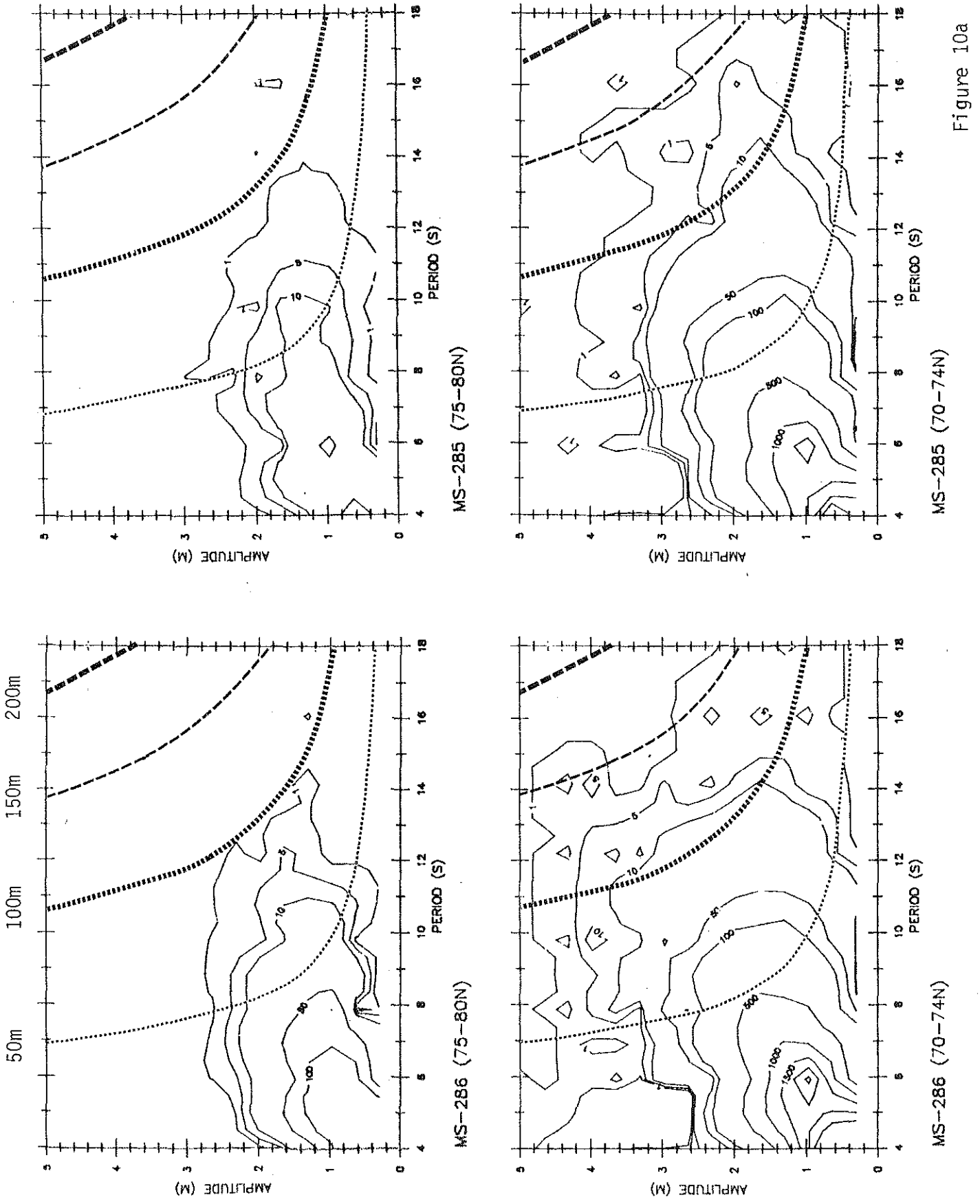
MS-285 (75-80N)
MS-285 (70-74N)
MS-286 (75-80N)
MS-286 (70-74N)
AMPLITUDE (M)
PERIOD (S)
50m
100m
150m
200m

Figure 10a

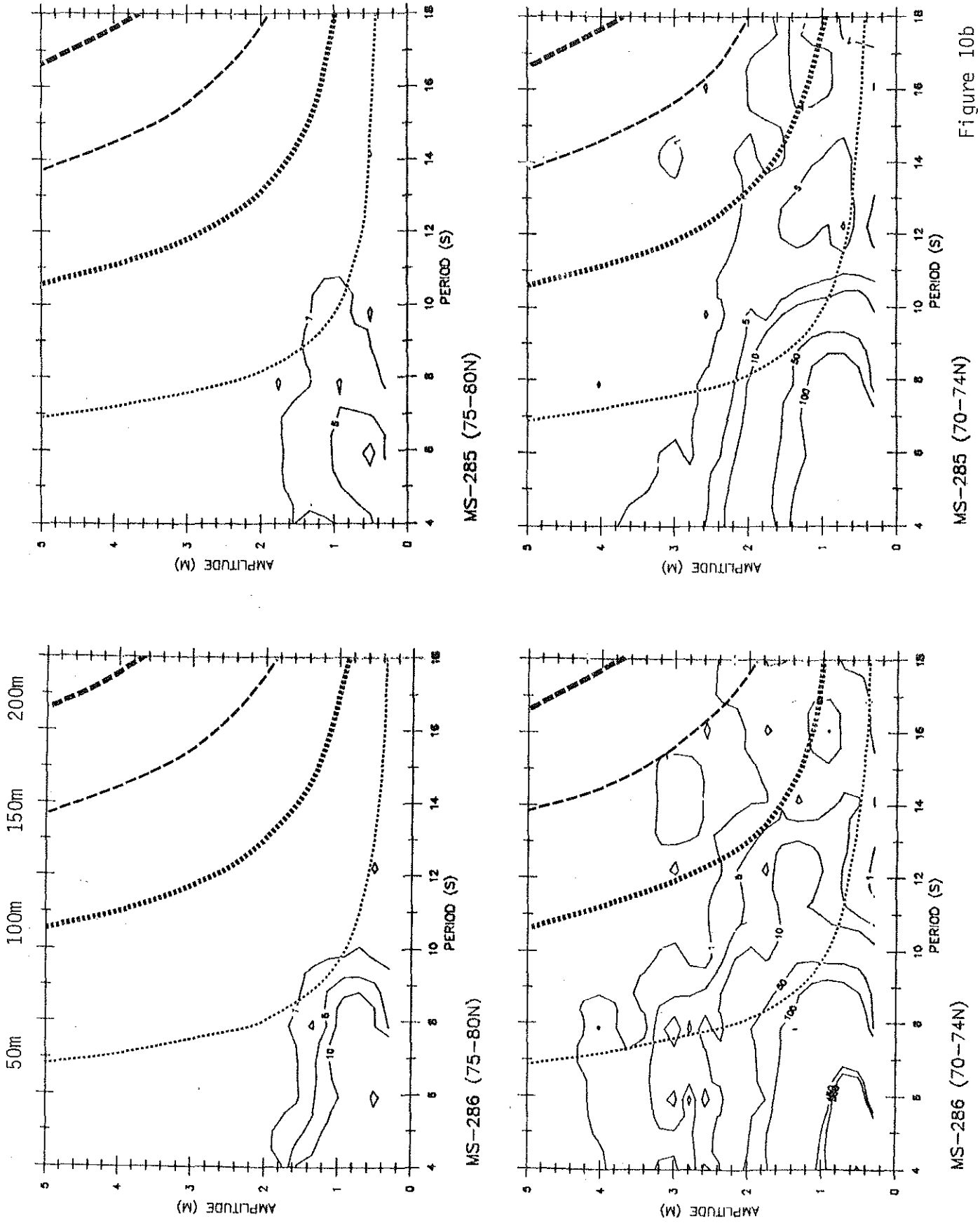
MS-285 (75-80N)
MS-285 (70-74N)
MS-286 (75-80N)
MS-286 (70-74N)
AMPLITUDE (M)
PERIOD (S)
50m
100m
150m
200m

Figure 10b

In order to determine the probability that these critical wave conditions occur in the Barents Sea, shipboard observations of sea surface conditions are plotted against the critical wave requirements (figure 10). The number of shipboard observations are limited in the northern Barents Sea because of sea-ice (figure 1), and sea-ice also dampens surface-wave activity thus decreasing the importance of surface waves in the northern Barents Sea. The data suggest that in the southern Barents Sea the less than 63μm fraction of surface sediments can be resuspended in shallow depths (less than 100m) by fairly small surface waves (2m amplitude), and occasional large storms may resuspend fine sediments to water depths of 150m. Similar open-ocean swell was observed by Sternberg and Larsen (1975) to resuspend bottom sediments at 167m water off the coast of California, suggesting that it is not unreasonable to expect erosion of sediment at these water depths in southern portions of the epicontinental Barents Sea.

If waves are superimposed on mean currents, the shear stress required to erode bottom sediments is markedly decreased (Madsen and Grant 1976). Tidal and mean current velocities discussed above may be high enough to cause bottom resuspension with the aid of a surface wave field.

In summary, the modern surface sediment texture is probably the result of reworking of the upper Wisconsin surface. Ice gouging, wind waves, and tidal currents (?) are the most important for redistribution of sediment in water depths less than 100m and occasional large storms possibly coupled with tidal and mean currents can cause resuspension in water depths of 100-200m. In water depths greater than 200m, mean currents must be stronger to resuspend sediment, since velocity of surface waves and tidal currents decreases with water depth. Transfer of fine-grained material winnowed from shallow regions to the deep basins, and regions of sea-floor reworking are considered in the following section.

Deep-water deposits

Although the surface sediment texture of deep water deposits (deeper than 200m) are generally fine-grained, there are no obvious recent sources for fine-grained material, other than winnowing of fine material from the shallower banks. Siberian river supply of suspended sediments to the Barents Sea is negligible, except in close proximity to the river mouths (Klenova 1960). Sediments suspended in glacial meltwater similarly are of only local importance since they are deposited within 40km of the glacial source (Pfirman, et al. 1982, chapter 4). Transport of sediment in suspension from glaciers or rivers are not likely sources for Holocene material deposited in deep basins.

However, there are several deep water regions with coarse surface sediments. The eastern slope of Spitsbergenbanken is the most

striking (figure 2: area A) and has coarse surface sediments in water depths exceeding 300m. In the northern Barents Sea several locations along the periphery of basins similarly have greater than 10% sand (calculated on a gravel-free basis) and greater than 2% gravel, indicating that winnowing or non-deposition has occurred (figure 2: areas B, C, D, and E). If winnowing is presently occurring, resuspension and advection of fine-grained sediments should be observed as a bottom nepheloid layer in these regions.

Near-bottom excess turbidity distribution delineates regions of modern resuspension and advection of bottom sediments. In general, stations with greater than 0.3mg/l excess turbidity (figure 11) are contained within or on the margins of deep basins where surface sediment texture is fine-grained. A shallow-water exception is the region with high excess turbidity east of Edgeoya (figure 11), which may correspond with the high velocity Hopen-Bjornoya Current (figure 6). Surface sediment texture is coarse in this region.

The strongest deep water bottom nepheloid layers (greater than 0.5mg/l excess turbidity) are located in the narrow strait east of Nordaustlandet (area B: figures 2 and 11), in the basin south of Nordaustlandet, in the narrow strait north of Kong Karls Land (area E: figures 2 and 11), and east of Edgeoya. A hydrographic and excess turbidity cross-section at 77°N shows that stations with greatest excess turbidity correspond with regions of near-bottom current shear (figure 8). This region of current shear is located near 200m water depth along the east coast of Spitsbergenbanken, between cores of Arctic and Atlantic water. At 78°N a similar temperature structure

Figure 11. Regional distribution of excess near-bottom turbidity. Hatched areas are greater than 0.3mg/1, cross-hatched regions have greater than 0.5mg/1 excess turbidity. Nephelometer stations shown by open squares. Open circles show SPM samples from 1m above bottom that are 0.3-0.6mg/1, filled circles are greater than 0.6mg/1. Heavy lines show suspended matter and hydrographic transect locations for figures 7, 8, 9 and 12.

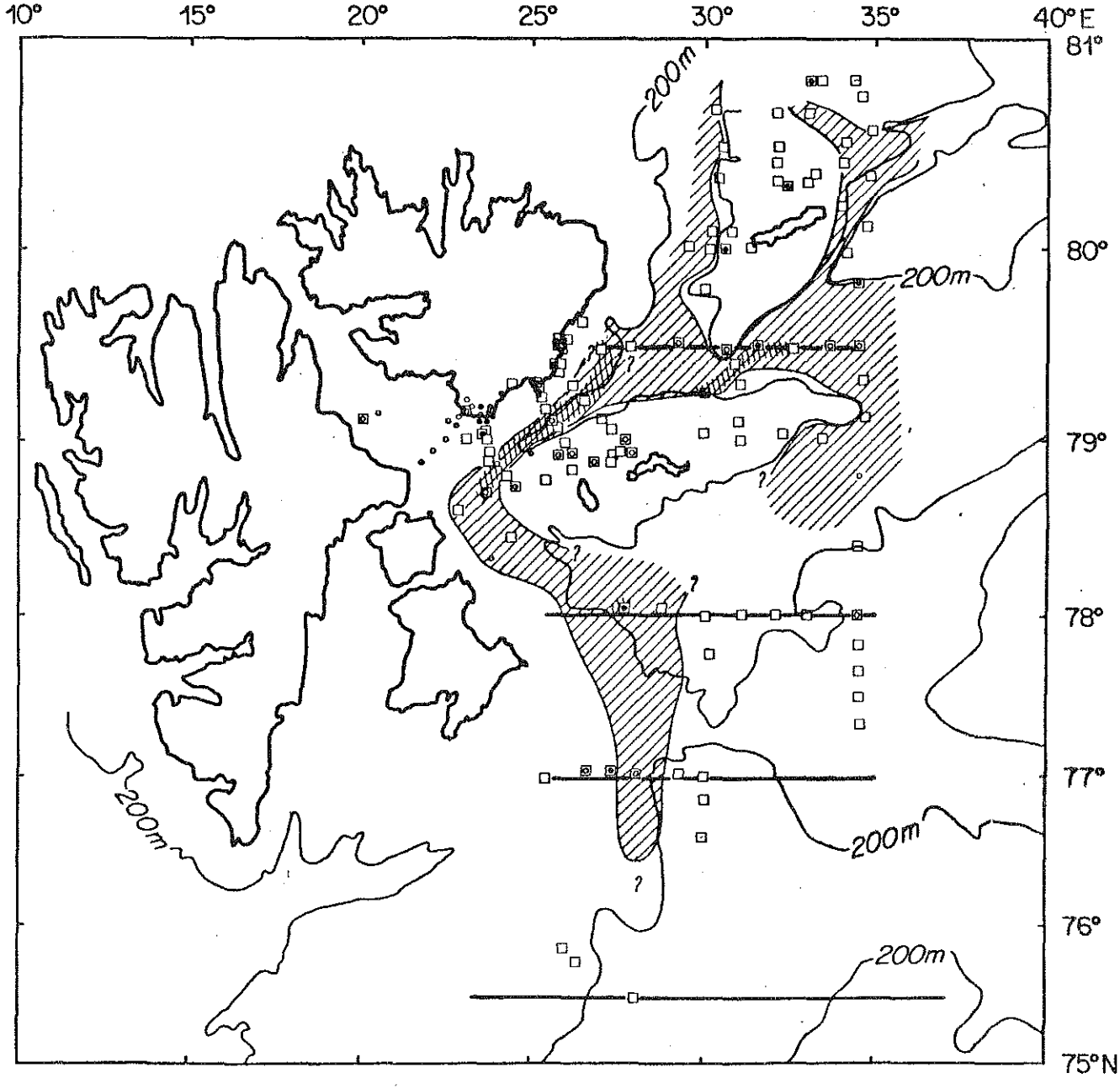
10°
15°
20°
25°
30°
35°
40°E
81°
80°
79°
78°
77°
76°
75°N
200m
200m
200m
200m
200m
?

Figure 11

is observed (figure 9), but the 1981 transect does not extend far enough west to determine if a similar region of current shear occurs (figure 9). On both of these transects turbid water is observed down the western slope, suggesting that fine-grained sediments are also transported to deep basins in a bottom nepheloid layer. High current shear associated with Atlantic water on the 78°N transect (1981), however, does not correspond with an exceptionally strong bottom nepheloid layer (1980) although the water mass structure looks similar both years. Nepheloid layer thickness averages about 30m, corresponding with the Ekman layer thickness (height above sea floor that currents will begin to "feel bottom") of 36m for these latitudes (from Pond and Pickard 1978).

Although suspended matter data is not available further south at 75° 30'N, geostrophic calculations indicate a region of near-bottom current shear at 250m (figure 7). This area was identified earlier as a deep region with notably coarse surface texture (area A, figure 2), suggesting non-deposition or erosion of fine surfical sediment. Influence of bottom current activity near this region is also observed in reworking of ice gouges (figure 5). Berms appear winnowed leaving a reflective deposit (probably of coarse lag material) observed on side-scan sonar profiles, while the gouge troughs are filled in with less reflective (fine-grained) sediment. Elverhoi and Solheim (1983) suggested that sea-floor erosion occurred here because of current intensification associated with the Polar Front (which is actually located shallower, near 100m - Johannessen and Foster 1978). The temperature transect (figure 7) shows that high velocities actually

occur in the cold, modified Atlantic water which flows southwest along the deep eastern slope of Spitsbergenbanken (figure 6 and chapter 1). Current shear on this southern transect is higher than calculated for 77°N, perhaps because additional southward-flowing cold deep water is entrained along the slope.

North of Kong Karls Land at 79° 30'N the highest excess turbidity occurs along the eastern slope of Nordaustlandet (figure 12). A detached nepheloid layer extends eastward from the slope, intruding into the basin east of Nordaustlandet at water depths of 230m.

A region with high excess turbidity is also observed in the eastern part of this transect (area D; figures 2, 11, and 12). High turbidity is probably associated with flow of Atlantic water, although the velocity structure is not known in this region because measurements of salinity are not available. A side-scan sonar profile south of the transect, but through the region of high turbidity, indicates sea-floor deposition controlled by bottom currents. Large sediment waves (5m wavelength) are orientated transverse to current flow, with furrows (10 m across) parallel to the inferred westerly current direction (figures 6 and 13).

DISCUSSION AND CONCLUSIONS

A discontinuitity in the modern surface sediment texture generally is associated with the 200m bathymetric contour (Elverhoi

Figure 12. Water column observations for 79° 30'N (1980).

A. Near-bottom excess turbidity and SPM

B. Temperature

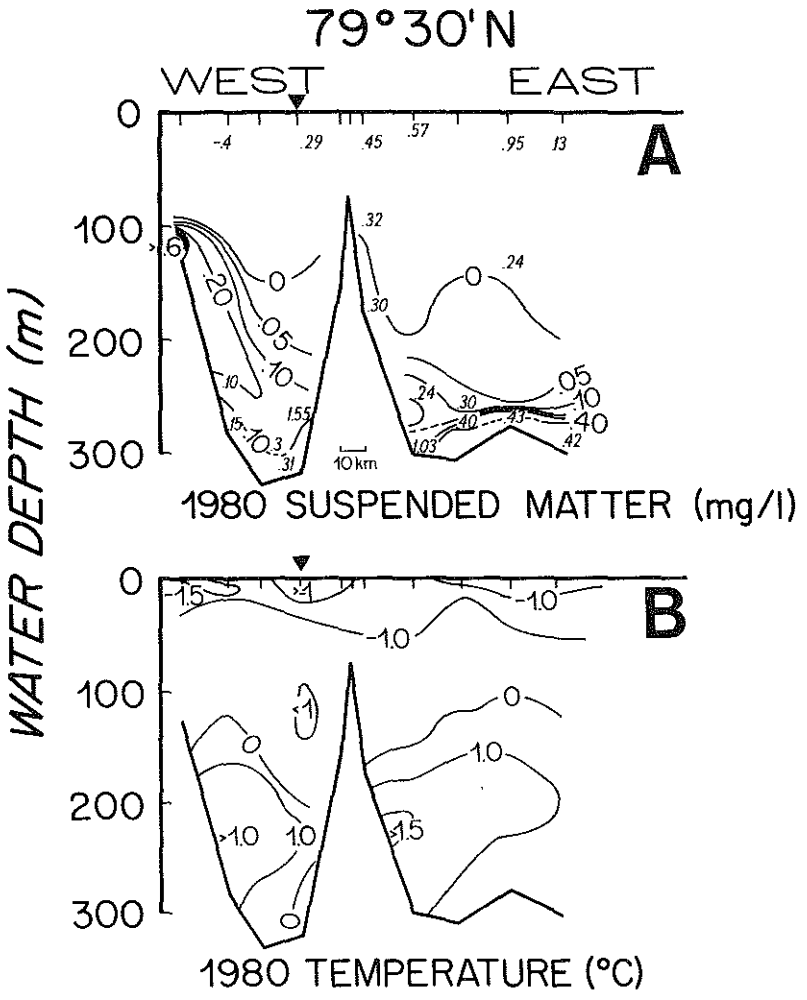
79°30'N
WEST
EAST
A
B
WATER DEPTH (m)
0
100
200
300
10 km
1980 SUSPENDED MATTER (mg/l)
1980 TEMPERATURE (°C)

Figure 12

Figure 13A. Side-scan sonar sonograph (50khz towfish and 600m swath width, orthogonally rectified) showing deep bedforms observed north of Kong Karls Land near region with large near-bottom excess turbidity. Wavelength of sediment waves approximately 5m (see figure 1 for location).

B. 3.5kHz profile.

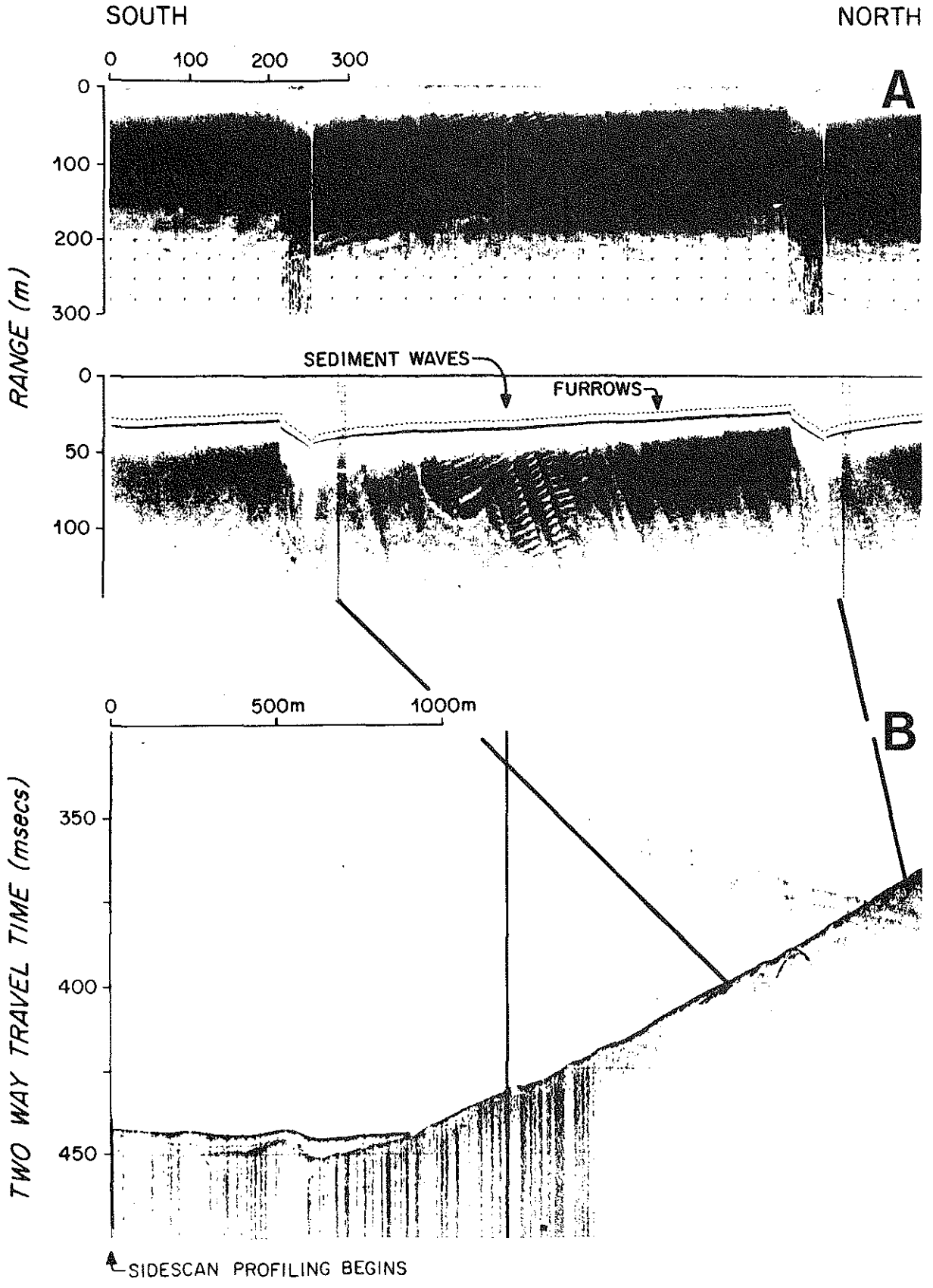
SOUTH
NORTH
0
100
200
300
A
RANGE (m)
SEDIMENT WAVES
FURROWS
0
50
100
0
500m
1000m
B
TWO WAY TRAVEL TIME (msecs)
350
400
450
SIDESCAN PROFILING BEGINS

Figure 13

and Solheim 1983). Surface sediments in water shallower than 200m are blue-gray, poorly sorted sandy muds with abundant gravel. In deeper waters, Holocene deposits of soft olive-gray fine-grained sediments predominate. The source of this fine-grained material seems to be redistribution of Pleistocene diamicton (tills and glaciomarine sediments). Redistribution must be rather extensive as Holocene sedimentation rates are estimated to be 3-5cm/1000yr for fine sediments in deposited in the basins (Klenova 1960, Forsberg 1983, Elverhoi and Solheim 1983), and the biologic component of surface sediments is low (Klenova 1960). Nepheloid layers are ubiquitous in the Barents Sea indicating that modern redistribution is indeed occuring, but concentrations of SPM are low; they only locally exceed 0.5mg/l excess turbidity (figure 11). Siberian river input of fine-grained sediments is negligible, except in close proximity to the river mouths in the southern Barents Sea (Klenova 1960). Modern glacial meltwater input similarly appears to have only local importance, within 30km of the glacial source (Pfirman, et al. 1982, chapter 4). Ice rafting is apparently also not extensive (Elverhoi and Solheim 1983, Forsberg 1983). The fine-grained deposits in the basins probably are not the result of original deposition beneath the Wisconsin glaciers because 1) they contain a warm water fauna, and 2) available dates of this material are less than 8000yrBP (Elverhoi, pers. comm.) and raised shorelines dated at 10,000yrBP indicate that much of the Barents Ice Sheet had already retreated by this time.

Reworking of sea-floor sediments is caused by different processes at different depths. Substantial redistribution of the surface sediments could have

occurred immediately after withdrawal of the Barents Ice Sheet. Although water depths were deeper during ice sheet disintegration, circulation may have been more intense, resulting in winnowing of the shallow banks. All surface sediments in water depths less than 125m are sandy. These sediments are probably reworked by modern surface waves (figure 10), are possibly influenced by tidal currents, and are reworked by modern icebergs. Sediments in water depths greater than 125m are affected only by waves with periods greater than 14sec and wave heights greater than 2m (figure 10), and are not gouged by modern icebergs.

Regions of pronounced resuspension/advection are:

1) in the narrow straits west and south of Kvitoya, and

2) along the southern margin of Nordaustlandet and eastern margin of Spitsbergenbanken.

Based on analysis of geostrophic velocity calculations, regions of high current shear are associated with increased near-bottom excess turbidity, and the geostrophic velocities calculated for 1981 in these regions appear high enough to resuspend some bottom sediments (figures 8 and 9). However, it is possible that material in suspension is being advected downstream from a higher velocity region. The velocity calculations could underestimate the actual velocity because 1) the reference level could have been chosen wrong, 2) a significant barotropic component was neglected in the calculation of a baroclinic current, or 3) superimposed surface wave activity increased the bottom

shear stress enough to resuspend bottom sediments. However, side-scan profiling in a region with a strong bottom nepheloid layer does show evidence of sea-floor reworking by currents, indicating that erosion is probably occurring in this region today.

Although highest SPM concentrations occur on western slopes of basins, nepheloid layers extend into the basins (figures 8, 9, and 12). Suspended sediments may be transported downslope (as well as along-slope), away from the erosional site, thereby advecting fine-grained sediments into the interior of basins.

ACKNOWLEDGEMENTS

The manuscript benefitted by critical reviews from John Milliman (WHOI), Tore Vorren (from the Tromso, Norway Insitute for Geological Research), and Anders Solheim (from the Norwegian Polar Research Institute (NPRI) in Oslo, Norway). The NPRI analyzed surface sediment texture, Tor Gammelsrod at the Geophyscial Institute in Bergen and Harald Loeng at the Institute for Marine Research in Bergen provided hydrographic information.

The Office of Naval Research supported this research under contract #N00014-01-C-009. The NPRI provided ship time and logistical. The captain, Terje Langvik, and the crew of the R/V Lance, from which most research was carried out, greatly aided data collection by intrepidly navigating in difficult sea-ice and uncharted waters. Additional travel funds were provided by the Norwegian Marshall Fund for Scientific Research and the Woods Hole Oceanographic Institution (WHOI) Education Department.

REFERENCES

Aagaard, K., A. Foldvik, T. Gammelsrod, and T. Vinje (1984) A one-year record of currents and bottom pressure in the Northeast Land - White Island Strait, Svalbard 1980-81.

Baker, E.T. and J.W. Lavelle (in press) The effect of particle size on the light attenuation coefficient of natural suspensions. J.G.R. 37pp.

Boulton, G.S., C.T. Baldwin, J.D. Peacock, A.M. McCabe, G. Miller, J. Jarvis, B. Horsefield, P. Worsley, N. Eyles, P.N. Chroston, T.E. Day, P. Gibbard, P.E. Hone, V. von Bunn (1982) A glacio-isostatic facies model and amino acid stratigraphy for late Quaternary events in Spitsbergen and the Arctic. Nature 298:437-441.

Butman, B. and J.A. Moody (1983) Observations of bottom currents and sediment movement along the U.S. east coast continental shelf during winter. Chapter 7, 60pp.

Denton, G.H. and and T.J. Hughes (1981) The Last Great Ice Sheets. John Wiley and Sons.

Dibner, V.D. (1970) "Ancient clays" and the relief of the Barents - Kara shelf as direct proof of its sheet glaciation during the Pleistocene. in Problems of Polar Geography ed. M. I. Below. Israel Program Scien. Translation Ltd. Jerusalem.

Eittreim, S., E.M. Thorndike, and L. Sullivan (1976) Turbidity distribution in the Atlantic Ocean. Deep-Sea Research 23:1115-1127.

Ellertsen, B., H. Loeng, F. Rey, S. Tjelmeland (1981) The feeding conditions of capelin during summer: Field observations in 1979 and 1980. Fisken og Havet 1981(3):1-68.

Elverhoi, A. and A. Solheim (1983a) The Barents Sea ice sheet - A sedimentological discussion. Polar Research 1:23-42.

Elverhoi, A. and A. Solheim (1983b) Western Barents Sea: Surface sediment distribution. Norsk Polarinstitutt Skrifter 179A.

Emelyanov, E.M., V.M. Litvin, V.A. Levchenko, and G.P. Martynova (1971) Geomorphological signs of action of the Scandinavian, Novaya Zemlya, and Spitsbergen ice sheets on the floor of the Barents Sea. Oceanology 20(4):440-447

Forsberg, C.F.(1983) Sedimentologic and early diagenic studies in the Barents Sea. unpub. thesis. University of Oslo

Grosswald, M.G. (1980) Late Weichselian ice sheet of northern Eurasia. Quaternary Research. 13:1-32.

Holtedahl, H. (1981) Distribution and origin of surface sediments on the Norwegian continental margin between 62°N and 65°N, with some remarks on the Late Quaternary litho- and biostratigraphy. in The Norwegian Coastal Current (eds.) R. Saetre and M. Mork. University of Bergen. p768-792.

Holtedahl, H. and K. Bjerkli (1982) Late Quaternary sediments and stratigraphy on the continental shelf off More - Trondelag, Western Norway. Marine Geology 45:179-226.

Johannessen, O.M. and L.A. Foster (1978) A note on the topographically controlled oceanic Polar Front in the Barents Sea. J.G.R. 83(C9):4567-4571.

Kellog, T.K. (1976) Late Quaternary climatic changes: evidence from cores of Norwegian and Greenland Seas. In: Investigation of Late Quaternary Paleo-oceanography and Paleoclimatology (eds.) R.M. Cline and J.D. Hays. Geol. Soc. Am. Mem. 145:77-110.

Klenova, (1960) The Barents Sea geology. Moscow. Akad.Nauk. SSSR 367pp.

Madsen, O.S. and W.D. Grant (1976) Sediment transport in the coastal environment. M.I.T. - Department of Civil Engineering. Report #209 105pp.

Moody, J.A. and B. Butman (in prep.) Light attenuation and scattering as a function of particle size.

Novitskiy, V.P.(1961) Permanent currents of the Northern Barents Sea. Trudy Gosudarstvennogo Okeanograficheskogo Tnstituda. 64:1-32 Leningrad. (Translated by U.S.N.O. 1967)

Pfirman, S.P., J.D. Milliman, and A. Elverhoi (1982) Recent flux of suspended material near glacier front, Svalbard Archipelago. AGU/ASLO Joint Meeting San Antonio, Texas. Abstracts with Program.

Pond, S. and G.L. Pickard (1978) Introductory Dynamic Oceanography Pergamon Press. 241pp.

Ruddiman, W.F. and A. McIntyre (1973) Time-transgressive deglacial retreat of polar waters from the North Atlantic. Quaternary Research 3:117-130.

Salvigsen, O. (1981) Radiocarbon dated raised beaches in Kong Karls Land, Svalbard and their consequences for the glacial history of the Barents Sea area. Geogr. Ann. 63A:283-291.

Solheim, A. (in press) Pockmarks along eastern slope of Spitsbergenbanken. Polar Research

Solheim, A. (in prep.) Acoustic character of surficial sediments of the northern Barents Sea.

Solheim, A. and Y. Kristoffersen (in press) Sediment distribution above upper regional unconformity and glacial history of the Barents Sea. Norsk Polarinstitutt Skrifter 179b.

Solheim, A. and S.L. Pfirman (in press) Sea-floor morphology outside a grounded, surging glacier: Brasvellbreen, Svalbard. Marine Geology.

Sternberg, R.W. and L.H. Larsen (1975) Threshold of sediment movement by open ocean waves. Deep-Sea Res. 22:299-309.

Tantsiura, A.I. (1959) On the currents of the Barents Sea. PINRO 11:35-53.

Vinje, T.E. (1984) Frequency distribution of sea ice, ridges, and water openings in the Greenland and Barents Seas - A preliminary report on the 'Birds Eye' observations. Norsk Polarinstitutt Nr. 15 Oslo 27pp.

Vorren, T.O., I.F. Strauss, O.-W. Lind-Hansen (1978) Late Quaternary sediments and stratigraphy on the continental shelf off Troms and West Finnmark, northern Norway. Quaternary Research 10(3):340-365.

Vorren, T.O. M. Hald, M. Edvardsen, O.-W. Lind-Hansen (1983) Glacigenic sediments and sedimentary environments on continental shelves: General principles with a case study from the Norwegian Shelf. in ed. J. Ehlers Glacial Deposits in Northwest Europe p61-73.

Vorren, T.O. and Y. Kristoffersen (in prep.) Late Quaternary glaciation in the southwestern Barents Sea.

Wright, P.L.(1974) Recent sediments of the southwestern Barents Sea. Mar. Geol. vol 16:51-62.

Young, R.A. and J.B. Southard (1978) Erosion of fine-grained marine sediments: Sea floor and laboratory experiments. Geol. Soc. of Am. Bull. 89:663-672.

CHAPTER 3

Sea-Floor Morphology Outside a Grounded, Surging Glacier; Brasvellbreen, Svalbard

Anders Solheim
Norwegian Polar Research Institute
P.O. Box 158, N-1330 Oslo Lufthavn
Norway

Stephanie Pfirman
Woods Hole Oceanographic Institution
Department of Geology and Geophysics
Woods Hole, Massachusetts

ABSTRACT

Acoustical profiling and bottom photography reveal several different sea floor morphological features adjacent to the grounded Brasvellbreen glacier on Svalbard, northwestern Barents Sea. Some of the features and their distribution are closely related to a major glacial surge in 1936-38, and as such are valuable in identifying former surges in other locations. A continuous end moraine with a characteristic asymmetrical cross-section runs subparallel to the present glacier front, and defines the maximum extent of the surge. Part of this moraine was probably pushed up in front of the glacier as it advanced, and part was deposited from meltwater during the surge. Subsequent slumping down the distal flank of the moraine modified the surface topography. A rhombohedral pattern of 5m high discontinous ridges inside the end moraine probably reflects sediment accumulation in crevasses formed at the base of the glacier at the end of the surge. Discontinuous arcuate ridges and swales within 1km of the modern ice front define local, minor readvances and retreats an active glacier. Iceberg plough marks are most frequent seaward of the end moraine; their orientation is controlled by a combination of a longshore current, offshore katabatic winds, and sea-floor topography. Superimposed on the plough marks are secondary features such as a "washboard pattern" and striae, most likely caused by push-up of overconsolidated material during gouging, and multi-keel icebergs, respectively. Bottom sediments observed in photographs and cores are composed of normally consolidated pebbly mud with a high

variability in clast content, resting on overconsolidated material, probably basal till. Cores obtained up to 40km from the ice front coarsen upwards, perhaps because ice rafting increased during the surge. Mud deposition from meltwater outflows presently prevails close to the glacier.

INTRODUCTION

Glacial readvances during a general deglaciation are usually interpreted as expressions of climatic fluctuations. However, glacial surges are important in many areas today, and were probably also common in the past. Local glacier surges can occur independently of climatic variations, although they do imply sufficiently high precipitation over a period of time to build up an unstable mass distribution. Prest (1969) considered, for example, the possibility that several of the Laurentide readvances were due to surging on a local scale with no climatological significance. Similarly, Holdsworth (1977), suggests that surge activity on Baffin Island may have been important during the decay of the last ice sheet. Glacier thinning through surges, according to Holdsworth (1977), may also help to explain the apparent difficulties of accounting for the rapid decay rates of large ice sheets in terms of the energy requirements for melting ice (Hare, 1976).

Glacial surges occur intermittently at intervals of 30 to 100 years (Meier and Post, 1969). A surge usually lasts 1-2 years (Paterson, 1981), during which time the glacier front advances rapidly. Surges constitute a common form of glacier advance on Svalbard (Liestol, 1969). On Spitsbergen, the largest island in the archipelago, advances up to 12km in less than one year have been measured (Liestol, 1969). The foreward movement of the glacier ceases at the end of the surge, and in the case of tidewater glaciers, calving causes retreat of the ice front.

Brasvellbreen glacier (1110 km^2) is part of an ice cap (8130 km^2) situated on Nordaustlandet in the Svalbard archipelago, northwestern Barents Sea (figure 1). Between 1936 and 1938, Brasvellbreen surged up to 20km (figure 2; Schytt, 1969), and has retreated 0.5-3.5km since that time. This surge is the greatest movement so far recorded (Paterson 1981). Extensive crevassing during the surge is documented from aerial photography (figures 3 and 4). Surge boundaries probably were controlled by underlying bedrock topography in central parts of the Nordaustlandet ice cap (Schytt, 1964; O. Liestol, pers. comm.). Aerial photographs in 1957 show that the glacier had retreated to approximately its present position (figure 2; Blake 1962). The glacier terminus is presently grounded in water depths ranging from 30 to 100m and forms a vertical wall 25 to 35m above sea level. The terminus presently appears stable and crevassing is limited to a few parallel fractures (figure 5). According to satellite images, large scale features of the ice front, like embayments and protrusions, have persisted at least since 1976 (chapter 4).

This situation presents a unique opportunity to study the effects of glacier advances on sea-floor parameters such as morphology, sediment distribution and composition, and geotechnical properties.

DATA ACQUISITION

Data were collected during two cruises in August 1982 and August 1983 (figure 6) aboard the R/V Lance. Acoustic instrumentation consisted of a hull-mounted 3.5 kHz echo-sounder (O.R.E. tranceiver

Figure 1. Distribution of glaciated areas (tick pattern) and exposed land (dotted) on the island of Nordaustlandet. Map area is shown by hatching in the location map. Heavy line shows Brasvellbreen glacier front.

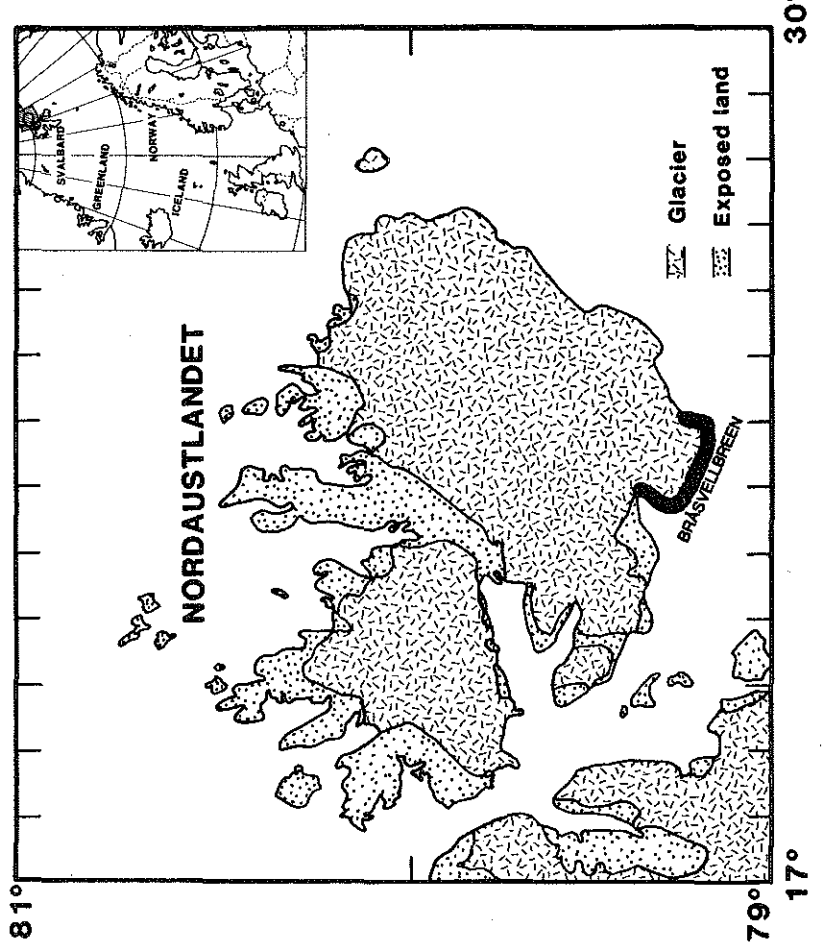
81°
79°
17°
30°
NORDAUSTLANDET
BRASVELLBREEN
Glacier
Exposed land
SVALBARD
GREENLAND
NORWAY
ICELAND

Figure 1

Figure 2. Ice front positions 1934 (probably the same in 1936), 1938, 1957, and 1984 (from Blake 1961).

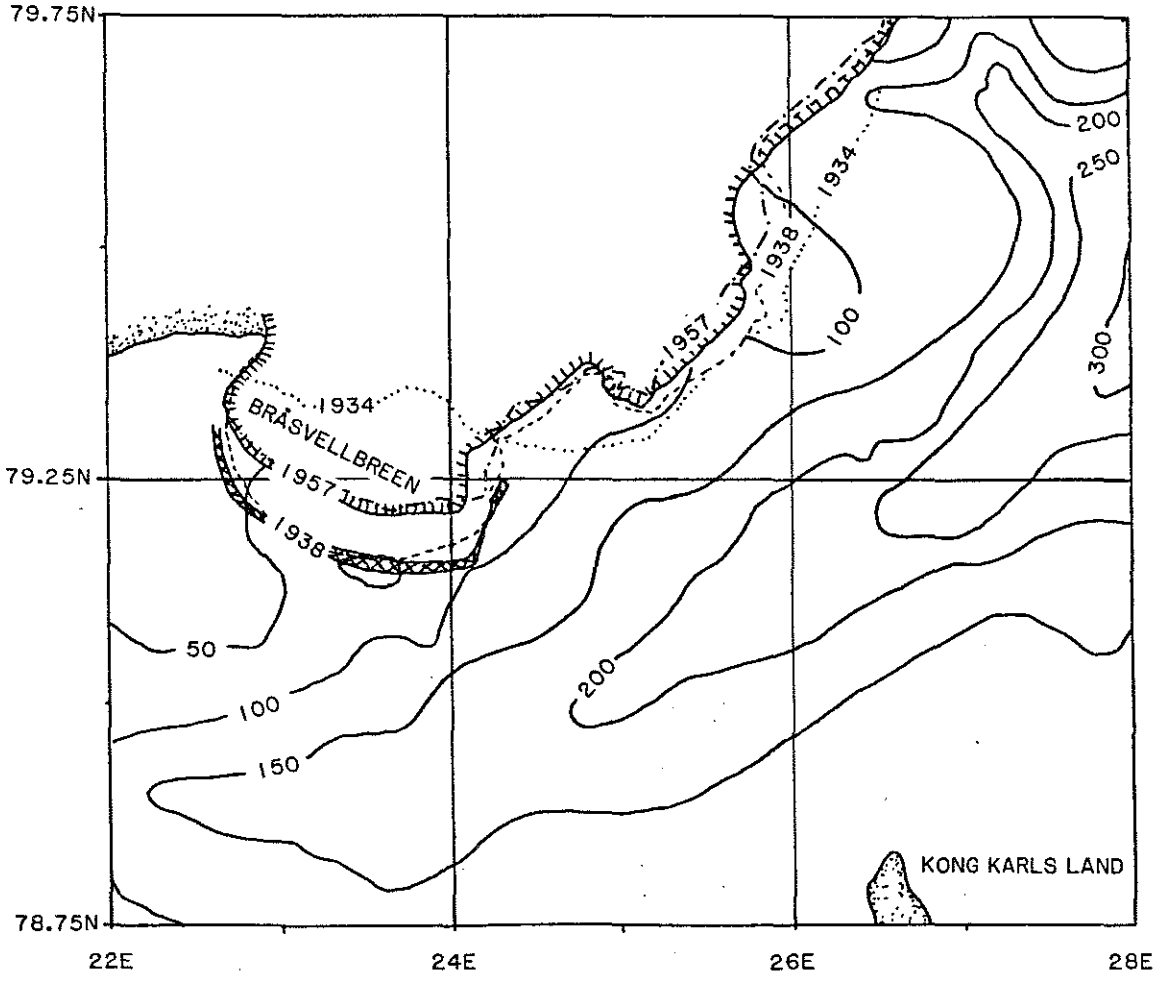
79.75N
79.25N
78.75N
22E
24E
26E
28E
BRÅSVELLBREEN
1934
1957
1938
50
100
150
200
100
200
250
300
KONG KARLS LAND

Figure 2

Figure 3. Photo taken in 1938 of the eastern part of Brasvellbreen. Note how the extensively crevassed glacier surface contrasts with the present-day situation shown in figure 5. Also note the "old" ice-front (without many crevasses) in the right-hand part of the photo, and the boundary between crevassed (surge) and uncrevassed glacier towards central parts of the ice cap. Flight height is approximately 2200m, camera lens 210mm, looking northeast. (Norsk Polarinstitutt photo S-38, 1958).

Figure 3

Figure 4. Photo taken in 1938, showing pattern of crevassing on the eastern flank of Brasvellbreen. Also note the boundary between the surging glacier and the "old" glacier, shown by the marked difference in crevasse patterns. Flight height is approximately 1800m, camera lens 210mm, looking east. (Norsk Polarinstitutt photo S-38, 1921).

Figure 4

Figure 5. Photo taken from helicopter in 1982, showing the present-day Brasvellbreen. Exact location and flight height is unknown, camera lens 28mm, looking north.

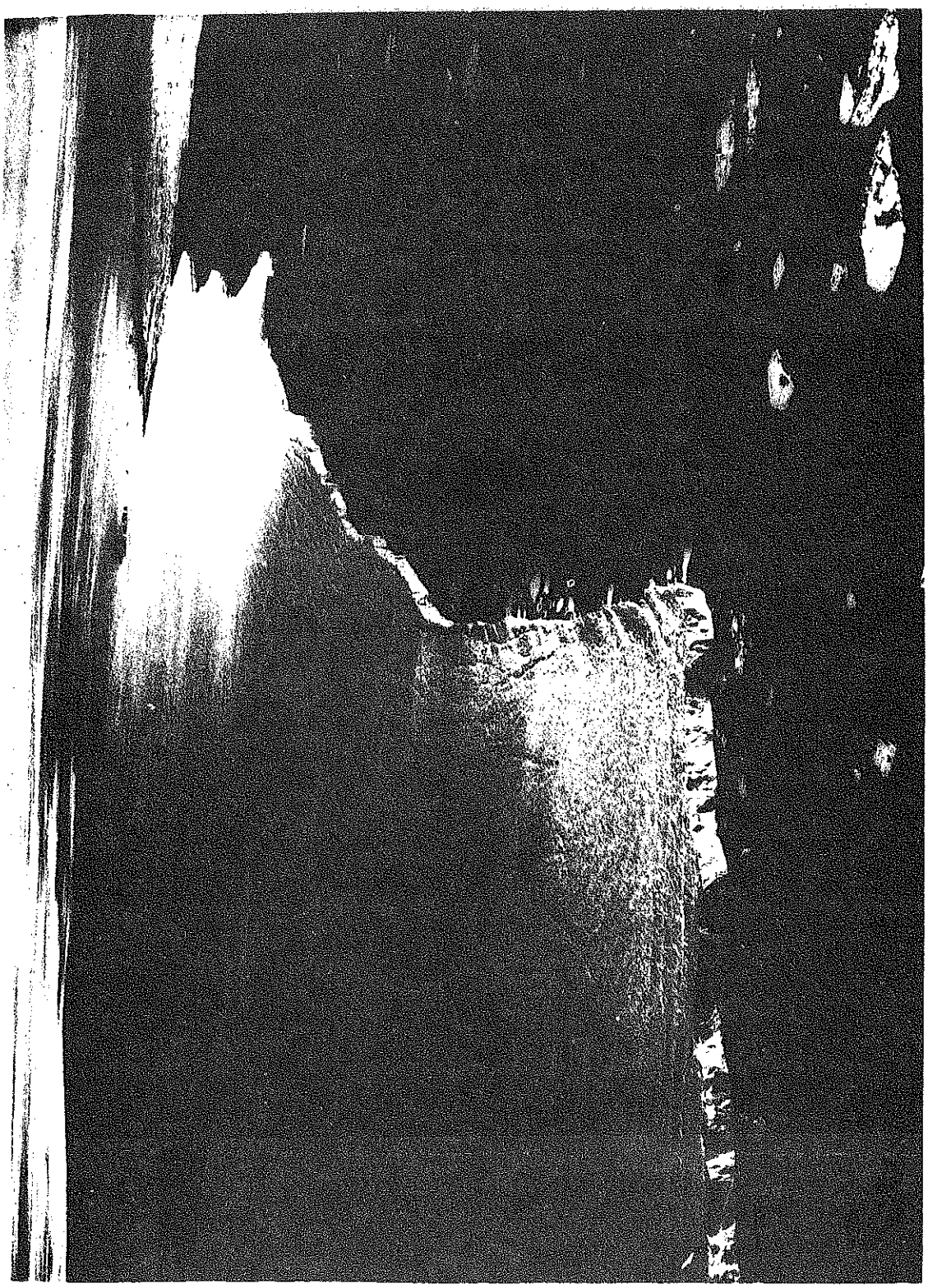

Figure 5

Figure 6. The survey area outside Brasvellbreen glacier showing track lines.

A. Numbers on heavy lines and crosses refer to later figures.

B. Core station locations.

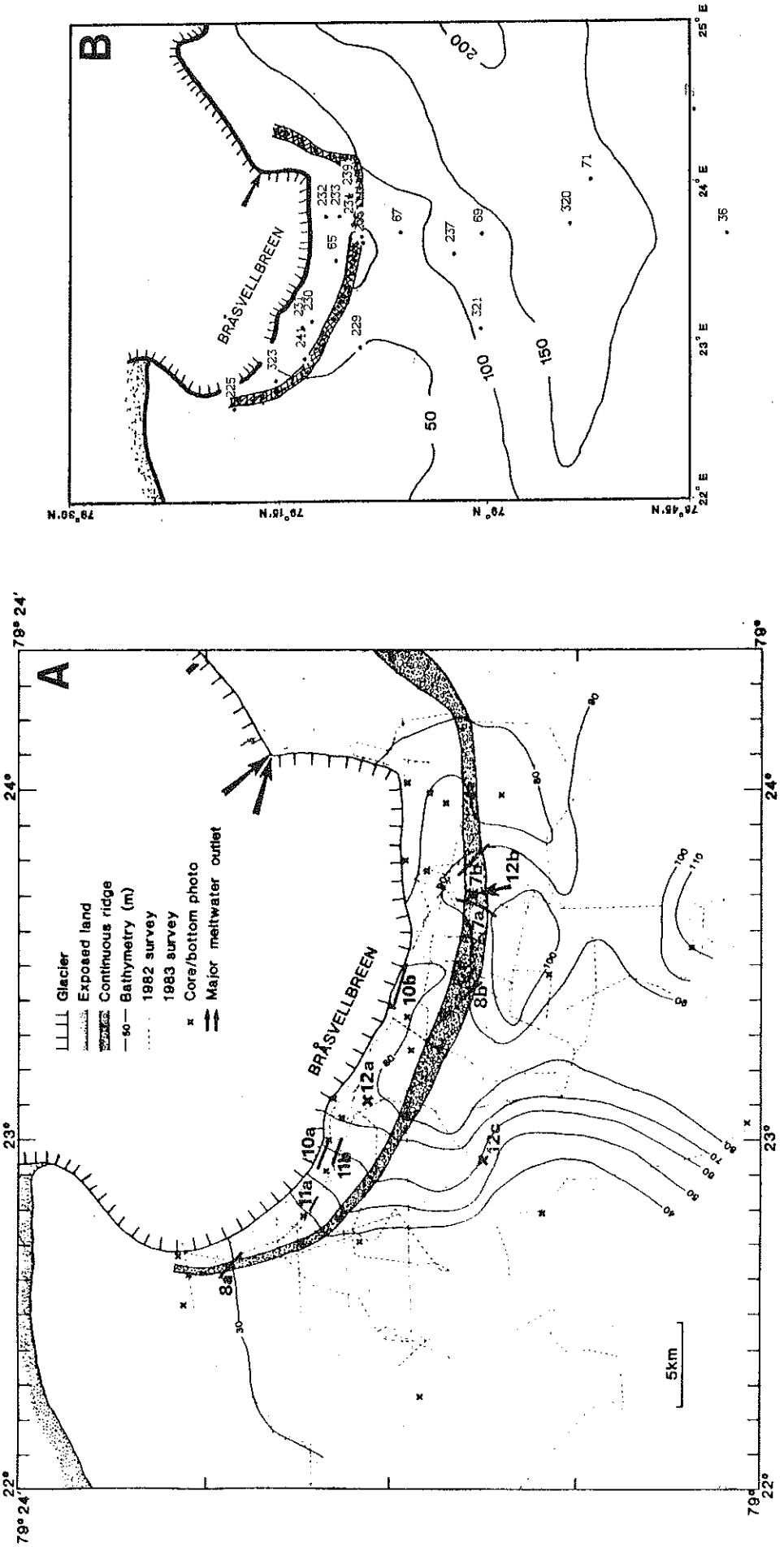
A
B
Glacier
Exposed land
Continuous ridge
Bathymetry (m)
1982 survey
1983 survey
Core/bottom photo
Major meltwater outlet
BRÅSVELLBREEN
5km
79° 24'
24°
23°
22°
79°
79°30'N
79°12'N
79°N
78°45'N
22° E
23° E
24° E
25° E
50
100
150
200

Figure 6

with an EPC 3200 analogue graphic recorder), a Klein 50 kHz side-scan sonar system and an E.G.&G. one kJ sparker system (only in 1983) with a single-channel streamer (pass band 100-600 Hz). Bottom photographs were taken with a Benthos deep-sea camera, and 44 sediment cores were acquired with a 110mm diameter gravity-corer and 90mm diameter vibro-corer. Shear strength (s_u (kPa)) of sediment cores was measured with a pocket penetrometer and falling-cone apparatus. Textural analysis of the top 5cm of the sediment samples was carried out by standard seive and pipette methods (Folk 1968) Mineralogy of the less than 63μm fraction was determined by x-ray diffraction (XRD). Unweighted major peak areas from the diffractograms were measured and calculated to 100% to show relative changes in the amounts of quartz, calcite, dolomite, and feldspar in the pro-glacial region (appendix B). Sediment texture and geotechnical results are presented more fully in Solheim (in prep.).

Due to severe sea-ice conditions, the side-scan survey of 1982 was limited to a narrow region of open water along the western part of the glacier front. However, extensive coverage was obtained with the 3.5 kHz echo-sounder, which was run continuously. In 1983, the area was almost ice-free, and additional profiling provided more extensive coverage with side-scan sonar and sparker, totalling 150km of side-scan sonar profiles and 400km of 3.5 kHz echo-sounder profiles.

MORPHOLOGICAL FEATURES

Brasvellbreen glacier thins to the west, exposing bare land and forming the southwestern boundary of the Nordaustlandet ice cap

(figure 1). The tidewater glacier front of the ice cap continues northeastward from the study area for another 120 km. Water depths increase to the east in the study area, from less than 30m to 100m, with the steepest bathymetric slope being midway along the front where a broad depression runs perpendicular to the glacier (figure 6).

Several distinct bottom morphological patterns are present in the survey area. The most prominent feature is a continuous ridge, subparallel to the glacier front. The distance from the ridge crest to the glacier front varies from 500m in the western sector to 3.5km in the central, deeper regions (figure 6). Ridge height varies from 8 to 20m, and width ranges from 500 to 1700 m (figures 7 and 8). The ridge is highest and widest in the central bathymetric depression (figures 6 and 7). Gradients are 2-3 degrees on the distal side and 4-6 degrees (locally steeper) on the proximal side. The distal flank is acoustically more transparent than the central and inner portions of the ridge. A distinct contact with an underlying surface is visible on 3.5 kHz records near the seaward extent of the ridge (figure 7a). The underlying surface cannot be followed under the crest and inner slope on 3.5khz records, but sparker profiling reveals a flat seismic reflector underneath the deposit (figure 7b). Slumps are observed on the distal slope in side-scan profiles (figure 8b), with locally rougher surface morphology and lobate margins.

Sea-floor morphology inside the continuous ridge is quite different from that outside, with respect to both relief and type of features (figure 9). In general, the sea floor has a more chaotic appearance inside than the more regular, ice-ploughed surface outside

Figure 7. Seismic profiling of the continuous outer ridge (for location, see figure 6).

A. 3.5 kHz echo-sounding across the continuous outer ridge.

B. 1 kJ sparker record across the ridge.

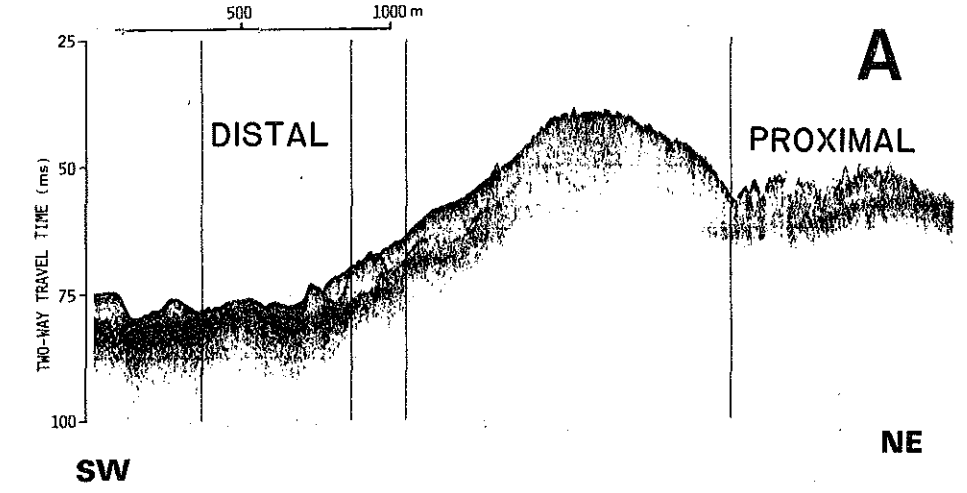
500
1000 m
25
50
75
100
TWO-WAY TRAVEL TIME (ms)
DISTAL
PROXIMAL
A
SW
NE

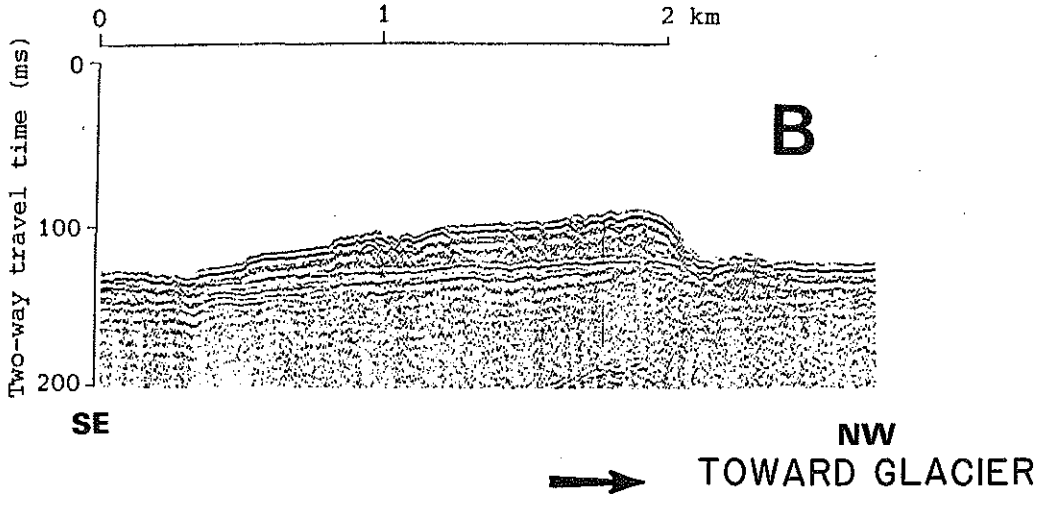
0
1
2 km
0
100
200
Two-way travel time (ms)
B
SE
NW
TOWARD GLACIER

Figure 7

Figure 8. Side-scan sonographs of continuous outer ridge (for location, see figure 6):

A. oblique profile across ridge showing rhombohedral pattern inside ridge and iceberg plough marks on distal flank, 3.5khz profile at bottom.

B. slump on distal flank of ridge, note rougher surface in slump region and lobate form of distal slump margin.

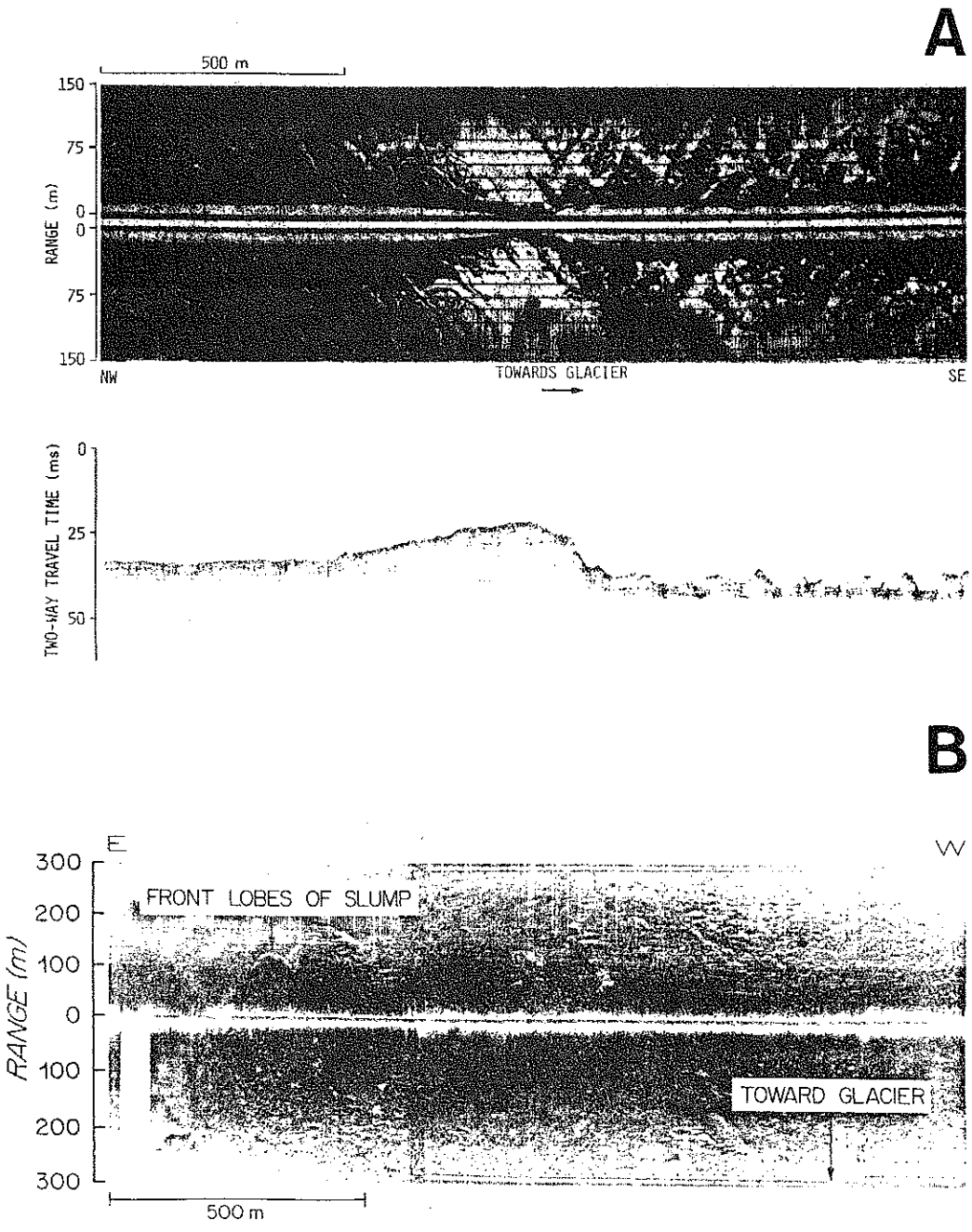
A
500 m
150
75
0
0
75
150
RANGE (m)
NW
TOWARDS GLACIER
SE
TWO-WAY TRAVEL TIME (ms)
0
25
50
B
E
W
300
200
100
0
100
200
300
RANGE (m)
FRONT LOBES OF SLUMP
TOWARD GLACIER
500 m

Figure 8

Figure 9. Location of sea-floor morphological types discussed in the text (based on interpretation of side-scan sonar and 3.5khz profiles).

End moraine crest is denoted by a heavy line, dotted line shows approximate outermost extent of end moraine material.

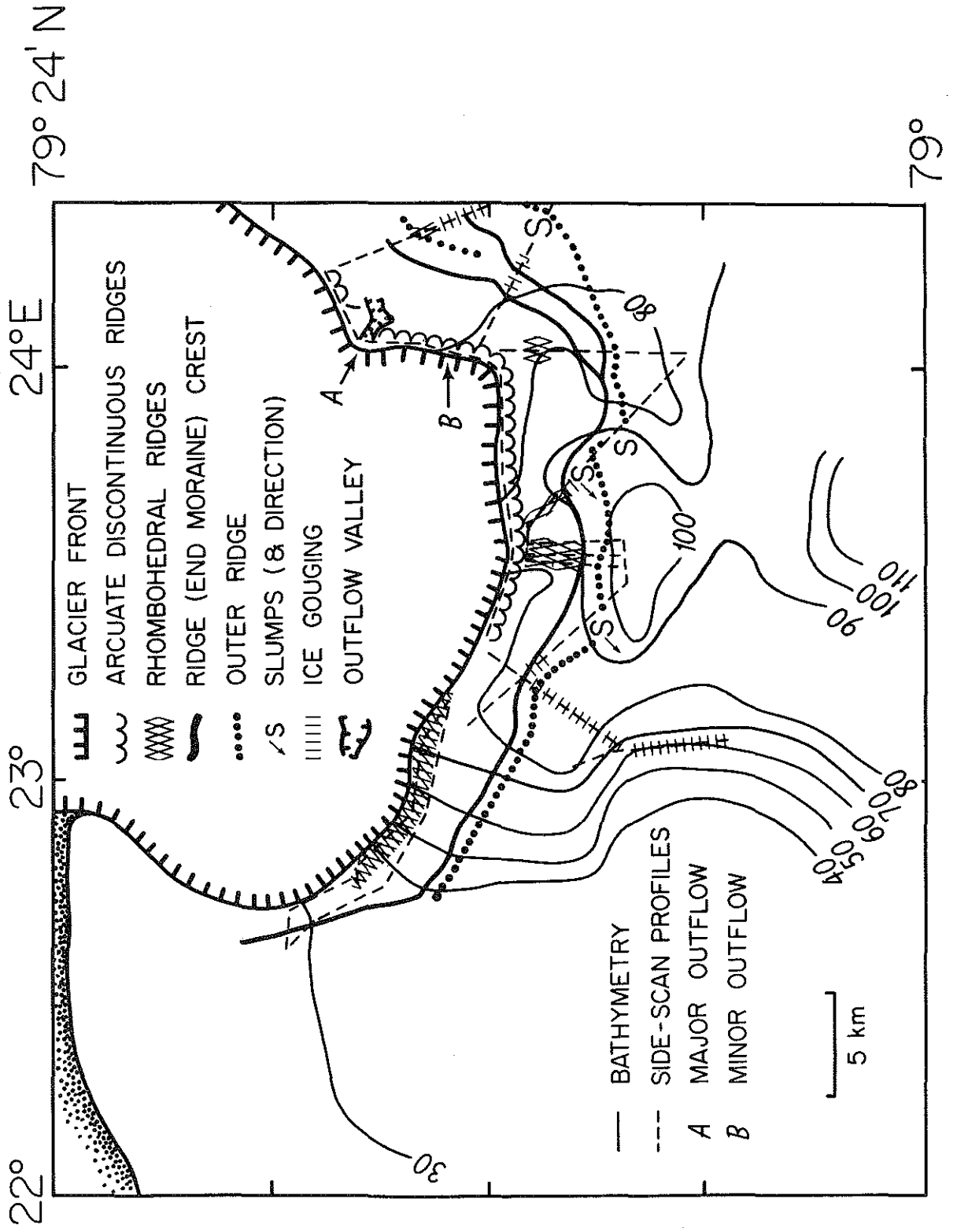
22°
23°
24°E
79° 24' N
79°
GLACIER FRONT
ARCUATE DISCONTINUOUS RIDGES
RHOMBOHEDRAL RIDGES
RIDGE (END MORAINE) CREST
OUTER RIDGE
SLUMPS (& DIRECTION)
ICE GOUGING
OUTFLOW VALLEY
A
B
S
30
40
50
60
70
80
90
100
110
BATHYMETRY
SIDE-SCAN PROFILES
A MAJOR OUTFLOW
B MINOR OUTFLOW
5 km

Figure 9

the ridge (figure 7a). Distinguishable features inside the ridge include:

1) Rhombohedral patterns, formed by linear discontinuous ridges with a relief of about 5m and 20-50m spacing (figure 10a). The network pattern has greater relief and is more closely spaced near the continuous ridge.
2) Irregularly distributed mounds up to 10m high (figure 10a).
3) Discontinuous arcuate ridges, running subparallel to the glacier front over short distances, concave towards the glacier front (figure 10b). The scale of the ridges varies considerably, but they tend to be less than 25m wide and 2-5m high.

Iceberg gouges are most prominent and frequent on the smoother sea floor outside the major ridge, with only a few occurrences closer to the glacier (figure 9). Furrow widths range from 10-30m (figure 11), and vertical relief is 2-5m. These dimensions have also been found in relict plough marks on the North Sea shelf (Belderson and Wilson, 1973), although most relict plough marks along the Norwegian coast are larger (Rokoengen, 1980; Lien, 1983). Most of the gouges show distinct levees. Plough directions are predominantly subparallel to the glacier front, but some at high angles are also observed, especially inside the ridge.

Secondary features are included within some of the ice gouges proximal to the glacier. A distinct "washboard pattern" (Lien, 1982) is observed at the outer edges of a wide plough mark proximal to the glacier (figure 11a), while other plough marks are striated parallel to the gouge direction (figure 11b).

Figure 10. Side-scan sonographs along the glacier front (for location, see figure 6):

A. rhombohedral ridge pattern and irregular mounds (3.5khz profile included for the same area),

B. discontinuous arcuate ridges paralleling the ice front

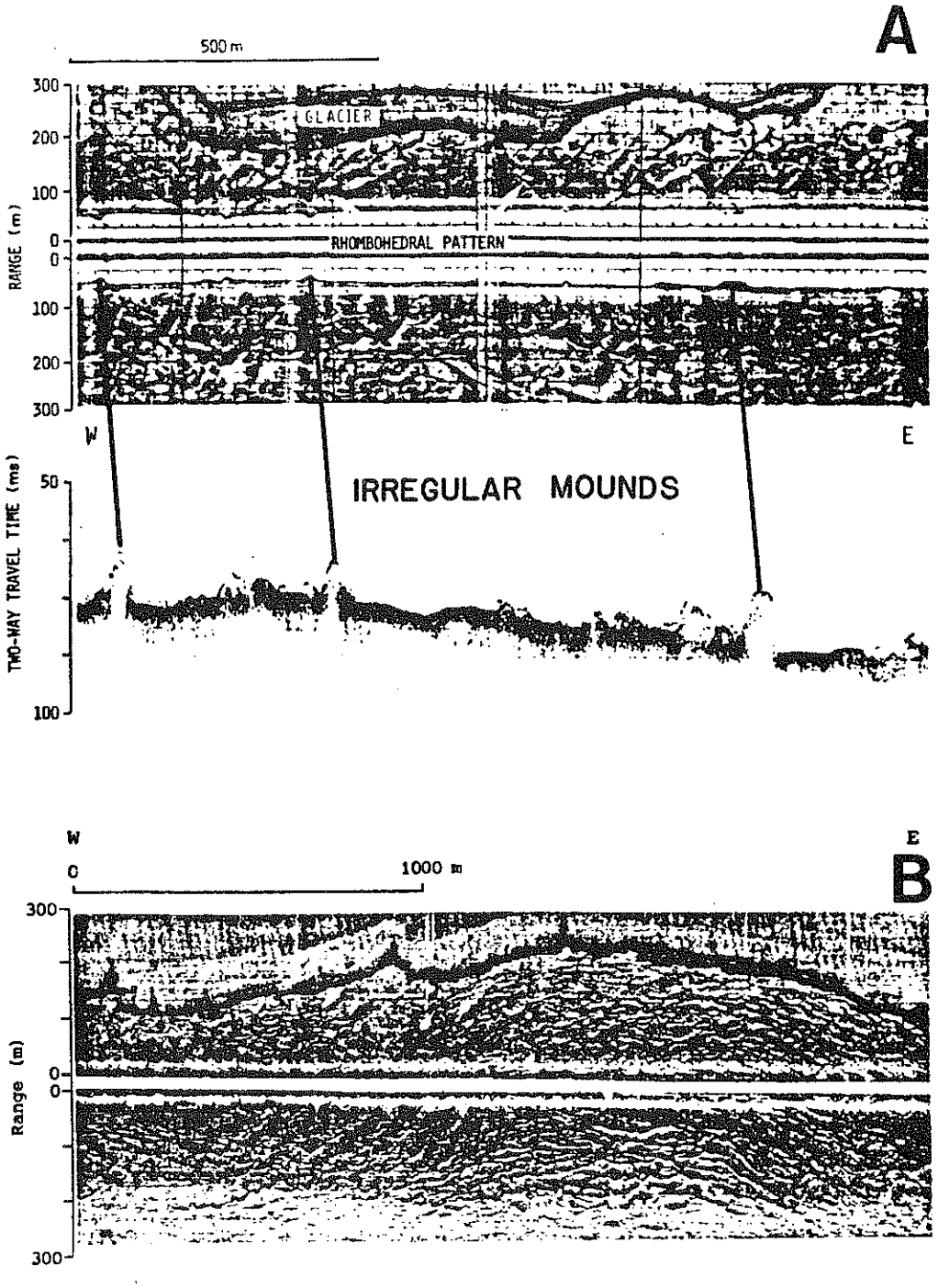
A
500 m
GLACIER
RHOMBOHEDRAL PATTERN
RANGE (m)
300
200
100
0
0
100
200
300
W
E
IRREGULAR MOUNDS
TWO-WAY TRAVEL TIME (ms)
50
100
W
E
0
1000 m
B
Range (m)
300
0
0
300

Figure 10

Figure 11. Side scan sonographs showing iceberg plough marks with secondary features (for location, see figure 6):

A. "washboard pattern" along edge of plough mark,

B. striated plough mark

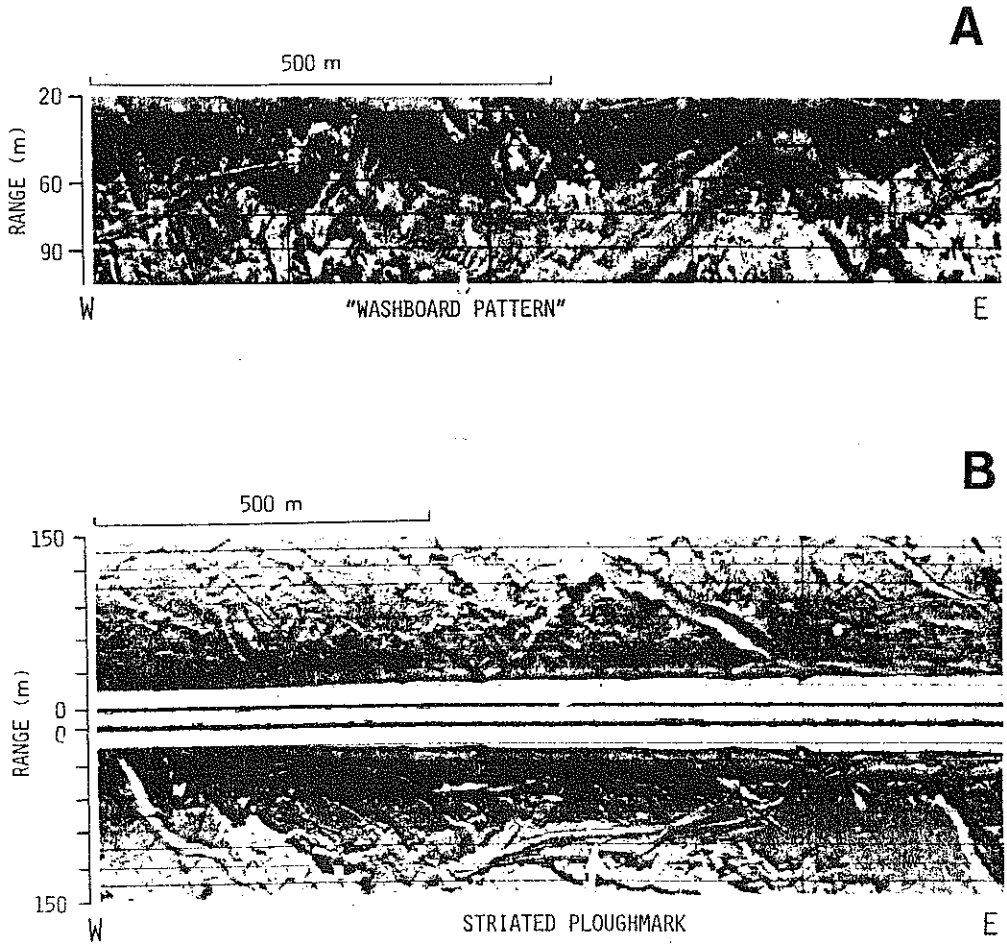
A
500 m
20
60
90
RANGE (m)
W
"WASHBOARD PATTERN"
E
B
500 m
150
0
0
150
RANGE (m)
W
STRIATED PLOUGHMARK
E

Figure 11

SEDIMENT DISTRIBUTION

Inside the ridge:

The surface sediments have high lateral variability in the study area. They are generally pebbly muds, but the pebble content shows considerable range both in cores and bottom photographs (figure 12). Photographs from four stations taken within 200m of the glacier front have turbid water obscuring most of the picture; however the sea floor appears to be muddy with few cobbles. Turbid bottom water was not observed in bottom photographs at greater distances from the glacier. Patchy regions of clean cobble pavement (figure 12c) are observed in bottom photographs outside the continuous ridge. Except for the presence of this pavement, no signs of current activity (i.e. ripples or scour marks) are seen in any bottom photographs.

Textural analyses of surface sediment samples near Brasvellbreen glacier reveal a uniform grain size distribution from -2 to 4ϕ indicative of poor sorting (figure 13). Station 65, located 2km from the ice front and inside the ridge is the sandiest core on the transect, and the proportion of coarse material remains relatively constant downcore (figure 14). This station has a significant gravel fraction throughout the entire core.

The main change down core inside the ridge is in the degree of consolidation. The top layer is usually an unconsolidated (s_u less than 10kPa) pebbly mud and is observed in 3.5khz profiles to form most of the surface topography. A thin and patchy layer of somewhat overconsolidated material (s_u 30-50 kPa) exists below the top layer inside the ridge. In a few cores, very stiff material (s_u in excess

of 100 kPa) was recovered below the slightly overconsolidated material. This lowermost layer forms an even reflector on the 3.5 kHz records and is interpreted to represent basal till, probably of late Weichselian (late Wisconsin) age. The intermediatly consolidated material may owe its overconsolidation to the overburden pressure of the surging glacier (Solheim, in prep.). This material is probably too patchy and has too small acoustic impedence contrast to be resolved with the seismic equipment used. The reflector beneath the continuous outer ridge (figure 7b) represents the assumed upper Wisconsin till.

Outside the ridge:

Outside the continuous ridge the general shape of the grain size distribution of the surface sediments stays the same as inside the ridge (figure 13), but with increasing distance from the glacier (from 1-40km) the percent of fine-grained material (less than 4um) increases while the gravel fraction (greater than 2mm) decreases. Lack of a dominant size mode suggests that surface sediments have not been reworked significantly by bottom currents. Cores from stations 67 and 69, located 9 and 20km from the glacier (outside the ridge) show decreases in the sand and gravel fraction down core (figure 14). Stations 319 at 30km and 71 at 34km also decrease in coarse fraction down core, but have have lower surficial gravel contents than stations closer to the glacier. Core 321 at 25km is exceptional as it is finest at the surface.

Figure 12. Bottom photographs (for location, see figure 6):

A. Muddy surface with dropstones located inside the end moraine.

B. On the end moraine, showing mud with high content of cobbles.

C. Outside the end moraine, showing variation between mud-dominated surface and clean cobble pavement.

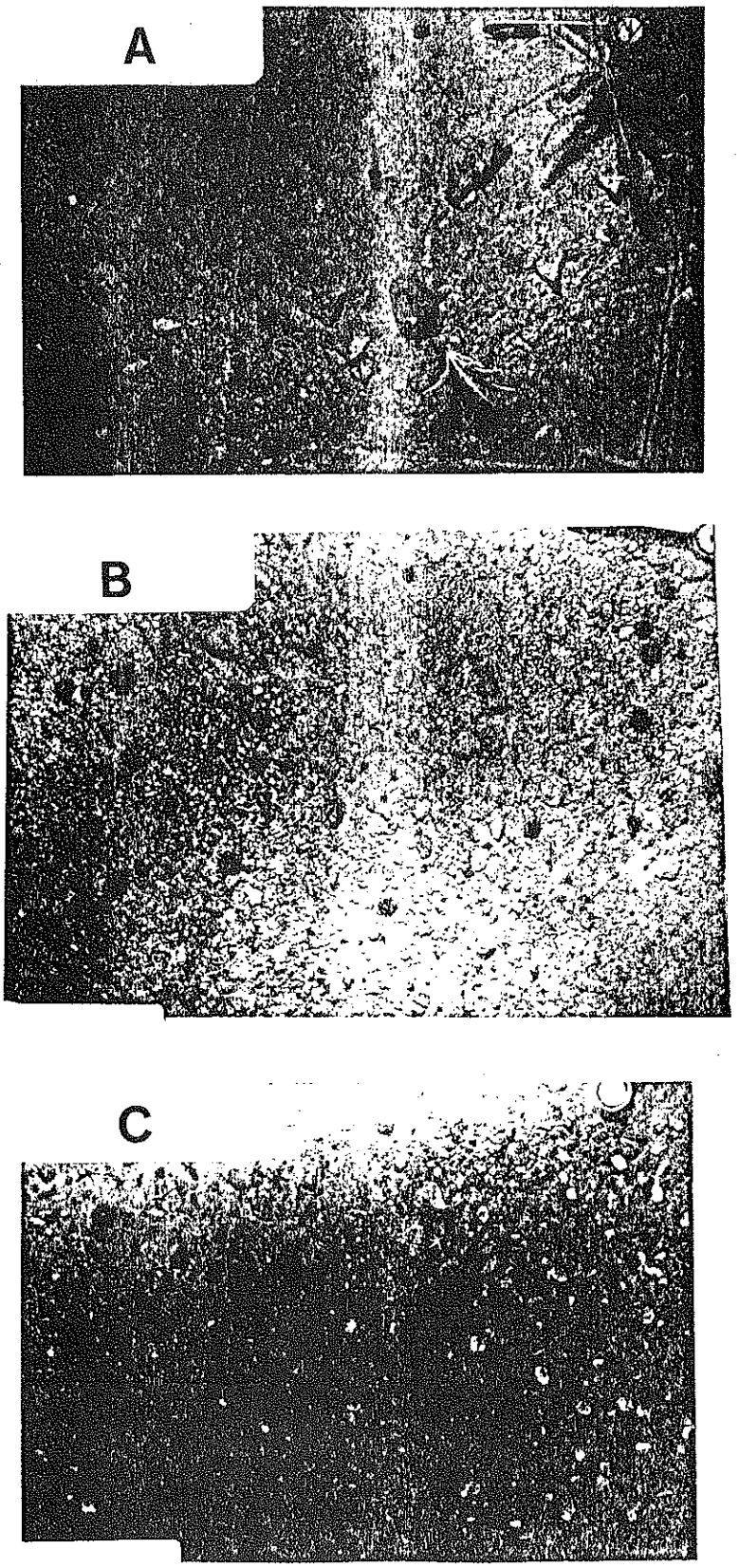

Figure 12

Figure 13. Grain size distribution of surface sediments for a transect of cores ranging from 1km to 35km from the present-day glacier front (see figure 6 for location). Percent of material smaller than 2mm (gravel) is calculated on gravel-free sample weights.

A. Inside the continuous ridge

B. Outside the continuous ridge

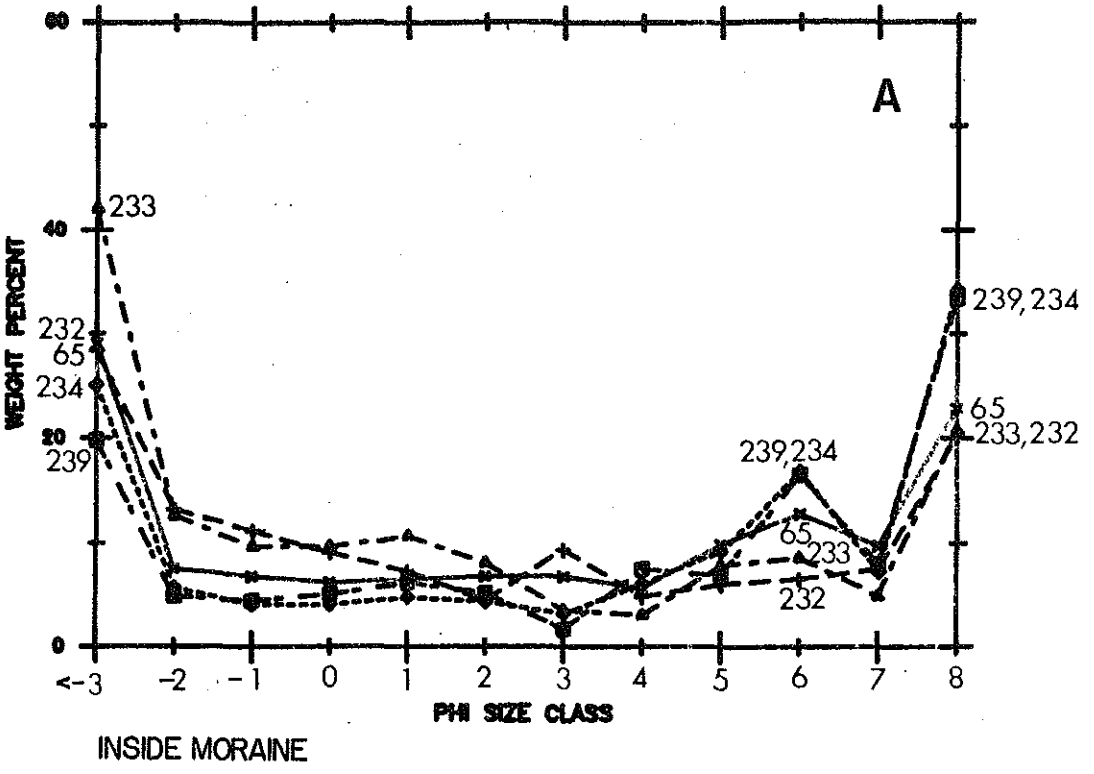
A
WEIGHT PERCENT
60
40
20
0
233
232
65
234
239
239,234
65
233,232
65
233
232
<-3
-2
-1
0
1
2
3
4
5
6
7
8
PHI SIZE CLASS
INSIDE MORAINE

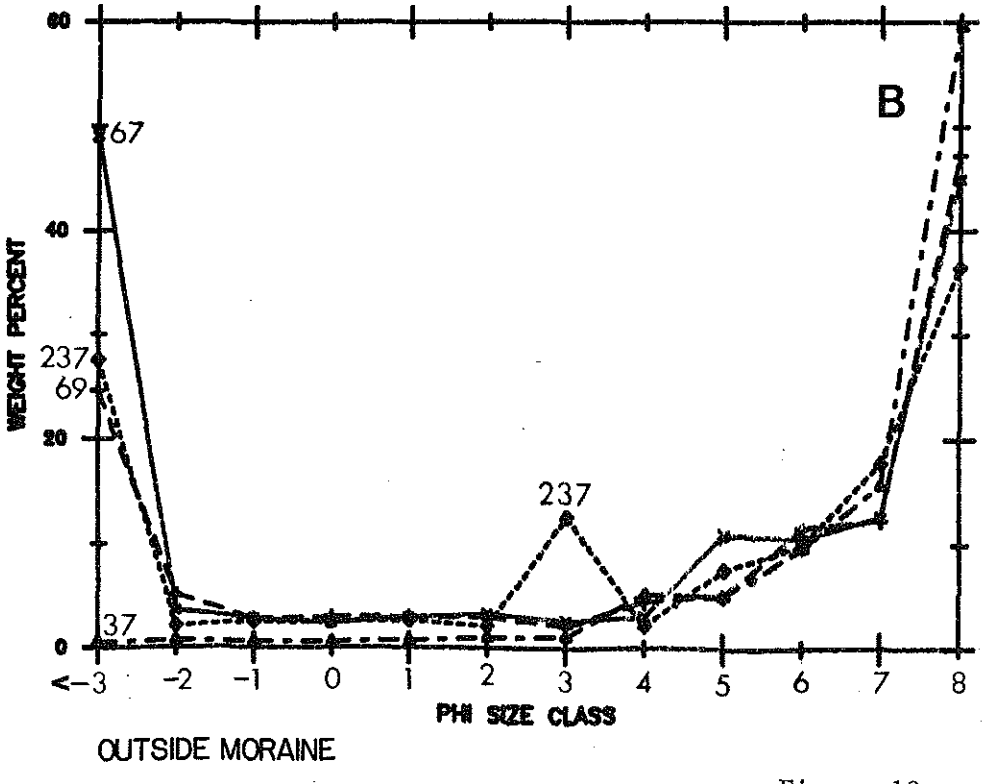
B
WEIGHT PERCENT
60
40
20
0
67
237
69
237
37
<-3
-2
-1
0
1
2
3
4
5
6
7
8
PHI SIZE CLASS
OUTSIDE MORAINE

Figure 13

Figure 14. Percent gravel (greater than 2mm), sand (2.0 - 0.063mm), and silt plus clay (less than 0.063mm) of down-core sediment samples form six cores (note that only top portion of triangular diagram is shown). Samples are denoted by station number followed by -depth (cm) down core (for station locations see figure 6).

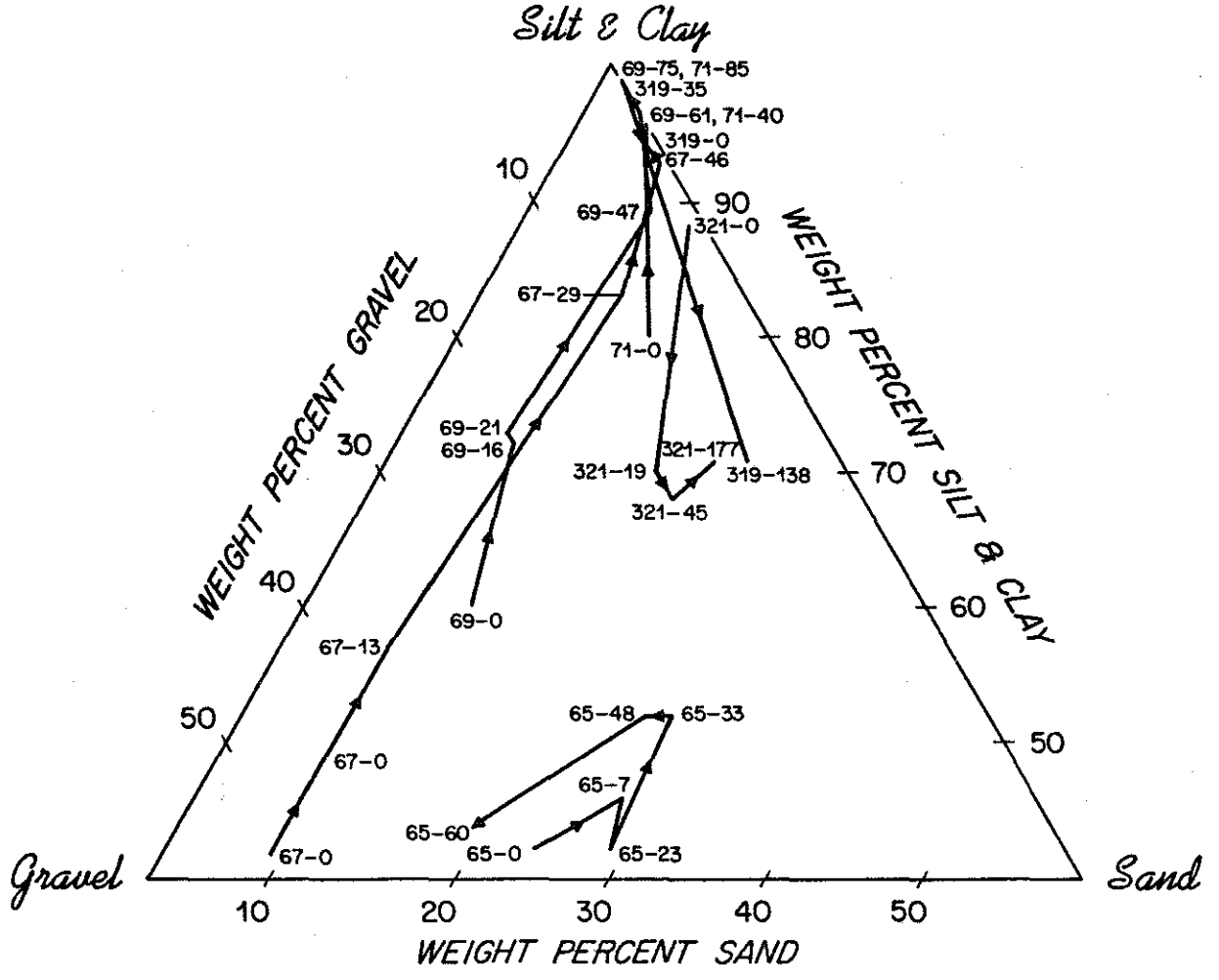
Silt & Clay
69-75, 71-85
319-35
69-61, 71-40
319-0
67-46
69-47
321-0
67-29
71-0
69-21
69-16
321-177
321-19
319-138
321-45
69-0
67-13
65-48
65-33
67-0
65-7
65-60
65-0
65-23
67-0
Gravel
Sand
WEIGHT PERCENT GRAVEL
WEIGHT PERCENT SILT & CLAY
WEIGHT PERCENT SAND
10
20
30
40
50
60
70
80
90

Figure 14

Erosional products of the Brasvellbreen glacier are probably the only major local source carbonate, because bedrock consisting of silicified carbonates and dolomites only occur in the southernmost region of Nordaustlandet (Orvin, 1969). Sediment supplied in meltwater by the present-day glacier or by meltwater released during the surge thus should be identified by an increase in the amount of fine-grained carbonate in core samples. X-ray diffraction (XRD) analysis of the less than 63μm fraction shows that surface sediments close to the glacier contain abundant carbonate (calcite and dolomite), along with quartz (figure 15). The relative amount of feldspar and clay minerals increases with distance from the glacier front, while dolomite remains approximately constant. If station 232 (the core obtained closest to the glacier) is assumed to contain 100% of the glacial-erosion mineralogy, then surface sediments at 22km from station 232 are 50% diluted by other material, while at 44km essentially no input from the glacier is observable in surface sediments (figure 15 and appendix B).

Sediment mineralogy also changes down core. The amount of calcite in the less than 63μm size fraction decreases below 12cm at stations 319 (25km from the glacier) and 321 (30km from the glacier) (appendix B). Core descriptions indicate that limestone makes up most of the gravel fraction above 12cm, but not below. The general coarsening-upward and mineralogic change observed in these cores outside the ridge may represent deposition from ice rafting and meltwater released during the 1936-1938 surge. If this is true, then 12cm of sediment at a distance of at least 30km are affected by a change in depositional patterns during the surge.

However, this discussion ignores down core mixing by bioturbation and biogenic carbonate contributions, so correlation with the recent surge cannot be confirmed until the cores are dated.

FORMATION OF THE MORPHOLOGICAL FEATURES

The continuous ridge is interpreted as the end moraine deposited during maximum extent of the recent glacier surge (figure 16), although effects from former surges can not be excluded. Evidence that the ridge probably formed as an ice-contact feature during 1936-38 is:

1) The ridge is continuous and subparallel to the recent glacier front.
2) The cross-sectional shape is characteristic of formation in close contact with an ice front, with the steepest slope toward the glacier (Elverhoi et al., 1983).
3) A marked change in bottom morphology occurs across the ridge, shown by all acoustic profiles.
4) Frequency of plough marks dramatically decreases inside the ridge indicating either a shorter period of exposure to iceberg gouging or that gouging was more frequent prior to the ice retreat.

Sediments incorporated in the end moraine are partly pushed up in front of the advancing glacier ("bulldozer effect"; Sugden and John 1976). The gentle slopes of the end moraine surface contrast with 45° slopes observed on submarine push-up ridges in Arctic Canada (Lewis et al., 1977), suggesting that the surface topography may be modified by later sedimentation. An internal reflector is often

Figure 15. Percent of calcite in surface sediments (based on comparison of unweighted peak areas from XRD analysis (appendix B)) vs. distance from station 232. All stations sampled outside of the region shown have zero relative calcite (see appendix B). Inset shows plan view of surface sediment samples. Stippled area is greater than 40% relative calcite, heavy dotted line is 30% and light dotted line is 20% contour.

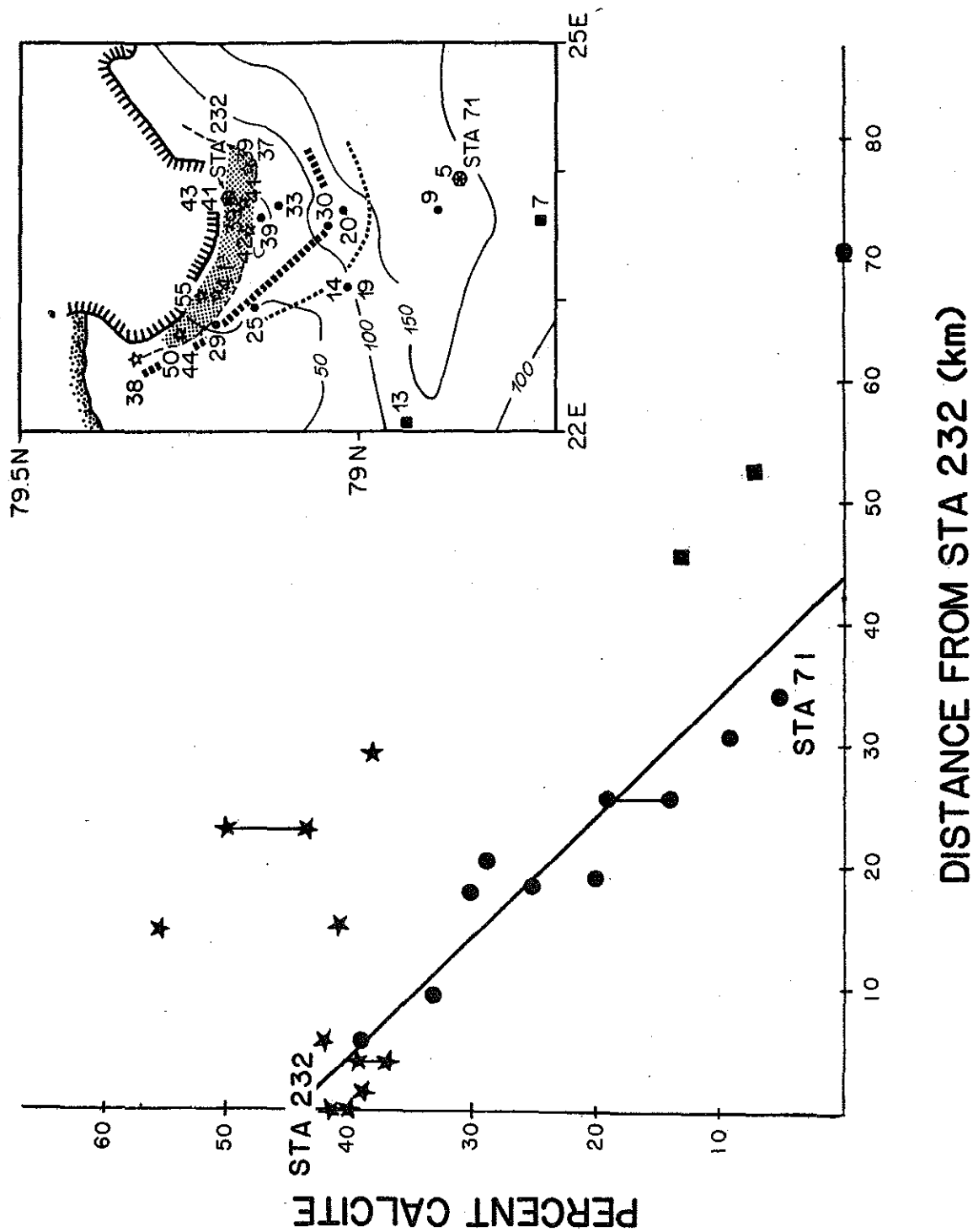
PERCENT CALCITE
DISTANCE FROM STA 232 (km)
STA 232
STA 71
79.5N
79 N
22 E
25E
50
100
150
100

Figure 15

Figure 16. Schematic profiles of Brasvellbreen glaciomarine environment:

A) at maximum extent of the surge (1938)

B) ice disintegration and calving from 1938(?) to 1957(?)

C) at present.

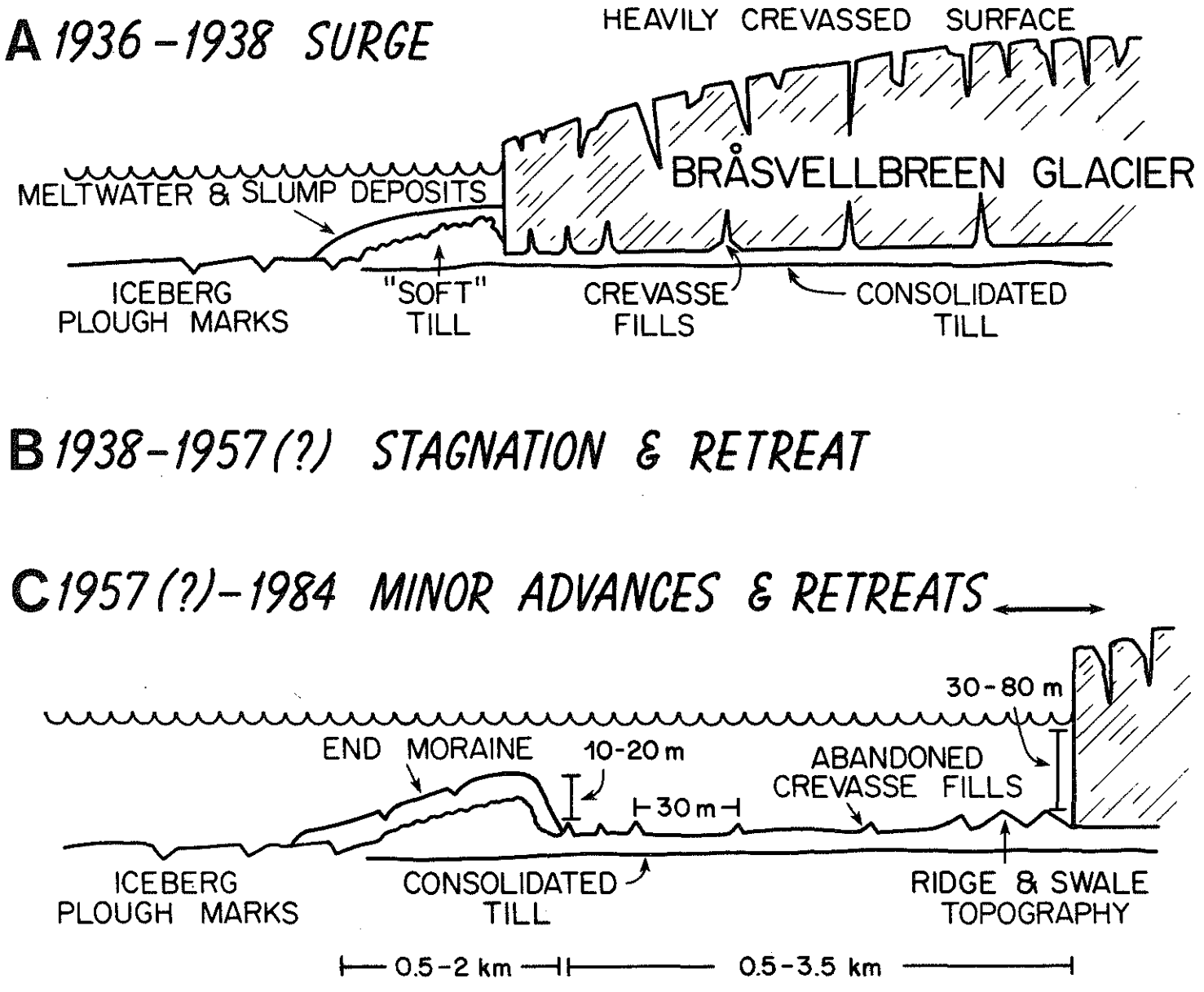
A 1936 - 1938 SURGE
HEAVILY CREVASSED SURFACE
BRÅSVELLBREEN GLACIER
MELTWATER & SLUMP DEPOSITS
ICEBERG PLOUGH MARKS
"SOFT" TILL
CREVASSE FILLS
CONSOLIDATED TILL
B 1938 - 1957 (?) STAGNATION & RETREAT
C 1957 (?) - 1984 MINOR ADVANCES & RETREATS
30 - 80 m
END MORAINE
10-20 m
30 m
ABANDONED CREVASSE FILLS
ICEBERG PLOUGH MARKS
CONSOLIDATED TILL
RIDGE & SWALE TOPOGRAPHY
0.5 - 2 km
0.5 - 3.5 km

Figure 16

covered by draped, acoustically semitransparent sediments in upper and distal parts of the end moraine (figure 7a). The internal reflector could be caused by an acoustic impedence contrast between ice push material and later deposits.

The continuous drape of overlying sediments suggests deposition along the entire ice front during maximum glacier extension. Both theory and field evidence for high rates of meltwater output during a surge indicate high material tranport capacity during a surge (Weertman, 1969; Thorarinson, 1976; Robin and Weertman, 1973; Sugden and John, 1976). Deposition of coarse material from meltwater occurs in close proximity to the discharge location (chapter 4), and may account for the continuous drape of sediment. Slumping (figure 8b) down the distal side probably modified the shape of the end moraine, and caused the abrupt termination observed on seismic profiles (figure 7b and mapped as "outer ridge" figure 9). The presence of slumps indicates unstable conditions caused by rapid deposition and possible oversteepening from glacier push.

The rhombohedral ridge pattern and the irregularly distributed mounds may be an expression of relief in the glacier sole during the surge. Similar features observed on land are inferred to be crevasse fills, formed by squeeze-up of underlying material (Gravenor and Kupsch, 1959; Flint, 1928). In order to preserve these features, Brasvellbreen glacier must have become stagnant and retreated by calving with minimal basal movement after maximum glacial extent (figure 16). Ice stagnation after a surge is also observed for other glaciers (Meier and Post, 1969).

The small, arcuate, discontinuous ridges (figure 10b) near the modern Brasvellbreen glacier are probably caused by minor glacier movements (Andrews and Matsch, 1983 p15). These features are morphologically similar to the swells and swales described by Gwynne (1942) and the washboard pattern of Elson (1957) and Gravenor and Kupsch (1959), which have been interpreted as annual events. The arcuate ridges are only observed in close proximity (less than 1km) to the present-day eastern glacier front (figures 9 and 16).

The two dominant directions for iceberg gouging are parallel and normal to the ice front. These directions are probably determined by currents, wind and bathymetry. A strong, westward, surface coastal current is observed along the ice front (Novitskiy, 1961; chapter 4), while offshore katabatic winds from the ice cap dominate the local wind field. Therefore icebergs should be transported either along the front, or offshore, depending on the relative strength of the wind or current. The western part of the study area is much shallower than the eastern part, so icebergs are either grounded in this region or deflected southward. The most prominent aspect of iceberg gouging, however, is the marked decrease in gouging frequency inside the continuous ridge (figure 9). Since the end moraine crest has variable water depth, it can not represent a barrier to icebergs in general. The decrease in plough mark frequency inside the moraine ridge may be because sea-floor inside the end moraine has only been exposed to marine conditions and drifting icebergs for less than 50 years. Alternately, ice gouging may not occur as frequently now as when the glacier was at its maximum extent. A decrease in the present-day frequency of ice gouging could be caused by a decrease in the size of

recent icebergs or a decrease in calving rate. Since Brasvellbreen probably disintegrated by calving after the surge, the icebergs produced during this time must have been too small to affect the sea floor. At present, only occasional large icebergs are observed in the study area.

Striated gouge patterns (figure 11b) are most likely caused by multi-keeled icebergs. Similar features are described from Arctic Canada by Lewis et al. (1968). Ice gouge "washboard patterns" (figure 11a), described from the Antarctic continental shelf by Lien (1982), are attributed to wobbling of grounded icebergs. The features described from Antarctica are, however, an order of magnitude larger than those observed in the Brasvellbreen study and are caused by tabular icebergs. Wobbling of icebergs by tides or waves may be a possible cause of the washboard pattern outside Brasvellbreen, but the tidal range is less than 1m (USNHO, 1958), and waves generally are small because of sea-ice cover. Another possibility is that the pattern arises from blocks of overconsolidated material that are pushed up during gouging (Barnes and Reimnitz, 1974; Lien, 1983).

DISCUSSION

The sea-floor morphologic features mapped outside the Brasvellbreen glacier may be summarized as follows:

1) A continuous ridge, subparallel to the glacier front at a distance of 0.5 to 3.5km, is interpreted as the end moraine deposited during maximum extent of the glacier surge in 1936-38. A part of the moraine may have been pushed up as the glacier advanced. However, the

cross-sectional acoustic stratigraphy seen on 3.5 kHz echo-soundings implies that later deposition, probably from basal meltwater, took place all along the surging ice front at the time of maximum glacier extension. Continuous deposition along the ice front during the surge contrasts with the modern sedimentary environment. At present, meltwater is discharged at only two major outlets for the entire Nordaustlandet ice cap (chapter 4). The original shape of the end moraine is partly modified by slumping on the distal flank.

Although sediment contained within the end moraine represents material eroded beneath the glacier during many years prior to the surge, it was deposited during only a few years. Estimates of the end moraine dimensions yield a sediment volume of 0.5 km^3. This volume of material is approximately equivalent to the annual sediment discharge of the Amazon River, which has the third largest sediment discharge of all the world rivers (Milliman and Meade, 1983). If all the material contained in the end moraine was derived from erosion of the bedrock underlying Brasvellbreen (over an area of 1110km^2), the subglacial surface would be lowered by 45cm. Judging from the amount of material moved during this latest Brasvellbreen surge, glacier surges may prove to be important mechanisms in the long-term transport history of glacial sediments.

2) A rhombohedral ridge pattern between the end moraine and the modern glacier may represent accumulation of sediment in crevasses in the glacier sole during the surge. Post-surge ice stagnation with disintegration by calving allowed preservation of these features. The rhombohedral pattern continues up to the western, shallow water ice front, but arcuate ridges forming swell and swale topography are

observed near the modern eastern glacier front. These features are most likely caused by minor, local readvances of the glacier, and indicate an active, though fairly stable glacier margin. A modern, stable glacier margin is consistent with satellite photographs showing no apparent activity since 1976 (chapter 4) and with minor crevassing in the present-day Brasvellbreen glacier observed in aerial photographs. The distribution of the crevasse fills and arcuate ridges indicates that the thicker eastern part of the glacier disintegrated approximately 3km through calving before becoming active. In its westernmost part, the glacier is probably still stagnant. Gradation from crevasse-fill deposits to swell and swale morphology in Pleistocene glacier reconstructions has also been interpreted as a shift from stagnant to active ice conditions (Gravenor and Kupsch, 1959).

3) Iceberg plough marks show two prevailing directions, E-W and N-S, most likely controlled by a combination of a westerly coastal current, offshore katabatic winds and sea floor topography. Plough mark frequency decreases markedly inside of the end moraine, indicating shorter time of exposure to drifting icebergs or a decrease in large iceberg activity since the surge and during disintegration of the surge ice. Striated plough marks are caused by multi-keel icebergs, and "washboard" pattern along plough marks inside the moraine ridge is most likely caused by push-up of small blocks of material during ploughing.

The end moraine and the general distribution of sea-floor morphological features are considered to be related to recent surge activity. The scale of these features may seem small when discussing larger ice sheets, but these morphologic features are important aids in interpreting Pleistocene and older glacigenic shelf accumulations. Orientation and distribution of such structures yield information on the direction and distance of glacier movement and the retreat history of the glacier.

ACKNOWLEDGEMENTS

We thank Robert Oldale, Reidar Lien, Tore O. Vorren and colleagues at the Norwegian Polar Research Institute (NPRI) and Woods Hole Oceanographic Institution (WHOI) for their critical comments on the manuscript. This work could not have been carried out without the cooperation of Captain Terje Langvik and his crew aboard the R/V Lance. This research was partly supported by the Norwegian Marshall Fund for Scientific Research. ARCO Norway, Inc. is acknowledged for financial support to data analysis. NPRI contribution no. 229, WHOI contribution no. 5743.

REFERENCES

Andrews, J.T. and Matsch, C.L., 1983. Glacial marine sediments and sedimentation; an annotated bibliography. Geo Abstracts Ltd., London, Bibliography no. II, 227 pp.

Barnes, P. and E. Reimnitz 1979. Ice gouge obliteration and sediment redistribution event: 1977-1978, Beaufort Sea, Alaska. U.S.G.S. Open File Report 79-848, 22pp.

Belderson, R.H. and Wilson, J.B., 1973. Iceberg plough marks in the vicinity of the Norwegian Trough. Norsk Geologisk Tidsskrift, 53:323-328.

Blake, W., 1962. Geomorphology and glacial geology in Nordaustlandet, Spitsbergen: Vol. I, II. 470pp. Ohio State University Thesis.

Elson, J.A., 1957. Origin of washboard moraines. Geol. Soc. Am. Bull., 68:1721.

Elverhoi, A., Lonne, O. and Seland, R., 1983. Glaciomarine sedimentation in a modern fjord environment, Spitsbergen. Polar Research, 1.

Flint, R.F., 1928 Eskers and crevasse fillings. Am. J. Sci., 15:410-416.

Folk, R.L., 1968 Petrology of sedimentary rocks. University of Texas. Geology 370K, 3831, 383M. 170pp.

Hare, F.F., 1976. Late Pleistocene and Holocene climates: some persistent problems. Quaternary Research 6:507-517.

Holdsworth, G., 1977. Surge activity on the Barnes Ice Cap. Nature 269: 588-590.

Gravenor, C.P. and Kupsch, W.O., 1959. Ice disintegration features in western Canada. J. Geol. 67:48-64.

Gywnne, C.S., 1942. Swell and swale pattern of the Mankato lobe of the Wisconsin drift plain in Iowa. J. Geol. 50:200-208.

Lewis, C.F.M., MacLean, B. and Falconer, R.K.H., 1968. Iceberg scour abundance in Labrador Sea and Baffin Bay; a reconnaisance of regional variability. Proc. of the 1st Can. Conf. on Marine Geotechnical Engineering, Calgary, Alberta:79-94.

Lewis, C.F.M., Blasco, S.M., Bornhold, B.D., Hunter, J.A.M., Judge, A.S., Kerr, J.Wm., McLaren, P. and Pelletier, B.R., 1977. Marine geological and geophysical activities in Lancaster Sound and adjacent fjords. Geol. Surv. Can., Paper 77-1A:495-506.

Lien, R., 1982. Sea bed features in the Blaaenga area, Weddell Sea, Antarctica. Proc. 6th, Int. Conf. on Port and Ocean Engineering under Arctic Conditions, Québec, Canada 1981:706-716.

Lien, R., 1983. Iceberg scouring on the Norwegian continental shelf. Continental Shelf Institute, Norway, Publ. 109, 147 pp.

Liestol, O., 1969. Glacier surges in West Spitsbergen. Canadian Journal of Earth Sciences, 6:895-897.

Meier, M.F. and Post, H., 1969. What are glacier surges? Canadian Journal of Earth Sciences, 6:807-816.

Milliman, J.D. and Meade, R.H., 1983. World-wide delivery of river sediment to the oceans. The Journal of Geology, 91:1-21.

Novitskiy, V.P., 1961. Permanent currents of the northern Barents Sea. Trudy Gosudarstvennogo Okeanograficheskogo Instituta, Leningrad, 64, 1-32, (U.S.N.O. translation 1967).

Orvin, A.K. (1969) Outline of the geological history of Spitsbergen. Skrifter om Svalbard og Ishavet. Nr. 78 Oslo 57pp.

Paterson, W.S.B., 1981. The Physics of Glaciers. Pergamon Press Ltd., Oxford, 380 pp.

Prest, V.K., 1969. Retreat of Wisconsin and recent ice in North America. Geol. Survey Can., Map 1257 A.

Robin, G. de Q. and Weertman, J., 1973. Cyclic surging of glaciers. J. Glaciol., 12:3-18.

Rokoengen, K., 1980. Shallow geology on the continental shelf off More and Romsdal. Description of 1:250,000 Quaternary geology map 6203. Continental Shelf Institute, Publ. no. 105, 49 pp.

Schytt, V., 1964. Scientific results of the Swedish glaciological expedition to Nordaustlandet, Spitsbergen, 1957 and 1958. Part I and part II. Geografiska Annaler, 46:243-281.

Schytt, V., 1969. Some comments on glacier surges in eastern Svalbard. Canadian Journal of Earth Sciences, 6:867-871.

Solheim, A., in prep. Sediment distribution and characteristics outside a grounded, surging glaicer, Brasvellbreen, Svalbard.

Sugden, D.E. and John, B.S., 1976. Glaciers and Landscape. A Geomorphological Approach. Edward Arnold Publishers, London, 376 pp.

Thorarinsson, S., 1969. Glacier surges in Iceland, with special reference to the surges of Bruarjokull. Canadian Journal of Earth Sciences, 6:875-882.

U.S. Navy Hydrographic Office 1958. Oceanographic Atlas of the Polar Seas; Part II Arctic. H.O. Pub. No. 705. 137pp.

Weertman, J., 1969. Water lubrication mechanism of glacier surges. Canadian Journal of Earth Sciences, 6:29-939.

CHAPTER 4

Input, Dispersal and Deposition of Glacial Sediment from Meltwater Plumes

Stephanie L. Pfirman
Woods Hole Oceanographic Institution
Woods Hole, Massachusetts

ABSTRACT

During Pleistocene deglaciations marine environments dominated by glacial meltwater were common on northern continental shelves. Suspended sediment supplied by meltwater to the open-marine environment is subject to coastal processes of larger scale than the restricted fjord-glacier environments that have been studied to date. Sediment-laden meltwater plumes were investigated at two localities along the open-marine glacier front of Nordaustlandet in the Svalbard archipelago. Suspended sediment concentrations decrease by at least an order of magnitude to normal Barents Sea levels within 18km offshore from the glacier front, but fine-grained sediment suspended in the plumes is advected at least 30km along the ice front in a westward coastal current. An 18km glacial surge in 1936 and recent glacial movements have reworked surface sediments near the outflow location and precludes clear definition of present-day depocenters. A model for meltwater plume dispersal and sediment deposition is developed in order to examine possible depositional patterns. This model is consistent with observed currents and suspended particulate concentrations, and predicts areal distribution and sedimentation rates for meltwater-dominated glaciomarine environments in Pleistocene and ancient glacial deposits.

INTRODUCTION

Surficial sediments of glaciated continental shelves reflect depositional and erosional conditions during deglaciation, when glaciers terminated as tidewater glacier fronts or ice shelves (Denton and Hughes 1981, Rust and Romanelli 1975). The volume of freshwater released in meltwater and by calving of icebergs during Pleistocene deglaciation may have been 1.5–2.0 times the freshwater supplied by the Amazon River (Jones and Ruddiman 1982). Glacial theory (Shreve 1972) and observations of Pleistocene outwash deposits (Rust and Romanelli 1975) indicate that meltwater from the glacier surface is often channeled into drainage networks at the base of the glacier, with discrete outflow points into the sea. When basal meltwater is present, 90% of glacial sediment transport occurs through outwash (Hagen et al. 1983). Deposition of suspended sediment discharged to the open sea in outflows of glacial meltwater is an important part of the glacial sedimentary cycle, and it is this phenomenon that is investigated in this study.

Previous investigations of modern glaciomarine environments have concentrated on the special conditions of the Antarctic continental shelf and fjord-glaciers of Alaska, Canada, and Norway. Biogenic deposition and low meltwater discharges characterize the modern Antarctic glacier margins (Anderson 1983). Although deposition from meltwater is important in fjord-glacier environments, sediments are largely trapped within the fjord (Farrow et al. 1983, Powell 1980). Important results from these studies are: 1) suspended sediment supply

is highly variable and is dependent on variations in meltwater discharge (Collins 1979) and glacial erosion (Elverhoi in press); 2) flocculation, pelletization, and agglomeration of fine-grained particles greatly increases sediment settling rates in the fjord environment (Syvitski and Murray 1981, Syvitski 1980); 3) meltwater may be discharged subaqueously through tunnels at the base of a glacier (Edwards 1978) or may migrate within the glacier up to sea level at some distance from the discharge point (Elverhoi et al. 1980); and 4) suspended sediment concentrations in meltwater outflows are rarely high enough (greater than the required 38g/l) to cause density underflows of turbid freshwater beneath seawater (Powell 1980, Gilbert 1978, Hoskin and Burrell 1972).

The northern Barents Sea environment today is similar to Pleistocene glaciated shelves. The open-marine area close to the Nordaustlandet ice dome (Svalbard Archipelago) is presently dominated by deposition of suspended sediment from meltwater plumes. Suspended sediment supplied via these plumes and its dispersal in the coastal environment is mapped in this study from Landsat satellite images and direct measurements. Recent glacial activity has reworked the surface sediments in this region (chapter 3); therefore the distribution of glaciomarine sediments observed in cores and acoustic profiles is not representative of modern conditions. However, processes controlling deposition can be analyzed using a plume model for dispersal and sedimentation, with variable freshwater supply and oceanographic conditions. The bulk of sediment suspended in meltwater outflow is both predicted and observed to be deposited close to the ice front,

but fine-grained sediments are transported alongshore in a westerly coastal current.

Study Area: Nordaustlandet

Nordaustlandet is the second largest island (14,600 sq.km) in the Svalbard Archipelago, located at the northwestern edge of the epicontinental Barents Sea. It is largely covered by an ice dome (figure 1) with maximum thickness greater than 550m near its northern boundary (Schytt 1964). Ice thickness decreases towards the southeastern glacier margin. The glacier is thought to be at the pressure melting point in the interior because of its thickness, while the perimeter may be frozen to the base (Schytt 1964, Hollins in prep.). The ice dome mostly overlies Caledonian crystalline rocks in the north and Jurassic silicified limestones and dolomites in the south (Orvin 1969).

The Nordaustlandet glacier is grounded along its entire length of 200km, making it the most extensive marine glacier in the northern hemisphere. The glacier front reaches maximum thicknesses of 130m with 5 to 30m above sea level, and 0-100m below sea level. Water depths along the ice front increase from less than 30m near western Brasvellbreen to more than 100m in the east, but bathymetry is well known only in the western area (figure 1 and Chapter 3, Kristoffersen et al. in press). Erik Eriksen Strait is 150m deep south of Nordaustlandet, and increases to greater than 300m deep to the east. The sea-floor gradient from Nordaustlandet south to Erik Eriksen Strait averages 0.2°.

Figure 1. Study area in southwest corner of Nordaustlandet, the Svalbard Archipelago. Region of Nordaustlandet glacier which was involved in the surge is delineated by heavy dashed line. Exposed land is stippled. Crosshatching in front of Brasvellbreen delineates end moraine deposited by 1936-1938 glacier surge. Stations connected by solid line are from 1980 survey, dotted line 1981 (and 1982) survey.
Stations numbered 0-100 obtained in 1980.
Stations numbered 100-199 obtained in 1981.
Stations numbered 200-299 obtained in 1982.
"A" indicates major western outflow.
"B" indicates minor western outflow.
"C" indicates major eastern outflow.

STATION LOCATIONS

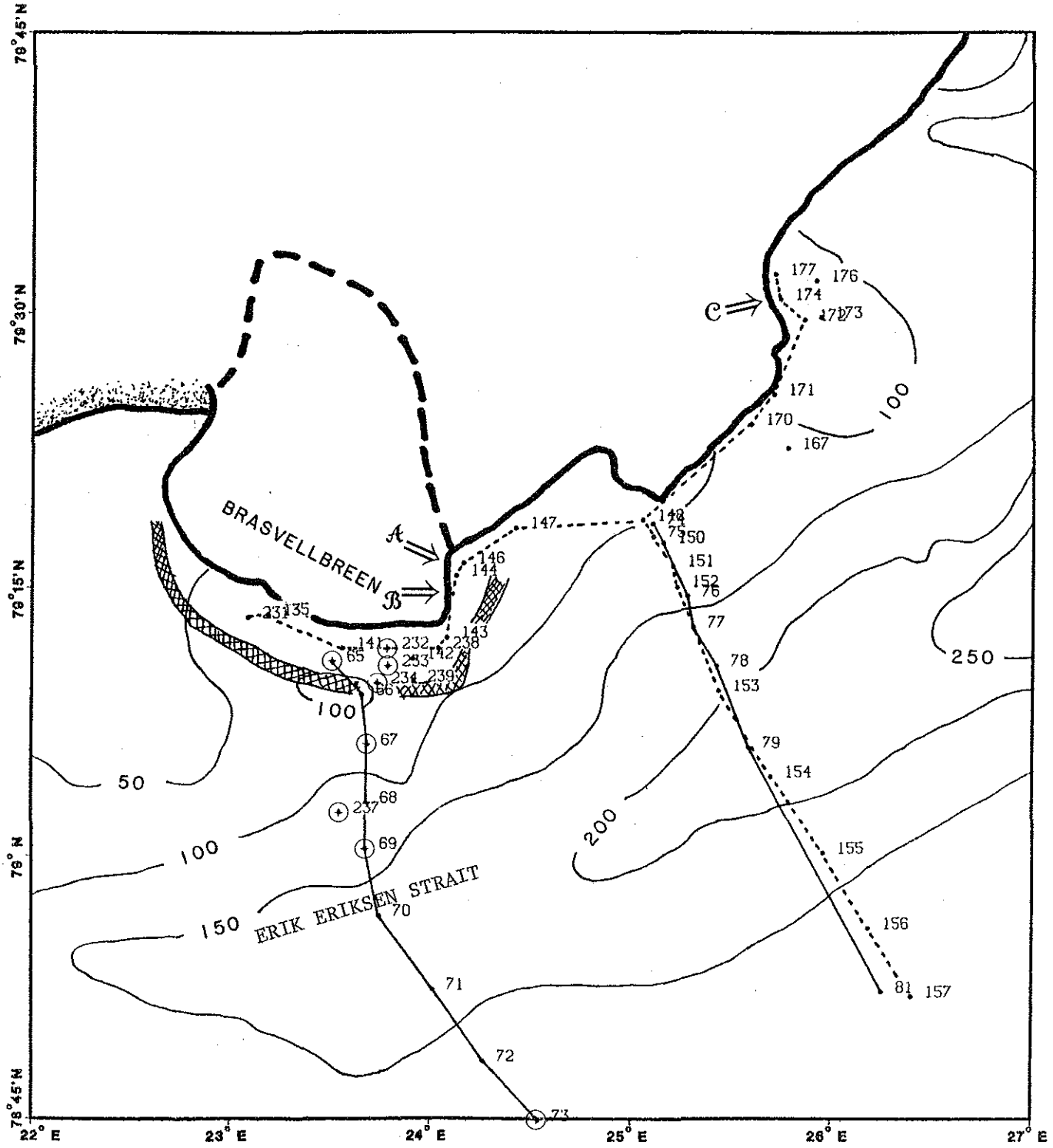

Figure 1

Brasvellbreen glacier, the southwestern sector of the Nordaustlandet ice dome, surged 18km between 1936 and 1938 (chapter 3; Schytt 1964). During the surge, large quantities of sediment-laden meltwater were probably discharged along the base of the glacier (chapter 3), contrasting with the present situatation where meltwater outflow is limited to two major discharge locations. A ridge composed of ice push material, meltwater deposited drape, and mass flow sediments was deposited at the outermost extent of the surge (figure 1 and chapter 3). By 1957 the ice front had retreated 0.5-3.5km to approximately the present position (Blake 1962). Sea-floor in the surge zone has only been exposed to marine conditions since sometime after 1938 and before 1957 (46-27 years ago). There does not appear to have been comparable glacier activity along the eastern Nordaustlandet glacier front (Blake 1962). Minor recent advances and retreats of the glacier front (perhaps annual oscillations) have formed a ridge and swale topography within 1km of the present ice front.

MATERIALS AND METHODS

Processes affecting dispersal and deposition of suspended sediment from meltwater plumes were investigated through analysis of the modern suspended sediment distribution. Twenty three Landsat images (band 4 obtained in 1976-1981) showed the location of major turbid meltwater discharges and variablity of the surface plumes

(figure 2). Width of the western plume was measured at 1km intervals downstream on 5 satellite photographs (figure 3). Frequent clouds and sea-ice precluded similar examination of the eastern plume, but average widths do not appear to differ from the western plume. Aerial photographs and shipboard observations at the discharge locations provided more details of plume behavior.

The water column was sampled along transects perpendicular to the glacier front in August of 1980, 1981, and 1982 (figure 1). Extensive sea-ice prohibited sampling of the plume sources in 1980 and 1982; one section parallel to and 0.5-1.0km from the glacier wall was obtained in 1981. CTD casts (conductivity, temperature, and depth with a Neil Brown CTD) were obtained at 60 stations. Geostrophic velocity was calculated for hydrographic sections perpendicular to the glacier front assuming zero velocity at the deepest station pair on each section. The calculated velocities indicate regions of current shear and are not absolute since no current meters were deployed in this region.

Suspended particulate matter (SPM) was measured by 72 light attenuation profiles (Montedoro-Whitney TMU transmissometer with one meter folded path length and white light source), and one to five water samples were filtered on 0.45μm Millipore filters at each station. Light attenuation was correlated with concentrations obtained from filtered water samples and is converted to concentration units (mg/l) (appendix C). Thirty SPM samples were analyzed for content of combustible organic material, and sediment grain size was estimated by microscopic examination of 54 filters from 17 stations

Figure 2. Satellite images of Nordaustlandet glacier and surrounding Barents Sea,

A. Landsat satellite photograph from 23 July 1976 showing western and eastern meltwater plumes (band 4).

B. Landsat satellite photograph from 7 September 1980 of survey area (band 4). Sea-ice in Nordaustlandet Coastal Current shows large eddies and current dimensions.

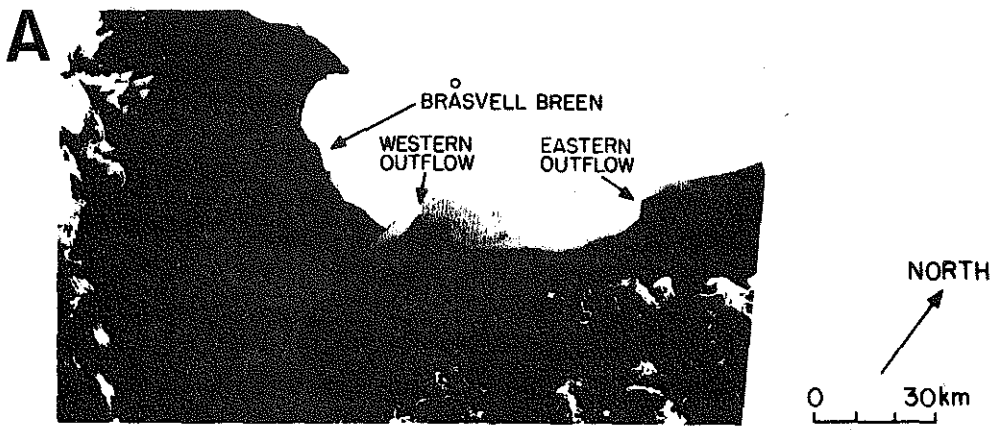
A
BRASVELL BREEN
WESTERN OUTFLOW
EASTERN OUTFLOW
NORTH
0
30km

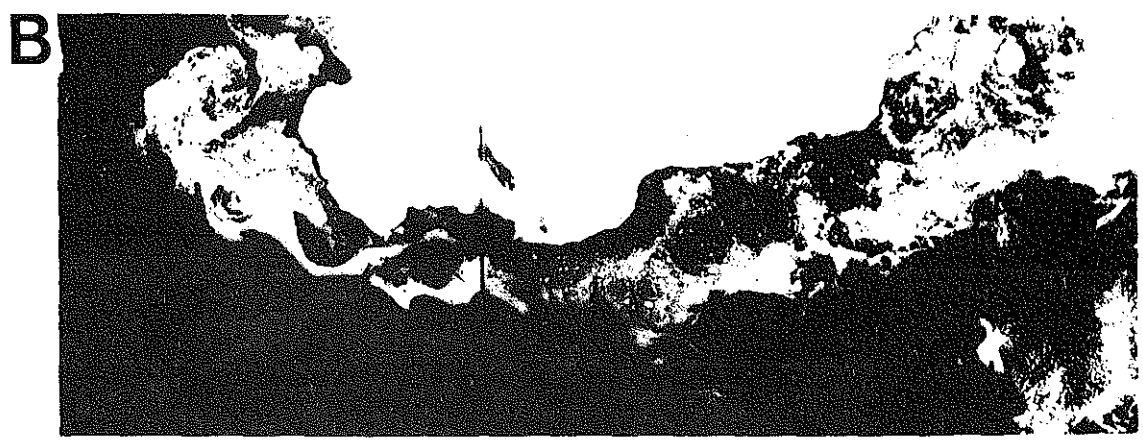
B

Figure 2

Figure 3. Average width of western meltwater plume based on 5 satellite photographs. Diamonds at 10.5km represent 90° corner in ice front discussed in the text.

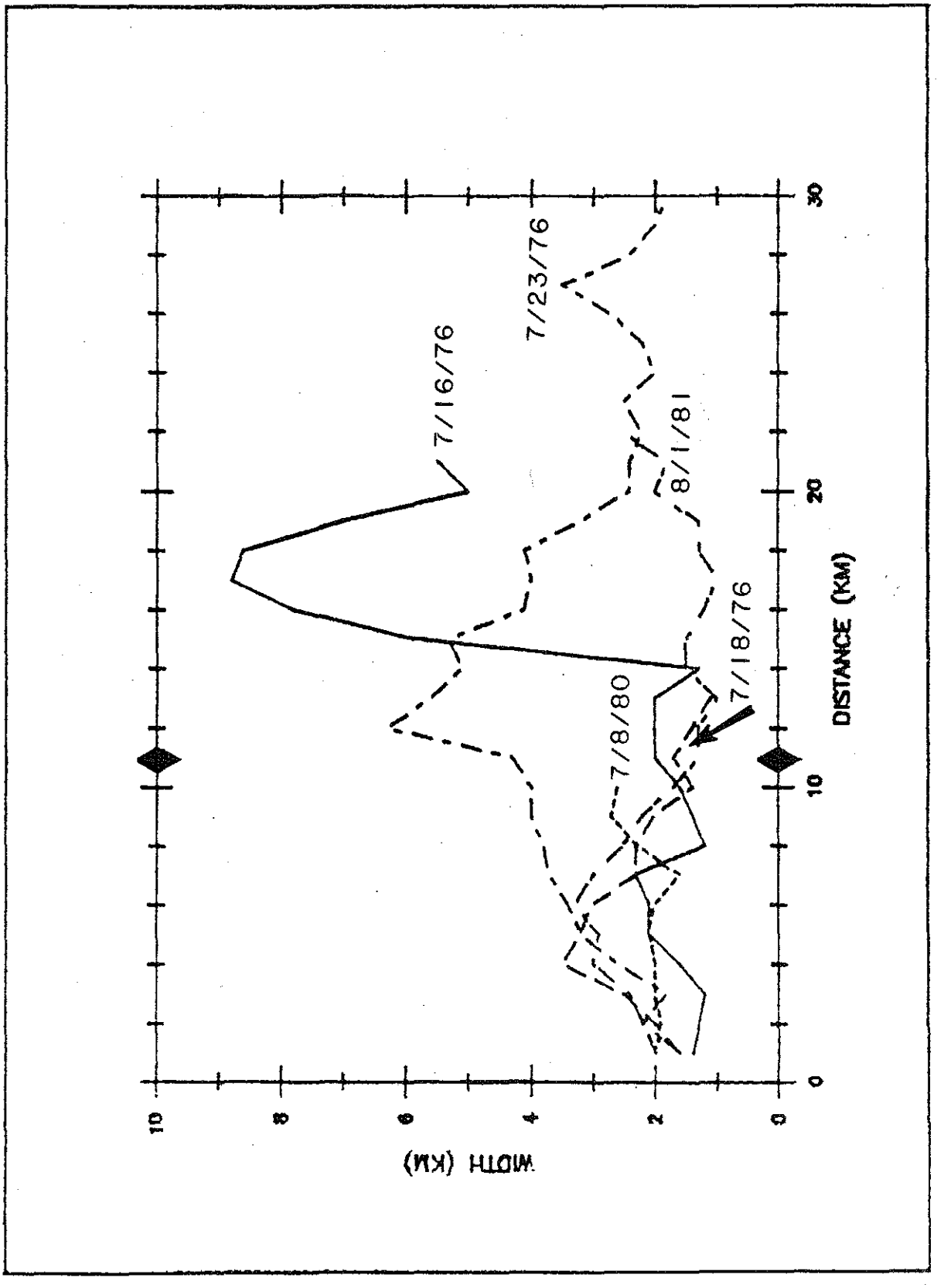
WIDTH (KM)
0
2
4
6
8
10
DISTANCE (KM)
0
10
20
30
7/16/76
7/23/76
8/1/81
7/18/76
7/8/80

Figure 3

(appendix C). The largest diameter of mineralogic grains was measured at 2μm intervals, beginning at 2μm. 50 to 150 grains were measured on each filter by counting the number of grains in each size class in 10 fields. Weight percent in each phi size class was calculated by assuming a density of 2.65g/cm^2, spherical particles, and ignoring contribution by grains smaller than 2μm.

Forty four sea floor samples were obtained in the vicinity of Brasvellbreen by a combination of vibracores, gravity cores, grab samplers, and dredges (figure 1); 19 of these stations also included bottom photographs. Results of textural of the top 5cm of nine sediment samples are discussed in this paper. For mineralogic analysis and further discussion see chapter 3 and Solheim (in prep.).

Sediment texture statistics for material in suspension and on the sea floor were calculated by the method of Folk (1968). These statistice are heavily dependent on the number of large grains observed on each SPM filter. Since large grains are often under-sampled, the statistics should be used with caution. Grain size is reported in ϕ units:

$$\phi = -\log_2(\text{size(mm)})$$

Mean grain size is calculated from a cumulative percentage curve, beginning with the coarsest samples (from small to large ϕ size classes). The 16th, 50th, and 84th percentiles are required:

$$M_z = (\phi 16+\phi 50+\phi 84)/3$$

TABLE 1

ϕ	Grain Size(μm)	Description
-1	2000	gravel
0	1000	very coarse sand
1	500	coarse sand
2	250	medium sand
3	125	fine sand
4	63	very fine sand

TABLE 1 (continued)

ϕ	Grain Size(μm)	Description
5	32	coarse silt
6	16	medium silt
7	8	fine silt
8	4	very fine silt
9	2	clay

Sediment dispersion (or sorting) is a measure of the sorting of the sediment sample. The 5th, 16th, 84th and 95th percentiles are required:

$$\sigma_I = (\phi 84-\phi 16)/4 + (\phi 95-\phi 5)/6.6$$

TABLE 2

$\sigma_I(\phi)$	Description
→0.35	very well sorted
0.35–0.50	well sorted
0.50–0.71	moderately well sorted
0.71–1.00	moderately sorted
1.00–2.00	poorly sorted
2.00–4.00	very poorly sorted
4.00→	extremely poorly sorted

Sediment skewness is a measure of the symmetry of the distribution:

$$Sk_I = (\phi 16+\phi 84-2\phi 50)/2(\phi 84-\phi 16) + (\phi 5+\phi 95-2\phi 50)/2(\phi 95-\phi 5)$$

Skewness is particularly sensitive to the presence of a few large grains which are difficult to sample without sediment traps. Therefore, although skewness is a useful parameter for discussion, absolute values determined by these methods cannot be strictly interpreted.

TABLE 3

Sk_I	Description
+1.00 - +0.30	strongly fine-skewed
+0.30 - +0.10	fine-skewed
+0.10 - -0.10	near-symmetrical
-0.10 - -0.30	coarse-skewed
-0.30 - -1.00	strongly coarse-skewed

Acoustic profiles consisted of 400km of 3.5khz echo sounder records (hull mounted O.R.E. transceiver with EPC 3200 analog graphic recorder) and 150km of side-scan sonar data (Klein, operated at 50khz) in the Brasvellbreen area (figure 1). Analysis of these acoustic profiles is reported in more detail in Chapter 3.

RESULTS

SUSPENDED SEDIMENT

Distribution of the turbid outflow plume in surface waters:

Landsat images of the northwestern Barents Sea show the region near Nordaustlandet to be covered by extensive sea-ice from November to May (chapter 2), with patchy sea-ice during the summer. Turbid water begins to discharge from the glacier front in July and ceases in September. Seasonality in the discharge indicates that a substantial portion of basal meltwater comes from melting of the glacier surface during July and August. A similar ablation season is observed on western Svalbard (Elverhoi et al. 1980) and western Nordaustlandet (Glen 1941).

Two major meltwater outflows are present each year in the same locations (figure 3a) and they are located in embayments of the ice front. Embayments form near meltwater outflows because the flow of water along the glacier base increases ice calving (Wright 1887, Powell 1980, Weertman and Birchfield 1982). Another peculiarity of the outflow region is that the glacier front often is 20m thicker, forming a dome-like structure over a 50m wide indentation or tunnel at the sea surface. Turbulent turbid water discharges from the tunnel, forming eddies at the sea surface. Birds feed at meltwater outflow points, as well as seals and whales, because of an increase in productivity in the outflow region (the so-called "brown zone" of Hartley and Dunbar (1937)).

Turbid water emanating from the embayments is generally deflected to the west, along the tidewater glacier front. The western plume discharges from the eastern margin of Brasvellbreen glacier (figure 2). Turbid surface water of the western plume spreads to a width of 1.8km within 1km from the ice front (figure 3). Four kilometers downstream the plume is 2.5km wide and maintains this width up to 10km from the outflow location. The width of the eastern plume appears in at least one satellite photograph (figure 2), to have approximately the same along-glacier distribution. The major difference between the two plumes is that near a 90° corner in the Brasvellbreen glacier (10km downstream) the western plume often separates from the ice front. The separation from the glacier front could be because the current is following the bathymetric contours which are also perpendicular to the ice front near the 90° corner

(figure 1). The western sediment plume spreads and becomes less distinct in the downstream region, sometimes forming large (15km diameter) eddies (figure 2).

Coastal hydrography:

Meltwater plumes observed in satellite photographs are deflected to the west; therefore they must be discharged into a westerly coastal current which has higher velocity than the local tidal current. Hydrographic transects obtained in August 1980 and 1981 (figures 4 and 5) show that a coastal water mass exists which is nearly isothermal (averaging 0°C). The coastal water mass is less saline at depth than the water in nearby Erik Eriksen Strait, causing downwarping of isohalines and isopycnals along the slope. Based on this hydrographic structure a westerly geostrophic current is calculated from the 1981 data (figure 4 and appendix A). The current is approximately 20km wide parallel to the glacier, with an outer limit centered over the 100m isobath (figure 4). Relative current shear increases toward the west from 4cm/sec on a transect north of Kong Karls Land, to greater than 16cm/sec near the western border of Brasvellbreen (appendix A). The coastal current transports both suspended sediment discharged in meltwater outflows (figure 2a) and sea-ice along the Nordaustlandet glacier front (figure 2b).

Surface waves are generally small in this region because of the perennial sea-ice cover.

Figure 4. Eastern hydrographic of eastern transect from 1981 obtained perpendicular to the Nordaustlandet glacier front. Station numbers are labelled across the top of each transect (location on figure 1, north is to the left):

A. temperature°C). The Nordaustlandet Coastal Current, surface water, Arctic Water (ArW), and Atlantic Water (AtW) are labelled.

B. salinity °/₀₀)

C. sigma-t

D. geostrophic velocity (cm/sec). Negative numbers indicate westward velocity (transect location figure 3b).

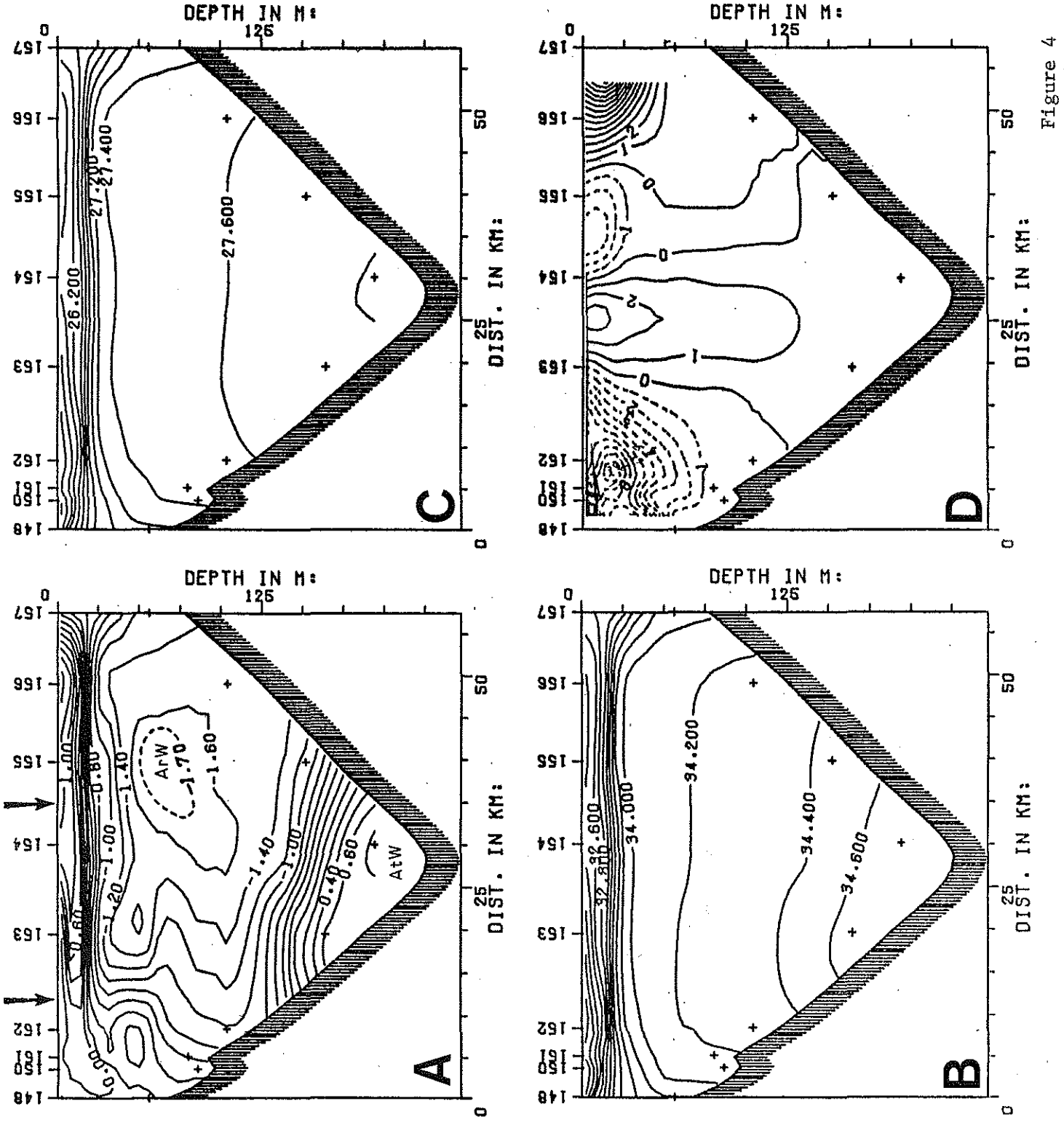
NORDAUSTLANDET COASTAL CURRENT SURFACE WATER
DEPTH IN M:
DIST. IN KM:
A
B
C
D
ArW
AtW
-1.70
-1.60
-1.40
-1.00
-0.80
-0.60
-0.40
-0.00
34.200
34.400
34.600
34.000
32.800
32.600
27.600
27.400
27.200
26.200

Figure 4

Figure 5. Transects obtained in 1980 perpendicular to ice front (locations on figure 1, north is to the left).

A. eastern transect temperature

B. eastern transect suspended matter. Calibrated attenuation is contoured, concentration of SPM from filtered waters samples are in italics

C. eastern transect percent non-combustible SPM

D. western transect temperature

E. western transect suspended matter

F. eastern transect percent non-combustible SPM

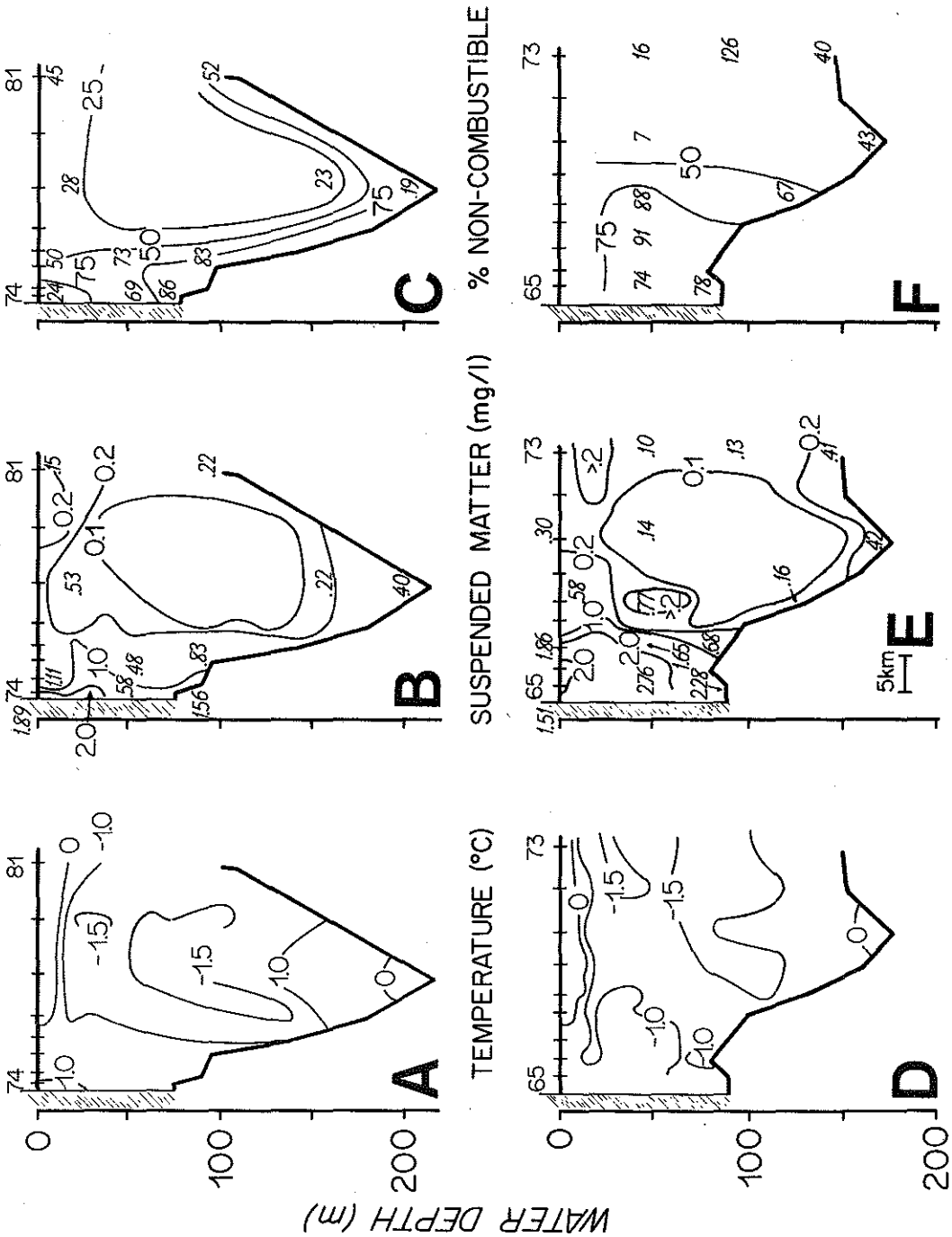
WATER DEPTH (m)
TEMPERATURE (°C)
SUSPENDED MATTER (mg/l)
% NON-COMBUSTIBLE
A
B
C
D
E
F
5km

Figure 5

Suspended sediment distribution:

The maximum concentration observed in a suspended matter sample at the eastern outflow was 15mg/l, and at the western outflow the maximum was 28mg/l (figure 6). Both samples are from the surface of the water column at stations located approximately 100m from the glacier front near the meltwater outflows. Average concentrations decrease rapidly within the first 3-5km westward along the ice front, downstream from the discharge locations (figure 6), although maximum plume concentrations may not have been sampled downstream because of difficulties in locating and sampling the plume axis. Concentration of SPM decreases downstream because the plume widens (figure 3) and coarse material settles from suspension. Suspended matter concentrations average 3.5mg/l west of the eastern plume (figure 6). The western meltwater outflow does not have a downstream extension of turbid water along the ice front, probably because the plume separates from the glacier wall as it passes the 90° corner as discussed above (figure 2). Suspended sediment appears to be transported southwards, out of the transect.

Two suspended matter profiles obtained in 1980 perpendicular to the ice front and west (downstream) of the outflow locations show the general cross-sectional features of the plumes (figure 5). Suspended sediment distribution for the eastern transect was similar in 1980 and 1981. Maximum concentrations, greater than 2mg/l, occur at stations closest to the glacier. These samples contain greater than 75% noncombustible material. Concentrations decrease offshore and reach normal Barents Sea background values (less than 0.2mg/l and less than

25% noncombustible material) at approximately 18km. This offshore distance corresponds to the outer limit of the coastal current defined by the 0°C isotherm (figures 4 and 5), suggesting that sediment supplied to the coastal current from meltwater plumes is not transported directly into Erik Eriksen Strait. However, glacial material originally deposited near the glacier may be transported offshore as well as alongshore by bottom currents, since near-bottom nepheloid layers occur in all transects perpendicular to the glacier front.

The turbid-water front observed in satellite photographs may be related to a seaward decrease in suspended matter concentration away from the ice front from greater than 2.0mg/l to less than 1.0mg/l (1980). This change occurs at 2km from the glacier on the eastern profile (figure 5b), but is detached from the glacier front on the western profile (figure 5e), as is also shown by satellite images.

Suspended sediment composition:

The two meltwater outflows discharge different sediment mineralogy which aids in distinguishing their sedimentary influence. Suspended sediment in the eastern outflow is composed of iron-stained quartz grains which results in brick-red SPM samples. A likely source for the sediment is rock flour from red sandstones. The western outflow is composed primarily of carbonate mineral grains and chert fragments derived from Jurassic silicified limestone (Orvin 1969). SPM samples obtained at station 144 (the western outflow samples) appear greenish-gray, but the SPM samples obtained downstream still have a slight reddish tinge indicating that some eastern outflow material is still in suspension.

Figure 6. Suspended matter profile obtained (1981 stations begin with 1, 1982 stations begin with 2) parallel to the Nordaustlandet ice front at distance of 0.5-1km (transect location figure 3).

A. Calibrated attenuation is contoured along ice front. Actual concentrations from filtered water samples are in italics.

B. Concentration (mg/l) of SPM samples, line is drawn through maximum concentration at each station. Dots are samples along the ice front, crosses are samples obtained offshore (see figure 1 for station locations).

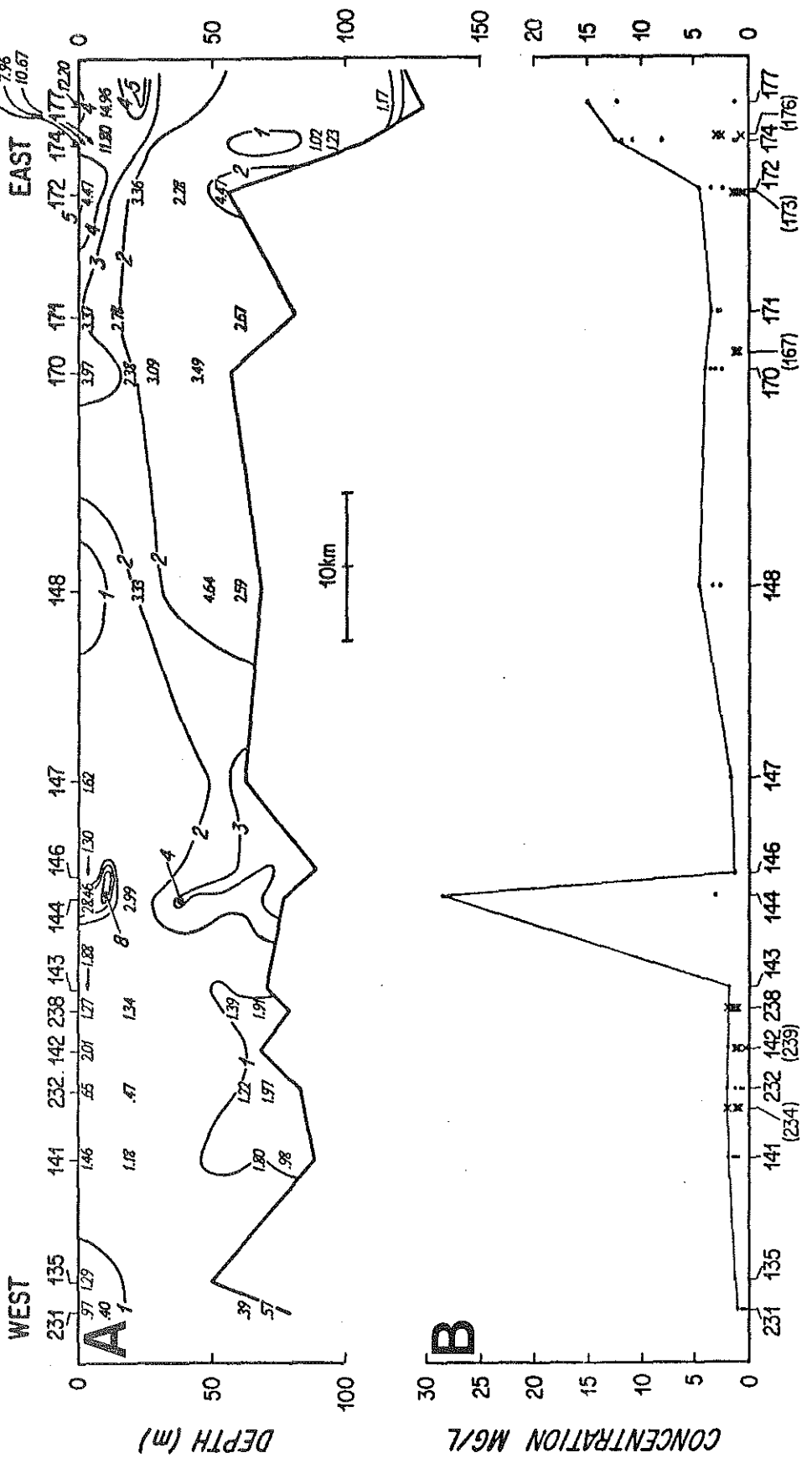

Figure 6

Suspended sediment texture:

On the average, mineral grains suspended in the eastern meltwater plume become finer-grained downstream from the discharge location (figure 7). The eastern plume has grains larger than 32μm only at the discharge location where they constitute 20% (by weight) of the greater than 2μm fraction of suspended matter (figure 7a). Grains of 16μm to 32μm size make up 50% of the greater than 2μm fraction at 2.5km (mean SPM ϕ 6), but have dropped to less than 30% at 10km. This coarse material settles from suspension within the first 10km, after which the grain size and concentration of material in suspension remains fairly constant with a mean size near 6.5ϕ (figures 6 and 7). The SPM samples have a large variation in sorting at a particular station, but a slight trend from moderately well sorted to moderately sorted is observed downstream. Skewness similarly is quite variable, but is generally slightly more positive (fine-skewed) in close proximity to the western outflow (stations 174 and 172). Skewness decreases downstream where the SPM grainsize distribution is near-symmetrical.

Offshore variations in suspended sediment texture are shown by stations 167, 173 and 176. These stations are outside the main axis of the plume and therefore have lower SPM concentrations (figure 6). Stations 176 and 167 have nearly the same mean size as the stations (174 and 170) located near the ice front. Station 173 is slightly finer-grained. Mean sorting for stations 173 and 176 are similar to the inner stations, while station 167 is less sorted. Station 176 has a very large variation in skewness, while stations 167 and 173 are

nearly the same as the inner stations. The offshore stations of the eastern plume do not appear very different from the inner stations, except that they have lower SPM concentrations.

Discussion of suspended sediment texture for the western plume is limited by the number of SPM stations in 1981; only two stations (144 and 141) had SPM samples at several water depths. In 1982 more SPM stations were obtained (231, 232, 234, 238, 239), but only downstream from the meltwater outflow (station 144 - 1981). The concentrations obtained from SPM samples are similar both years (figure 6), so textural data is plotted together (figure 7). Discussion of the western plume is also complicated because the plume appears to be detached from the ice front near the 90° corner (between stations 144 and 143, 238).

Comparison of alongshore suspended sediment texture shows that samples obtained upstream of station 144 in 1981, do not appear very different from station 147. The mean size is not coarser, and the sediments are slightly better sorted and are normally distributed. There is no evidence from the sediment textural parameters that these samples were obtained in a glacier meltwater outflow, except that the SPM concentration is an order of magnitude higher. Station 141 (18km downstream) has approximately the same mean size and sorting as station 144, but is strongly fine-skewed.

The 1982 surface SPM samples (station 238 and 232) are generally much coarser than 1981, bringing the mean size up to 5.85ϕ. Both samples are moderately sorted and station 238 is strongly fine-skewed while station 232 is fine-skewed. Station 231 (28km downstream from

Figure 7. Grain size distribution statistics measured from filtered water samples obtained along ice front in 1981 (and 1982).

A. Histograms of weight percent in 5,6,7,8,9ϕ classes.

B. Mean size (ϕ) of all SPM samples obtained at this station (vertical bars are 1σ)

C. Mean dispersion (ϕ)

D. Mean skewness

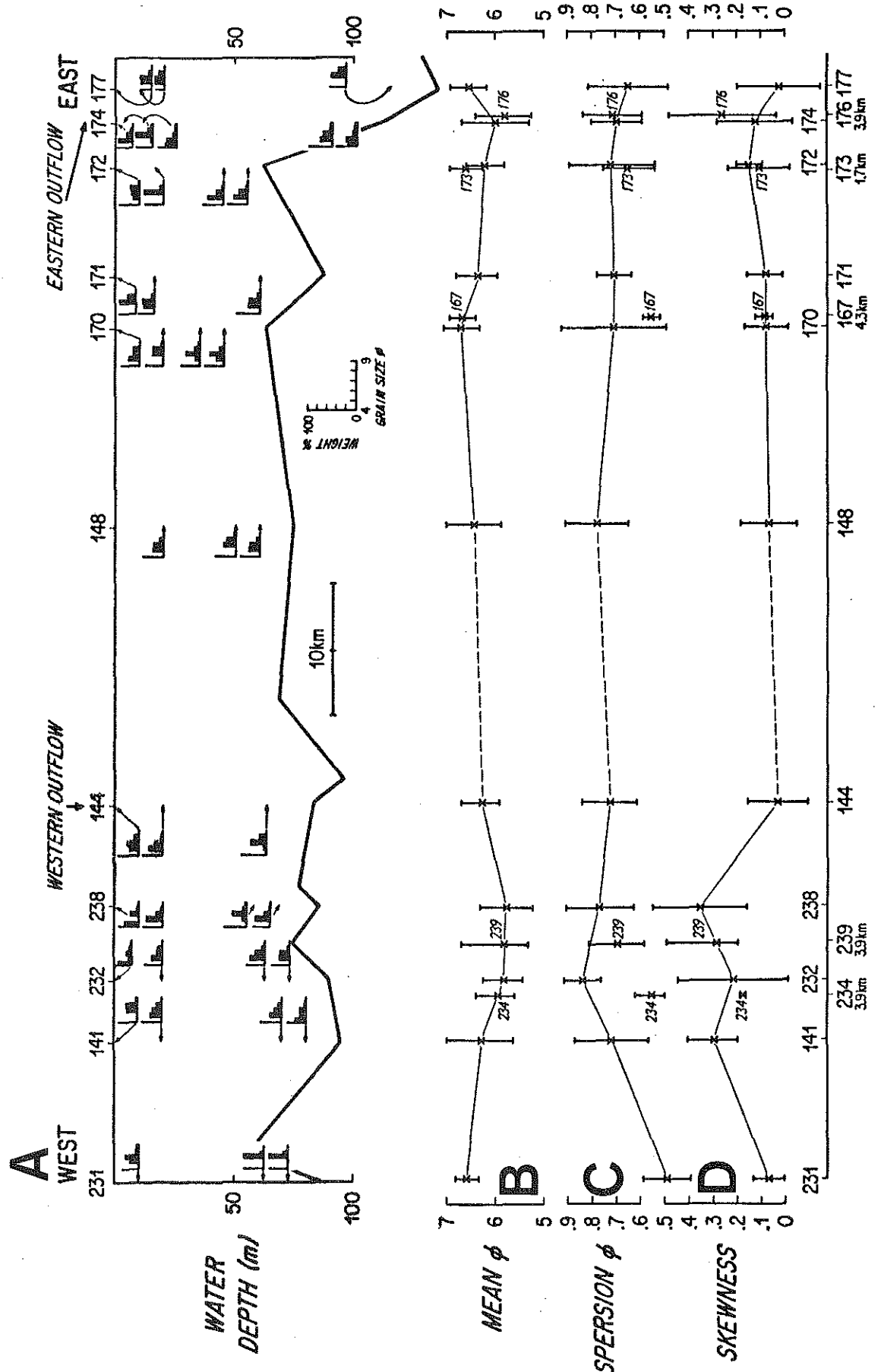
A
WEST
EAST
WESTERN OUTFLOW
EASTERN OUTFLOW
WATER DEPTH (m)
10km
WEIGHT %
GRAIN SIZE ϕ
B
MEAN ϕ
C
DISPERSION ϕ
D
SKEWNESS
231
141
232
238
144
148
170
171
172
174
177
234
239
167
173
176
3.9km
4.3km
1.7km

Figure 7

station 144) is probably out of the plume altogether as seen by the very low SPM concentrations. SPM is well sorted and is nearly normally distributed.

Because the western plume separates from the glacier front near the 90° corner, average SPM samples from stations 239 and 234 (3.9km away from the glacier front) have mean sizes and concentrations similar to the inner stations (figures 6 and 7). These outer stations are less dispersed (moderately well sorted), and have similar skewness as their inner counterparts. Although these textural statistics have large variations, it appears that the SPM samples offshore from the western plume have similar concentration and mean size as the inner stations, but are better sorted. There also may be a downstream trend from fine-skewed toward a more symmetrical distribution.

Suspended matter samples obtained at the western outflow location in 1981 (station 144) do not contain the coarse grains (greater than 32μm) observed downstream in 1982 (figure 7). Three possible explanations for this are that the coarse sediment observed in suspension downstream is resuspended from the sea floor, comes from a different source, or that at the time of sampling (1981) only fine-grained material was supplied by the glacier. Resuspension along the transport path is probably not a likely source for coarse material in suspension because the coarsest samples are high in the water column (figure 7). Turbid water emanating from other outflows is not observed on satellite photographs, but side-scan profiling of the glacier front revealed a small indentation of the ice front, 6km downstream from the major discharge location (figure 2). Coarse

sediment could be discharged at this location, but no water samples from this area are available. Temporal variation in sediment discharge is the most obvious explanation and is discussed later.

SEA-FLOOR SEDIMENT

Sediment deposited from meltwater plumes might be expected to extend as a drape of material westward from the outflow locations with an ice-rafted component superimposed on the meltwater deposits. The region downstream of the western plume was examined through sediment cores and acoustic profiles for evidence of deposition from the meltwater plumes.

Surface sediment texture:

Core samples obtained downstream from the western plume do show a general decrease in mean sediment size, from 2.5ϕ (station 232 and 233, 13.1km downstream from station 144) to 5.4ϕ (station 65, 18.7km downstream from station 144):

TABLE 4

Station	X	Y	Median	Mean	Dispersion	Skewness	%Gravel
232	0.7	13.1	2.495	2.649	3.811	0.034	28
65	1.9	18.7	4.348	3.662	3.505	-0.314	29
233	2.2	13.1	1.883	2.486	3.761	0.181	42
234	3.9	15.5	5.494	4.486	3.287	-0.510	25
239	3.9	11.8	5.476	4.412	3.309	-0.506	20
67	10.6		6.602	5.542	2.739	-0.686	49
237	16.7		6.278	5.386	2.637	-0.568	28
69	21.3		6.778	5.378	2.994	-0.784	25
73	53.3		7.160	6.664	1.393	-0.470	1

(X = distance offshore (km))
(Y = distance downstream from station 144 (km))
Statistics are based on gravel-free deposits (greater than 3mm).

Dispersion decreases slightly from 3.8 to 3.5ϕ downstream and skewness shifts from nearly symmetrical to strongly coarse-skewed at station 65.

An offshore transect of surface sediment samples shows a general decrease in mean size of surface sediments from very fine sand to medium silt at 21km offshore. The dispersion also decreases from very poorly sorted to poorly sorted, while the distribution becomes more coarse-skewed, up to to -0.8 (strongly negatively skewed). However, this offshore transect is probably not representative of modern deposition because of the recent glacier surge (chapter 3). Glaciomarine sediments deposited prior to the surge in 1936-38 were overrun and reworked by the glacier. In order for even 1cm of sediment to accumumlate since 1938 (-1957), sedimentation rates must be very high (20 - 40cm/1000yr). As will be seen later, such high accumulation rates will only occur in the outflow embayments and no cores are available from these regions.

Sea-floor morphology:

Side-scan profiling along the glacier front at the western plume shows an indentation in the ice front which is probably the major outflow tunnel (figure 8). The tunnel is approximately 200m wide at the glacier base and is located below a 50m wide surface indentation, from which high turbidity water emanates. A valley (approximately 20m deep and 800m wide) is located just to the west of the western meltwater outflow. Meltwater drainage of glaciers is predicted to occur preferentially in topographic depressions (Flint

1971, Weertman 1972), suggesting that this valley may continue westward under the glacier and is a conduit for meltwater outflow.

Arcuate ridges of acoustically transparent material are observed within the valley (figure 8). The ridges are similar to others occurring along the ice front downstream, but are at least twice as large in the outflow valley (figure 8). These swales and swells are interpreted to be material pushed up or deposited by the glacier during small advances and retreats (chapter 3). The fact that they are larger in the outflow region may indicate that more unconsolidated material is available. Other than these deposits, the only evidence from acoustic profiling for enhanced deposition in the outflow region is the smoother sea-floor near the tunnel, perhaps caused by recent deposition of sediment.

A small indentation, 50m wide, is observed 6km to the west of the major outflow (figure 9). An accumulation of acoustically transparent sediment is observed on the sea-floor in front of this tunnel. The deposit is 5m high and 400m wide. If this material accumulated since 1936 (-1957), the local sedimentation rate is 5m/(46-27yr) or 10-20cm/yr. However, the surface morphology of the deposit appears similar to the surrounding sea floor, indicating that it may have been deposited before 1936 and perhaps was overrun by the surging glacier.

Several unidentified targets were observed on side-scan profiles in front of the major western outflow (figure 8). They are approximately 40m high and 50m in diameter, and at least one was observed in 1981 as well as 1982. They appear to be discrete mounds

Figure 8. Side-scan sonar (A) and 3.5kHz (B) profiles along ice front (located in front of major western outflow "A", figure 1). Vertical lines on sonograph are due to interference from sparker profiler. Major outflow tunnel is observed as an embayment in the ice front, located to the east of the outflow valley seen on 3.5khz profile.

Several discrete unidentified side-scan targets also appear on this side-scan sonograph and 3.5khz profile. They are approximately 40m high and occur to the east of the outflow tunnel. At present their origin is in question.

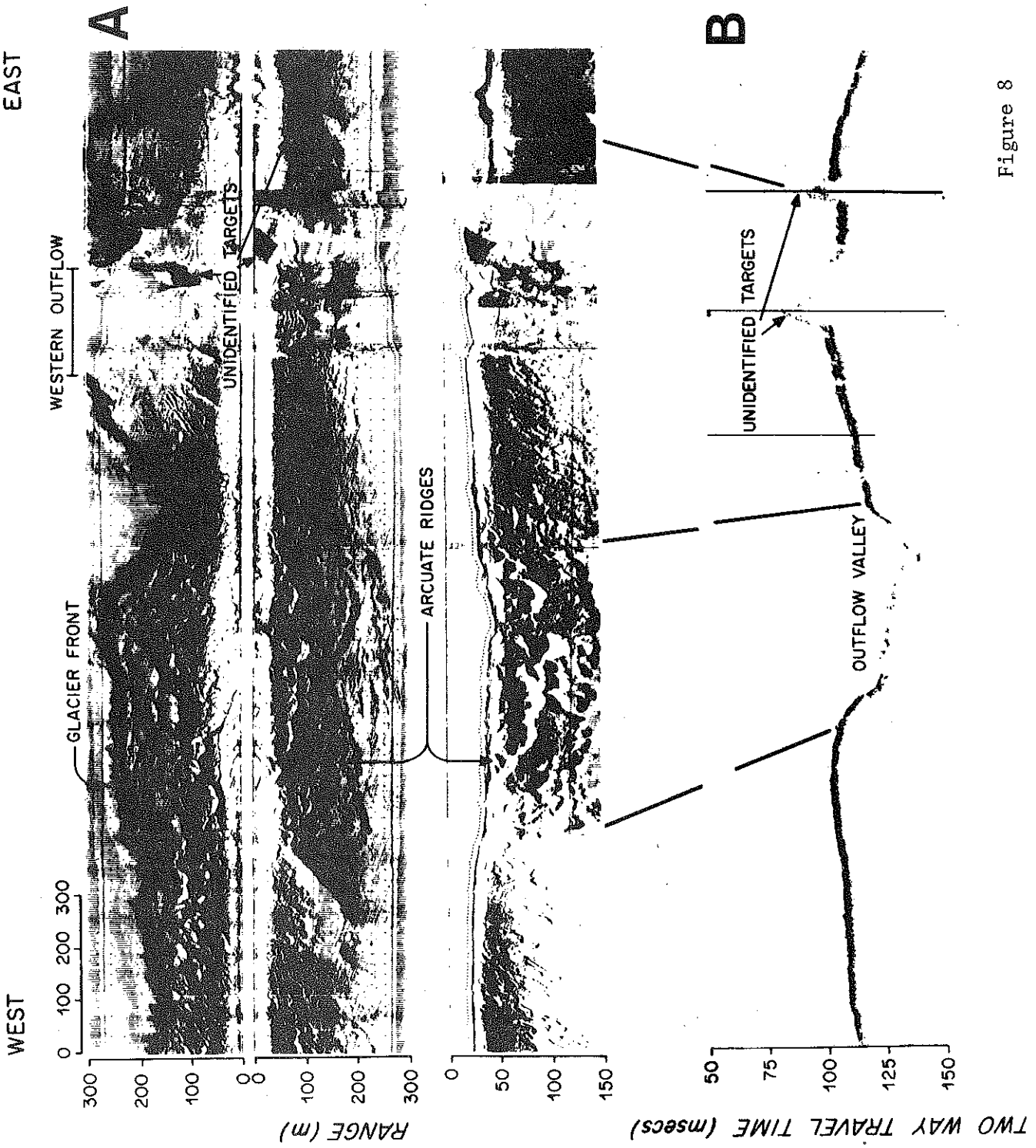
WEST
EAST
A
B
0 100 200 300
GLACIER FRONT
WESTERN OUTFLOW
UNIDENTIFIED TARGETS
ARCUATE RIDGES
OUTFLOW VALLEY
RANGE (m)
TWO WAY TRAVEL TIME (msecs)
300
200
100
0
50
75
100
125
150

Figure 8

Figure 9. Side-scan sonar (A) and 3.5kHz (B) profiles along ice front (located in front of minor western outflow "B", figure 1). Vertical lines are due to interference from sparker profiler. Minor outflow embayment observed in ice front corresponds with sediment accumulation observed on 3.5kHz profile.

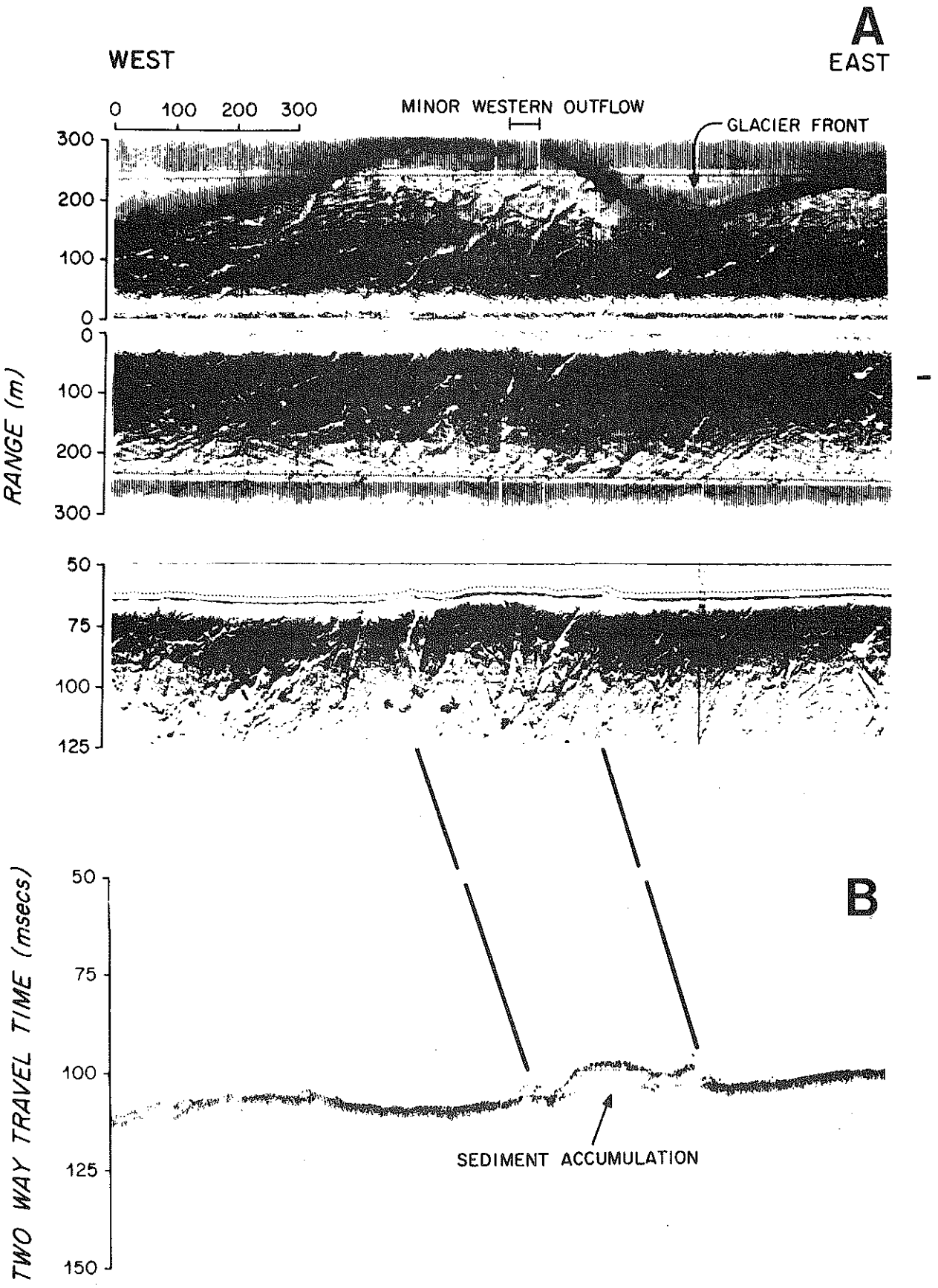
A
WEST
EAST
0 100 200 300
MINOR WESTERN OUTFLOW
GLACIER FRONT
RANGE (m)
300
200
100
0
0
100
200
300
50
75
100
125
B
TWO WAY TRAVEL TIME (msecs)
50
75
100
125
150
SEDIMENT ACCUMULATION

Figure 9

since they cast triangular shadows on the side-scan sonographs, and appear acoustically transparent on the 3.5khz profiles. The transparency and peakedness of the mounds may, however, be caused by side-echoes. The mounds may be composed of bedrock, ice, or sediment. Since the surrounding sea floor is smooth and the bedrock is nearly conformable to the sea surface in this region (Orvin, 1969), the mounds are probably not composed of bedrock. They could be formed by sediment-laden ice, calved from the glacier sole. The coastal current water temperature averages 0°C, which could mean that they would melt slowly. However, the sediment concentration would have to be extremely high in order to weigh down a 40m thick block of ice. The most obvious explanation is that they are mounds of sediment, accumulated in front of the outflow. If this is true, then the sedimentation rate has been extremely high in very localized regions during sporadic glacier retreat. Pleistocene esker deposits are often "beaded" (Flint 1971), perhaps reflecting a similar depositional environment. The very steep angle of repose of the unidentified targets would tend to imply that the deposits are very coarse. Obviously more observations need to be obtained in this region.

MELTWATER INPUT, DISPERSAL, AND DEPOSITION

Because SPM samples are limited at the Nordaustlandet ice front and the glacier surge probably reworked any recent deposits, deposition from meltwater plumes cannot be defined clearly by

available field observations. However, these observations can be used together with knowledge of the local geomorphology and glacier theory for a discussion of general features of the input, dispersal and deposition of suspended sediment from meltwater plumes in the marine environment. Specific questions that can be addressed are: Over what area are sediments deposited from meltwater plumes? What sedimentation rates can be expected? How will grain size distributions from different sources change sedimentation patterns under variable hydrographic conditions? The problem can be separated into consideration of source, near, intermediate, and far field regions (figure 10). Source conditions (A-B-C, figure 10) of interest are meltwater discharge (volume, velocity, and variability) and sediment transport (concentration, grain size, and variability). The near field (C-D, figure 10) concerns injection of material into the water column from a meltwater tunnel and the immediate buoyancy and momentum effects. The intermediate problem examines initial expansion of the plume and deposition of sand. In the far field (D-E, figure 10) a source grain size distribution and concentration is dispersed and allowed to settle from suspension in a coastal current.

Source:

Questions to be answered at the source are how much and what grain size of suspended material can be expected to be supplied via meltwater discharge, and what conditions must occur before the turbid plume is observed at the sea surface in satellite photographs. Behavior of meltwater introduced to the marine environment will depend

Figure 10. Schematic of sedimentary regime near meltwater outflow.

SCHEMATIC OF ICE FRONT

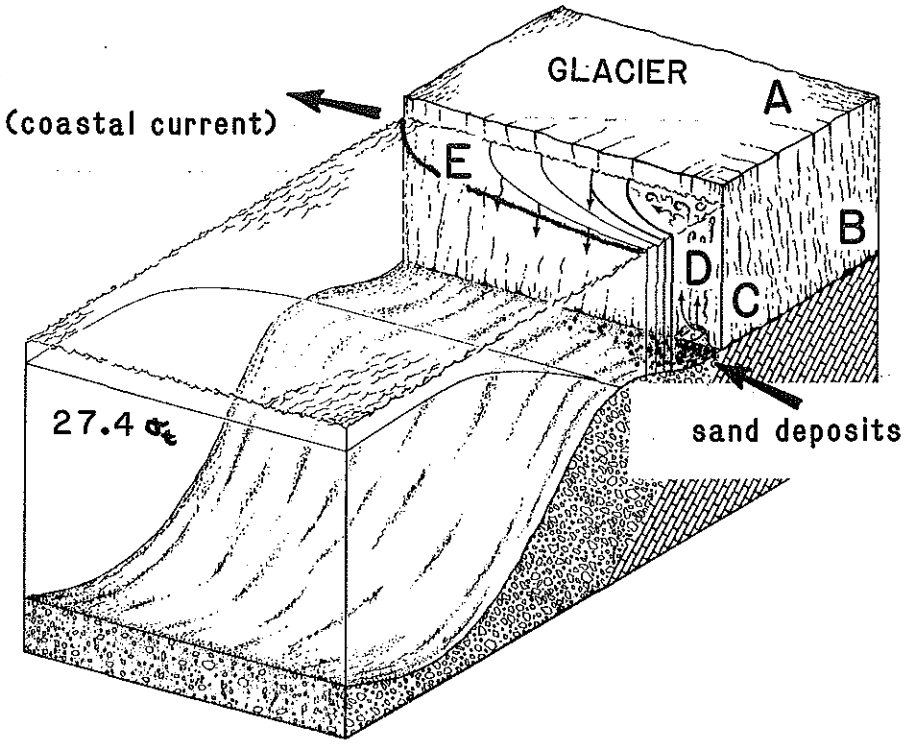

A SURFACE MELTWATER

B SUBGLACIAL STREAMS TRANSPORT GLACIAL EROSIONAL PRODUCTS

C SEDIMENT-LADEN MELTWATER DISCHARGED AT GLACIER FRONT

Near Field:	D SUSPENDED SEDIMENT RISES TO SEA SURFACE IN BUOYANT MELTWATER OUTFLOW	→ TRACTION LOAD DEPOSITS
Intermediate Field:	PLUME SPREADS IN OUTFLOW EMBAYMENT	→ SAND DEPOSITS
Far Field:	E TURBID PLUME ADVECTED IN COASTAL CURRENT	→ SILT DEPOSITS

Figure 10

on the volume discharge of meltwater and sediment, discharge velocity, dimensions of the outflow tunnel, the density difference between the fresh meltwater and the ambient seawater, the marine density stratification, and the coastal current velocity (Brooks 1973, Fischer et al. 1979). Since only the marine density stratification is known, the other parameters are estimated from glacial theory and the geomorphology and glaciology of the Nordaustlandet region.

Discharge of meltwater plus sediment is not known, but may be estimated from glacier theory (Shreve 1972, Weertman 1972), coupled with observations from this investigation, as follows. The drainage area for the western outflow point is estimated from the fact that water at the base of a glacier will generally flow parallel to the pressure gradient caused by the surface elevation of the glacier (Flint 1971, Weertman 1972). A drainage area of 900km^2 is estimated, roughly following the limits of Brasvellbreen glacier (Orvin 1969) (figure 1). Since discharge of turbid water is low in winter and high in July and August (based on satellite photographs), summer outflow must come from surface meltwater which is transported to the glacier base (A-B, figure 10). Weertman (1972) suggests that 1-2m of ice could be melted over the entire (Brasvellbreen) glacier surface during the summer ablation season. If 1m/yr is assumed here to be contributed to basal meltwater over the 900km^2 drainage area, an average discharge of 174m^3/sec will be released for the two summer months. Large variability in meltwater discharge can be expected during the summer because of meteorological fluctuations (Collins 1979).

Bounds on winter discharge may similarly be derived from a discussion by Weertman (1972). An average of 1.5cm/yr may be melted from the base of the glacier; including 0.5cm/yr from geothermal heating and 1.0cm/yr from frictional sliding (this value depends on the velocity of the glacier). If basal melting occurs over 900km^2, then an average winter discharge of 0.43m^3/sec is derived.

Channelization of meltwater occurs at the base of glaciers, forming a dendritic pattern in topographic lows of the bedrock similar to river networks (Flint 1971, Shreve 1972, and Weertman 1972). This results in several large stable meltwater outflows, located along valleys in the bedrock and flowing parallel to the glacier flow. If the tunnel is melted into the ice at the base of the glacier, dimensions of the meltwater tunnel and transport velocity can be estimated, using Weertman's (1972) equations:

R = tunnel radius melted into the ice (m)
$= [Q/\pi 8.5 P_g^{1/2}]^{3/8}$
V = velocity of meltwater in a tunnel beneath the glacier (m/sec)
$= 8.5 P_g^{1/2} R^{2/3}$

where: Q = discharge (m^3/s)
ρ = water density = 0.9998g/cm^3 (not including SPM)
ρ' = ice density = 0.917g/cm^3
g = gravity = 980cm/s^2
α = surface slope of the glacier = 0.0126
P_g = pressure gradient = $\rho' g\alpha + (\rho - \rho')g\alpha$

The radius of the meltwater conduit is estimated at 2m, with a discharge velocity of 13m/s for an average summer discharge of 200m^3/s. However, this estimate is probably a maximum velocity because the channel is probably bigger than the 4m diameter estimated by ice melting considerations. The channel is thought to be larger because it is observed to remain in the same location from year to

year, and so is probably related to bedrock topography of a larger scale. If 13m/s is assumed to be the velocity over the entire drainage length of 30km, then meltwater would take 38min to reach the glacier front (B-C, figure 10), and may be susceptible to daily meterological fluctuations. However, meltwater must first travel from the surface to the base of the glacier (A-B, figure 10), and then must be collected in a series of channels. The reservoir time at each of these stages is not well documented in the glacial literature (Shreve 1972, Embleton and King 1975 p. 327). Weekly variations in plume width and turbidity are observed from satellite photographs (figure 4), but these patterns could also be due to variations in the coastal current.

Possible velocities on the order of meters/second indicate that very coarse material may be transported in the meltwater channel along the glacier base. This result is consistent with observations of esker sediments which contain coarse sand and well rounded pebbles and cobbles and are thought to be deposits formed by subglacial rivers (Flint 1971, Embleton and King 1975). Channel dimensions and discharge velocity will change at the ice frontas the waters enters the ocean. Powell (1980) suggested that melting of the ice front by outflow turbulence (C-D, figure 10) can cause the outflow tunnel to migrate up to sea level, thus widening the discharge area and separating the meltwater from the sea-floor. Elverhoi et al. (1980) observed that meltwater with entrained seawater was discharged at the sea surface from the extensively fractured Kongsfjord glacier. The meltwater discharging from the glacier was fairly saline (28°/$_{oo}$)

with a suspended matter concentration of 500mg/l at the discharge location. Migration up to sea level within the glacier will not only decrease the exit SPM concentration and buoyancy (due to entrainment of seawater), but deposition of the traction load and suspended sand will begin at some distance behind the general ice front.

When discharge area of the conduit increases, discharge velocity decreases, but these numbers are difficult to quantify. The tunnel mouth cannot be greater than the 75m water depth. The indentation in the side-scan sonograph observed near the sea floor is 200m wide (figure 8), while the surface expression of the tunnel is approximately 50m wide. If the discharge is assumed to remain constant at $200m^3/s$, but the tunnel area increases to $100m^2$, then the exit velocity will decrease to 2m/s. Eddies are observed at the sea surface at the Nordaustlandet discharge locations. These eddies could result from buoyant flow discharged at depth (discussed also by Wright 1887, Edwards 1978, Powell 1980), therefore in the following discussion, meltwater is assumed to discharge from the base of the glacier. Consequences of surface discharge (as observed by Elverhoi et. al (1980)) are discussed later.

Initial sediment concentration in the meltwater plume is estimated from annual glacier erosion rates because 90% of glacier erosion products are transported in suspension when meltwater is present at the base of the glacier (Hagen et al. 1983). Sedimentary bedrock similar to that underlying Brasvellbreen is eroded at 1mm/yr on western Svalbard (Elverhoi et al. 1980), while crystalline basement is eroded at 0.4mm/yr (Hagen et al. 1983). If 0.8mm/yr of

fine-grained erosional products from the entire drainage area are transported to the glacier front, then the average concentration of suspended sediment in meltwater during the two month ablation season is estimated at a maximum of 2000mg/l (assuming sediment density is $2.65 g/cm^3$). This average value is consistent with suspended sediment concentrations measured in meltwater streams (see discussion in Jopling and McDonald 1975), but will vary during the ablation season because of variations in meltwater discharge and channel locations (Collins 1979). If sediment concentrations greater than 38,000mg/l occur, underflows (density currents) can develop when meltwater is discharged into the marine environment. Since such high concentrations have rarely been measured (Powell 1980), sediment concentration in the outflow is assumed to have a negligible effect on buoyancy.

Near Field:

Plume trajectory immediately after discharge into the sea depends on initial discharge velocity (M = momentum flux) and bouyancy (B = buoyancy flux) which determine how far from the source the outflow behaves as a jet (l_m) (Fischer et al. 1979). If the meltwater is discharged horizontally from the glacier base, l_m is the distance from the ice front that the meltwater will flow before it loses its initial momentum and starts to rise:

$$l_m = M^{3/4}/B^{1/2}$$

where: ρ_w = density of sea water = 1.0273
M = momentum flux = VQ
B = bouyancy flux = $Qg(\rho_w-\rho)/\rho$

Since 13m/s is an upper velocity for meltwater discharge based on previous calculations and l_m for 13m/s is only 48m, the outflow will be considered a bouyant plume from the start. (If the outflow velocity is 2m/s, then it will start to rise after it flows only 12m from the tunnel mouth.)

In a stratified coastal environment with no ambient velocity, the plume will have a terminal height of rise (h_B) dependent on its buoyancy (Fischer et al. 1979). Even though the meltwater outflow is more buoyant than seawater the height to which it can rise is limited because it entrains seawater as it rises, thereby increasing its density. A linear density stratification in the coastal water column is estimated from the 1981 density profile at station 144, located 100m from the outflow point (figure 11).

$$h_B = 3.8B^{1/4}/(g\varepsilon')^{3/8}$$

where:
- H = water depth
- h = depth to base of pycnocline
- ρ_{wd} = density of bottom water (at depth H)
- ρ_{ws} = density of water below pycnocline (at depth h)
- $\varepsilon' = (\rho_{wd} - \rho_{ws})/H\rho_{wd}$

Figure 11. Density stratification for 1981 station 144 (for location see figure 1), located 100m from western outflow.

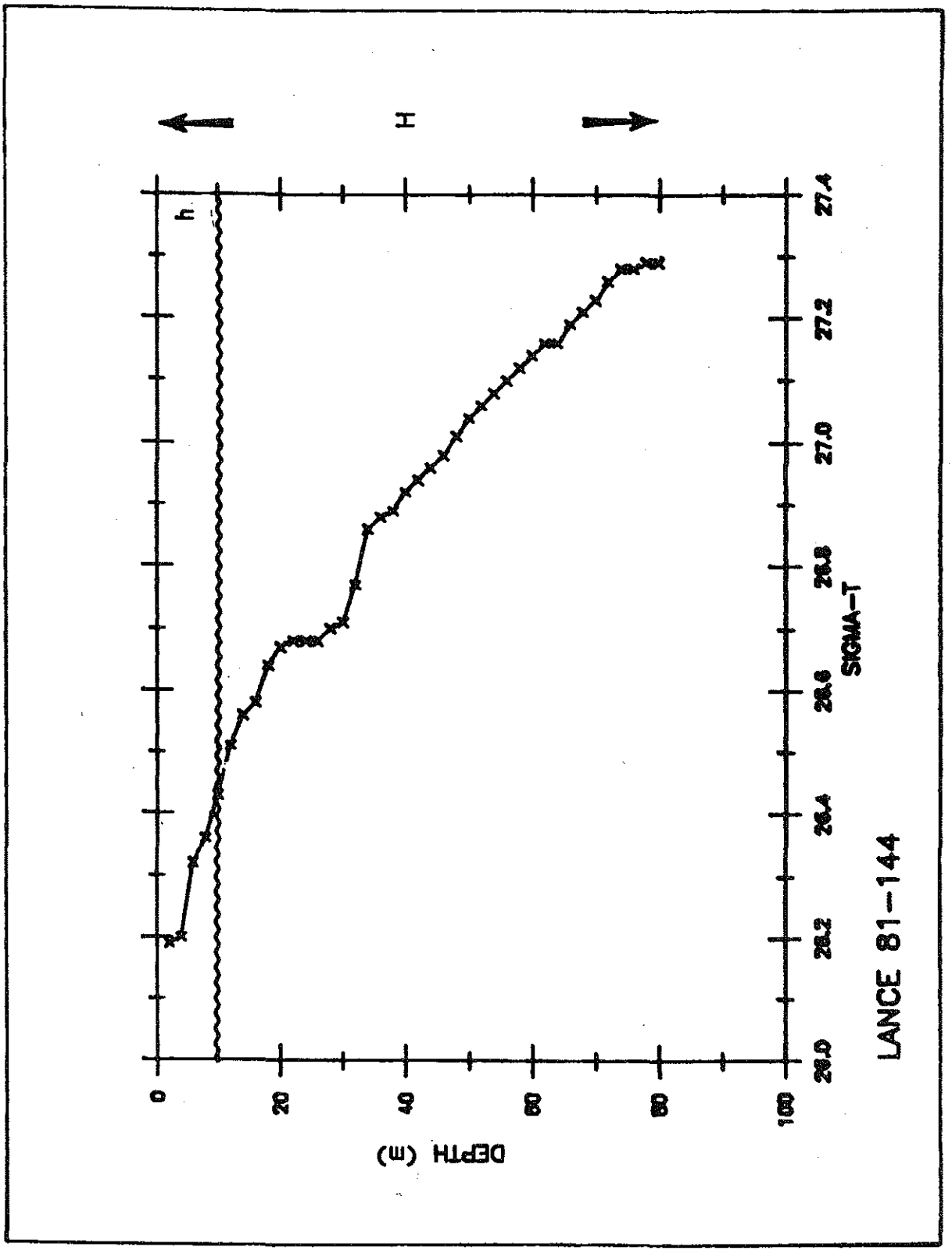
H
h
DEPTH (m)
0
20
40
60
80
100
26.0
26.2
26.4
26.6
26.8
27.0
27.2
27.4
SIGMA-T
LANCE 81-144

Figure 11

The average summertime discharge of $200m^3/sec$ produces a 293m terminal height of rise. Since water depth is only 75m, the plume will reach the surface under summer discharge conditions (C-D, figure 10). If discharge is less than $0.9m^3/sec$, the plume will reach a subsurface limit (determined by rearranging the above equation to solve for Q at h_B = 75m):

$$Q = h_B^4(g\varepsilon')^{3/2} \; / \; 3.8^4 g(\rho_w - \rho)/\rho$$

This result is consistent with winter discharge of turbid water being too low to be observed in satellite images. Since maximum winter discharge is estimated at $0.43m^3/sec$, it reaches a terminal height of 62m and will not be observed in satellite images. An ambient coastal current (velocity = U (m/sec)) will alter these estimates (Fischer et al. 1979):

Z_B = height of rise in an ambient current (without stratification)

$= B/U^3$

In order to advect the summer discharge plume downstream before it reaches the surface, the coastal current must have a velocity of 85cm/sec (this is actually an upper value since stratification is not considered).

The grain size distribution of material in suspension depends on the vertical velocity (W_m = maximum vertical velocity) of the meltwater plume near the discharge point as well as the type of sediment supplied by glacier erosion. The time of rise of the plume (T) and vertical velocity may be estimated from the buoyancy of the meltwater (does not include effects of stratification) from Fischer et al. 1979:

$W_m = 4.7(B/H)^{1/3}$

$T = H/W_m = 18\text{sec}$ ($H = 75\text{m}$, $B = 54.3$)

Particles greater than 1mm may be carried to the surface in the summer. While rising to the surface entrainment of seawater into the plume significantly decreases the concentration (C_o = source concentration) of material in suspension (Fischer et al. 1979):

C_m = maximum concentration

$= 9.1QC_o \; / \; B^{1/3}H^{5/3}$

C_{av} = average concentration (assuming a normal distribution across the axis of the plume)

$= C_m/1.4$

An initial concentration of 2000mg/l yields an average surface concentration of 509mg/l and a maximum concentration on the axis of the plume of 713mg/l, assuming no sedimentation during rise to the surface. Observed concentrations at Nordaustlandet are on the order of 10's of mg/l, suggesting either deposition from an initially coarse suspension has occurred before sampling, initial concentrations were lower than 2000mg/l (100's of mg/l), initial discharge was lower than $200m^3/s$, or more seawater has been entrained than is considered in the model. These estimates of velocity and concentration are based on plume theory which assumes a normal distribution of velocity and suspended sediment concentration across the plume axis (Fischer et al. 1979).

The source texture also depends on the glacier type and the bedrock lithology (Flint 1971). Predominately coarse-grained sediment may be discharged in meltwater from erosion of metamorphic, igneous,

or initially coarse-grained sedimentary rocks such as sandstones, conglomerates or breccias. In general, fine-grained initial size distribution occurs during erosion of carbonate rocks, siltstones, shales and mudstones, although the glacial thermal regime (therefore the type of erosion) and transport mechanism also has a large impact on the resultant particle size. A bimodal distribution may result from erosion of two different bedrock types, or erosion of a silicified carbonate. Since the two meltwater outflows at Nordaustlandet drain very different source regions, the initial grain size distributions should be different. Erosion of the eastern sandstone should produce a fairly uniform source without many large grains. The western source should be bimodal as chert fragments will be large, while glacial erosion of limestone produces fine-grained sediments. Surface samples obtained downstream from the western outflow in 1982 (stations 232 and 238) are indeed bimodal (figure 7).

Intermediate field:

Expansion of the plume occurs at the sea surface because of excess buoyancy of the summertime plume (Garvine 1982 and 1984). The small embayments associated with meltwater discharge locations along the Nordaustlandet ice front are observed to be filled with turbid water in satellite photographs, indicating that near-surface spreading may be limited by the geometry of the ice front. The turbid western plume observed in satellite images is 1.7km wide at 1km from the ice front; it continues to widen for approximately 4km downstream, where a constant width of 2.5km is attained (figure 3). Westward advection at

approximately 1km from the discharge location suggests that at this point the turbid water has dispersed from the embayment into the higher velocity coastal current. Within the 4km long initial spreading zone, average suspended sediment concentration drops to less than 5mg/l (figure 6) due to dilution by mixing and to fallout of material from suspension. The concentration and grain size of material in suspension remains fairly constant at distances greater than 3-5km from the outflow (figure 7). This intermediate field region is difficult to model, especially because it depends on the geometry of the ice front, but is important because sand settles from suspension in this region (figure 10):

TABLE 5

Size (μm)	w(cm/s)*	5cm/s	10cm/s	15cm/s+
2000	19.1	0.0196	0.0392	0.0588
1000	10.8	0.0347	0.0694	0.104
500	5.27	0.0711	0.142	0.213
250	2.12	0.177	0.354	0.530
125	0.695	0.539	1.14	1.62
64	0.198	1.89	3.78	5.67
32	0.0496	7.56	15.1	22.7
16	0.0124	30.2	60.5	90.7

*Fall velocity
+Fallout distance downstream(km) for 75m water depth and variable coastal current velocity

The fall velocities of the less than 100μm fraction are estimated by Stokes equation which assumes spherical particles and settling of individual sediment grains. Fall velocities of larger particles are estimated from Baba and Komar (1981). These estimates of fallout distance show that sediments smaller than 64μm escape from the outflow embayment even if the effective velocity is as low as 5cm/s.

If the small 400 by 5m deposit near the minor western outflow is assumed to extend 300m to the glacier front, $4.1\text{-}2.4 \times 10^{10}$g/yr have accumulated since the surge (assuming a sediment density of 1.86g/cm^3). This corresponds to deposition of 40-23mg/l for a discharge of 200m^3/s and an annual 2 month ablation season.

Far field:

In the far field the plume is advected along the Nordaustlandet ice front by a westerly coastal current and silt settles from suspension. Width, velocity, suspended matter concentration, and grain size distribution of the advected plume are of interest for location of depocenters and determination of accumulation rates (figures 10 and 12). The velocity of the coastal current determines the trajectory of different grain sizes of suspended material discharged in glacial meltwater.

The coastal current may be driven by regional winds, local winds, or density differences between the coastal water mass and the adjacent Barents Sea. Fresh water supplied along a coast and mixed throughout the water column can drive a westerly coastal current in the Northern Hemisphere (Csanady 1982, Griffiths and Linden 1983). Continual supply of meltwater may drive a summertime Nordaustlandet coastal current, since the velocity of the current is observed to increase as it flows along the glacier front (appendix A). Also, the sea-ice distribution observed in wintertime satellite photographs does not require the presence of a coastal current.

Katabatic winds from the glacier may also contribute to formation of the coastal current. These winds form by air cooling near the glacier surface, forming a downslope density flow of cold air which can extend 50km away from a glacier front (Flint 1971). The temperature difference between the glacier surface and air is greatest in the summer, causing highest velocity winds when meltwater discharge is greatest. Increased winds also cause increased ablation (Martin 1975, Shcheglova and Chizhov 1981) probably resulting in increased meltwater discharge. A 10m/s offshore wind is not unusual for katabatic inversion winds (Whillans 1975), and might drive a coastal current flowing to the right of the glacier front. These offshore winds could also widen the surface plume. It is not possible at this stage to partition and accurately calculate the effects of density and wind in driving a coastal current with the data available. However, it seems likely that a fast and narrow coastal current can develop along marine glacier margins by a combination of meltwater-produced density gradients and katabatic winds. Such a current is also likely to be influenced by the larger scale coastal flow created by regional hydrographic and meteorologic conditions. Nordaustlandet coastal current velocities of 5 and 10cm/s are estimated from geostrophic velocities calculated for transects through the coastal region (appendix A).

Generalities of sediment deposition from a meltwater plume in both the near and far field are illuminated through a one dimensional settling and accumulation model (figure 12). An initial concentration

Figure 12. Schematic of one dimensional advection and settling model.

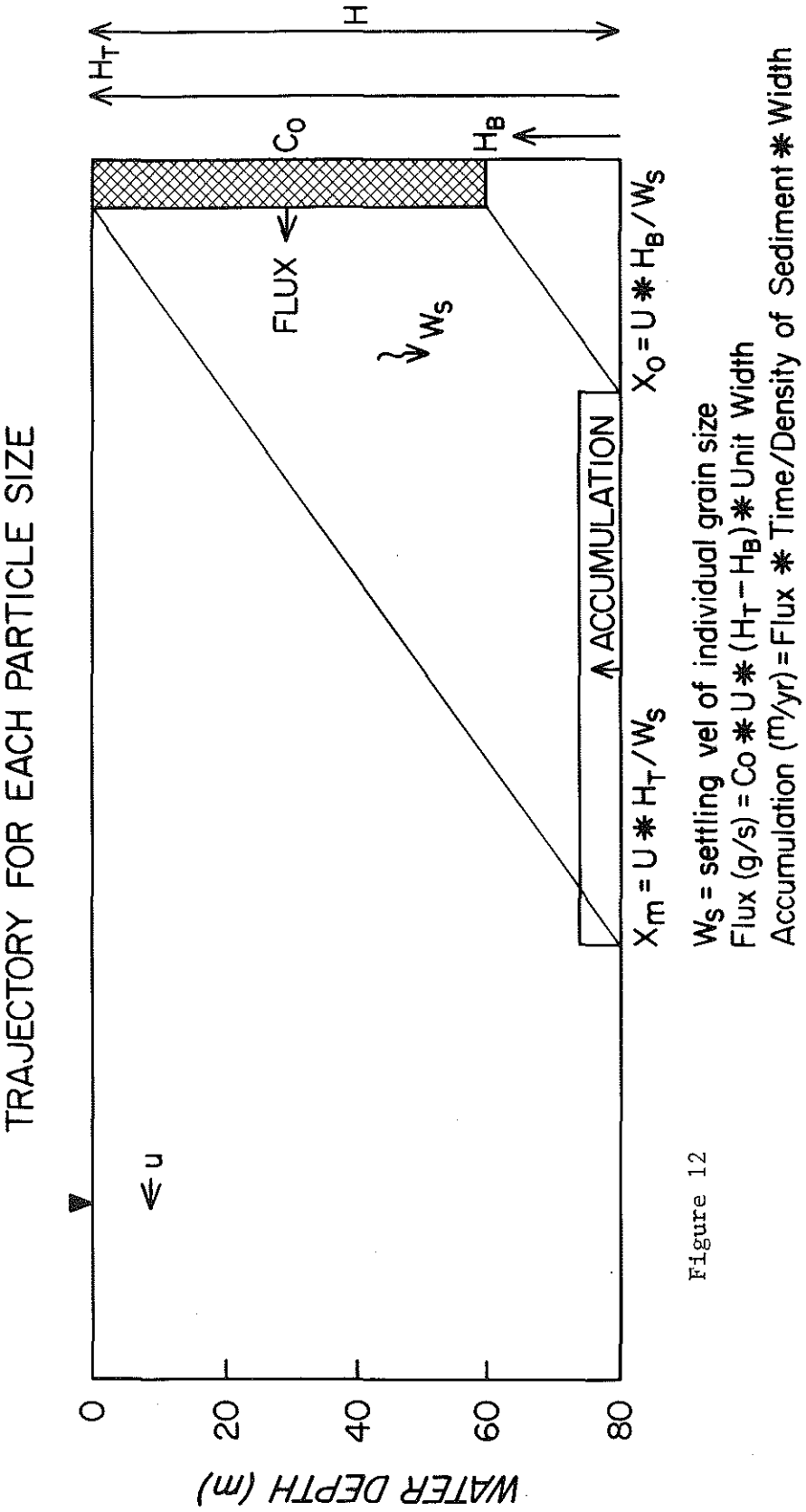
TRAJECTORY FOR EACH PARTICLE SIZE
WATER DEPTH (m)
0
20
40
60
80
u
H_T
H
C_O
H_B
FLUX
W_S
ACCUMULATION
$X_m = U * H_T / W_S$
$X_O = U * H_B / W_S$
W_S = settling vel of individual grain size
Flux (g/s) = $C_O * U * (H_T - H_B) *$ Unit Width
Accumulation (^{m}/yr) = Flux * Time/Density of Sediment * Width

Figure 12

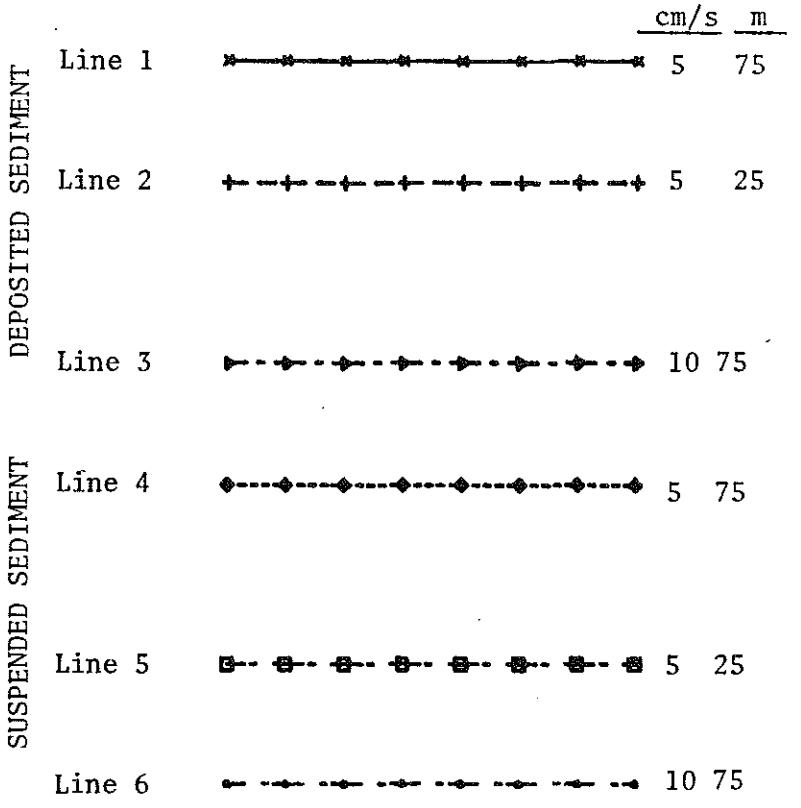

Figure 13. Downstream plume behavior for 25mg/l initial suspended concentration advected along the ice front for a normally distributed source grain size distribution.
A. Source grain size distribution.
B. Concentration downstream
C. Accumulation rate of material downstream
D. Mean size of material in suspension and deposited on the sea floor
E. Dispersion of material in suspension and deposited on the sea floor
F. Skewness of material in suspension and deposited on the sea floor

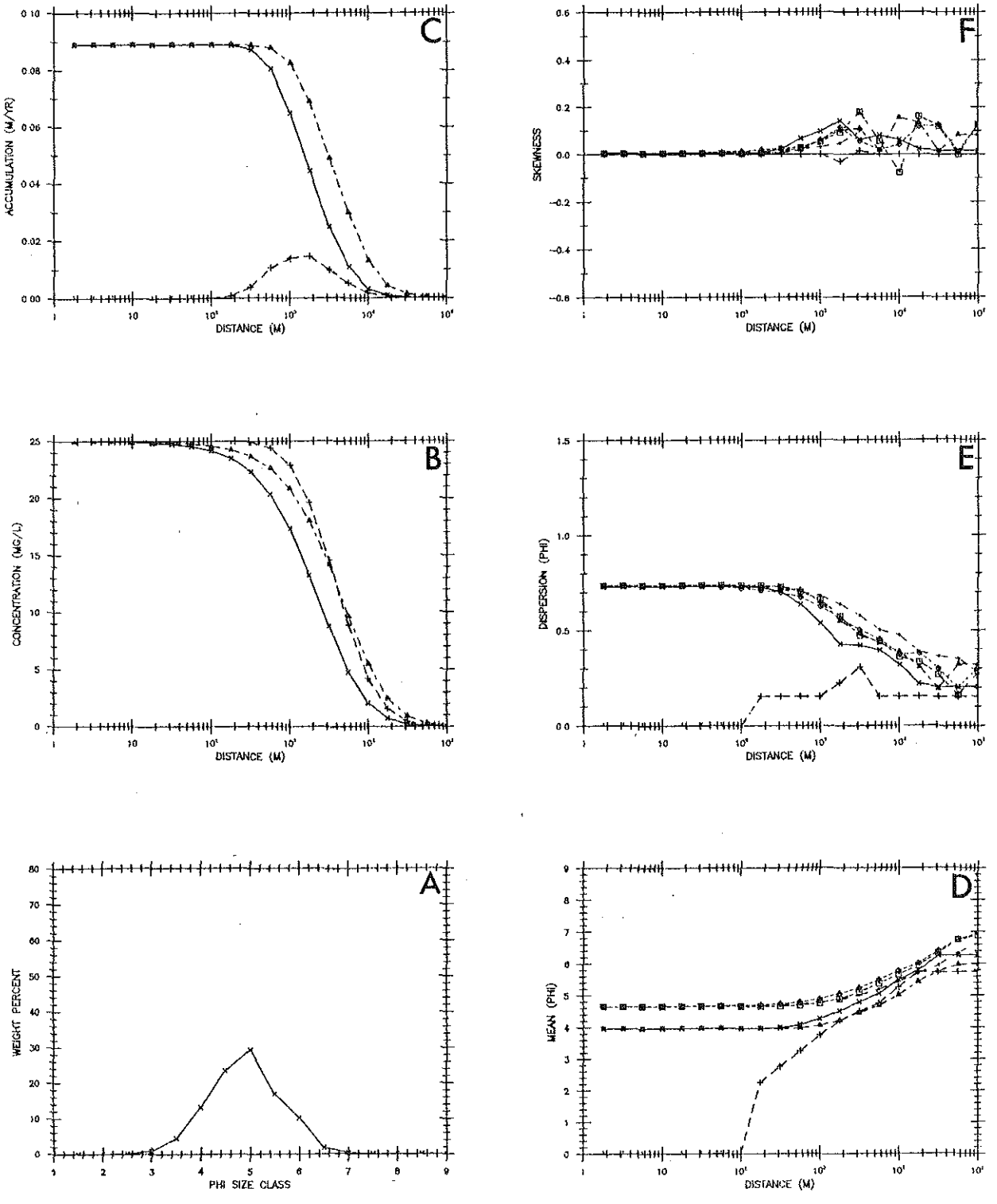
C
ACCUMULATION (M/YR)
DISTANCE (M)
F
SKEWNESS
DISTANCE (M)
B
CONCENTRATION (MG/L)
DISTANCE (M)
E
DISPERSION (PHI)
DISTANCE (M)
A
WEIGHT PERCENT
PHI SIZE CLASS
D
MEAN (PHI)
DISTANCE (M)

Figure 13

Figure 14. Downstream plume behavior for 25mg/l initial suspended concentration advected along the ice front for a coarse source grain size distribution.

A. Source grain size distribution.

B. Concentration downstream

C. Accumulation rate of material downstream

D. Mean size of material in suspension and deposited on the sea floor (note change of scale)

E. Dispersion of material in suspension and deposited on the sea floor

F. Skewness of material in suspension and deposited on the sea floor

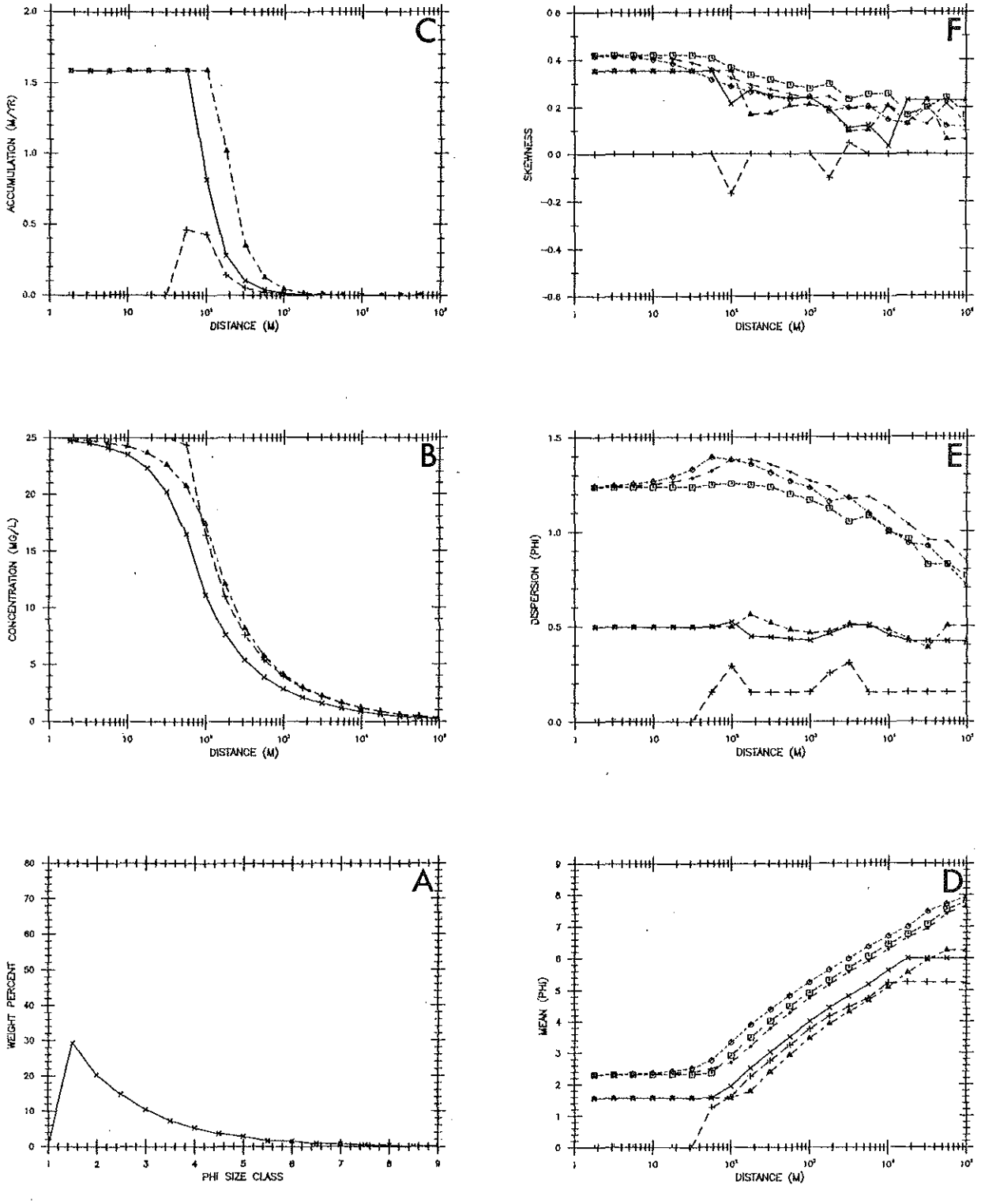
C
ACCUMULATION (M/YR)
DISTANCE (M)
F
SKEWNESS
DISTANCE (M)
B
CONCENTRATION (MG/L)
DISTANCE (M)
E
DISPERSION (PHI)
DISTANCE (M)
A
WEIGHT PERCENT
PHI SIZE CLASS
D
MEAN (PHI)
DISTANCE (M)

Figure 14

Figure 15. Downstream plume behavior for 25mg/l initial suspended concentration advected along the ice front for a fine source grain size distribution.

A. Source grain size distribution.

B. Concentration downstream

C. Accumulation rate of material downstream

D. Mean size of material in suspension and deposited on the sea floor

E. Dispersion of material in suspension and deposited on the sea floor

F. Skewness of material in suspension and deposited on the sea floor

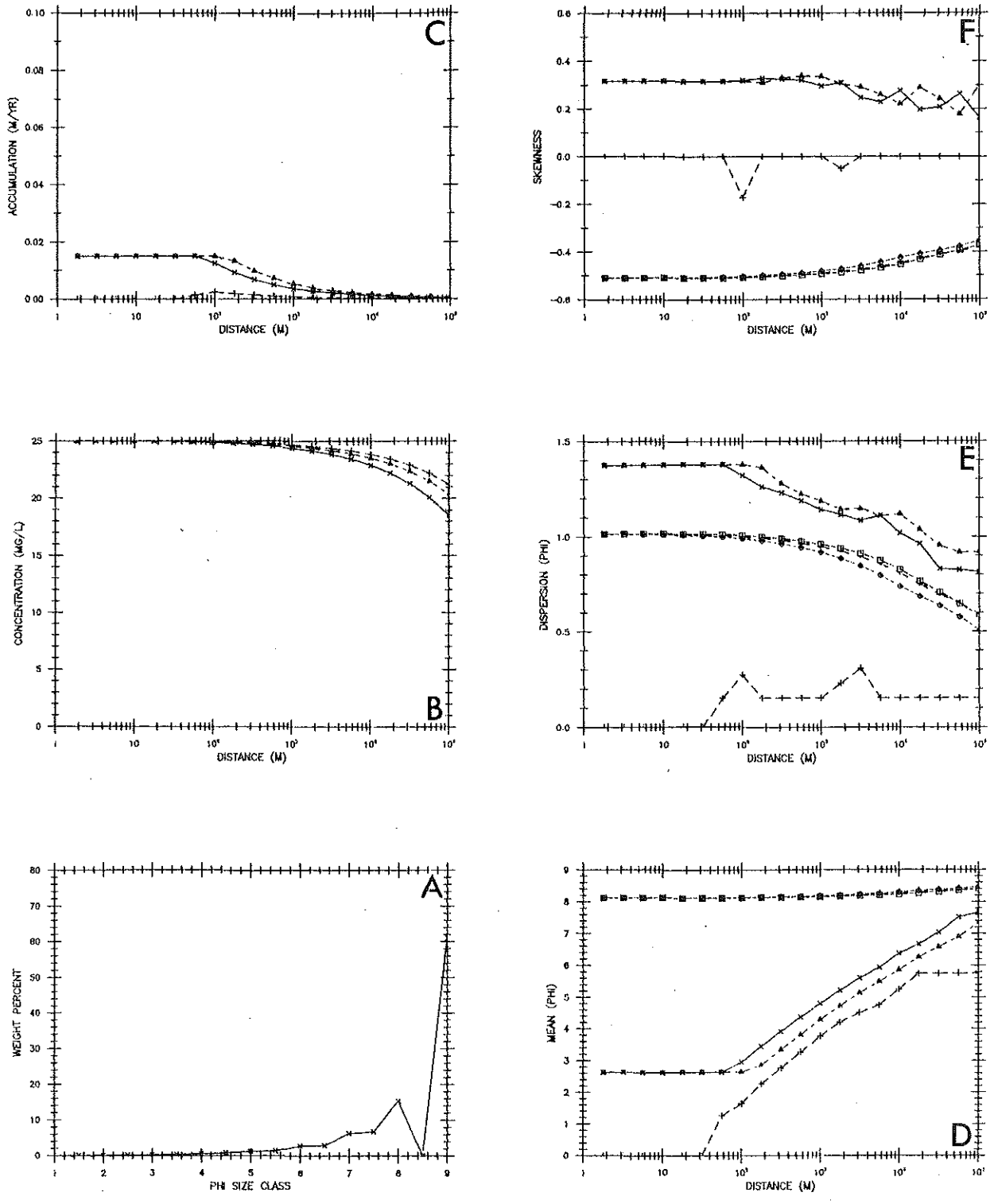
C
ACCUMULATION (M/YR)
DISTANCE (M)
F
SKEWNESS
DISTANCE (M)
B
CONCENTRATION (MG/L)
DISTANCE (M)
E
DISPERSION (PHI)
DISTANCE (M)
A
WEIGHT PERCENT
PHI SIZE CLASS
D
MEAN (PHI)
DISTANCE (M)

Figure 15

Figure 16. Downstream plume behavior for 25mg/l initial suspended concentration advected along the ice front for station 174 (10m) source grain size distribution.

A. Source grain size distribution.

B. Concentration downstream

C. Accumulation rate of material downstream

D. Mean size of material in suspension and deposited on the sea floor

E. Dispersion of material in suspension and deposited on the sea floor

F. Skewness of material in suspension and deposited on the sea floor

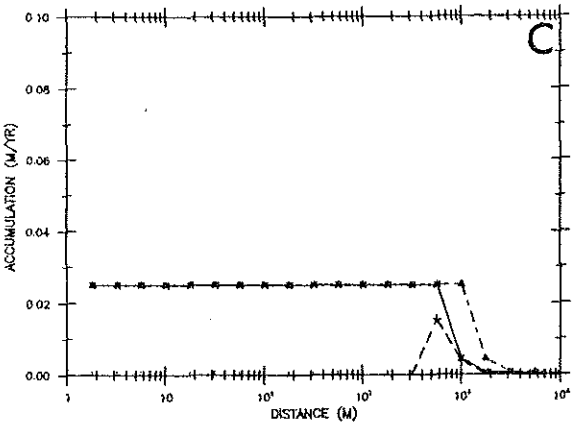
C
ACCUMULATION (M/YR)
DISTANCE (M)

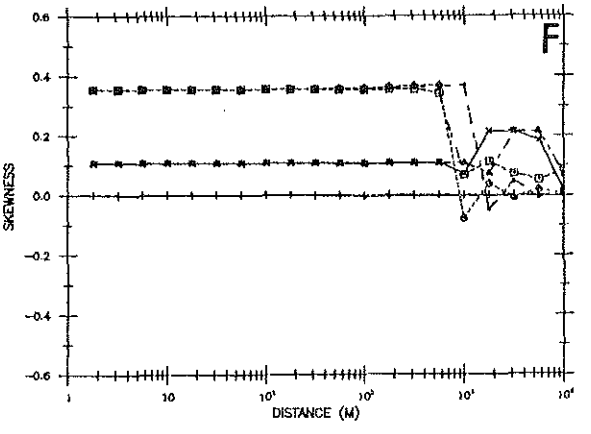
F
SKEWNESS
DISTANCE (M)

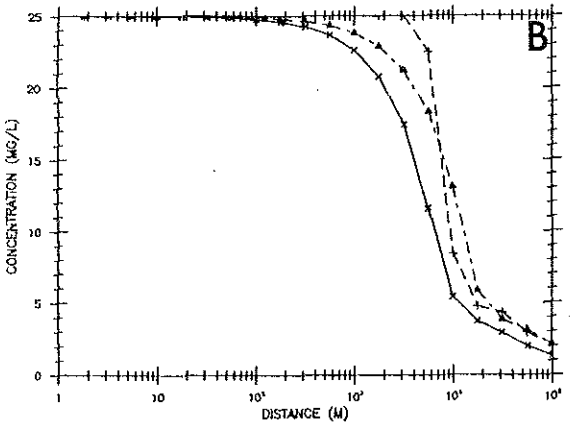
B
CONCENTRATION (MG/L)
DISTANCE (M)

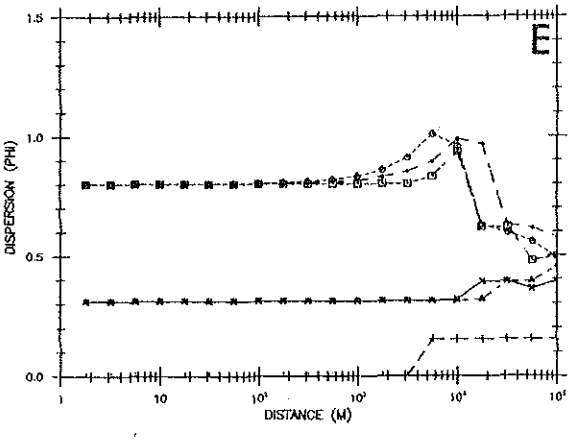
E
DISPERSION (PHI)
DISTANCE (M)

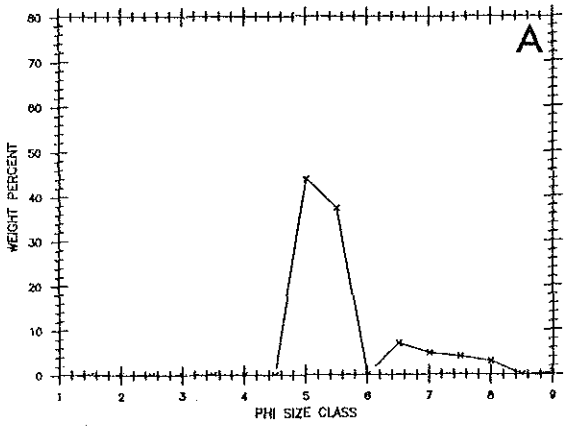
A
WEIGHT PERCENT
PHI SIZE CLASS

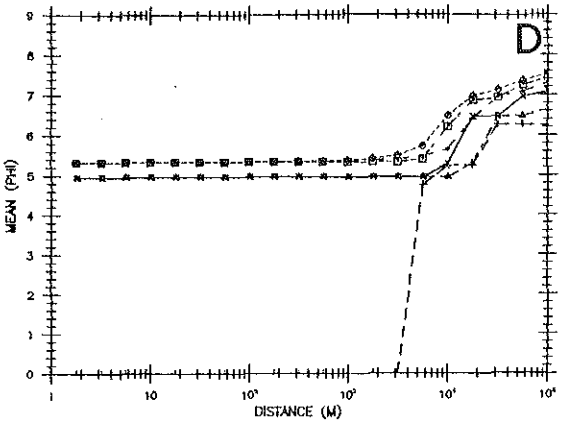
D
MEAN (PHI)
DISTANCE (M)

Figure 16

with various source grain size distributions is supplied to a unit width of either the entire water column ($H = H_T$, $H_B = 0$) or to a surface layer ($H = H_T$, $H_B \rightarrow 0$). The flux of material for these different conditions does not remain constant. The sediment-laden plume is then advected by variable coastal current velocities (u = 5, 10cm/sec). Sediment is assumed to settle as single particles using Stokes' velocities (w_s) for sediment smaller than 100μm, and Baba and Komar (1981) for the larger grains. Suspended sediment concentration, deposited sediment accumulation rates, and grain size distribution statistics are computed for three ambient conditions: uniform plume over whole water depth at 5cm/s coastal current velocity, 25m thick surface layer plume in 5cm/s coastal current, and a uniform plume over whole water depth at 10cm/s. The intial concentration (C_o) is assumed to be 25mg/l and sediment is accumulated on the sea floor for 2 months (or 1 year, assuming a 2 month ablation season). Average water depth is 75m. Four initial size distributions are examined: normally distributed (figure 13), coarse (positively skewed) (figure 14), fine (negatively skewed) (figure 15), and the natural distribution obtained from the 10m water depth sample from station 174 (the coarsest sample from the eastern plume) (figure 16). These results are then compared with Nordaustlandet SPM observations.

Several major features appear on model runs for all source grain size distributions. Deposition from the surface layer plume does not begin until some distance downstream. Sediment accumulated on the sea floor from the surface plume always has the same statistics,

regardless of the source distribution. The deposits are well-sorted and are normally distributed (not skewed). Other general features are: sediment in suspension has a smaller mean grain size than sediment depositing at the same distance downstream; mean grain size, dispersion, and skewness of both deposited sediments and sediments in suspension generally decrease downstream; doubling the current speed stretches out the accummulation zone downstream; and for coarser source size distributions the sedimentation rate near the source is higher.

If a normal distribution (mean 4.7ϕ and $\sigma 2\phi$) is supplied to the whole water column, then concentrations of suspended sediment should remain near source levels until about 1km downstream (figure 13). Concentrations then decrease fairly rapidly until about 10km downstream where most of the modal material is deposited from suspension. In this depositional region, sediment accumulates at a rate of 9cm/yr with a mean size of 4ϕ. The deposits are moderately sorted and normally distributed. Deposition from the surface plume does not begin until about 100m from the source and it also decreases after 10km.

Sediment in suspension maintains the source statistics until about 500m downstream. After this point the grain size distribution of material in suspension decreases logarithmically and becomes more well sorted and slightly positively skewed.

If the source distribution is initially coarse, sediment falls out sooner from suspension (figure 14), thus accumulating faster (1.6m/yr) over a narrower region (0-200m downstream), up to 75m in 50 years! These rates are similar to those obtained in fjord

sedimentations studies (reviewed by Syvitskiy, in prep., Powell, pers.comm.). A well-developed delta should form with very coarse sediments (mean 1.5ϕ) which are positively skewed (except for deposits from the surface plume, which are normally distributed) deposited within the first 50-70m.

Sediment in suspension decreases markedly between 10m and 1km from the coarse source. Between 10m and 100km from the source the mean ϕ of material in suspension increases from 2.5 to 8. The suspended sediments are poorly sorted at the source and then become more poorly sorted near 30km downstream. Further downstream the material in suspension is moderately sorted. Sorting decreases at intermediate distances from the source because of the strong initial positive skewness. As coarse material is deposited, the sediments become less skewed so the statistical dispersion increases until a normal distribution is attained. Then as material continues to fall from suspension, the dispersion decreases. A downstream increase in dispersion of suspended sediments should be apparent in all initial strongly fine-skewed distributions.

A fine-grained, negatively skewed suspended sediment source has very different downstream behavior (figure 15). The concentration of suspended particulate matter does not decrease because only a very small amount of coarse material is falling from suspension. Therefore the mean size of material in suspension is nearly constant and remains strongly negatively skewed. Sorting decreases and shifts from moderate to moderately well-sorted at distances greater than 10km.

Only 1.5cm of sediment is predicted to accumulate in the 1-14m range downstream, and for the surface plume only 0.2cm accumulates in this region. The mean size of deposited material decreases markedly with increasing distance from the source. Sorting decreases slightly, from poorly sorted to moderately sorted at distances greater than 20km. These sediments are initially strongly positively skewed and become positively skewed downstream.

Grain size measured from SPM sample obtained from 10m water depth at station 174 was chosen as the natural sediment source (figure 16), because this sample was the coarsest obtained at the western plume outflow. The source grain size distribution is strongly positively skewed, moderately sorted, and has a mean of 5.2ϕ. The predicted downstream concentrations and accumulation region are similar to the normal distribution discussed earlier, but the grain size statistics are more reminiscent of the strongly positively skewed coarse source. Concentration decreases between 2 and 11km as the coarse sediment settles from suspension. Approximately 2.5cm of sediment should accumulate in 1 year in this region. Deposits from the surface plume accumulate between 2 and 10km from the source. The mean size of these sediments is similar to that in suspesion, 5ϕ, but the sediments are well sorted and only slightly fine-skewed to nearly normally distributed.

Sediment in suspension retains the source mean size until 4km where the dispersion begins to increase and the skewness drops sharply. Once sediment in suspension is approximately normally distributed, dispersion begins to decrease, as noted earlier for the coarse source.

These model results may be compared with actual grain statistics measured up to 25 and 28km downstream from the meltwater outflows along the Nordaustlandet ice front (figures 6 and 7). Some of the features predicted by the simple advection and settling model are observed in these samples, but because of the large variablity in natural suspended matter samples only general tendencies can be discussed.

Between 3 and 5km downstream the Nordaustlandet concentration drops to a nearly constant value as predicted for a positively skewed initial distribution (compare figures 6 and 14). Mean grain size should decrease downstream from about 5.5 to 7.5ϕ at 30km. The eastern source show some evidence of a decrease in grain size from 6 to 6.5ϕ. SPM sorting is predicted to decrease downstream, since the source is strongly positively skewed, but there is no real evidence for this at the eastern plume and the western plume SPM samples were obtained in different years. Dispersion for the natural distribution (station 174) model run increased between 4 and 10km downstream to 1.0ϕ and then decreased to 0.5ϕ. In general, these values correspond with the 0.5-0.9ϕ range observed at both eastern and western Nordaustlandet plumes. Skewness should decrease from an initial positive skewness to a nearly symmetrical distribution. There is some evidence for this in SPM samples from both plumes.

Approximately 1m of sediment is predicted to accumulate since the Nordaustlandet glacier surge using the natural grain size distribution and 4.5m if the coarse initial distribution is used. These values appear reasonable since a subaqueous fan is not oberved near the

western outflow location. Recent glacier activity has formed a swale and swell morphology along the innermost 1km which could mask these deposits.

DISCUSSION

Further aspects of glaciomarine deposition can now be discussed with reference to the basic sedimentation model depicted above and preservation potential in the geologic record.

Several source grain size distributions were used above to show that sediment accumulation rates and location of depocenters are sensitive to the type of material which is supplied by the glacier. The initial texture is determined largely by the type of bedrock eroded by the glacier, the glacial thermal regime, and the transport efficiency of the subglacial meltwater conduit. The grain size distribution of sediment supplied to the ice front will probably be positively skewed. Fine-skewness results from deposition of the coarse tail, truncating the normal distribution. This occurs when the fresh meltwater stream encounters seawater. The very coarse sediments found in eskers (Flint 1971, p.216; Embleton and King 1975, p.467) support this supposition. Because the meltwater is bouyant, it will rise and the traction load will be deposited. 30m-wide sand lenses observed above glacier till by Rust and Romanelli (1975) may be Pleistocene analogs to this depositional environment.

Glacial outflows are intrinsically different from river discharge because they originate at some depth below the sea surface and are buoyant, thus will maintain coarse material in suspension. If outflow turbulence or calving and crevassing of the glacier leads to migration of the tunnel to sea level within the glacier, then a coarse deposit will form at some distance behind the general ice front. Sand may settle from suspension before the meltwater is discharged as a surface plume. Sediments deposited from a surface plume typically are normally distributed and very well sorted. Deposition from suspension before discharge at the glacier front may cause the initial low concentrations observed and fine grain size (no grains coarser than 40μm) of Nordaustlandet suspended matter samples. If discharge occurs from a tunnel at the glacier base, then the plume may be more or less distributed over the entire water column. Deposits will be strongly fine-skewed and well sorted with a very well-defined accumulation region having a nearly constant mean grain size. The outer border of the depocenter is defined by the coastal current velocity and the time it takes the mean grain size to settle from the sea surface to the sea floor.

However, at least some of the fine-grained material in suspension could be incorporated into fecal pellets. Packaging of mineralogic material into larger pellets by grazing organisms is well documented in fjord-glacier environments (Syvitski 1980, Syvitski and Murray 1981). This process is certainly important at Nordaustlandet particularly in view of the high productivity observed at the meltwater outflows. Intact fecal pellets containing mineral grains

are observed on some filtered water samples. Incorporation of sediment into fecal pellets by zooplankton and agglomeration of grains into composite particles leads to deposition of fine-grained material much closer to the discharge location than suggested by the model, increased accumulation rates, and deposition of unsorted sediment; this essentially adds a random fine component to the meltwater deposits. Flocculation would have the same effect, and may also be important where the meltwater outflow first encounters seawater. If the suspended sediments are not settling particle-by-particle, then the mean grain size of material in suspension would not be expected to have a systematic trend, although the absolute maximum size in suspension might be related to the settling velocity.

Ice rafting will add an essentially random coarse component to the surface sediments. Sediments may be ice rafted from ice bergs calved from the glacier front, or from sea ice transported with the coastal current. Ice rafting is observed mostly in the coarse fraction because even a very small amount of coarse material skews the sediment texture.

Because of the combined effects of a probable positively skewed source and biologic aggregation, "significant" accumulations from meltwater plumes may be limited to a range of about 10-30km from the discharge location. "Significant" accumulation in the Barents Sea is considered to be greater than the average of 5cm/1000yr (Elverhoi and Solheim 1983). In the geologic record thick accumulations of marine meltwater deposits should indicate that the ice front was within about

10km, because the source flux of fine-grained material must be very high for enough silt and clay to be carried in suspension downstream that significant accumulation rates occur at greater distances.

Fine silt and clay will remain in suspension for distances greater than 30km downstream, if they escape aggregation. Because transport distances of fine silt and clay are so large, material discharged at one outflow may be superimposed on the next outflow downstream. This continual rain of fine material results in a negatively skewed surface texture (since all paticles less than 2μm are presented as one class in most size analyses). When a coarse (positively skewed), ice-rafted component is superimposed on the fine meltwater deposit, a saddle-shaped grain size distribution results (chapter 3).

Deposition has been considered only in the downstream direction. The width of the plume will determine the offshore extent of glacial meltwater impact. At Nordaustlandet, the surface plume is several kilometers wide. Concentration decreases with distance from the ice front, but grain texture is not appreciably different. The offshore concentration decrease may be caused by mixing with ambient coastal water. Textural characteristics of meltwater deposits should not vary as rapidly offshore as they do downstream, but accumulation rates will decrease, corresponding with the decrease in SPM concentration.

In this discussion the meltwater outflow locations have been assumed to remain constant. Subglacial drainage is determined partly by topography of the glacier surface and partly by topography of the underlying bedrock. Variations in either surface may result in a

shift in the drainage pattern. The glacier surface changes as ablation and accumulation vary. The bedrock surface is continually eroded both by the glacier and subglacial streams, although the general topography remains fairly constant. Also the actual discharge location may migrate on a local scale since the ice front is a dynamic region. If the drainage pattern shifts dramatically the lens of coarse material deposited near the ice front will be covered by silty clay from upstream plumes, while minor shifts in outflow location will spread out coarse deposits over a broader region.

Because grounded-marine glacier margins are generally shallow (otherwise the glacier would not be grounded), the glaciomarine environment is subjected to reworking by a number of different processes. Ice bergs calved from the glacier and transported along the glacier front in the coastal current may gouge the sea floor, reworking the upper few meters of sediment. At Nordaustlandet, there are surprisingly few ploughmarks in the recent surge deposits along the ice front (chapter 3). The coastal current not only prevents fine material from being deposited near the ice front, but may have high enough velocity to rework sea floor sediments. Also, surface waves and tidal currents, although not important at Nordaustlandet, may be significant for sea-floor reworking along other glaciated shelves.

In addition, meltwater discharge implies that the glacier is melting. Subglacial meltwater drainage associated with large eskers appears to form during the waning stages of glaciation when the surface gradient is low and the discharge of meltwater is high (Shreve 1972). Depositional environments similar to the present-day

Nordaustlandet ice front were probably widespread on continental margins during late Pleistocene deglaciation (e.g. Rust and Romanelli 1975). After deglaciation, isostatic rebound results in shallowing water depths and even subaerial exposure, therefore many glaciomarine sequences have been extensively reworked and they grade into sandur deposits or glaciofluvial sequences.

CONCLUSIONS

Meltwater outwash plumes discharged from the Nordaustlandet ice dome dominate the modern offshore sedimentary regime. Although field observations along the glacier front are limited, comparison of suspended sediment concentration, grain size, suspended sediment sorting and skewness, against estimates of glacier erosion rates, meltwater discharge, and coastal hydrography provides a framework for discussion of the glaciomarine sedimentary environment. Because meltwater plumes are observed in satellite images only during the summer, meltwater is assumed to be derived primarily from melting of the glacier surface. Since the meltwater is turbid as it discharges at the ice front, it must flow along the glacier base where resuspension of glacial erosional products occurs. Topographic depressions in the bedrock surface guide the subglacial dentritic drainage network. Meltwater discharge therefore occurs at discrete and limited outflows near bathymetric depressions along the ice cap margin. Embayments tend to form around the outflow location because meltwater at the base increases calving of the ice front.

Coarse material can be transported in the high velocity subglacial meltwater streams. When the meltwater encounters the open ocean it rises buoyantly to the sea surface and deposits the traction load but carryies coarse sand to the sea surface. Sand is deposited from this coarse, positively skewed suspended matter in the outflow embayment; it forms an outflow delta if the flux of coarse material is high enough and if the ice front and discharge location remain stable during deposition. Depending on biologic activity, appreciable amounts of silt and clay may be deposited within fecal pellets of zooplankton. Deposition of silt and clay in fecal pellets, with a possible additional component of agglomerated and flocculated material will superimpose a random, fine component on the sandy outflow deposits.

A coastal current (flowing to the right in the northern hemisphere) may be set up by a combination of katabatic winds off the glacier surface and the summertime discharge of low salinity (and therefore low density) water along the glacier front. Although the outflow embayments are to some degree protected from the general ice-front coastal current, silt and clay will escape the embayment and be transported along the ice front. Silt and clay plumes supplied at several discharge points will overlap and more or less continually deposit sediment during the summer melt season. In general, glaciomarine sediments along the ice front therefore will be negatively skewed, when all the less than 2μm particles are presented as one size class.

The width of the turbid plume along the Nordaustlandet ice front, as observed in both satellite photographs and offshore concentration

of suspended matter, is approximately 2.5km. Although the concentration of mineralogic material in suspension decreases offshore, sediment textural parameters do not appear to vary. Therefore, accumulation rates will be highest near the glacier front but similar sediment textures will be observed several kilometers away from the ice front. Sharp bends in the ice front or bathymetric changes may cause the coastal current to detach from the glacier front, advecting suspended glacial material farther offshore.

Meltwater outwash deposits in the marine environment should form lenses of fairly well-sorted sand in eskers and in ridge and swale deposits typical of active, but fairly stable, ice fronts. They will probably be located behind end moraines and amidst ice-disintegration features (like crevasse fills) caused by glacier surges (chapter 3). In the geologic record glaciomarine deposits are likely to be reworked. They are accumulated in largest volume on shallow shelves of receding or disintegrating ice margins. Because of the shallow water depth and high local sedimentation rate, the combined effects of the ice front coastal current, surface waves, tidal currents, and iceberg gouging may rework the sea floor. After the glacier has retreated, the previously glaciated surface will isostatically rebound, prehaps even causing subaerial exposure of the meltwater deposits.

Further analysis of depositional conditions near meltwater outflows would be greatly facilitated by sediment traps, current meters, and coring at the exit point, as well as vertical side-scan profiling of the ice front to determine discharge tunnel dimensions and location.

ACKNOWLEDGEMENTS

Support for this research came from the Office of Naval Research under contract # N00014-01-C-009, and could not have been completed without ship time and logistical support from the Norwegian Polar Research Institute (NPRI) and the crew of the R/V Lance. Travel funds were provided by the Norwegian Marshall Fund for Scientific Research and the Woods Hole Oceanographic Institution Education Department. The manuscript benefitted by early reviews from David Aubrey, John Milliman, Paul Speer, Keith Stolzenbach, and Anders Solheim (NPRI). Tor Gammelsrod at the Geophyscial Institute in Bergen provided hydrographic information, Sharon Downey measured grain sizes of suspended sediments, and Nancy Murphy drafted the figures.

REFERENCES

Anderson, J.B., C. Brake, E. Domack, N. Meyers, R. Wright (1983) Development of a polar glacial-marine sedimentation model from Antarctic Quaternary deposits and glaciological information. in Molnia, B.F. (ed.) Glacial Marine Sedimentation. Plenum Press p.233-264.

Baba, J. and P.D. Komar (1981) Measurements and analysis of settling velocities of natural quartz sand grains. J. Sed. Pet. 51:631-640.

Beardsley, R.C. and J. Hart (1978) A simple theoretical model for the flow of an estuary onto a continental shelf. J. Geophs. Res. 83:873-883.

Blake, W. (1962) Geomorphology and glacial geology in Nordaustlandet, Spitsbergen: vol I, II. 470pp. Ohio State Univ. Ph.D. thesis.

Brooks, N. (1960) Dispersion in Hydrologic and Coastal Environments. In: Proc. 1st Int. Conf. on Waste Disposal in the Marine Environment, Pergamon Press, p.246.

Collins, D.N. (1979) Sediment concentration in meltwater as an indicator of erosion processes beneath an alpine glacier. J. Glaciol. 23:247-257.

Csanady, G.T. (1973) Turbulent Diffusion in the Environment D. Reidel Pub. Co. p.106.

Csanady, G.T. (1982) Circulation in the Coastal Ocean. D. Reidel Pub. Co. Dordrecht, Holland. 279pp.

Denton, G.H. and T.J. Hughes (1981) The Last Great Ice Sheets John Wiley and Sons. 484pp.

Edwards, M.B. (1978) Glacial Environments. in Reading, H.G. (ed.) Sedimentary Environments and Facies. Elsevier p416-438.

Elverhoi, A. (in press) Glacigenic and associated marine sediments in the Weddell Sea, fjords of Spitsbergen, and the Barents Sea: a review. Mar. Geol.

Elverhoi, A. and A. Solheim (1983) The Barents Sea ice sheet - A sedimentological discussion. Polar Research 1:23-42.

Elverhoi, A., O. Liestol, J. Nagy (1980) Glacial erosion, sedimentation, and microfauna in the inner part of Kongsfjorden, Spitsbergen. Nor. Polarinst. Skr. 172:33-58.

Embleton C. and C.A.M. King (1975) Glacial Geomorphology. John Wiley and Sons. 573pp.

Farrow, G.E., J.P.M. Syvitski, V. Tunnicliffe (1983) Suspended particulate loading on the macrobenthos in a high turbid fjord: Knight Inlet, British Columbia. Can. J. Fish. Aquat. Sci. 40 (suppl. 1):273-288.

Fischer, H.B., E.J. List, R.C.Y. Koh, J. Imberger, N.H. Brooks (1979) Mixing in Inland and Coastal Waters Academic Press. 483pp.

Flint, R.F. (1971) Glacial and Quaternary Geology. John Wiley and Sons, Inc., New York. 892pp.

Folk, R.L., 1968 Petrology of sedimentary rocks. University of Texas. Geology 370K, 3831, 383M. 170pp.

Garvine, R.W. (1984) Radial spreading of bouyant, surface plumes in coastal aters. J. Geophys. Res. 89:1989-1996.

Garvine, R.W. (1982) A steady state model for bouyant surface plume hydrodynamics in coastal waters. Tellus 34:293-306.

Gilbert, R. (1978) Observations on oceanography and sedimentation at Pangnirtung Fjord, Baffin Island. Maritime Sed. 14:1-10.

Glen, A.R. (1941) A subarctic glacier cap: the west ice of North East Land. Geograph. J. 98:135-146.

Griffiths, R.W. and P.F. Linden (1983) The stability of bouyancy-driven coastal currents. Dynamics of Atm. and Oceans 5:281-306.

Hagen, J.D., B. Wold, O. Liestol, C. Ostrem, J.L. Sollid (1983) Subglacial process at Bondhusbreen, South Norway: Some preliminary results. Ann. Glaciol. 4:000-000.

Hartley, C.H. and M.J. Dunbar (1937) On the hydrodynamic mechanism of the so-called brown zones associated with tidal glacier. J. Mar. Res. 1:305-311.

Hollins (in prep.) The Brasvellbreen surge.

Hoskin, C.M. and D.C. Burrell (1972) Sediment transport and accumulation in a fjord basin; Glacier Bay, Alaska. J. Geol. 80:539-551.

Jones, G.A. and W.F. Ruddiman (1982) Assessing the global meltwater spike. Quaternary Res. 17:148-172.

Jopling, A.V. and B.C. McDonald Glaciofluvial and Glaciolacustrine Sedimentation. Soc. Econ. Pal. Min. 23

Loeng, H. (1980) Physical oceanography of the Barents Sea. Fisken Hav. (in Norwegian).

Kristofferson, Y., J.D. Milliman, J.P. Ellis (in press) Unconsolidated sediments and shallow structure of the northern Barents Sea. Nor. Polarinst. Skr.

Martin, S. (1975) Wind regimes and heat exchange on glacier de Saint-Sorlin. J. Glaciol. 14:91-105.

Orvin, A.K. (1969) Outline of the geological history of Spitsbergen. Skrifter om Svalbard og Ishavet. Nr. 78 Oslo 57pp.

Pfirman, S.P., J.D. Milliman, and A. Elverhoi (1982) Recent flux of suspended material near glacier front, Svalbard Archipelago. AGU/ASLO Joint Meeting San Antonio, Texas. Abstracts with Program.

Pfirman, S.L. (1984) Input of recent glacial sediment to the northern Barents Sea. 13th Annual Arctic Workshop. INSTAAR abstracts with program. p.63.

Pfirman, S.L. (in prep.) Water mass distribution of the northern Barents Sea.

Powell, R. (1980) Holocene glacimarine sediment deposition by tidewater glaciers in Glacier Bay, Alaska. Ohio State Univ. Ph.D. thesis 420pp.

Rust, B.R. and R. Romanelli (1975) Late Quaternary subaqueous outwash deposits near Ottawa, Canada. in Jopling, A.V. and B.C. McDonald Glaciofluvial and Glaciolacustrine Sedimentation. Soc. Econ. Pal. Min. 23:177-192.

Schytt V. (1964) Scientific results of the Swedish glaciological expedition to Nordaustlandet, Spitsbergen, 1957 and 1958. Part I and II. Geografiska Annaler 46:243-281.

Shcheglova, O.P. and O.P. Chizhov (1981) Sediment transport from the glacial zone, central Asia. Ann. Glaciol. 2:103-108.

Shreve R.L. (1972) Movement of water in glaciers. J. Glaciol. 11:205-214

Solheim, A. (in prep.) Sediment distribution and characteristics outside a grounded surging glacier; Brasvellbreen, Svalbard.

Syvitski, J.P.M. (1980) Flocculation, agglomeration, and zooplankton pellitization of suspended sediment in a fjord receiving glacial meltwater. in Fjord Oceanography. p615-623.

Syvitski, J.P.M. and J.W. Murray (1981) Particle interaction in fjord suspended sediment. Mar. Geol. 39:215-242.

Weertman, J. and G. E. Birchfield (1982) Subglacial water flow under ice streams and West Antarctic ice sheet stability. Ann. Glaciol. 3:316-320.

Weertman, J. (1972) General theory of water flow at the base of a glacier or ice sheet. Rev. Geophys. Space Phys. 10:287-333.

Whillans, I.M. (1975) Effect of inversion winds on topographic detail and mass balance on inland ice sheets. J. Glaciol. 14:85-90.

Wright, G.F. (1887) The Muir Glacier. Am. J. Sci. 33:1-18.

Appendix A

Hydrographic Data

1978

All data is from the Institute for Marine Research, in Bergen.

Figure 1A. Surface temperature

B. Surface salinity

C. Arctic Water temperature

D. Arctic Water salinity

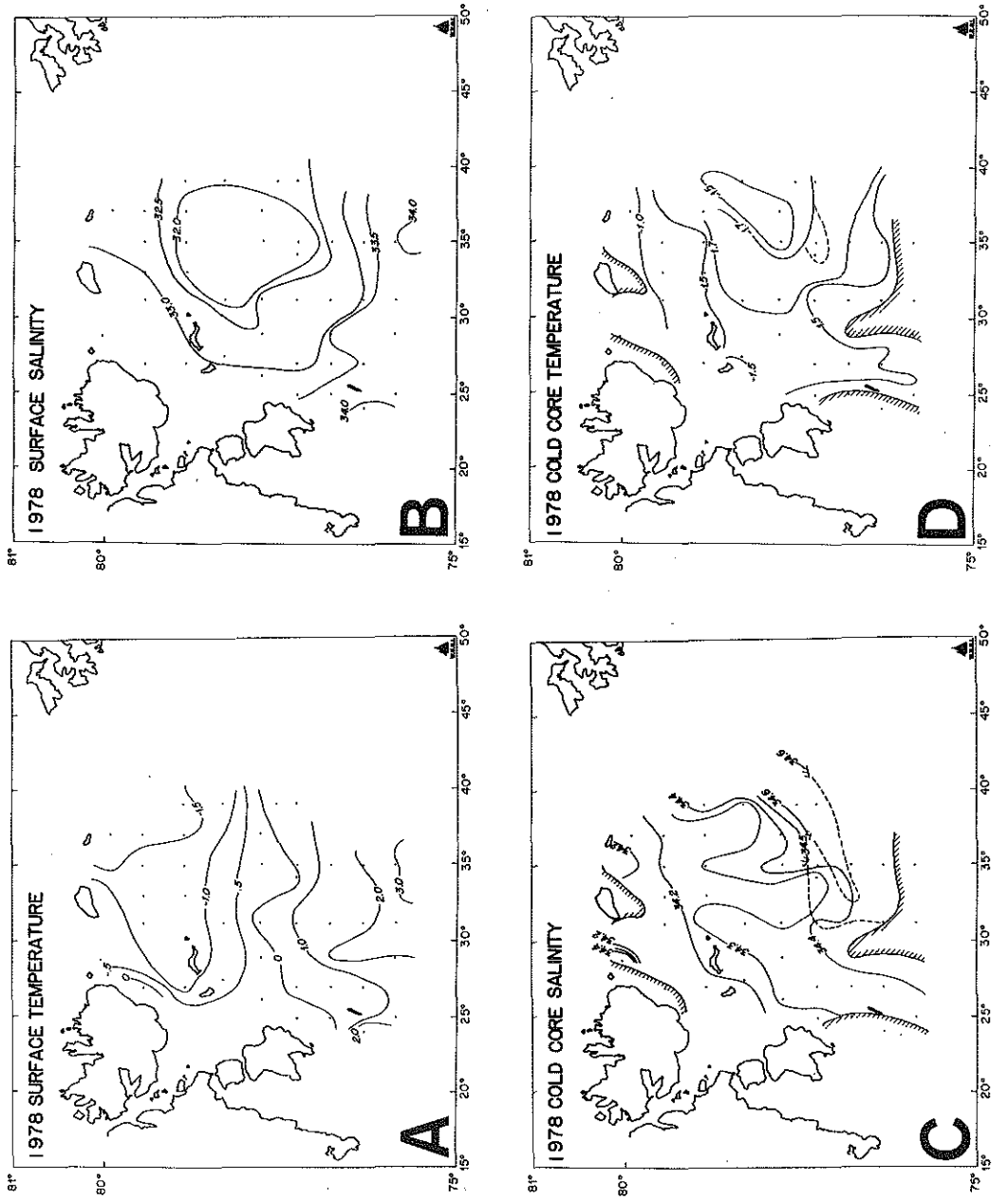
1978 SURFACE TEMPERATURE
A
1978 SURFACE SALINITY
B
1978 COLD CORE SALINITY
C
1978 COLD CORE TEMPERATURE
D

Figure 1

Figure 2A. Atlantic Water temperature

B. Atlantic Water salinity

C. Bottom water temperature

D. Bottom water salinity

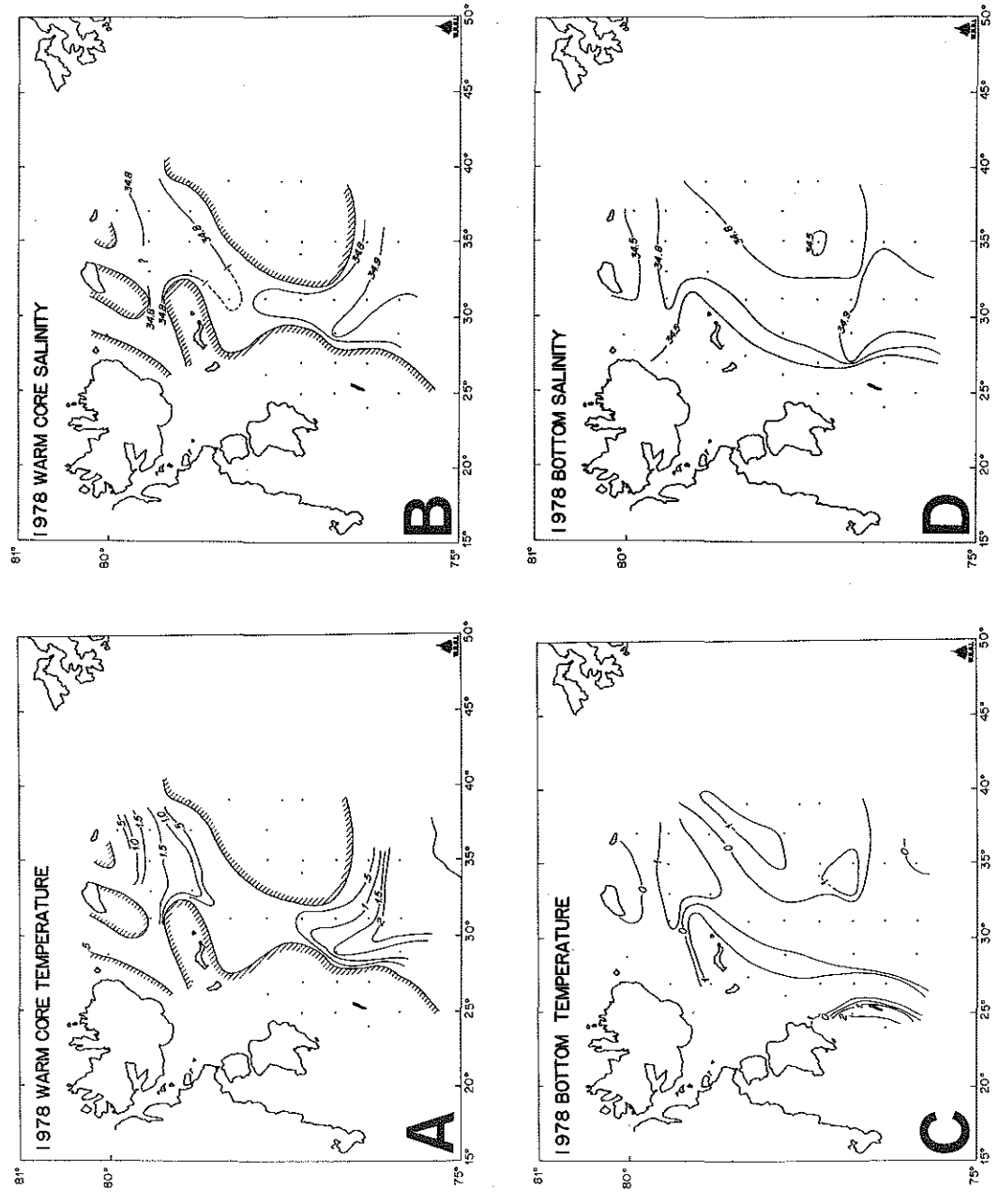
1978 WARM CORE TEMPERATURE
A
1978 WARM CORE SALINITY
B
1978 BOTTOM TEMPERATURE
C
1978 BOTTOM SALINITY
D

Figure 2

1980

All data was collected on the Norwegian Polar Research Institute cruise of 1980 to the northern Barents Sea, from the Norvarg. Further details of the cruise, including station locations, may be found in the NPRI cruise report prepared by Yngve Kristoffersen.

Figure 3. 1980 station locations. Hatching in the north denotes region with heavy sea-ice.

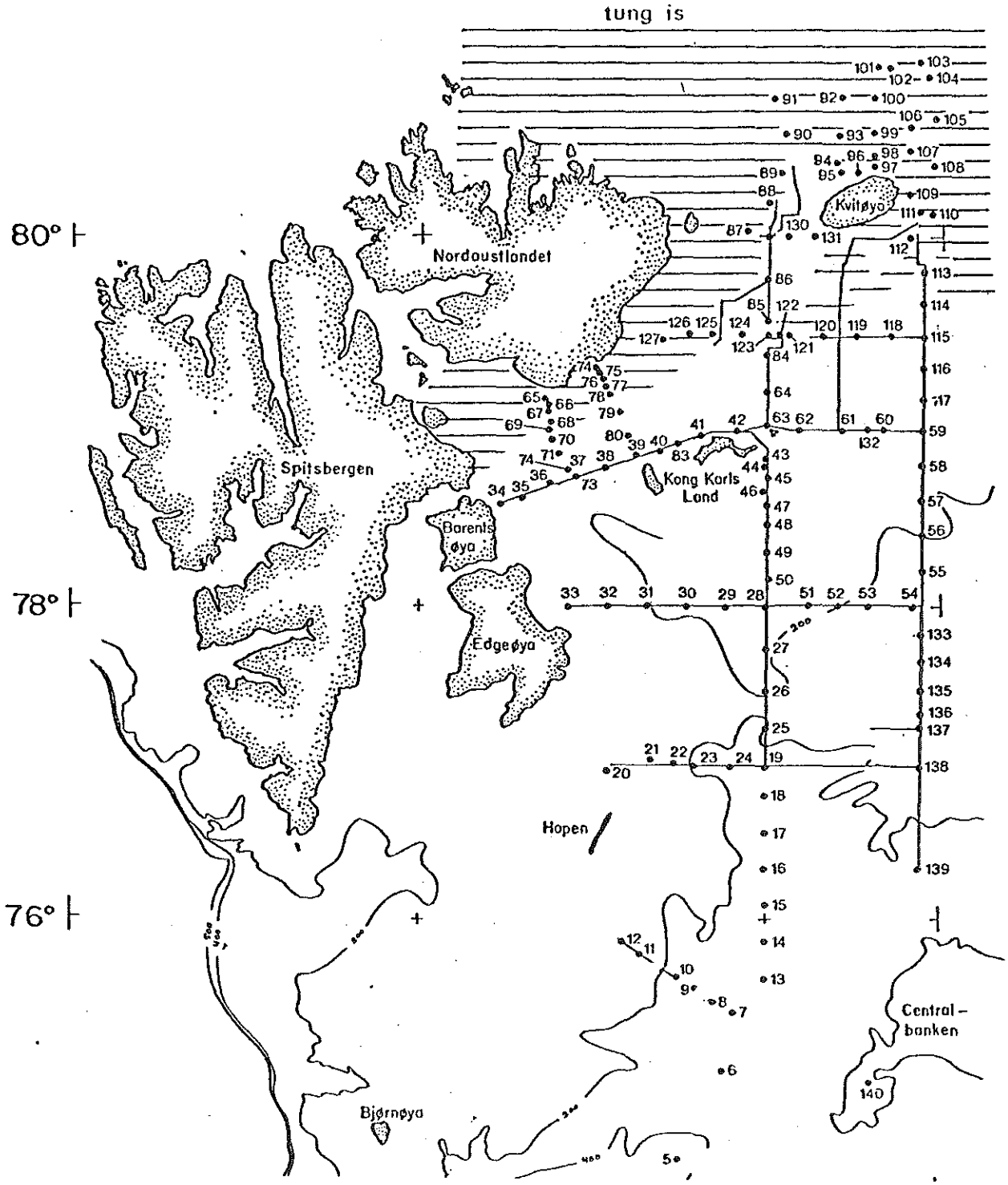
tung is
Nordaustlandet
Kvitøya
Spitsbergen
Barents øya
Kong Karls Land
Edgeøya
Hopen
Bjørnøya
Central-banken
80°
78°
76°

Figure 3

Figure 4A. Surface temperature

B. Surface salinity

C. Bottom water temperature

D. Bottom water salinity

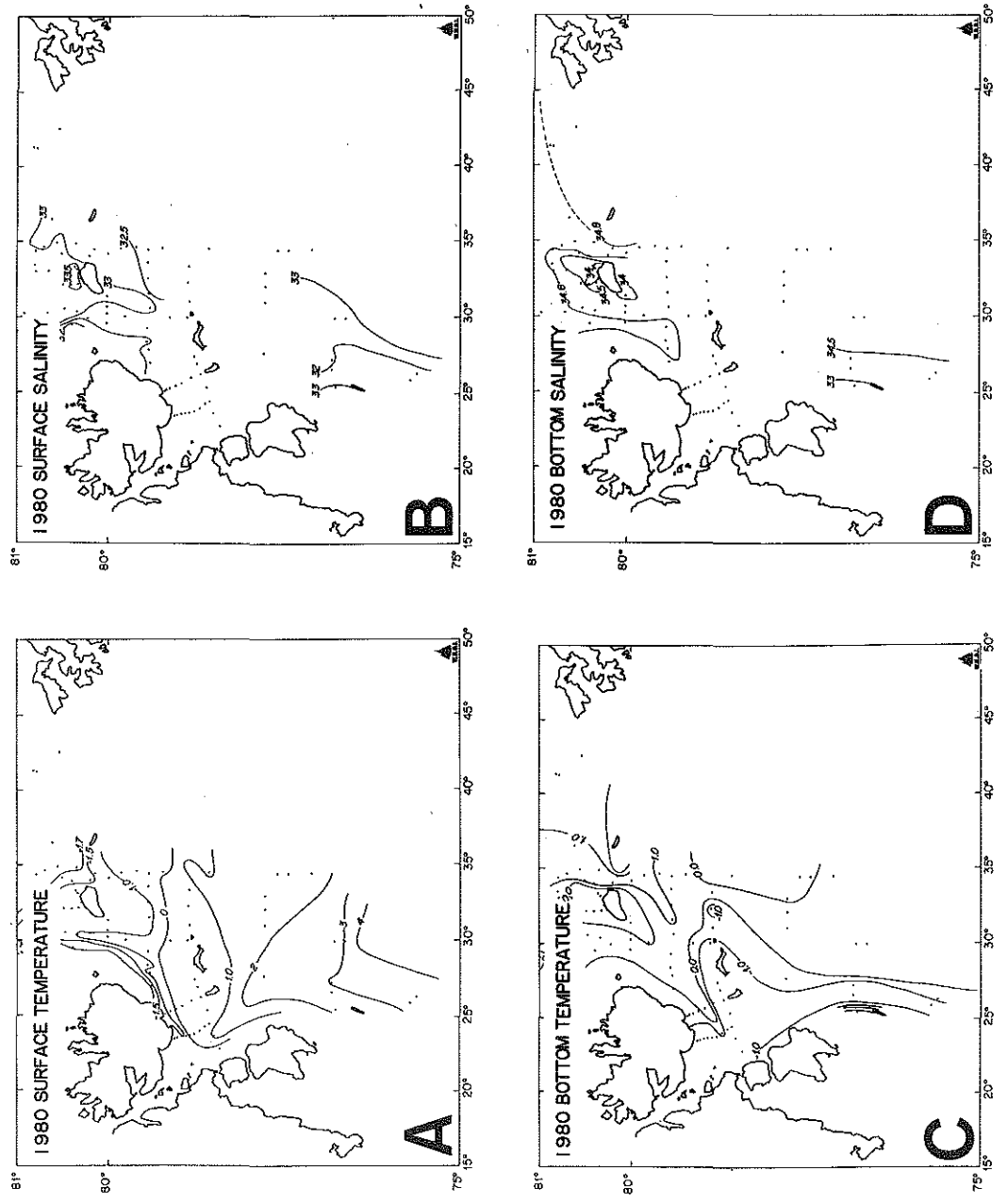
1980 SURFACE TEMPERATURE
A
1980 SURFACE SALINITY
B
1980 BOTTOM TEMPERATURE
C
1980 BOTTOM SALINITY
D

Figure 4

1981

Hydrographic data complied from both a NPRI cruise to the northern Barents Sea and the Institute for Marine Research cruise to the southern Barents Sea. Further information on the 1981 NPRI cruise can be obtained from the cruise report by Anders Elverhoi and Anders Solheim, NPRI.

Figure 5. Station locations for 1981 NPRI cruise.

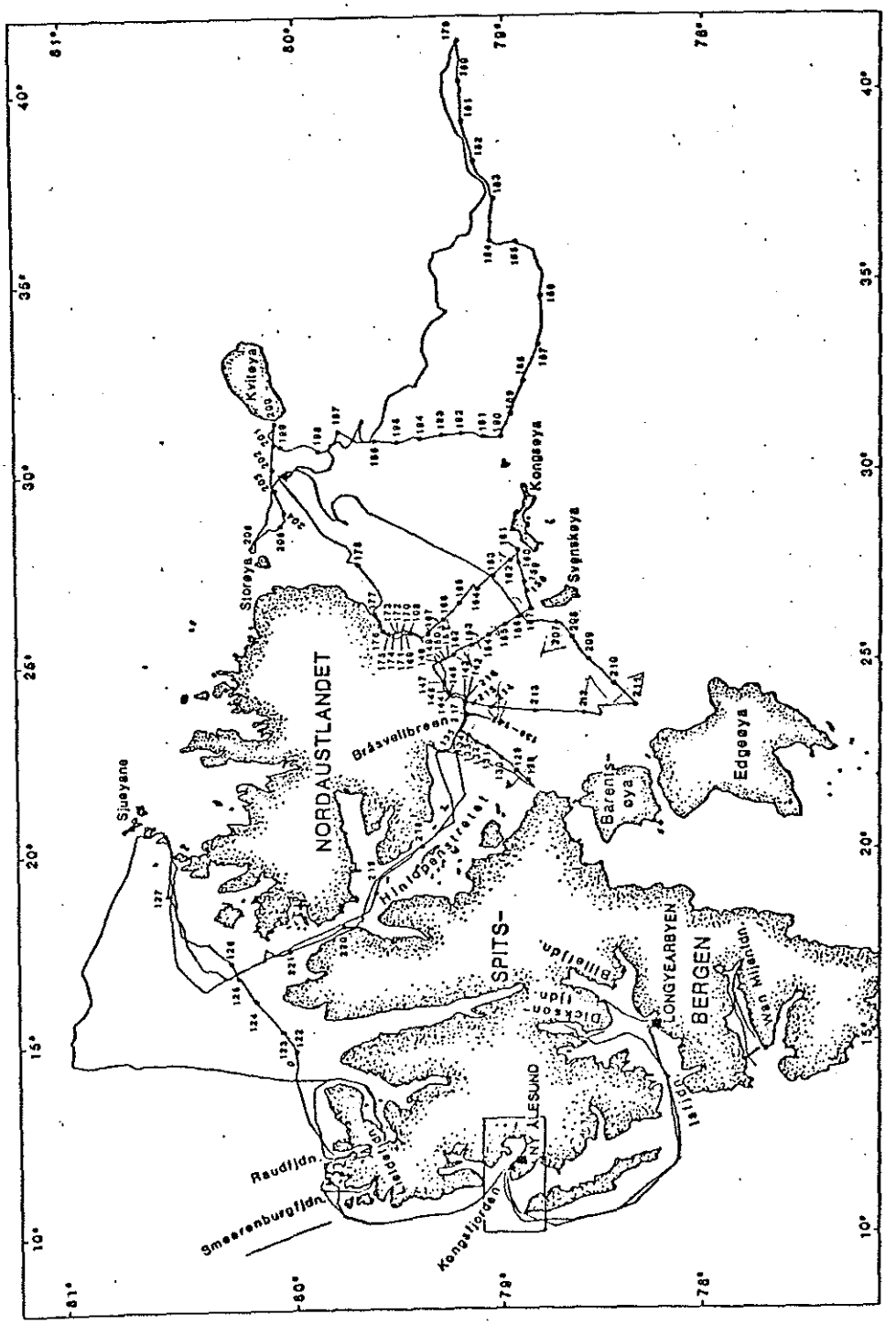
NORDAUSTLANDET
SPITS-
BERGEN
NY ÅLESUND
LONGYEARBYEN
Kvitøya
Kongsøya
Svenskøya
Storøya
Barentsøya
Edgeøya
Sjuøyane
Brøsvalibreen
Hinlopenstretet
Raudfjorden
Smeerenburgfjorden
Kongsfjorden
Billefjorden
Dickson-fjorden
Isfjorden
Wijdefjorden

Figure 5

Figure 6. Hydrographic transects for Nordaustlandet region. Data collected and processed by Tor Gammelsrod, Geophysics Department, University of Bergen.

a. Stations 128-136

b. Stations 211-216

c. Stations 148-157

d. Stations 162-167

e. Stations 207-211

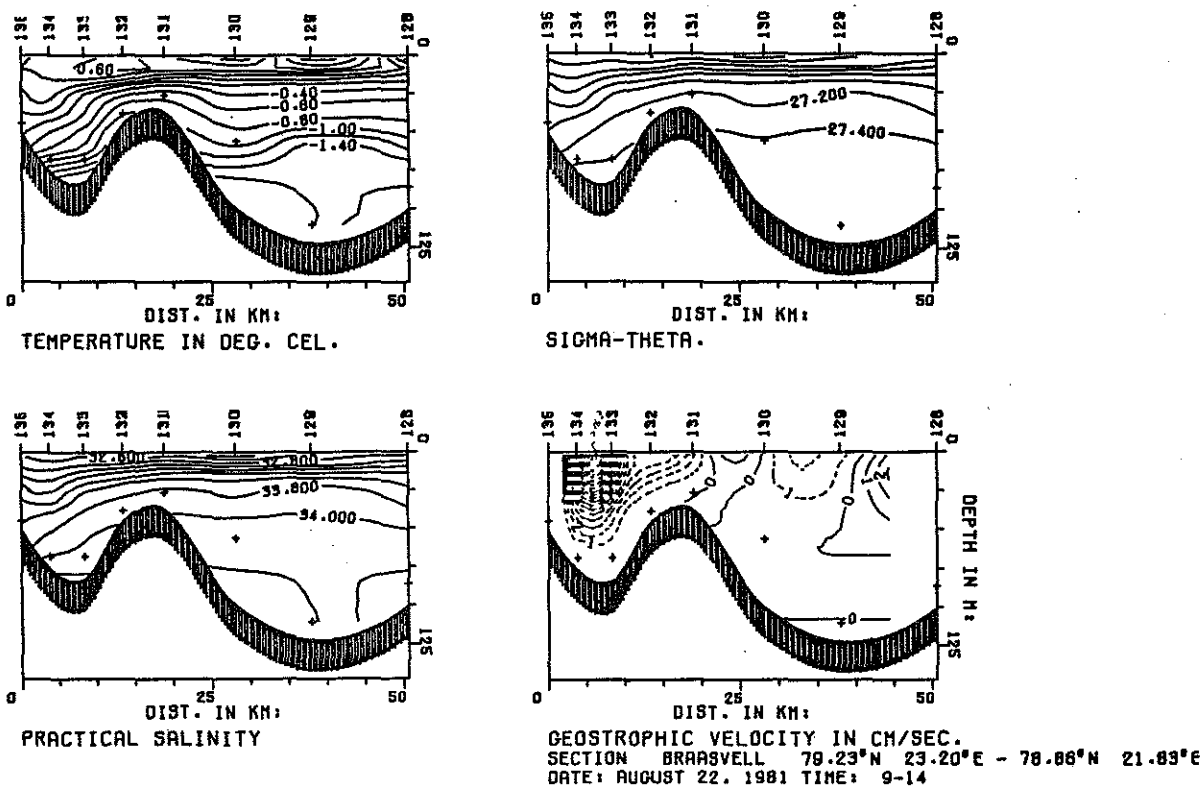
DIST. IN KM:
TEMPERATURE IN DEG. CEL.
-0.60
-0.40
-0.80
-1.00
-1.40
DIST. IN KM:
SIGMA-THETA.
27.200
27.400
DIST. IN KM:
PRACTICAL SALINITY
33.800
34.000
DIST. IN KM:
DEPTH IN M:
GEOSTROPHIC VELOCITY IN CM/SEC.
SECTION BRAASVELL 79.23°N 23.20°E - 78.86°N 21.83°E
DATE: AUGUST 22. 1981 TIME: 9-14

Figure 6a

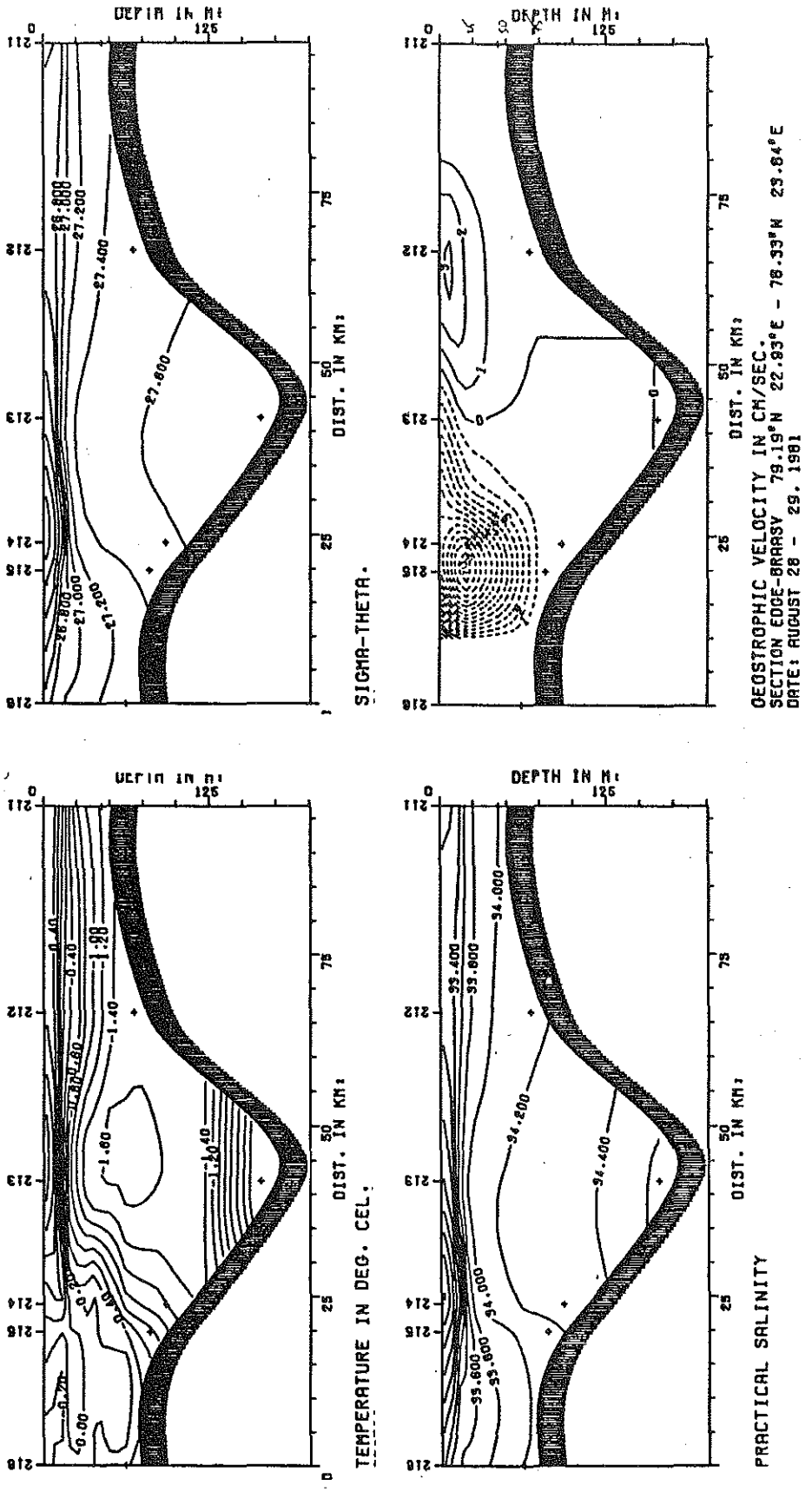
DEPTH IN M:
DIST. IN KM:
SIGMA-THETA.
GEOSTROPHIC VELOCITY IN CM/SEC.
SECTION EDGE-BRARSV 79.19°N 22.83°E - 78.33°W 23.84°E
DATE: AUGUST 28 - 29, 1981
TEMPERATURE IN DEG. CEL.
PRACTICAL SALINITY

Figure 6b

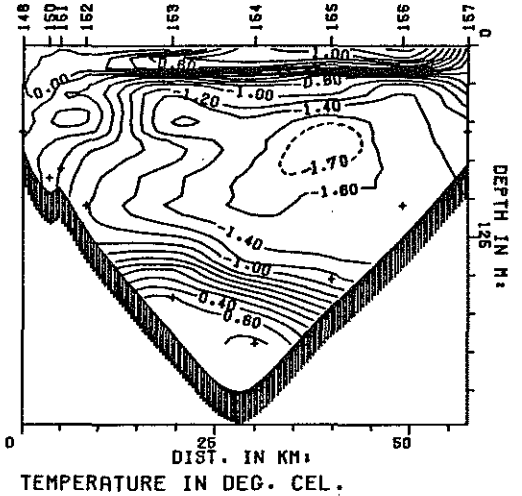

TEMPERATURE IN DEG. CEL.

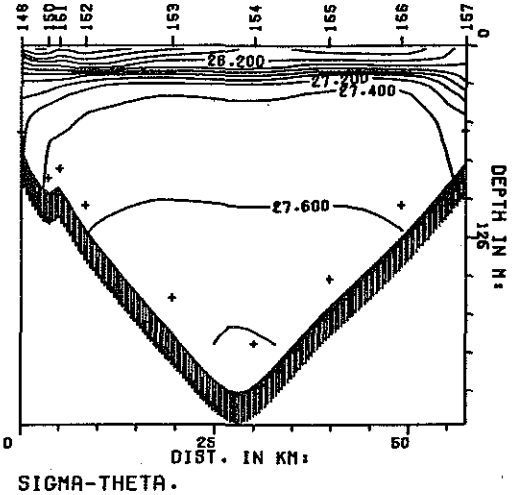

SIGMA-THETA.

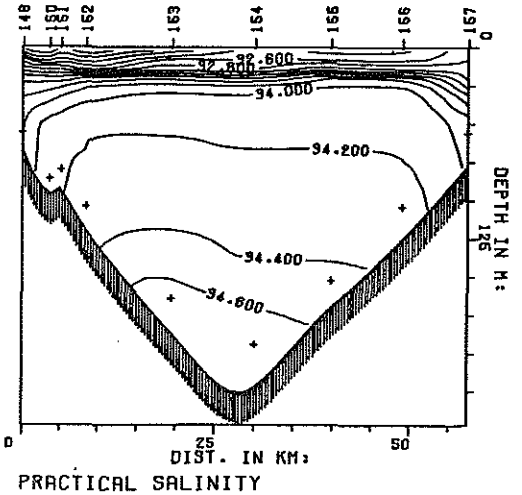

PRACTICAL SALINITY

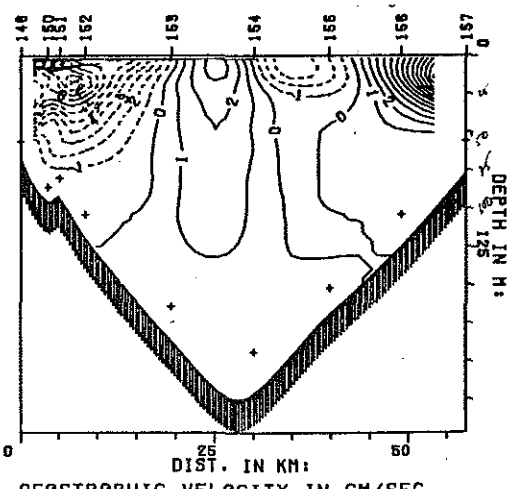

GEOSTROPHIC VELOCITY IN CM/SEC.
SECTION MOHN-SVENSK 79.32°N 25.05°E - 78.87°N 26.40°E
DATE: AUGUST 23. 1981 TIME: 3- 8

Figure 6c

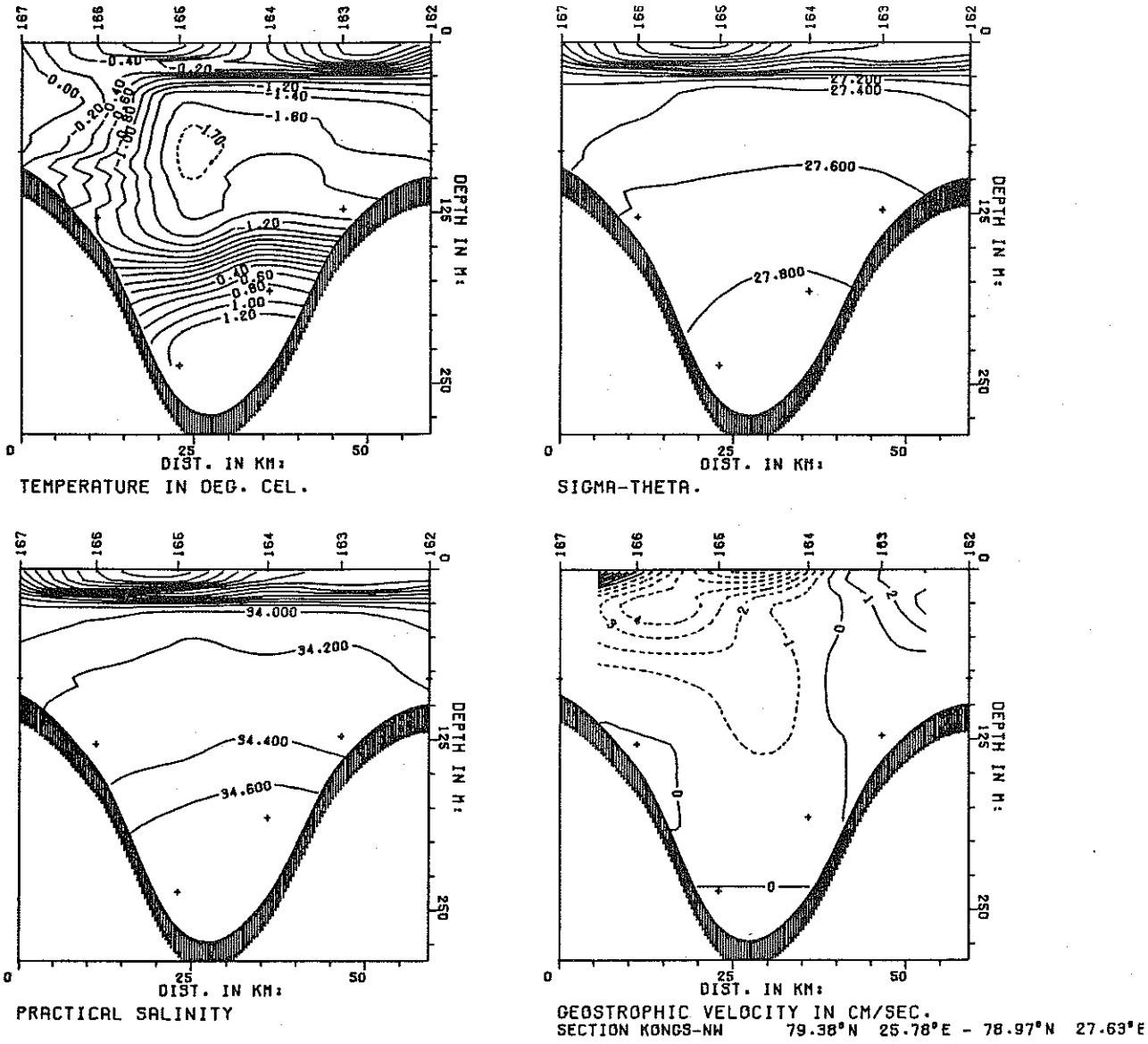
167
166
165
164
163
162
0
-0.40
-0.20
0.00
-1.20
-1.40
-1.60
-1.70
-0.60
-0.80
-1.00
-1.20
0.40
0.60
0.80
1.00
1.20
DEPTH IN M:
125
250
0
25
50
DIST. IN KM:
TEMPERATURE IN DEG. CEL.
27.200
27.400
27.600
27.800
SIGMA-THETA.
34.000
34.200
34.400
34.600
PRACTICAL SALINITY
-3
-2
-1
0
1
2
GEOSTROPHIC VELOCITY IN CM/SEC.
SECTION KONGS-NW 79.38°N 25.78°E - 78.97°N 27.63°E

Figure 6d

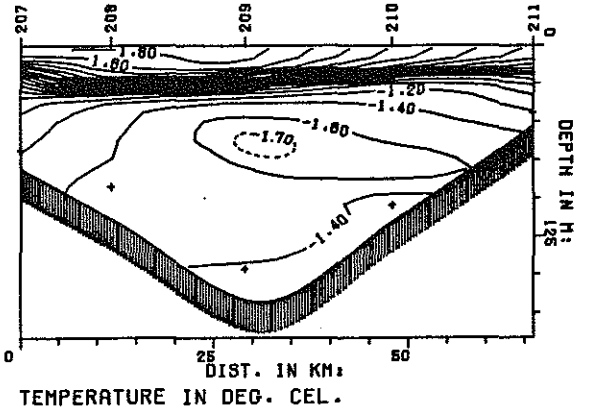

TEMPERATURE IN DEG. CEL.

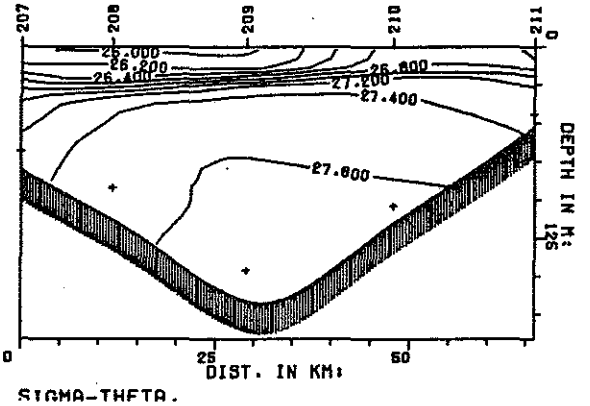

SIGMA-THETA.

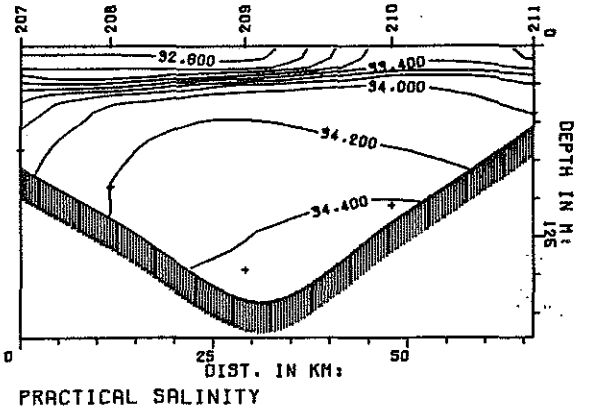

PRACTICAL SALINITY

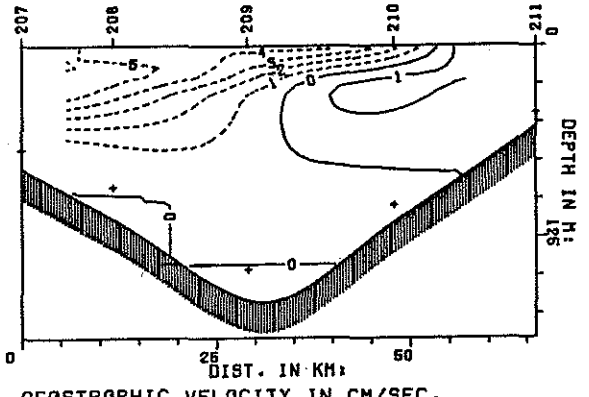

GEOSTROPHIC VELOCITY IN CM/SEC.
SECTION SVENSK-EDOE 78.73°N 26.07°E - 78.33°N 23.84°E
DATE: AUGUST 28, 1981 TIME: 13-18

Figure 6e

Figure 7. Surface water properties:

Property	Average	Standard Deviation
Depth	2.1	0.8m
Temperature	2.10	1.91°C
Salinity	32.95	2.33°/$_{oo}$
σ_t	26.33	1.84

A. Surface temperature

B. Surface salinity

C. Surface density

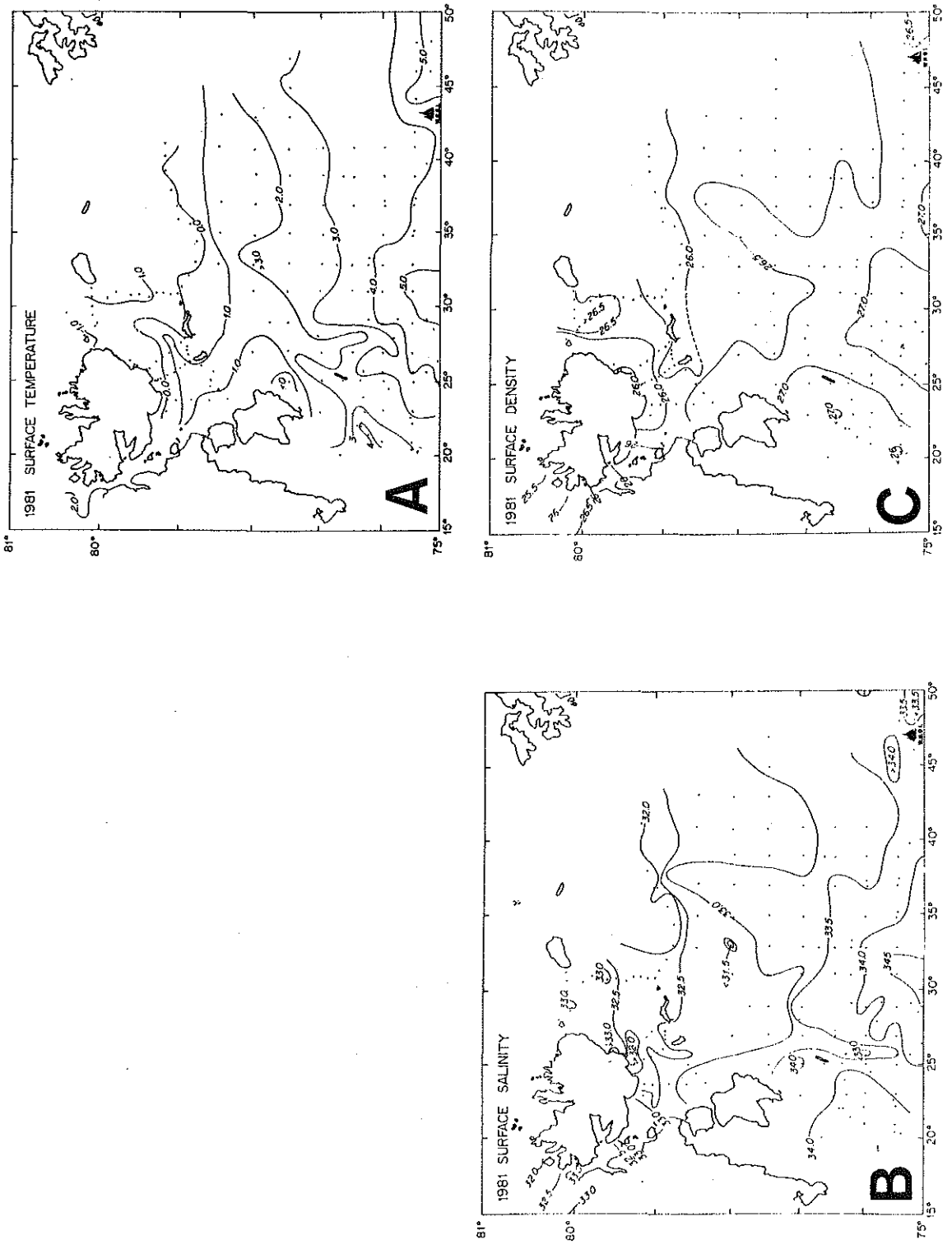
1981 SURFACE TEMPERATURE
A
1981 SURFACE DENSITY
C
1981 SURFACE SALINITY
B

Figure 7

Figure 8. Arctic water core properties:

Property	Average	Standard Deviation
Depth	70.9	20.5m
Temperature	-1.48	0.37°C
Salinity	34.37	0.20°/$_{oo}$
σ_t	27.68	0.17

A. Arctic water depth

B. Arctic water temperature

C. Arctic water salinity

D. Arctic water density

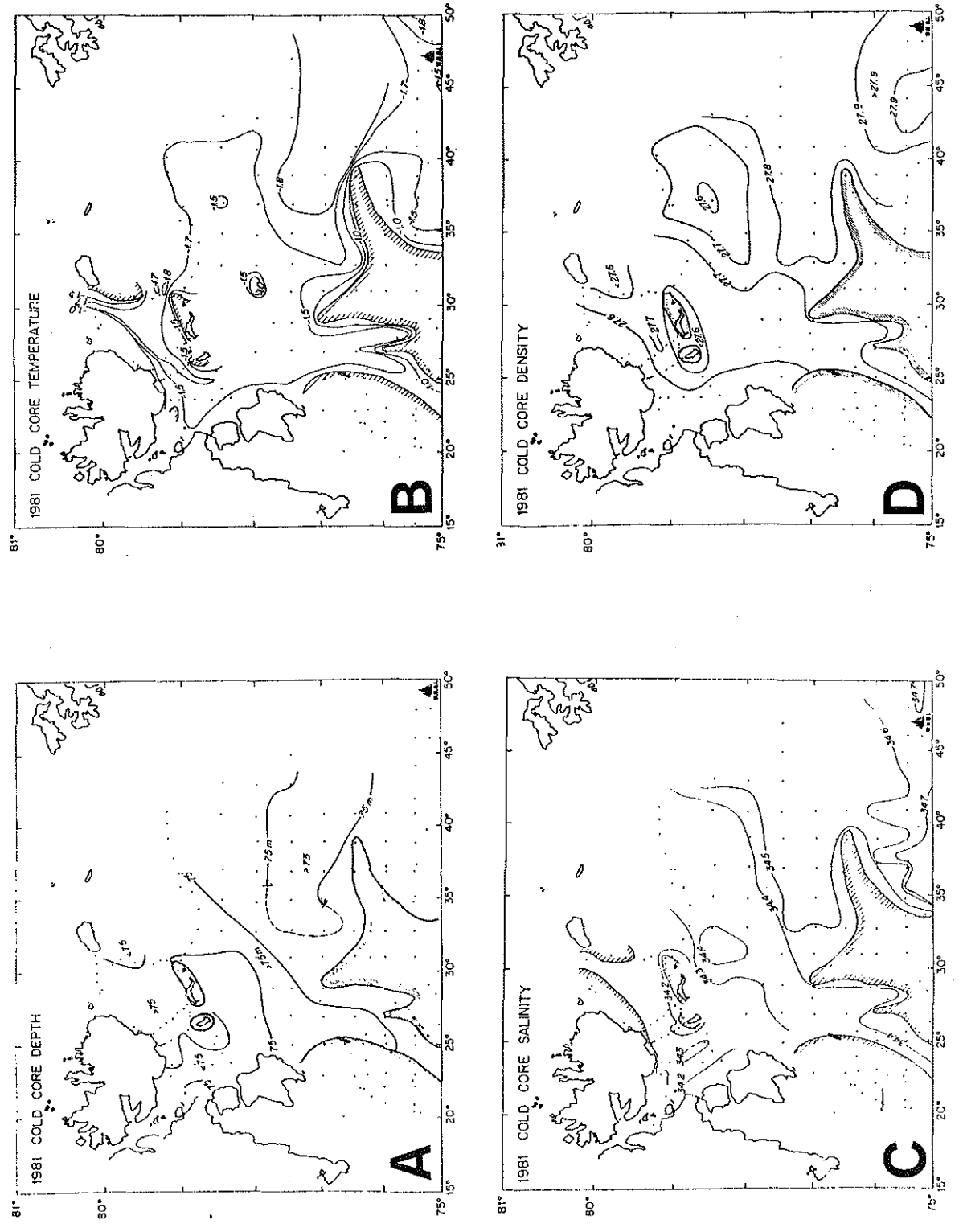
1981 COLD CORE DEPTH
A
1981 COLD CORE TEMPERATURE
B
1981 COLD CORE SALINITY
C
1981 COLD CORE DENSITY
D

Figure 8

Figure 9A. Location of stations with extreme water mass characteristics

B. Temperature - salinity plot of Arctic water core data

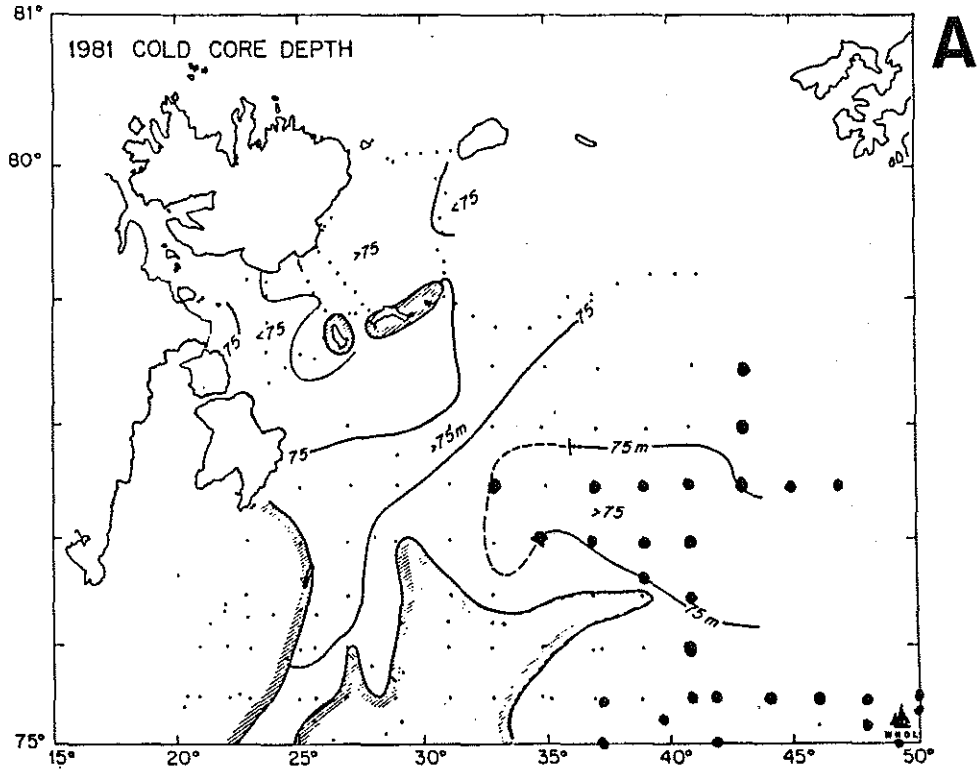
1981 COLD CORE DEPTH
A
81°
80°
75°
15°
20°
25°
30°
35°
40°
45°
50°
<75
>75
75
>75m
75m

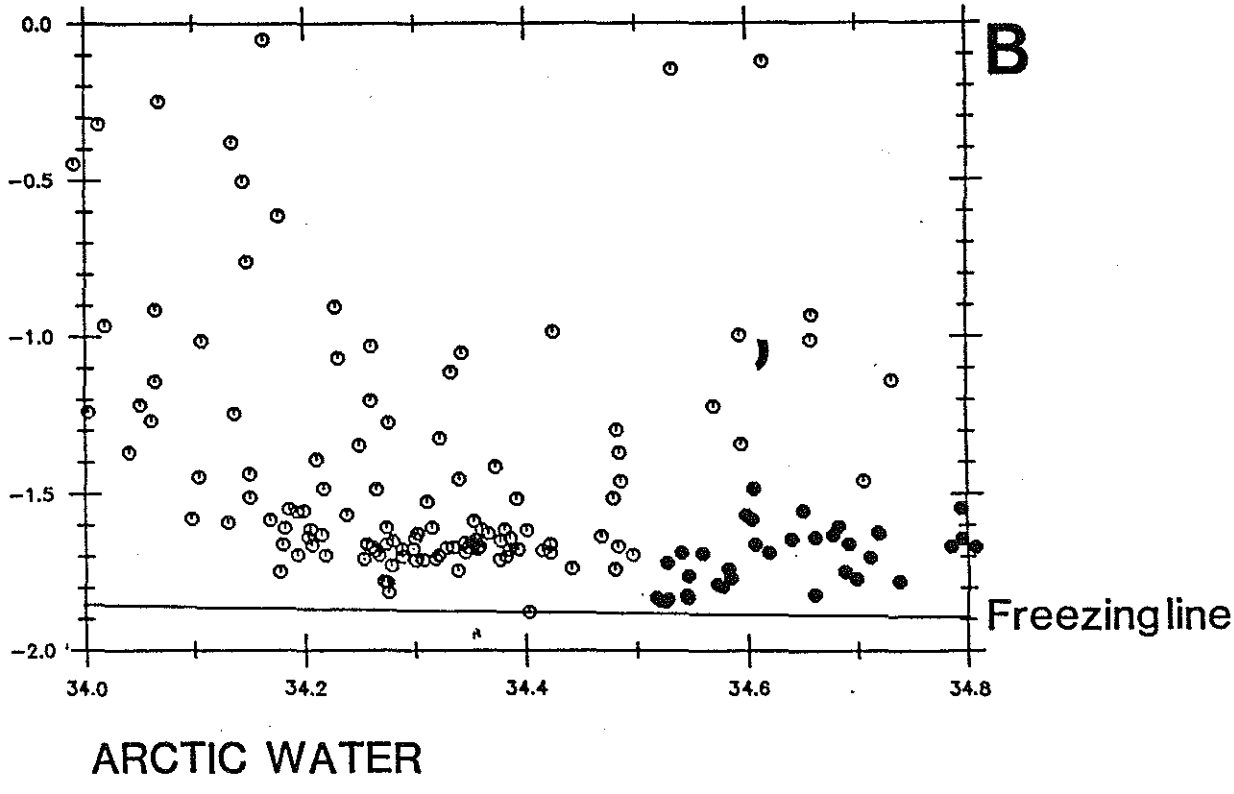
B
0.0
-0.5
-1.0
-1.5
-2.0
34.0
34.2
34.4
34.6
34.8
Freezing line
ARCTIC WATER

Figure 9

Figure 10. Atlantic water core properties:

Property	Average	Standard Deviation
Depth	149.4	73.6m
Temperature	1.35	1.12°C
Salinity	34.86	0.11°/$_{oo}$
σ_t	27.92	0.11

A. Atlantic water depth

B. Atlantic water temperature

C. Atlantic water salinity

D. Atlantic water density

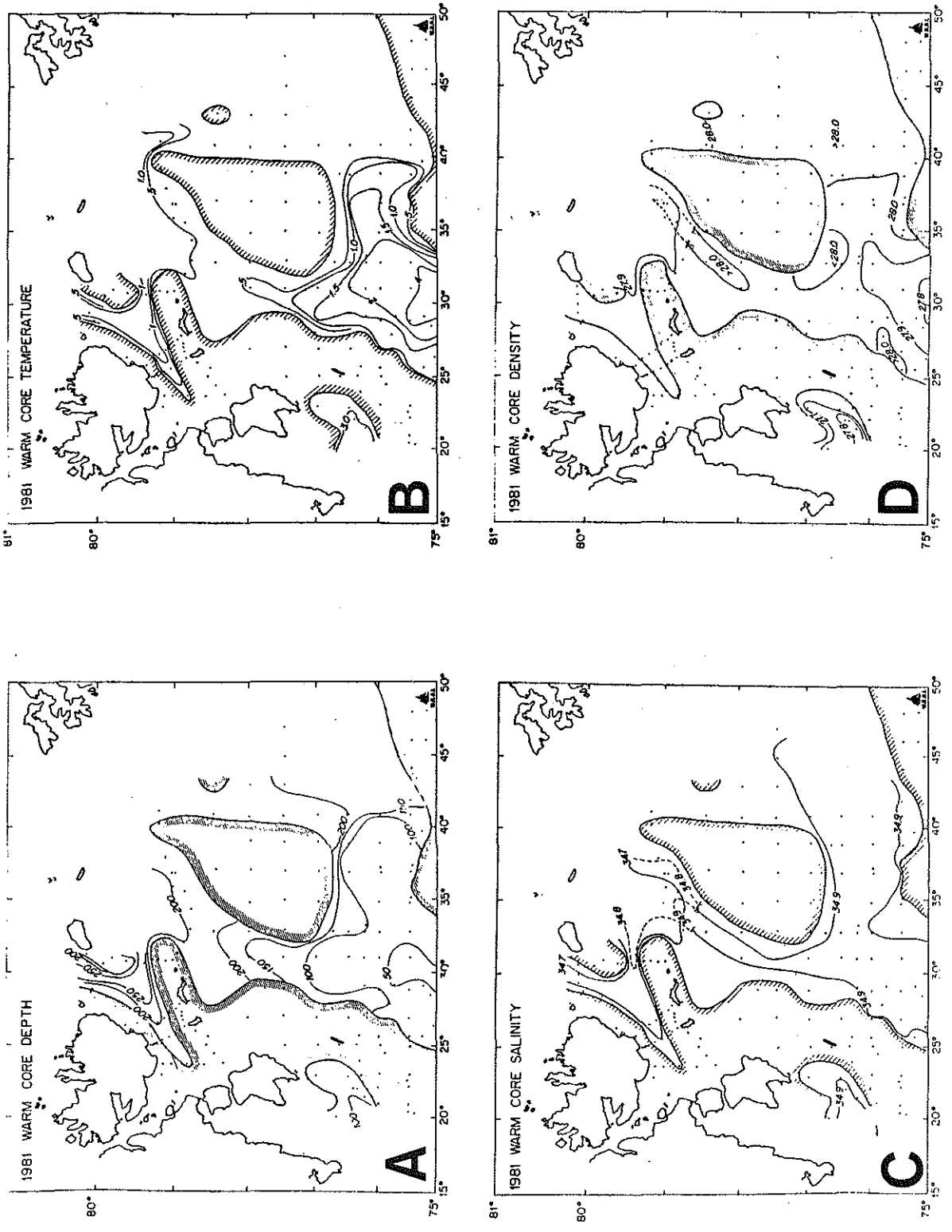
1981 WARM CORE DEPTH
A
1981 WARM CORE TEMPERATURE
B
1981 WARM CORE SALINITY
C
1981 WARM CORE DENSITY
D

Figure 10

Figure 11A. Location of stations with extreme water mass characteristics

B. Temperature - salinity plot of Atlantic water core data

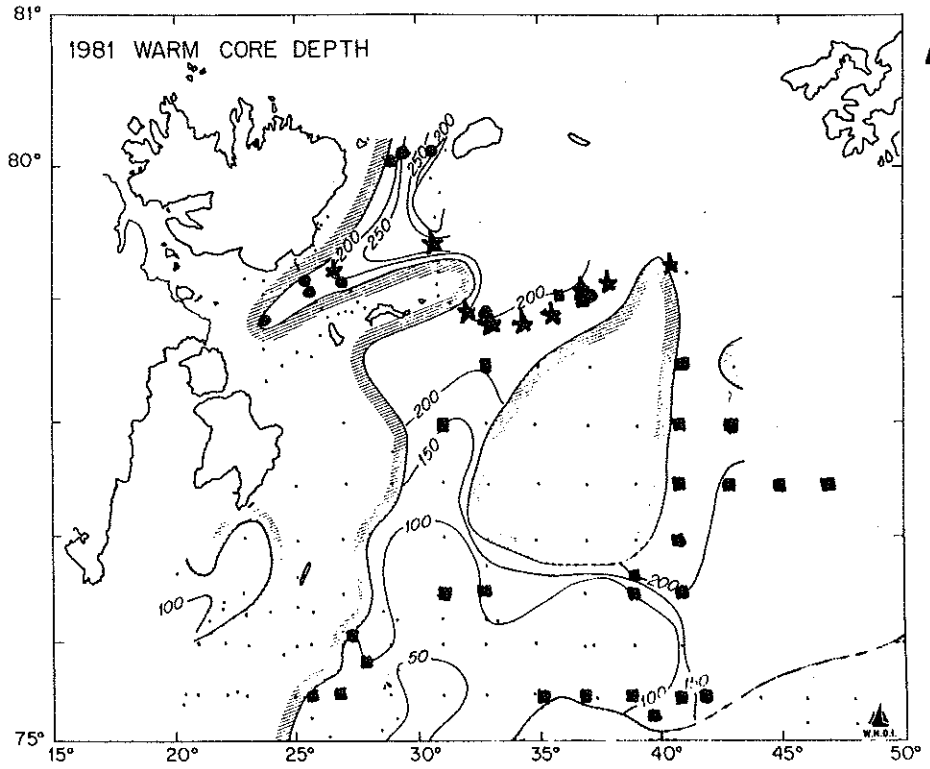
A
1981 WARM CORE DEPTH
81°
80°
75°
15°
20°
25°
30°
35°
40°
45°
50°
300
250
200
150
100
50

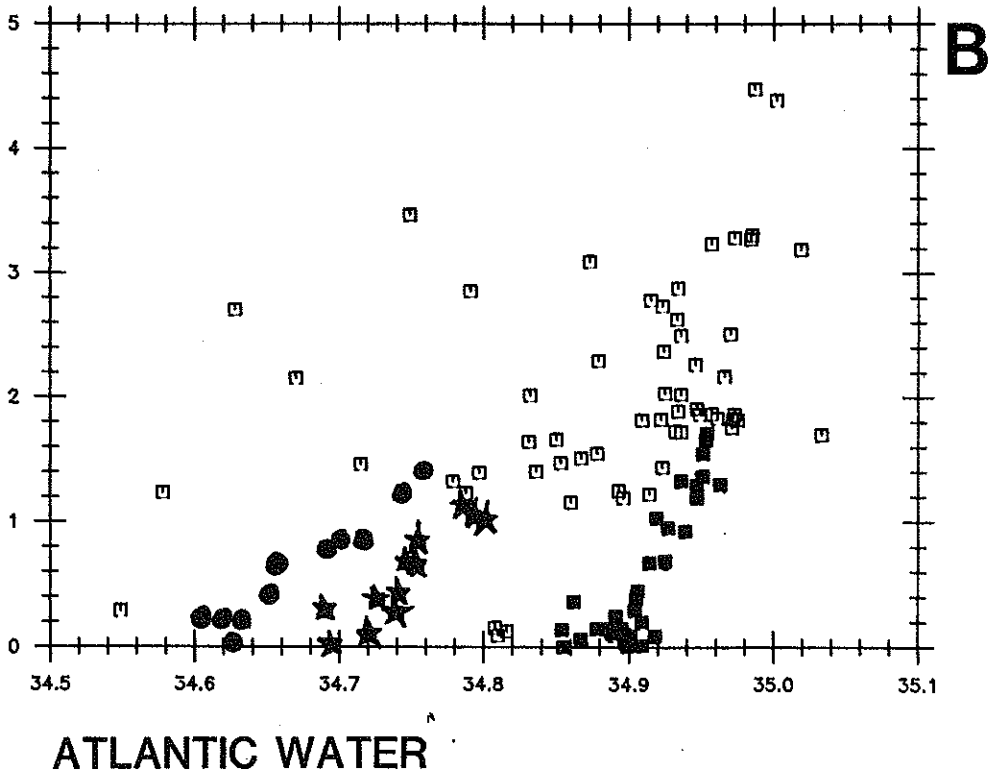
B
5
4
3
2
1
0
34.5
34.6
34.7
34.8
34.9
35.0
35.1
ATLANTIC WATER

Figure 11

Figure 12. Cold deep water core properties:

Property	Average	Standard Deviation
Depth	234.1	51.7m
Temperature	-0.75	0.58°C
Salinity	34.88	0.05°/$_{oo}$
σ_t	28.06	0.05

A. Cold Deep Water depth

B. Cold Deep Water temperature

C. Cold Deep Water salinity

D. Cold Deep Water density

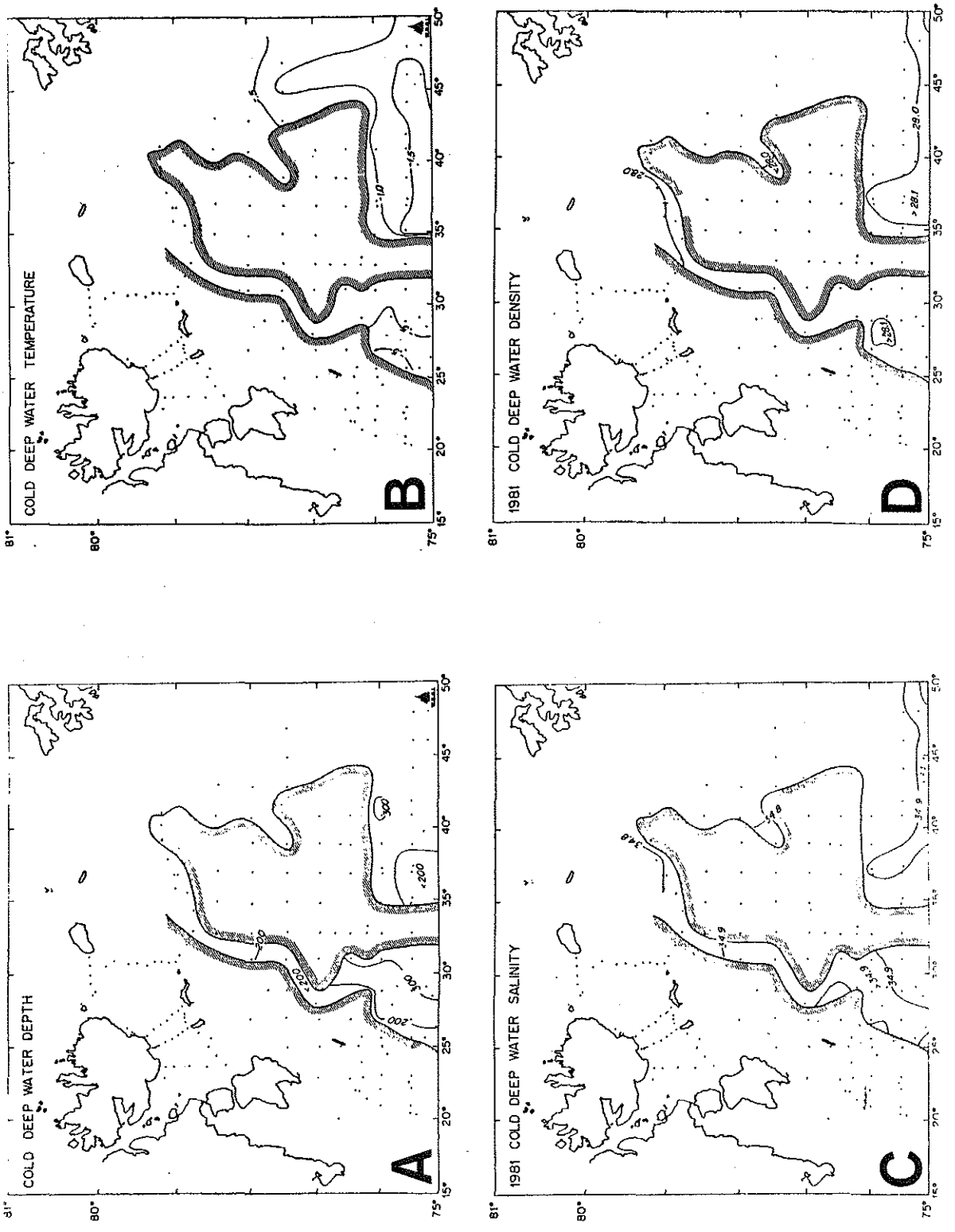
COLD DEEP WATER DEPTH
A
COLD DEEP WATER TEMPERATURE
B
1981 COLD DEEP WATER SALINITY
C
1981 COLD DEEP WATER DENSITY
D

Figure 12

Figure 13A. Location of stations with extreme water mass characteristics

B. Temperature - salinity plot of cold deep water core data

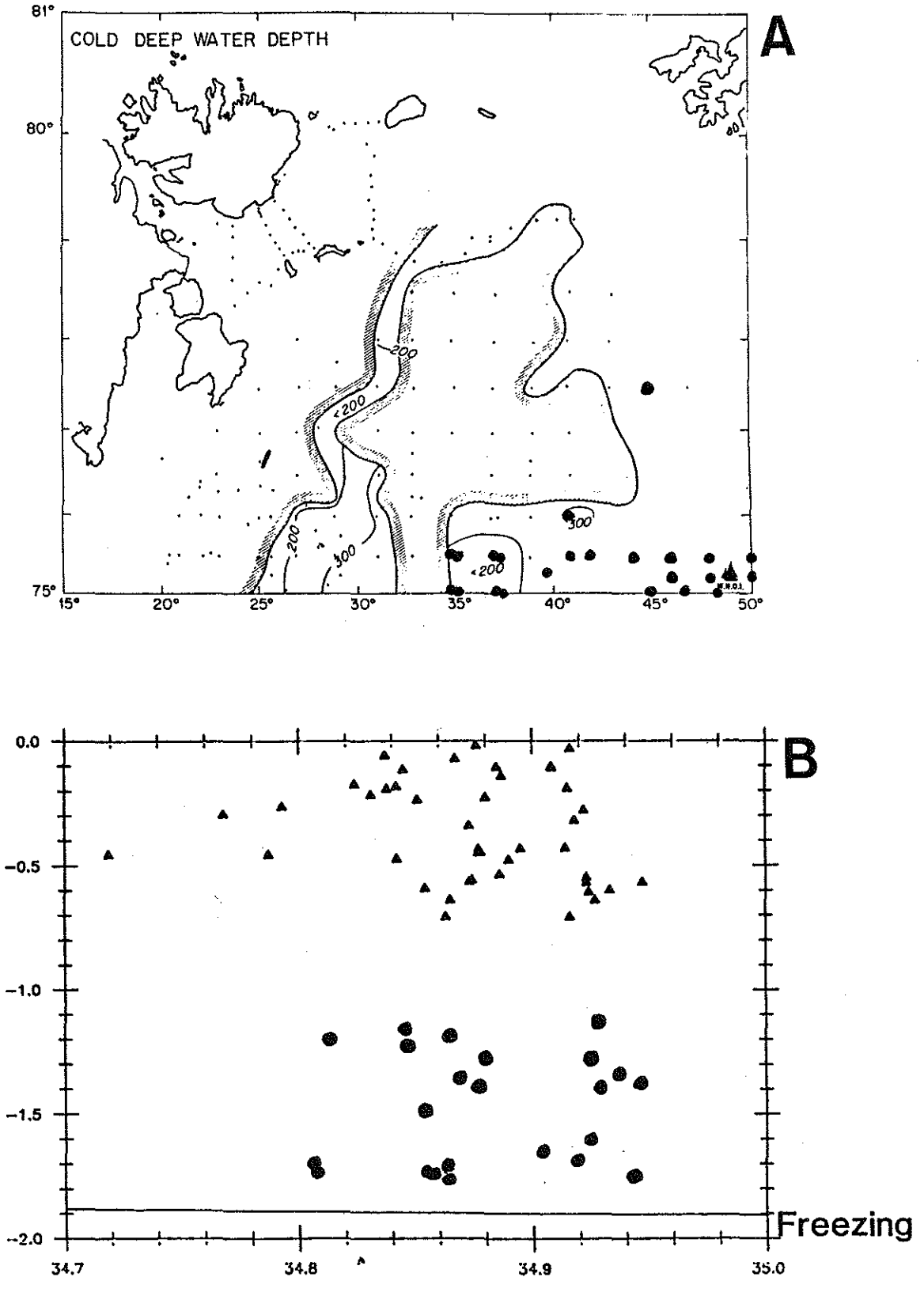
A
COLD DEEP WATER DEPTH
81°
80°
75°
15°
20°
25°
30°
35°
40°
45°
50°
<200
200
300
B
0.0
-0.5
-1.0
-1.5
-2.0
34.7
34.8
34.9
35.0
Freezing
COLD DEEP WATER

Figure 13

Figure 14. Bottom water properties:

Property	Average	Standard Deviation
Depth	174.2	91.2m
Temperature	-0.11	1.19°C
Salinity	34.44	2.31°/$_{oo}$
σ_t	27.67	1.86

A. Bottom temperature

B. Bottom salinity

C. Bottom density

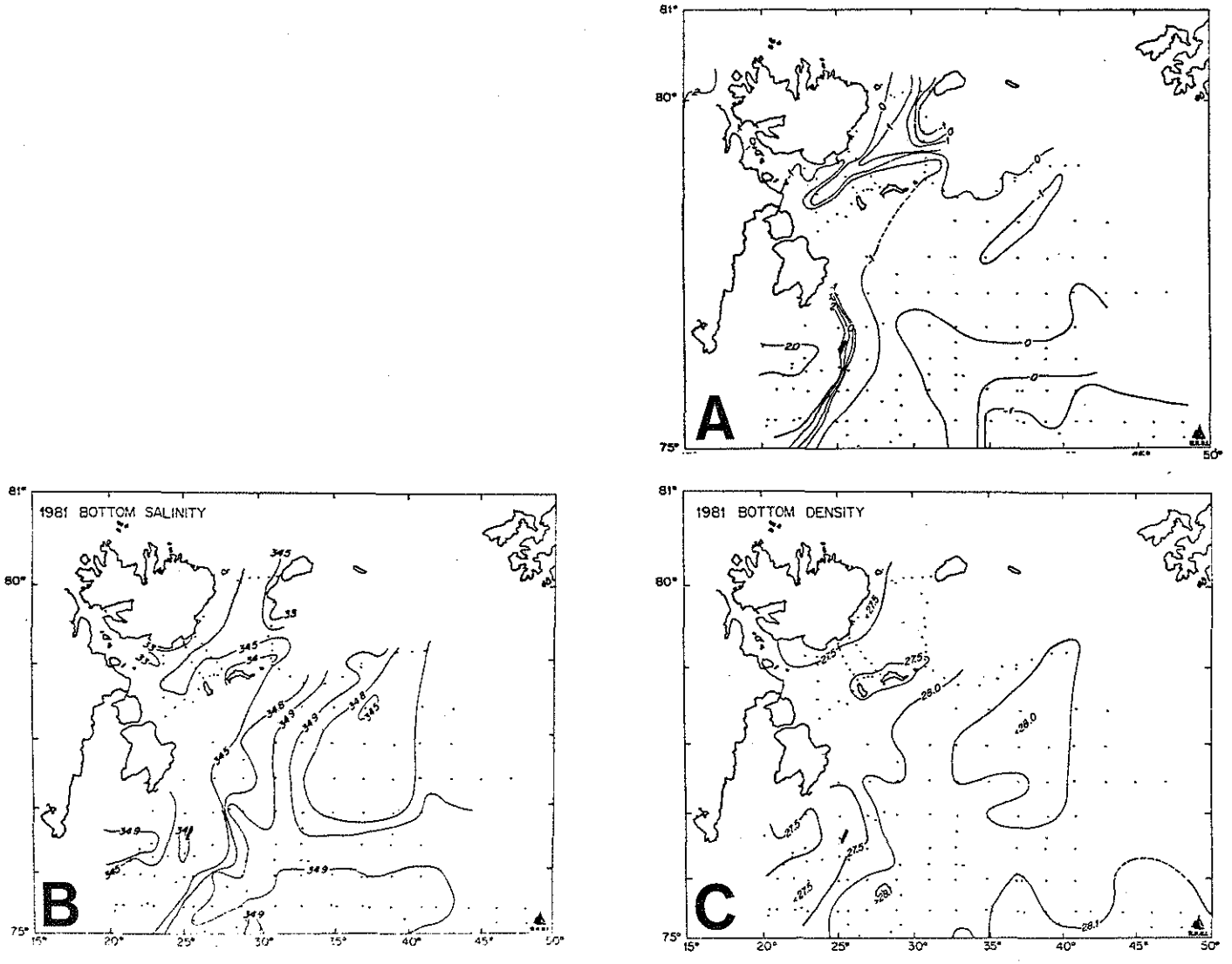
A
B
C
1981 BOTTOM SALINITY
1981 BOTTOM DENSITY
81°
80°
75°
15°
20°
25°
30°
35°
40°
45°
50°

Figure 14

Figure 15. Hydrographic properties at 100m water depth

A. Temperature

B. Salinity

C. Density

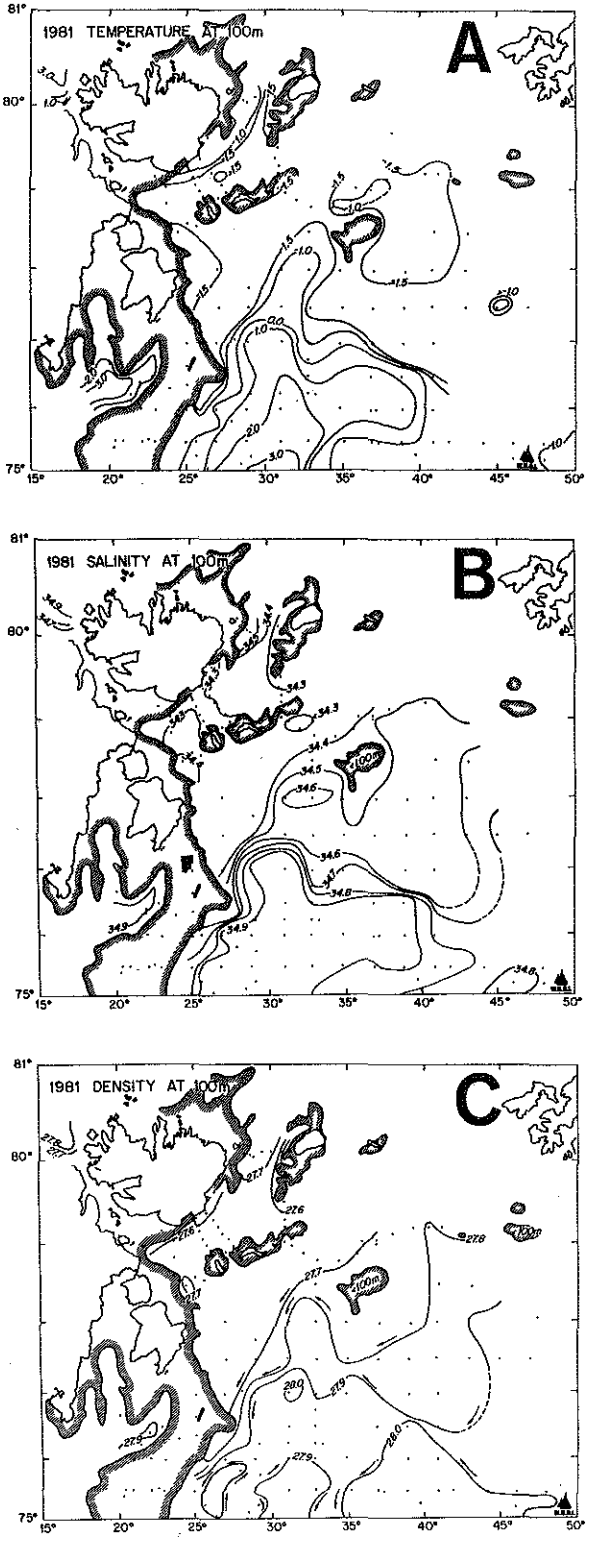
1981 TEMPERATURE AT 100m
A
1981 SALINITY AT 100m
B
1981 DENSITY AT 100m
C
81°
80°
75°
15°
20°
25°
30°
35°
40°
45°
50°

Figure 15

δO^{18} analysis for samples obtained from station casts in the northwestern Barents Sea. All samples were analyzed in Richard Fairbank's lab at the Lamont-Doherty Geophysical Observatory:

Station #	Depth	δO^{18}	Salinity	Temperature
238	0	0.13	31.753	-0.686
	20	0.05	33.512	-0.769
	70	0.19	34.158	-1.100
248	0	0.29	33.534	-1.311
	109	0.30	34.105	-1.058
281	0	0.23	32.598	-0.189
	28	0.17	33.814	-1.659
	75	0.25	34.308	-1.484
	300	0.41	34.866	0.154
299	0	0.14	32.219	-0.955
	10	0.13	32.579	-0.207
	30	0.26	34.061	-1.698
	75	0.21	34.355	-1.671
	225	0.45	34.867	0.242
318	0	0.05	31.732	-1.127
	30	0.11	34.181	-1.712
	75	0.14	34.236	-1.836
	190	0.38	34.720	0.994
331	30	0.29	33.970	-1.337
	75	0.23	34.222	-1.525
	300	0.32	34.768	1.055
335	20	0.28	34.067	2.776
	75	0.43	34.947	3.265
	870	0.24	34.923	0.463
338	0	-.60	32.302	1.689
	10	-.13	32.949	3.201
	300	0.35	34.874	2.166

Figure 16. Station locations for δO^{18} samples. Labelled stations were analyzed.

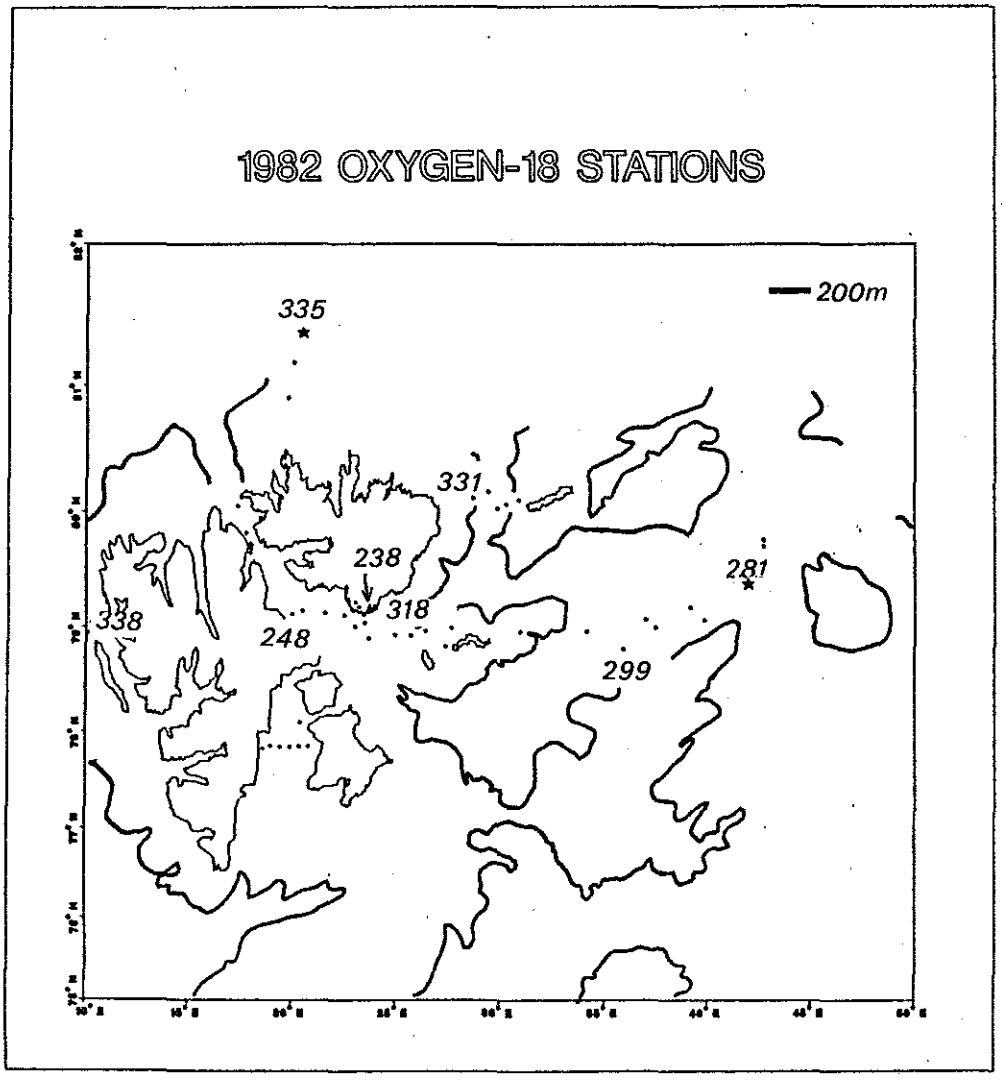

Figure 16

Figure 17A. Temperature - salinity plot for analyzed δO^{18} samples.

B. δO^{18} - salinity plot.

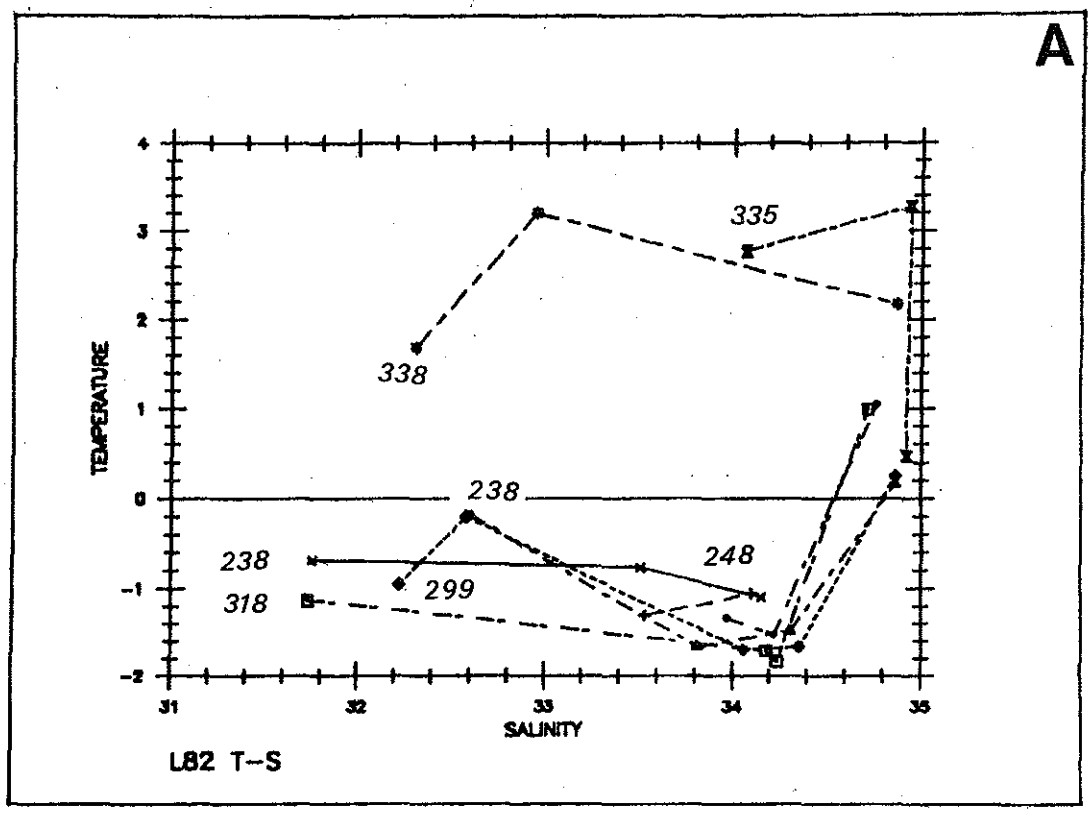
A
TEMPERATURE
SALINITY
335
338
238
238
248
299
318
L82 T-S

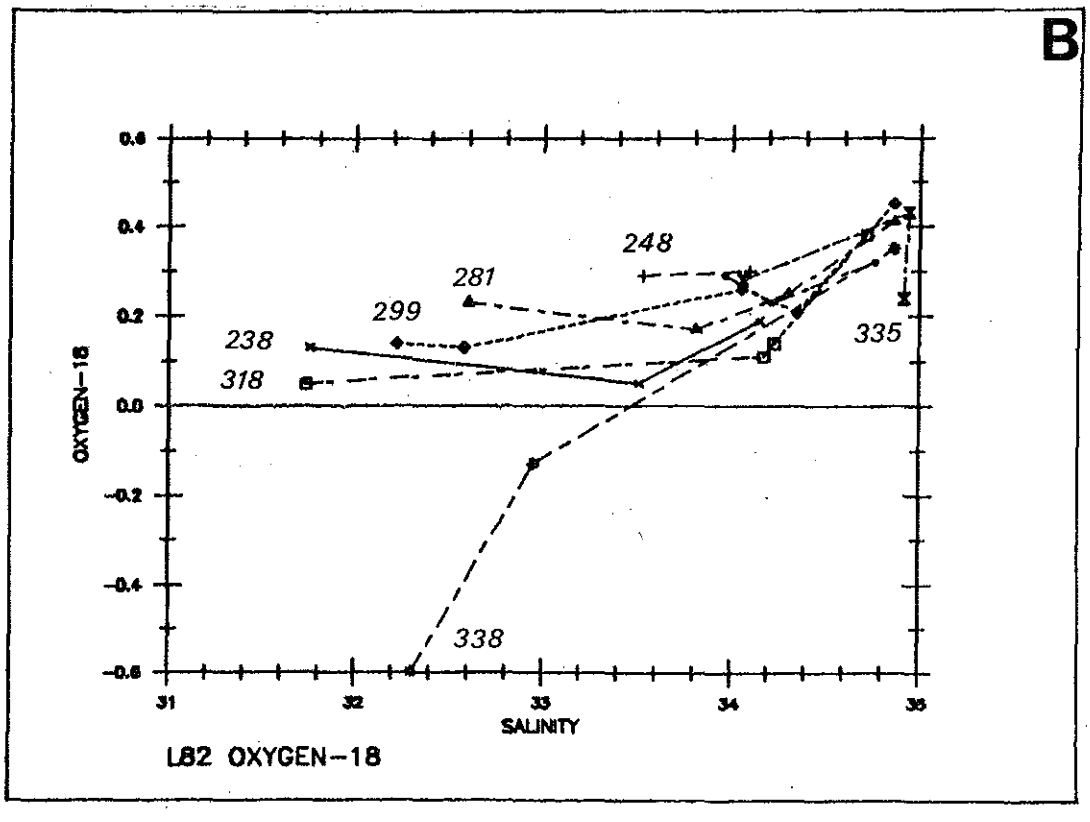
B
OXYGEN-18
SALINITY
248
281
299
238
318
335
338
L82 OXYGEN-18

Figure 17

1982

Hydrographic data for 1982 is compiled from the NPRI cruise to the northern Barents Sea and data from the Institute for Marine Research in Bergen. Further information on the NPRI cruise can be obtained from the cruise report and the prelimiary data report by Tor Larsen, NPRI. The data report contains hydrographic transects and profiles of light attenuation.

Figure 18. Station locations for the NPRI cruise.

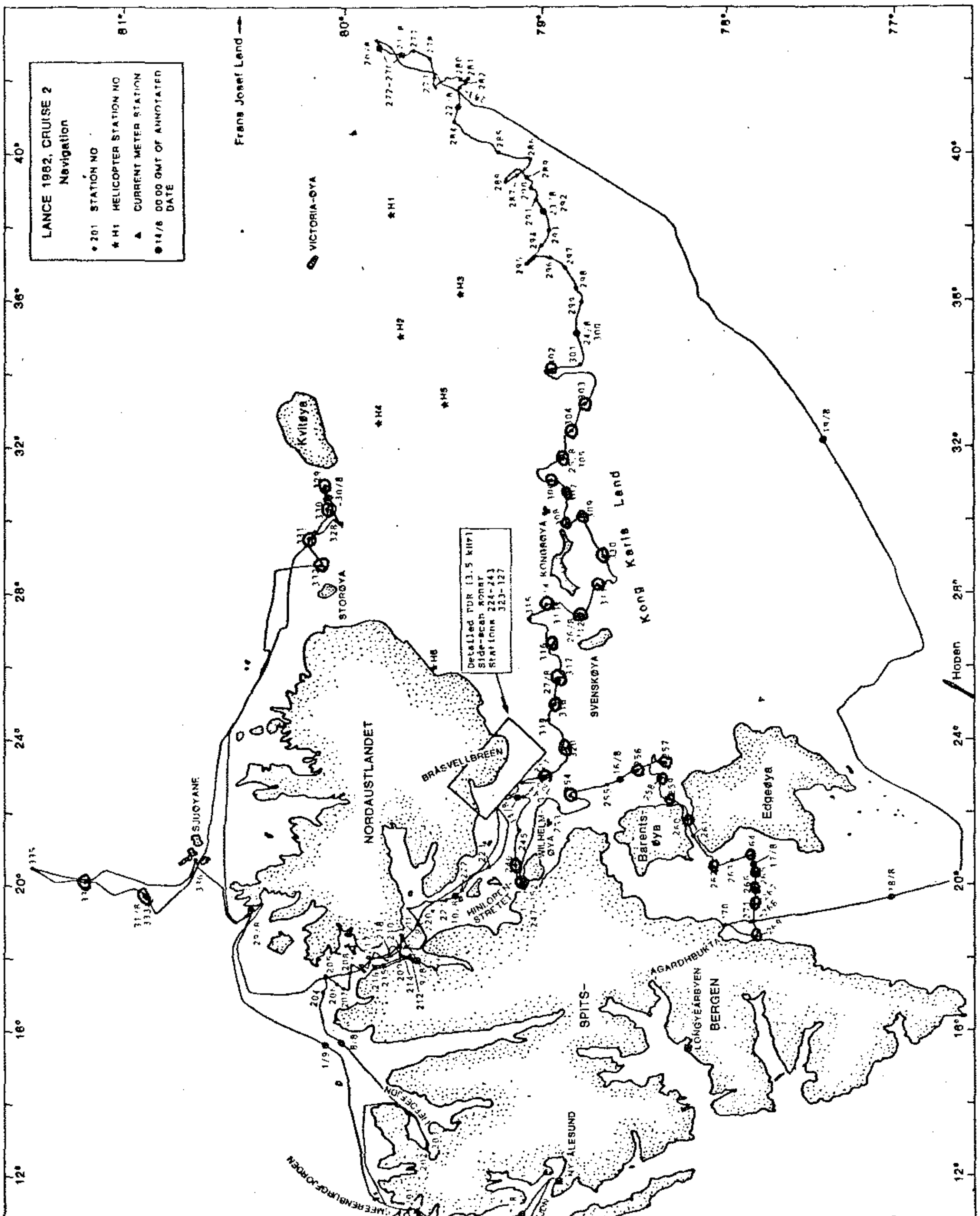
LANCE 1982, CRUISE 2
Navigation
• 201 STATION NO
★ H1 HELICOPTER STATION NO
▲ CURRENT METER STATION
● 14/8 00.00 GMT OF ANNOTATED DATE
Frans Josef Land
VICTORIA-ØYA
Kvitøya
STORØYA
SJUØYANE
NORDAUSTLANDET
BRÅSVELLBREEN
KONGSØYA
Kong Karls Land
SVENSKØYA
WILHELMØYA
HINLOPENSTRETET
Barentsøya
Edgeøya
AGARDHBUKTA
SPITSBERGEN
LONGYEARBYEN
NY ÅLESUND
KONGSFJORDEN
SMEERENBURGFJORDEN
Hopen
81°
80°
79°
78°
77°
12°
16°
20°
24°
28°
32°
36°
40°

Figure 18

Appendix B

Surface Sediment Data

Sediment grain size for down core at 1ϕ intervals was analyzed by standard sieve and pipette techniques (determined by the NPRI). Sediment smaller than 2mm (-2ϕ) is presented as weight percent of the gravel-free sediment:

1980 - 37

Depth(cm)	-3	-2	-1	0	1	2	3	4	5	6	7	8 ϕ
000-005	00.5	0.7	0.6	0.6	0.7	1.0	1.1	5.2	5.1	9.8	15.7	59.5
053-059	00.0	0.0	0.0	0.0	0.0	0.2	0.3	7.4	9.6	14.6	13.3	54.4
083-088	00.0	0.0	0.0	0.0	0.0	0.1	0.3	11.1	8.6	14.2	13.9	51.6
107-113	00.0	0.0	0.0	0.0	0.0	0.2	0.3	3.2	9.6	15.6	18.4	52.6
143-147	01.3	1.3	1.3	1.5	1.6	2.5	5.0	5.5	10.4	12.2	10.6	48.2
147-151	00.4	0.3	0.3	0.2	0.8	11.1	16.0	11.8	7.1	10.6	8.4	33.5
155-158	07.8	0.6	0.9	0.9	1.2	1.3	1.9	15.2	7.0	10.0	11.9	49.0
182-186	04.5	4.0	3.0	1.8	2.3	2.0	2.1	15.1	8.5	10.2	10.9	40.1
212-220	05.7	4.9	3.4	2.2	2.1	1.8	1.9	15.0	5.4	12.0	11.5	39.6

1980 - 65

Depth(cm)	-3	-2	-1	0	1	2	3	4	5	6	7	8 ϕ
000-007	29.0	7.5	6.8	6.2	6.5	6.8	6.8	5.7	9.9	12.8	9.7	22.8
007-013	17.5	10.0	7.6	6.7	6.8	7.2	5.8	4.0	7.4	11.6	14.5	17.8
023-028	22.6	8.1	8.1	7.4	7.2	7.4	6.8	8.8	4.6	11.1	15.3	15.3
033-038	12.7	8.4	6.9	6.1	6.0	6.7	6.4	17.0	6.0	8.5	10.0	18.0
048-053	16.4	7.3	6.4	5.8	5.7	6.7	6.5	10.0	8.0	8.5	10.5	24.7
060-064	30.1	9.7	5.9	4.8	5.1	5.9	5.8	7.5	5.2	13.1	12.1	24.8

1980 - 67

Depth(cm)	-3	-2	-1	0	1	2	3	4	5	6	7	8 ϕ
000-011	49.1	3.6	2.8	2.4	2.9	3.3	2.6	3.0	11.1	10.6	12.7	44.9
000-007	41.2	3.9	2.4	2.1	2.4	2.9	2.5	7.4	1.6	10.7	14.4	49.6
013-019	31.9	6.8	3.1	2.0	1.8	1.8	1.7	-3.1	7.3	10.0	13.9	54.5
046-050	0.0	0.7	0.9	1.1	1.5	1.9	2.0	6.5	6.5	12.0	12.6	54.8
066-069	0.3	0.3	0.6	0.5	0.9	1.1	1.2	-3.9	7.6	15.8	14.6	61.4

1980 - 69

Depth(cm)	-3	-2	-1	0	1	2	3	4	5	6	7	8 ϕ
000-010	24.6	5.1	2.8	3.0	3.0	3.0	2.1	4.5	5.1	11.7	12.4	47.2
016-021	18.6	2.0	1.8	1.9	2.0	2.5	2.1	-9.4	6.7	11.3	15.0	64.0
021-026	17.1	4.0	1.6	1.5	1.6	1.9	1.9	6.8	6.4	12.4	9.4	52.6
047-052	00.9	2.0	1.2	1.2	1.5	2.1	2.4	14.2	3.2	13.0	11.4	47.7
061-066	00.0	0.0	0.0	0.2	0.6	1.0	1.3	-1.5	10.6	12.5	14.9	60.2
075-078	00.0	0.0	0.0	0.0	0.0	0.3	0.4	11.7	4.9	17.8	12.9	51.6

Depth(cm)	-3	-2	-1	0	1	2	3	4	5	6	7	8 φ
1981 - 232.2												
000-000 28.4	13.2	11.2	9.1	7.3	4.5	9.4	4.9	6.1	6.6	7.5	20.1	
1981 - 233.1												
000-000 42.1	12.6	9.7	9.7	10.7	8.1	3.6	3.1	7.9	8.6	5.0	20.7	
1981 - 234.2												
000-000 25.1	5.7	4.1	4.1	4.8	4.4	3.2	6.1	9.2	16.8	7.2	34.2	
1981 - 237												
000-000 27.5	2.1	2.5	2.5	2.6	2.1	12.6	2.1	7.7	10.1	17.8	36.4	
1981 - 239												
000-000 19.8	4.9	4.5	5.1	6.2	5.2	1.7	7.5	7.0	16.5	8.0	33.3	

Surface Sediment Data:

Grain size and Composition

Surface texture separated into larger than 2mm (g = gravel), between 2mm and 0.063mm (s = sand), and less than 0.063mm (f = fine sediments). Sand and finer sediments (sf) equals the weight of the gravel-free fraction.

Surface sediment composition was determined by x-ray diffraction of the less than 0.063mm siz fraction. Peak areas on the diffractogram were estimated by measuring the peak height and the width at half the peak heigth. Major peak areas were measured for quartz (qtz), calcite (cal), dolomite (dol), and feldspar (fel), and each peak area was divided by the total area to determine relative percentages (Jack Hathaway, pers. comm.). These percentages are reported for each sample under "XRD" data.

Grain size data:								XRD data:			
yr	no	d	f	s	g	f/sf	s/sf	qtz	cal	dol	fel
80	15	310	59.0	37.0	04.0	61.0	39.0				
80	19	230	78.0	21.0	00.4	79.0	21.0				
80	22	140	70.0	18.0	12.0	80.0	20.0				
80	29	300	97.0	02.4	00.0	97.0	02.4	86.0	00.0	00.0	14.0
80	30	330	99.0	01.0	00.0	99.0	01.0	76.0	02.0	06.0	16.0
80	31	175	98.0	01.7	00.0	98.0	01.7	73.0	00.0	08.0	19.0
								77.0	00.0	06.0	16.0
80	32	135	94.0	03.0	04.7	97.0	03.1	73.0	00.0	08.0	19.0
80	36							64.0	07.0	17.0	11.0
80	37	150	94.7	03.9	01.3	96.0	03.2				
80	38	120	34.0	59.0	07.0	37.0	63.0	81.0	00.0	00.0	19.0
80	39	107	23.0	77.0	00.2	24.0	76.0	81.0	00.0	00.0	19.0
80	44	130	71.0	17.0	12.0	81.0	19.0				
80	45	125	69.0	19.0	13.0	78.0	22.0				
80	46	230	72.0	21.0	07.0	77.0	23.0				
80	50	325	97.6	05.4	00.0	97.6	05.4				
80	52	200	89.0	11.0	00.0	89.0	11.0				
80	53	125	48.0	42.0	10.0	53.0	47.0				
80	55	250	99.8	00.2	00.0	99.8	00.2				
80	56	100	36.0	56.0	07.0	39.0	61.0				

Grain size data:								XRD data:			
yr	no	d	f	s	g	f/sf	s/sf	qtz	cal	dol	fel
80	57	210	97.5	02.5	00.0	97.5	02.5				
80	58	330	99.4	00.5	00.0	99.5	00.5				
80	59	305	99.1	00.9	00.1	99.1	00.9				
80	60	345	90.0	09.5	00.4	90.0	09.5				
80	61	130	67.0	26.0	06.0	72.0	28.0				
80	62	225	74.0	22.0	04.0	77.0	23.0				
80	64	320	98.0	01.4	00.2	99.0	01.4	75.0	00.0	07.0	18.0
80	65	085	43.0	23.0	34.0	65.0	35.0				
80	66	080	68.2	20.0	12.0	77.0	23.0	48.0	39.0	13.0	00.0
80	67	080	49.0	07.0	44.0	87.0	13.0	52.0	33.0	15.0	00.0
80	67	080	42.0	07.0	51.0	86.0	14.0				
80	69	135	61.0	10.5	28.5	85.0	15.5	64.0	20.0	16.0	00.0
80	71	178	80.0	12.5	07.5	86.0	14.0	80.0	05.0	15.0	00.0
80	84	320	97.8	01.3	00.8	99.0	01.3	73.0	00.0	06.0	21.0
80	85	250	56.6	03.0	00.0	95.0	05.0	75.0	00.0	11.0	14.0
80	86	142	68.0	22.0	10.0	76.0	24.0	74.0	05.0	07.0	14.0
80	87	255	97.2	02.5	00.4	97.0	02.5	64.0	07.0	08.0	21.0
80	88	275	98.2	01.6	00.2	98.0	01.6	72.0	00.0	07.0	22.0
80	89	275	38.0	41.0	21.0	48.0	52.0	78.0	00.0	08.0	14.0
80	90	225	60.0	27.0	13.0	69.0	31.0	74.0	00.0	06.0	19.0
80	91	295	98.1	01.9	00.2	98.1	01.9				
80	93	140	86.5	11.5	01.5	88.0	12.0				
80	101	170	37.0	45.0	18.0	45.0	55.0				
80	102	170	59.0	40.0	02.0	60.0	40.0				
80	104	180	55.0	35.0	10.0	61.0	39.0				
80	105	149	40.0	43.0	16.0	48.0	52.0				
80	106	165	51.0	19.0	25.0	73.0	27.0				
80	107	185	78.0	19.0	03.0	80.0	20.0				
80	108	175	55.2	44.8	00.0	55.2	44.8				
80	109	260	34.4	34.2	27.2	50.0	50.0				
80	111	215	86.8	12.5	00.0	86.8	12.5				
80	112	147	42.6	18.7	38.8	69.0	31.0				
80	113	214	82.0	17.5	00.1	82.0	17.6				
80	114	340	97.0	03.0	00.0	97.0	03.0				
80	115	300	90.0	09.2	00.8	91.0	09.2				
80	116	262	95.0	04.9	00.0	95.0	04.9				
80	118	280	99.0	01.0	00.0	99.0	01.0				
80	119	307	99.3	00.7	00.0	99.3	00.7				
80	121	175	65.0	24.0	12.0	73.0	27.0				
80	124	330	99.0	00.9	00.3	99.0	00.9	74.0	00.0	07.0	19.0
80	125	330	97.0	01.5	01.5	98.0	01.5	71.0	00.0	07.0	22.0
80	126	285	98.0	03.0	00.3	97.0	02.9	76.0	00.0	06.0	18.0
80	127	130	67.0	24.0	09.0	74.0	26.0	62.0	05.0	08.0	25.0
80	128	265	85.0	14.0	01.0	86.0	14.0	72.0	00.0	06.0	22.0
80	131	115	35.0	13.0	52.0	73.0	27.0				
80	134	165	92.6	07.4	00.0	92.6	07.4				
80	137	125	57.1	42.3	00.6	57.0	43.0				
82	225	036	71.2	12.0	16.0	86.0	14.0	56.0	38.0	06.4	00.0
82	229	055	51.6	18.0	29.0	74.0	26.0	62.0	25.0	13.0	00.0
82	230	081	59.7	22.0	18.0	73.0	27.0	46.8	41.1	12.1	00.0

Grain size data:									XRD data:			
yr	no	d	f	s	g	f/sf	s/sf		qtz	cal	dol	fel
82	231	083	52.4	34.0	13.0	61.0	39.0		35.2	55.4	09.4	00.0
82	233	101	26.8	19.4	54.0	59.0	41.0		48.6	38.8	10.6	01.9
82	234	079	64.6	21.0	14.0	75.0	25.0		50.0	41.0	09.0	00.0
82	235	106	49.0	11.0	40.0	82.0	18.0		48.0	42.0	10.0	00.0
82	237	105	82.9	09.0	08.0	90.0	10.0		53.0	30.0	17.0	00.0
82	239	087	68.7	22.0	09.0	76.0	24.0		52.0	37.0	10.0	00.0
82	239	087	41.4	13.0	46.0	76.0	24.0		48.0	39.0	12.0	00.0
82	241	057	43.7	15.0	41.0	74.0	26.0		63.3	28.6	08.1	00.0
82	253	124	89.8	08.0	02.0	92.0	08.0		65.0	13.0	22.0	00.0
82	232	082	39.5	31.5	28.9	56.0	44.0		50.7	40.7	08.7	00.0
									46.7	42.8	10.5	00.0
82	317	142	88.6	10.0	01.0	90.0	10.0		87.0	00.0	13.0	00.0
82	320	181	91.8	06.0	00.0	94.0	06.0	319	60.0	09.0	11.0	09.0
82	321	099	79.8	11.0	01.0	88.0	12.0					
82	321	099	75.4	08.0	17.0	90.0	10.0		64.0	19.0	17.0	00.0
									62.0	14.0	16.0	08.0
82	323	039	40.6	31.0	29.0	57.0	43.0		42.8	49.8	06.1	01.3
82	323	039	73.1	24.0	03.0	75.0	25.0		48.7	43.8	07.5	00.0

Appendix C

Suspended Sediment Data

Filtered Water Samples
Concentration data

yr	sta	d	conc	d	conc	d	conc	d	conc	d	conc
80	003	400	0.78	025	0.05	005	0.22				
80	021	109	0.25	040	0.25	020	0.31				
80	023	157	0.27	030	0.25	010	0.13				
80	028	279	0.02	025	0.20	010	0.16				
80	030	229	0.69								
80	032	134	0.14	115	1.98	075	0.45	035	0.41	015	0.26
80	034	021	2.22	003	1.94						
80	036	124	0.32								
80	038	119	0.21	018	0.93	003	0.28				
80	051	215	0.14	005	0.15						
80	052	199	0.15	030	0.10	005	0.14				
80	053	130	0.16	050	0.26	025	0.33	005	0.23		
80	054	217	0.32	040	0.27						
80	058	329	0.48	030	0.29						
80	060	244	0.18	145	1.95						
80	062	224	0.22	175	0.02	100	0.23				
80	064	225	0.52	160	0.06	030	0.24				
80	065	087	2.28	050	2.76	003	1.51				
80	067	089	0.68	050	1.65	003	1.86				
80	069	134	0.16	050	0.77	003	0.58				
80	071	177	0.42	050	0.14	002	0.30				
80	073	149	0.41		0.13	050	0.10				
80	074	086	2.56	050	1.58	003	1.89				
80	075	100	0.83	050	0.48	003	1.11				
80	079	214	0.40	161	0.22	020	0.56				
80	081	099	0.22	050	1.44	003	0.15				
80	083	121	0.21	072	0.43	020	1.01				
80	086	141	0.19	090	0.25	030	0.50				
80	089	179	0.21	130	0.74	030	0.54				
80	091	264	0.32	065	0.22	005	0.32				
80	096	132	1.00	070	1.91	020	0.82				
80	101	164	0.61	030	1.02						
80	113	213	0.60	150	0.20	030	0.50				
80	115	299	0.42	030	0.13						
80	118	299	0.43	130	0.24	030	0.95				
80	120	299	1.03	250	0.24	020	0.57				
81	122	080	0.17	065	0.10	020	0.34				
81	123	134	0.24	050	0.20	020	0.43				
81	124	239	0.29	075	0.26	025	0.44				
81	125	348	0.51	110	0.20	035	0.41	020	0.70		
81	126	085	0.31	025	0.64	001	0.80				
81	128	090	0.71	020	0.59	001	1.22				
81	129	114	0.35	020	0.98	002	0.26				
81	130	060	0.48	020	0.90	002	0.28				
81	131	030	0.74	020	0.63	002	0.38				

yr	sta	d	conc	d	conc	d	conc	d	conc	d	conc	d	conc
81	132	041	0.41	020	1.42	002	0.35						
81	133	074	0.50	060	0.50	021	1.24	002	0.21				
81	136	098	0.51	088	0.46	020	0.50	001	0.29				
81	141	079	0.99	070	1.80	020	1.18	001	1.46				
81	144	020	2.99	00128.46									
81	148	060	2.59	050	4.64	020	3.33						
81	150	090	2.22	080	1.52	020	3.47	001	2.89				
81	151	085	2.06	075	1.09	020	0.89	001	0.69				
81	152	110	0.81	100	0.93	020	3.92	001	0.48				
81	153	170	1.86	160	0.86	020	1.17	001	0.31				
81	154	200	0.38	190	0.29	020	0.31	001	0.00				
81	155	155	0.28	145	0.19	020	0.26	001	0.27				
81	156	110	0.53	100	0.25	020	0.72	001	0.58				
81	157	060	0.33	050	0.35	020	0.48	001	0.55				
81	158	055	0.46	045	0.40	020	0.67	001	1.27				
81	159	090	0.13	080	0.19	020	0.37	001	0.30				
81	161	060	0.33	050	0.38	020	0.50	001	0.49				
81	162	086	0.13										
81	163	124	0.17	114	0.09	019	0.32	001	3.12				
81	164	201	0.12										
81	165	239	0.63	228	0.28	099	0.01	019	0.33	002	0.31		
81	166	184	0.26										
81	168	065	1.78	050	1.78	020	1.34	001	1.08				
81	170	045	3.49	035	3.09	020	2.38	001	3.97				
81	171	060	2.67	016	2.78	000	3.37						
81	172	055	4.47	045	2.30	020	3.36	000	4.47				
81	173	054	1.29	045	0.55	020	0.81	000	0.64				
81	174	100	1.23	090	1.02	01011.80		00510.67		00112.33		000	7.92
81	176	110	2.55	010	2.78	000	0.65						
81	177	115	1.17	01014.96		00012.20							
81	178	075	1.36	065	1.47	010	5.88	000	8.15				
81	208	100	0.00	080	0.30								
81	209	155	0.06	145	0.06	020	0.16	001	0.27				
81	210	105	0.45	095	0.15	020	0.22	001	0.18				
81	211	045	0.33	020	0.51	001	0.84						
81	215	085	0.66	075	0.37								
82	212	047	0.51	040	0.38	017	1.03						
82	213	063	0.31	010	0.65								
82	214	137	0.27	130	0.34	010	0.29						
82	215	076	2.03	033	0.57	000	2.50						
82	228	009	0.82	007	0.93	000	0.57						
82	229	042	0.56	032	0.38	020	0.80	000	2.23				
82	231	072	0.57	062	0.39	020	0.34	020	0.46	000	0.97		
82	232	072	1.97	062	1.22	020	0.47	000	0.65				
82	233	088	0.47	020	0.67	000	1.14						
82	234	077	1.11	020	0.83	000	1.83						
82	236	087	0.70	077	0.55	020	0.29	000	0.41				
82	237	102	0.38	089	0.32	020	0.29	000	0.81				
82	238	067	1.91	057	1.39	020	1.34	000	1.27				
82	243	068	0.87	000	1.02								

yr	sta	d	conc	d	conc	d	conc	d	conc	d	conc	d	conc
82	244	025	0.44	000	0.34								
82	246	068	0.53	000	1.51								
82	247	109	0.74	000	1.06								
82	248	109	0.43	000	1.02								
82	249	109	0.37	000	0.91								
82	250	109	0.67	000	2.60								
82	251	109	0.46	000	0.97								
82	252	109	0.54	000	1.35								
82	314	100	0.32	020	0.55	000	0.79						
82	317	127	0.33	030	0.83	000	0.43						
82	318	190	0.65	020	0.62	000	0.58						
82	337	130	0.94	010	1.07	000	1.30						
82	338	298	0.53	010	0.43	000	1.58						

Bottom Filtered Water Samples
Concentration and position

yr	sta	sd	wd	conc	long	lat
80.0	3.0	350.0	400.0	0.78	23.29	73.19
80.0	21.0	100.0	109.0	0.25	26.60	77.04
80.0	23.0	160.0	157.0	0.27	28.03	77.02
80.0	28.0	275.0	279.0	0.02	30.03	77.99
80.0	30.0	230.0	229.0	0.69	27.69	78.03
80.0	32.0	135.0	134.0	0.14	25.45	78.02
80.0	34.0	22.0	21.0	2.22	22.06	78.59
80.0	36.0	125.0	124.0	0.32	23.66	78.71
80.0	38.0	120.0	119.0	0.21	25.39	78.78
80.0	51.0	215.0	215.0	0.14	31.10	78.00
80.0	52.0	200.0	199.0	0.15	32.05	77.99
80.0	53.0	125.0	130.0	0.16	32.97	78.00
80.0	54.0	215.0	217.0	0.32	34.44	78.00
80.0	58.0	330.0	329.0	0.48	34.51	78.80
80.0	62.0	225.0	224.0	0.22	30.99	79.00
80.0	65.0	85.0	87.0	2.28	23.51	79.18
80.0	67.0	80.0	89.0	0.68	23.68	79.10
80.0	69.0	135.0	134.0	0.16	23.67	79.01
80.0	71.0	178.0	177.0	0.42	24.01	78.87
80.0	73.0	150.0	149.0	0.41	24.54	78.75
80.0	74.0	85.0	86.0	2.56	25.10	79.31
80.0	75.0	90.0	100.0	0.83	25.10	79.30
80.0	79.0	212.0	214.0	0.40	25.58	79.10
80.0	81.0	100.0	99.0	0.22	26.25	78.87
80.0	83.0	111.0	121.0	0.21	27.41	78.95
80.0	86.0	142.0	141.0	0.19	29.99	79.79
80.0	96.0	119.0	132.0	1.00	32.41	80.31
80.0	101.0	170.0	164.0	0.61	33.05	80.81
80.0	113.0	214.0	213.0	0.60	34.48	79.83
80.0	115.0	300.0	299.0	0.42	34.49	79.51
80.0	118.0	280.0	299.0	0.43	33.62	79.51
80.0	120.0	300.0	299.0	1.03	31.53	79.51
80.0	121.0	175.0	193.0	0.30	30.59	79.49
80.0	124.0	330.0	325.0	0.31	29.25	79.52
80.0	126.0	285.0	284.0	0.15	27.85	79.50
80.0	128.0	265.0	275.0	0.12	29.50	80.02
80.0	130.0	125.0	106.0	0.52	30.57	80.00
80.0	133.0	168.0	187.0	0.28	34.48	77.83
80.0	135.0	188.0	191.0	0.16	34.50	77.50
81.0	126.0	105.0	85.0	0.31	17.16	80.30
81.0	128.0	105.0	90.0	0.71	21.80	78.88
81.0	129.0	127.0	114.0	0.35	22.13	78.94
81.0	130.0	74.0	60.0	0.48	22.50	79.01
81.0	131.0	42.0	30.0	0.74	22.81	79.08
81.0	132.0	50.0	41.0	0.41	22.90	79.13
81.0	133.0	88.0	74.0	0.50	23.08	79.17
81.0	136.0	109.0	98.0	0.51	23.58	79.14
81.0	141.0	94.0	79.0	0.99	23.56	79.19

yr	sta	sd	wd	conc	long	lat
81.0	144.0	82.0	63.0	9.99	24.13	79.26
81.0	148.0	73.0	60.0	2.59	25.05	79.31
81.0	150.0	102.0	90.0	2.22	25.15	79.29
81.0	151.0	98.0	85.0	2.06	25.20	79.27
81.0	152.0	124.0	110.0	0.81	25.23	79.25
81.0	155.0	175.0	155.0	0.28	25.96	79.00
81.0	156.0	130.0	110.0	0.53	26.18	78.93
81.0	158.0	66.0	55.0	0.46	26.82	78.88
81.0	159.0	104.0	90.0	0.13	27.07	78.90
81.0	161.0	76.0	60.0	0.33	27.93	78.93
81.0	164.0	210.0	201.0	0.12	26.93	79.13
81.0	166.0	151.0	184.0	0.26	26.16	79.30
81.0	168.0	76.0	65.0	1.78	25.61	79.40
81.0	170.0	62.0	45.0	3.49	25.60	79.40
81.0	172.0	61.0	55.0	4.47	25.86	79.49
81.0	173.0	56.0	54.0	1.29	25.94	79.50
81.0	174.0	107.0	100.0	1.23	25.74	79.51
81.0	176.0	129.0	110.0	2.55	25.92	79.53
81.0	177.0	128.0	115.0	1.17	25.71	79.53
81.0	208.0	117.0	100.0	0.00	25.67	78.54
81.0	209.0	171.0	155.0	0.06	25.02	78.57
81.0	211.0	59.0	45.0	0.33	23.84	78.33
81.0	215.0	97.0	85.0	0.66	23.85	79.14
82.0	212.0	54.0	47.0	0.51	18.01	79.66
82.0	213.0	80.0	63.0	0.31	18.06	79.69
82.0	215.0	0.0	76.0	2.03	17.80	79.82
82.0	228.0	21.0	9.0	0.82	22.63	79.31
82.0	229.0	55.0	42.0	0.56	22.96	79.15
82.0	231.0	83.0	72.0	0.57	23.09	79.22
82.0	232.0	82.0	72.0	1.97	23.79	79.19
82.0	233.0	101.0	88.0	0.47	23.79	79.18
82.0	234.0	79.0	77.0	1.11	23.73	79.16
82.0	236.0	97.0	87.0	0.70	23.49	79.11
82.0	237.0	105.0	102.0	0.38	23.55	79.04
82.0	238.0	83.0	67.0	1.91	24.04	79.19
82.0	243.0	79.0	68.0	0.87	23.27	79.18
82.0	244.0	39.0	25.0	0.44	22.56	79.11
82.0	246.0	83.0	68.0	0.53	20.56	79.15
82.0	247.0	124.0	109.0	0.74	20.06	79.12
82.0	248.0	123.0	109.0	0.43	20.06	79.12
82.0	249.0	123.0	109.0	0.37	20.06	79.12
82.0	250.0	123.0	109.0	0.67	20.06	79.12
82.0	251.0	119.0	109.0	0.46	20.06	79.12
82.0	252.0	119.0	109.0	0.54	20.06	79.12
82.0	314.0	112.0	100.0	0.32	27.71	79.00
82.0	317.0	142.0	127.0	0.33	25.77	78.92
82.0	318.0	207.0	190.0	0.65	25.00	78.93
82.0	337.0	136.0	130.0	0.94	12.02	78.96
82.0	338.0	308.0	298.0	0.53	11.98	78.93

Suspended sediment data

Number of grains in each size class:

1980:

Sta.	Depth	-4	-6	-8	-10	-12	-14	-16	-18	-20	-22	-24	-26	-28
21	109	25	15	7	4	5	1	3	1	1	0	1		
23	157	27	17	10	3	7	1	0	0	1	1(28μm), 1(30μm)			
120	299	30	29	7	4	5	4							
126	235	22	18	8	3	1	0	0	0	0	1			
126	284	30	26	11	6	2	4	2	1	1	0	1		

1981:

Sta.	Depth	-4	-6	-8	-10	-12	-14	-16	-18	-20	-22	-24	-26	-28
141	1	31	24	9	3	3								
141	20	24	16	11	4	2	1	1	0	2				
141	70	38	31	7	4	5	1	0	2	0	1			
141	80	34	21	11	7	7	4	1	1	1(28μm), 1(38μm)				
144	1	19	28	17	6	7	2	2	1	0	0	1		
144	20	35	27	12	8	7	5	1	3	0	1	2		
144	63	35	47	27	15	8	3	2	1					
145	0	36	29	11	2	0	1							
148	20	32	27	13	7	3	3	0	1	0	0	1		
148	50	99	49	17	10	4	0	1						
148	60	24	26	13	6	7	4	1	1	0	0	2		
167	0	18	15	9	3	1	1							
167	20	20	12	6	1	4	3	2	0	1				
167	75	20	18	9	6	3	2	1						
167	85	20	15	10	8	4	1	2						
170	1	41	40	10	3	3	1	0	0	0	0	0	1	
170	20	21	19	5	2	2								
170	35	26	24	12	3	5	2	2	0	1				
170	45	27	35	18	10	12	3	3	1	1	1			
171	0	31	23	7	1	4	1	1						
171	16	24	25	7	7	6	1	3	1	1	0	1		
171	60	37	33	16	10	6	6	1	3	1	0	1		
172	0	211	154	54	8	3	7	3	1	2	0	1		
172	16	32	19	7	10	4	6							
172	45	39	43	18	7	7	5	3	2	3	1	4		
172	55	27	34	25	11	12	3	5	3	0	2	2	2	

Suspended sediment data (cont')

Number of grains in each size class:

1981:

Sta.	Depth	-4	-6	-8	-10	-12	-14	-16	-18	-20	-22	-24	-26	-28
173	0	22	15	5	3	2	1	1	0	1				
173	20	14	15	5	3	4	1	0	1					
173	45	6	13	4	3	1								
173	54	24	25	12	2	5	0	3	1	0	1			
174	0	9	12	5	2	3	0	2	1(32μm)					
174	1	50	48	18	13	15	4	2	1					
174	5	30	29	14	2	5	3	1						
174	10	33	39	19	5	3	2	2	2(26μm), 1(32μm), 2(34μm)					
174	90	27	21	11	2	4	2	4	1	1	1(28μm)			
174	100	27	14	11	3	6	3	2 (28μm), 1(36μm)						
176	0	5	8	5	4	2	0	2	1					
176	10	9	14	7	6	1	2	3	0	0	1	1(42μm)		
176	110	23	16	12	5	2	1	0	3	0	0	0	1	
177	0	18	11	6	4	6	1	0	1	1				
177	10	57	84	49	18	10	7	2	1	2	1	0	0	1 1
177	115	22	26	12	8	4	1							

1982:

Sta.	Depth	-4	-6	-8	-10	-12	-14	-16	-18	-20	-22	-24	-26	-28
231	20	7	9	5	3	3	1	1	0	1				
231	62	7	5	5	3	3	1	1						
231	72	11	8	5	5	4	1							
232	0	24	23	4	2	3	4	1	1	1	1(38μm)			
232	20	26	28	18	8	3	1	0	0	0	0	0	0	1
232	62	23	13	4	6	4	1	0	0	0	0	0	0	1
232	72	25	16	12	1	7	5	2	1	1(30μm)				
234	20	18	8	5	2	4	0	2	2					
234	77	15	7	4	0	3	2	3	1	3	1	2		
238	0	19	23	11	9	5	2	2	1(36μm)					
238	20	12	14	7	4	5	2	1	1(28μm), 1(32μm)					
238	57	29	20	6	5	3	3	0	1					
238	67	33	22	9	3	4	5	0	1	2	1	1		
239	0	42	35	9	5	5	1	1						
239	20	21	13	8	4	6	1	1	1(34μm), 1(38μm)					
239	60	19	8	3	3	1	2	0	0	1	1			
239	70	31	17	11	2	1	2	2	1	1(30μm)				

Averaged suspended matter data

Eastern Plume:

	Distance	ϕ5	ϕ6	ϕ7	ϕ8	ϕ9	Avg Conc
Station 174	0.0	13.54%	33.80%	38.17%	13.17%	1.33%	12.33mg/l
Station 172	2.8	0.0	50.71	29.98	16.83	2.15	3.65
Station 171	10.0	0.0	29.14	51.03	17.43	2.40	2.94
Station 170	13.7	0.0	23.87	46.22	26.71	3.70	3.23
Station 148	27.6	0.0	29.09	43.60	23.36	3.95	3.52

Western Plume:

	Distance	ϕ5	ϕ6	ϕ7	ϕ8	ϕ9	Avg Conc
Station 144	0.0	0.0	32.60	48.21	17.93	1.26	28.46
Station 232	6.3	14.41	37.71	35.88	10.58	1.43	1.48
Station 238	11.7	14.91	40.61	31.65	11.52	1.31	1.08
Station 141	16.5	11.6	29.10	34.50	21.80	3.00	1.36
Station 231	26.7	0.0	10.57	71.79	16.22	1.43	0.58

Transmissometer/Nephelometer Calibrations

The transmissometers and nephelometers used in this atudy are manufactured by the Montedoro-Whitney Corporation. The transmissometer has a one meter folded path length. and uses a white light source. The same light source is used for the nephelometer which has a prism orientated at 90° to the source. This instrument has been extensively calibrated in a laboratory test tank at the U.S. Geological Survey in Woods Hole (figure 1). While working for Bradford Butman at the U.S.G.S., I built the tank and began the calibrations. They have since been continued by John Moody, and his results on natural sediments will be presented here (Moody and Butman in prep.). Calibration has also been done with glass beads of various sizes, and recently with diatom cultures.

Sediments used in this experiment were from the same station location but were separated into different size classes by pipetting. They were then introduced into the test tank in increasing concentrations. The same three T/N units were used in all experiments. Concentrations were determined by filtration of water samples and normalization to the clean tank sample.

The light attenuation calculated from the light transmisson (tr) referenced to the light transmission in clear water (tr_{cw}):

$$a = -\ln(tr/tr_{cw})$$

is shown to be linearly dependent on the concentration of suspended material (figure 2). Any instrumental gain factor on the transmissometer is normalized out of the equation, so need not be

Figure 1. Schematic of test tank.

TRANSMISSOMETER CALIBRATION TANK

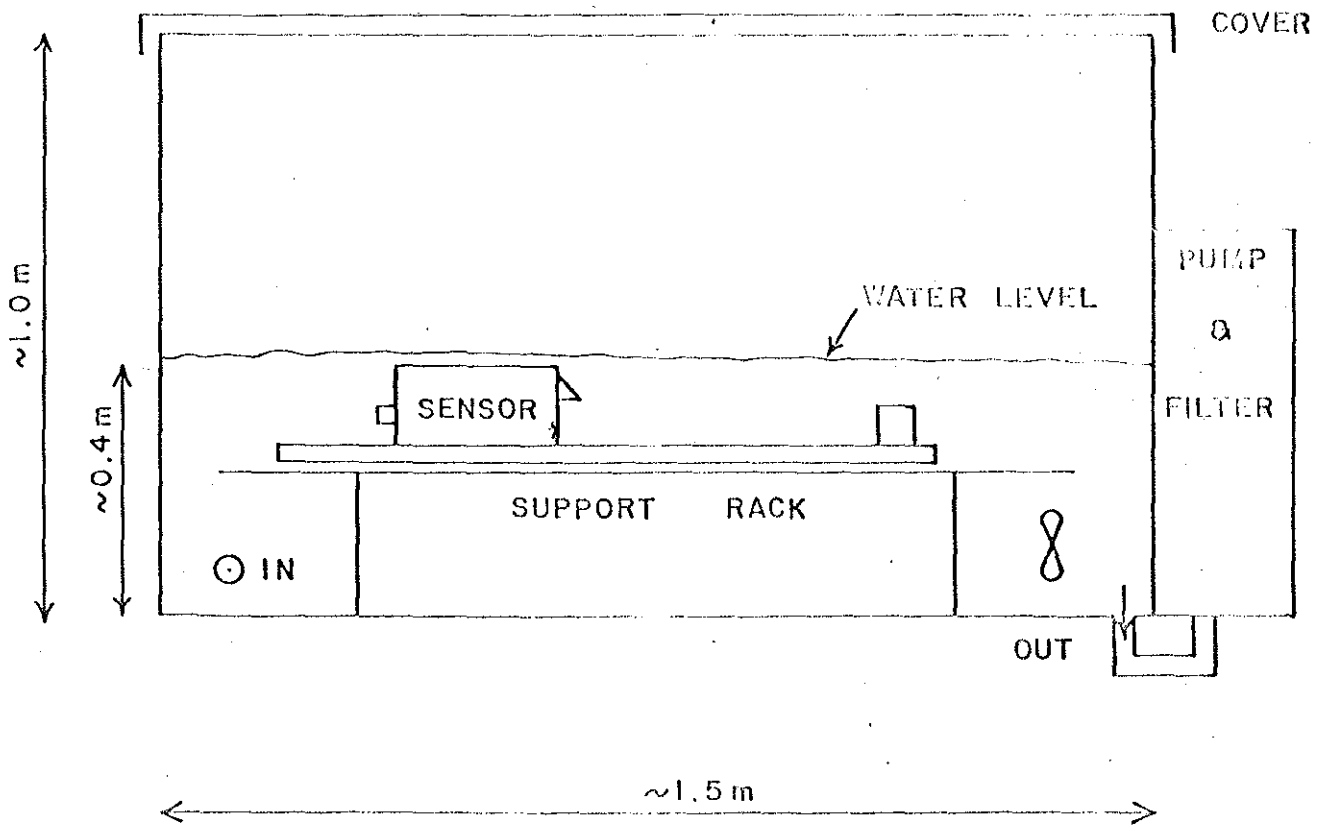

Figure 1

considered. The beam attenuation actually measured in the tank is the sum of the attenuation by the water itself, plus the attenuation by the suspended particles.

When different grain size size material is used the relationship of concentration and attenuation remains linear, but with different slopes (figure 2). Therefore, if the grain size of the suspended material is known, then the concentration can be determined, and vice versa. In the field, it is often assumed that only a single grain size distribution of material is in suspension, so the measured concentrations are linearly regressed with the optical measurements (e.g. Spinrad et al 1983). The slope becomes steeper with coarser material, that is the larger the grain size the less it attenuates for the same weight concentration (mg/l) of material. (This might be expected, as the weight is dependent on the volume, rather than the cross-sectional area which is being measured optically.)

Scattering measured through at 45-90° by the nephelometer, also is linearly related to concentration for a specific grain size (figure 3). The value used is the scattering measured at the particular concentration (ne) with the scattering in clear water (ne_{cw}) subtracted:

$C_{ne} = (ne - ne_{cw}) / f$

f = gain factor

There is a problem with the nephelometers in that the gain range can be set differently for the instrument, and this gain factor is not normalized out of the computation as it is in the transmissometer beam attenuation calculation. Therefore Moody found that application of a "gain factor" was necessary in order to compare the instruments. This

Figure 2. Light attenuation vs. concentration (mg/l)

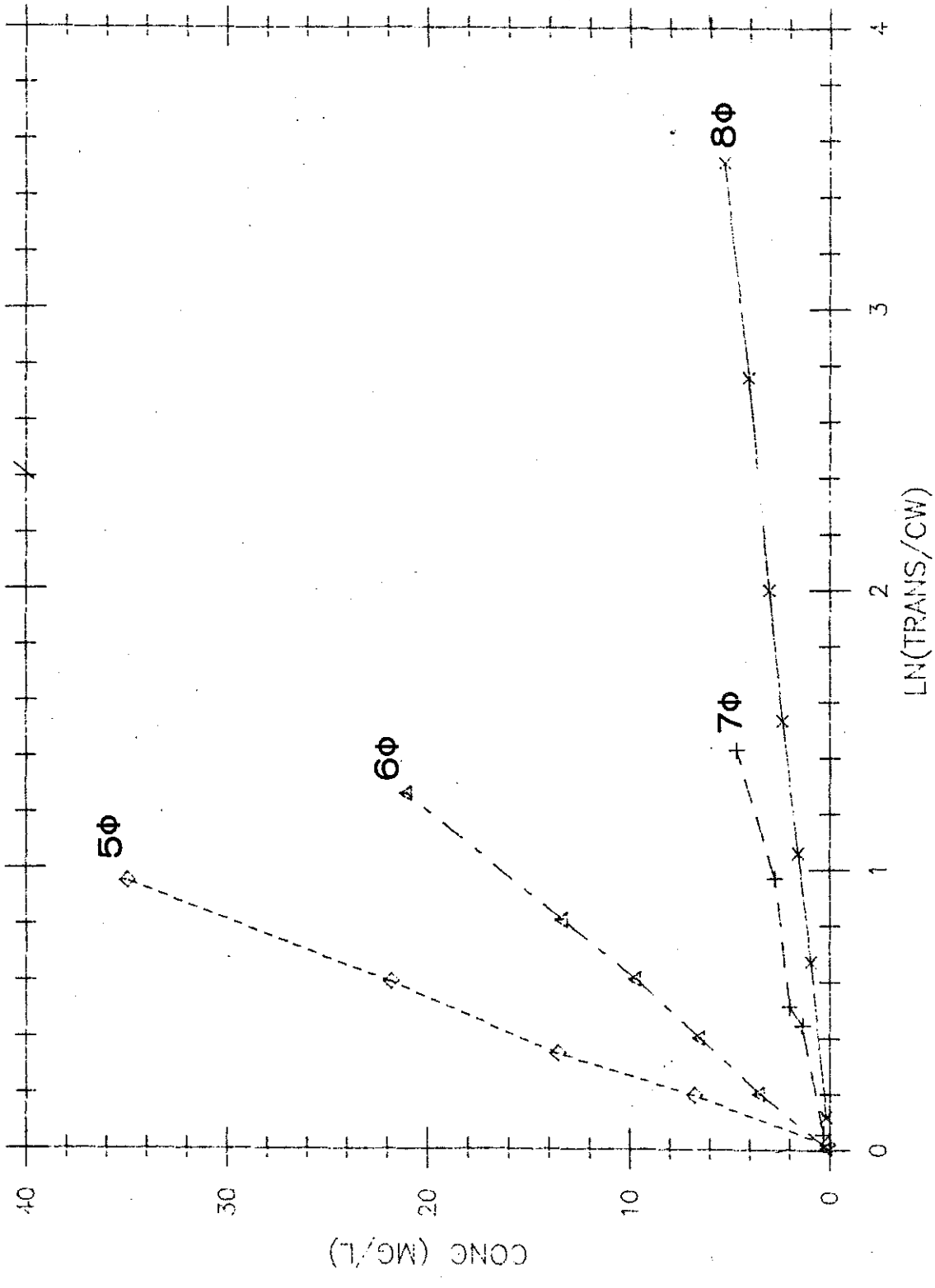

Figure 2

Figure 3. Light scattering vs. concentration (mg/1)

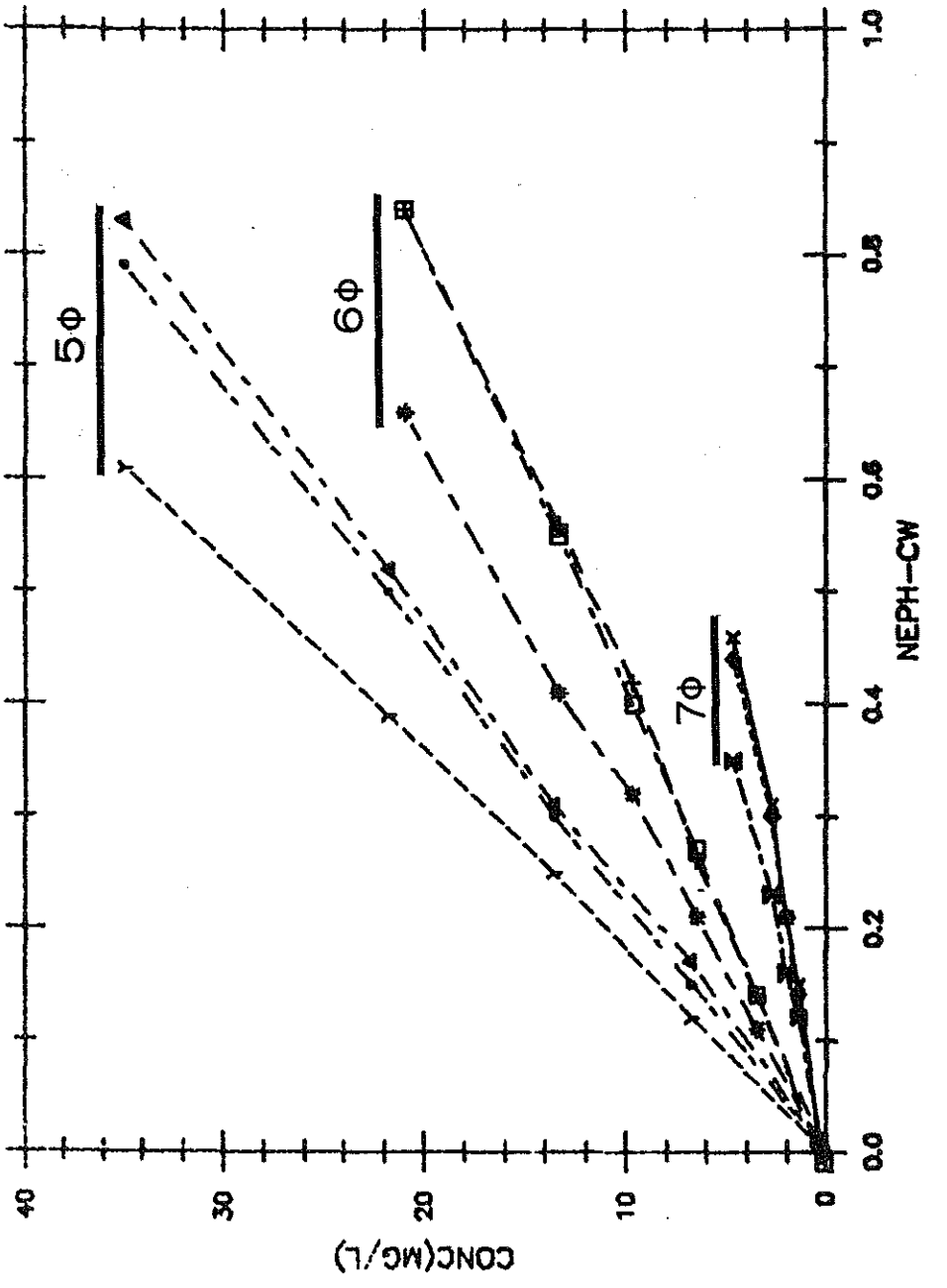

Figure 3

Figure 4. Flourescence (line A) and light attenuation (line B - not normalized)vs. pressure (db = depth (m)).

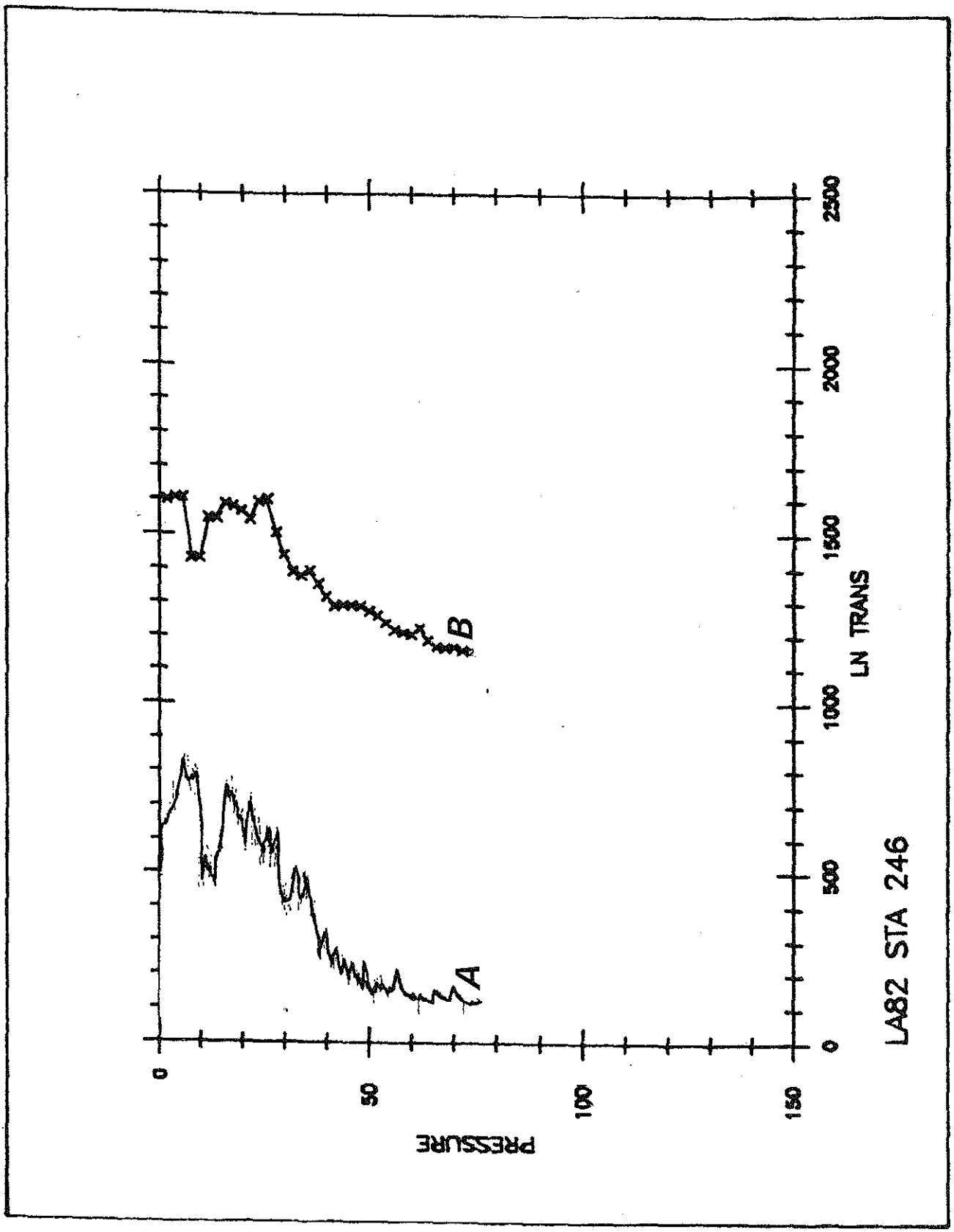
LA82 STA 246
LN TRANS
0
500
1000
1500
2000
2500
PRESSURE
0
50
100
150
A
B

Figure 4

Figure 5. Clear water values for 1980.

A. Nephelometer

B. Transmissometer

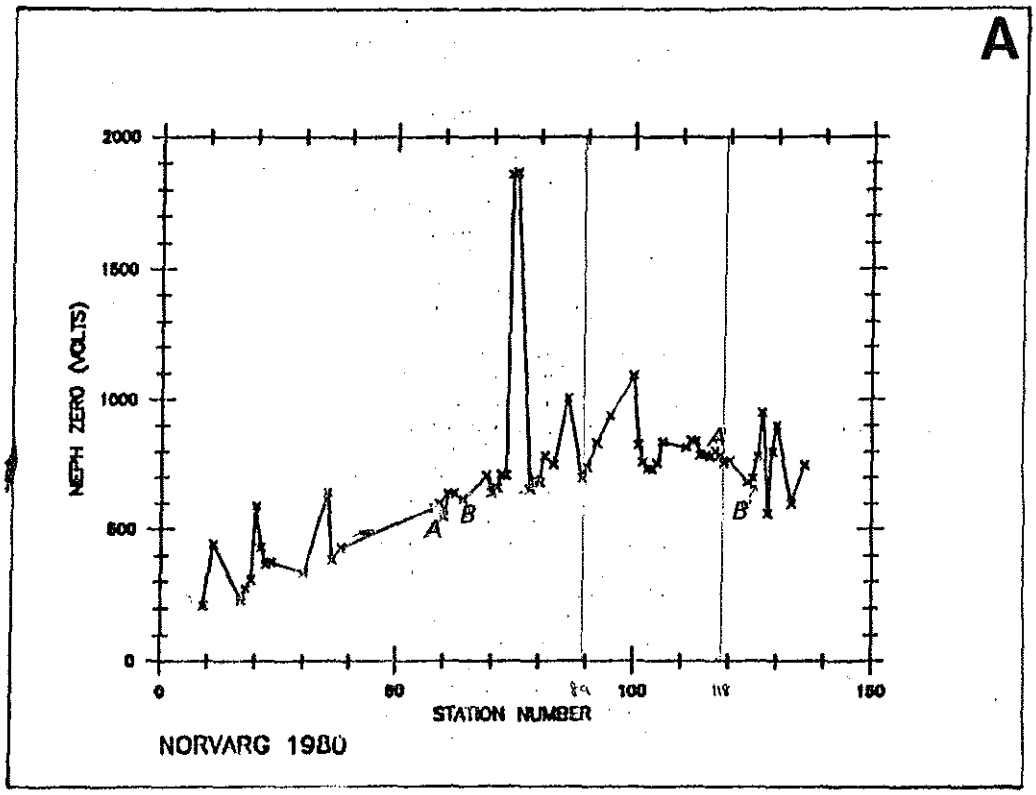
A
2000
1500
1000
500
0
NEPH ZERO (VOLTS)
0
50
100
150
STATION NUMBER
A
B
A'
B'
NORVARG 1980

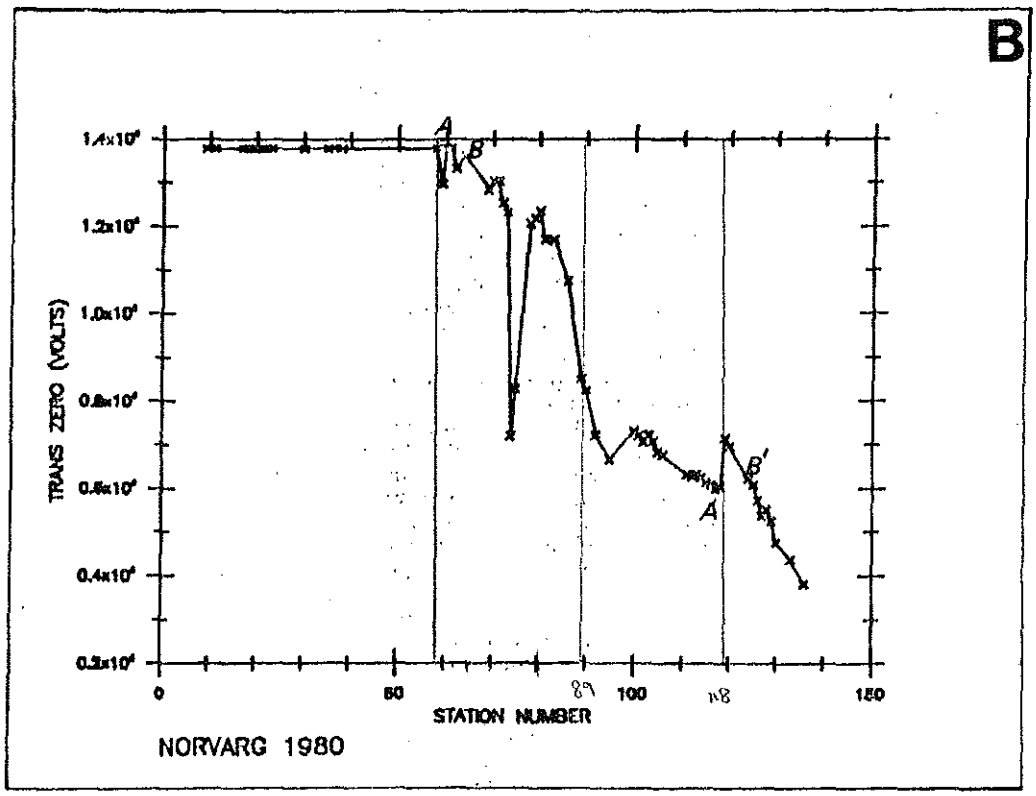
B
1.4x10⁶
1.2x10⁶
1.0x10⁶
0.8x10⁶
0.6x10⁶
0.4x10⁶
0.2x10⁶
TRANS ZERO (VOLTS)
0
50
100
150
STATION NUMBER
A
B
A'
B'
NORVARG 1980

Figure 5

gain factor was determined by correlating the results all to one standard nephelometer. Alternatively, the instruments can all be set as close as possible before deployment to a standard concentration. However, this was not done before use in the Barents Sea resulting in problems discussed below.

A typical suspended matter profile in the Barents Sea has a near-surface maximum, a mid-depth clear water minimum and a near-bottom maximum (figure 4). The nephelometer was flooded by surface light in the upper 30m, so light scattering can only be used in the near-bottom nepheloid layer. The near-surface maximum in light attenuation is generally caused by biologic activity, shown by the fact that phytoplankton abundance (estimated by a flourometer which measures chlorophyll) is very well correlated to light attenuation above the clear water minimum (figure 4).

Light scattering measurements were used in the regional distribution of suspended matter in the Barents Sea (chapter 2), because data from the transmissometer was not recorded on scale for many stations south of Kong Karls Land in 1980 (before station 58) (figure 5). At each station cast, the clear water value for that cast was subtracted, yielding excess turbidity. However, because of instrument drift during the 1980 cruise and the fact that nephelometers used on different cruises were not set originally at the same scale, the gain factor mentioned previously is missing. Light scattering must somehow be correlated with measured suspended sediment concentrations from filtered water samples and the light scattering adjusted by this factor. In this study, calibration was done by first

determining a reference value (ne_{ref}) which should be equal to the clearest water in the Barents Sea, subtracting the reference value from the scattering measured in volts, and then correlating this value with the concentration measured for samples below the clear water minimum (C_{ws}, figures 6, 8, 10):

$C_{ne} = (ne_v - ne_{ref})$ (volts)

$f_{ne} = C_{ne}/C_{ws}$ (volts/(mg/l))

Ne_{ref} was determined by plotting the clear water values (in volts) for each station, and drawing an assumed clear water value for the Barents Sea below this (figures 5, 7, 9). Actual values used were:

Year	Stations	Calibration	fac
1980	0- 89	ne_{ref} = (sta#-30)0.006+0.333	0.8
	90-118	ne_{ref} = 0.730	
	119-138	ne_{ref} = (sta#-119)0.022-0.753	
1981	all	ne_{ref} = 1.470	2.4
1982	all	ne_{ref} = 3.696	2.0

Excess turbidity was multiplied by f_{ne} in order to adjust for the gain factor, and at the same time allow contouring of estimated excess "concentration". Calculation of f_{ne} assumes that the gain factor did not drift when the gain range did.

In analysis of the suspended sediment distribution near Nordaustlandet, the suspended matter distribution of the entire water column was of interest. Light attenuation from the transmissometer must be used because the nephelometer was contaminated by sunlight near the surface and whole water column observations are important in this region. As discussed above, there is no problem with a gain factor for the calibration of light transmission, but in order to look

Figure 6. 1980 suspended matter calibration data:

A. Light scattering vs. concentration (mg/l)

B. Light attenuation vs. concentration (mg/l)

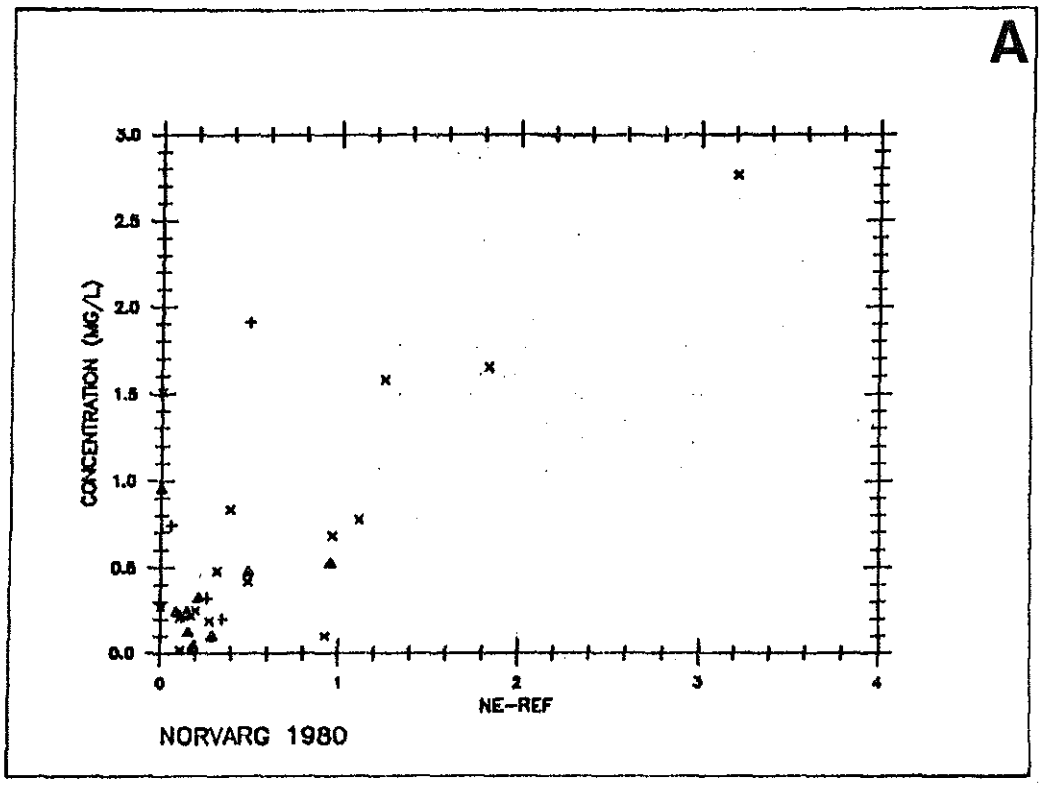
A
CONCENTRATION (MG/L)
3.0
2.5
2.0
1.5
1.0
0.5
0.0
0
1
2
3
4
NE-REF
NORVARG 1980

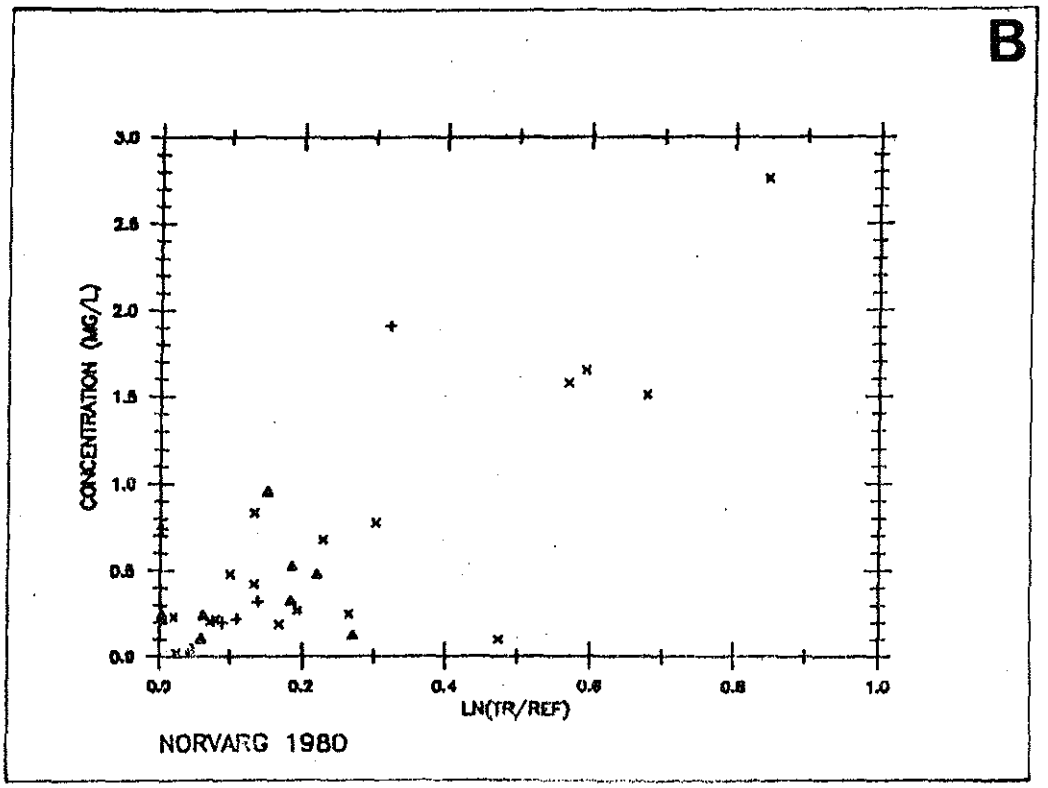
B
CONCENTRATION (MG/L)
3.0
2.5
2.0
1.5
1.0
0.5
0.0
0.0
0.2
0.4
0.6
0.8
1.0
LN(TR/REF)
NORVARG 1980

Figure 6

Figure 7. Clear water values for 1981.

A. Nephelometer

B. Transmissometer

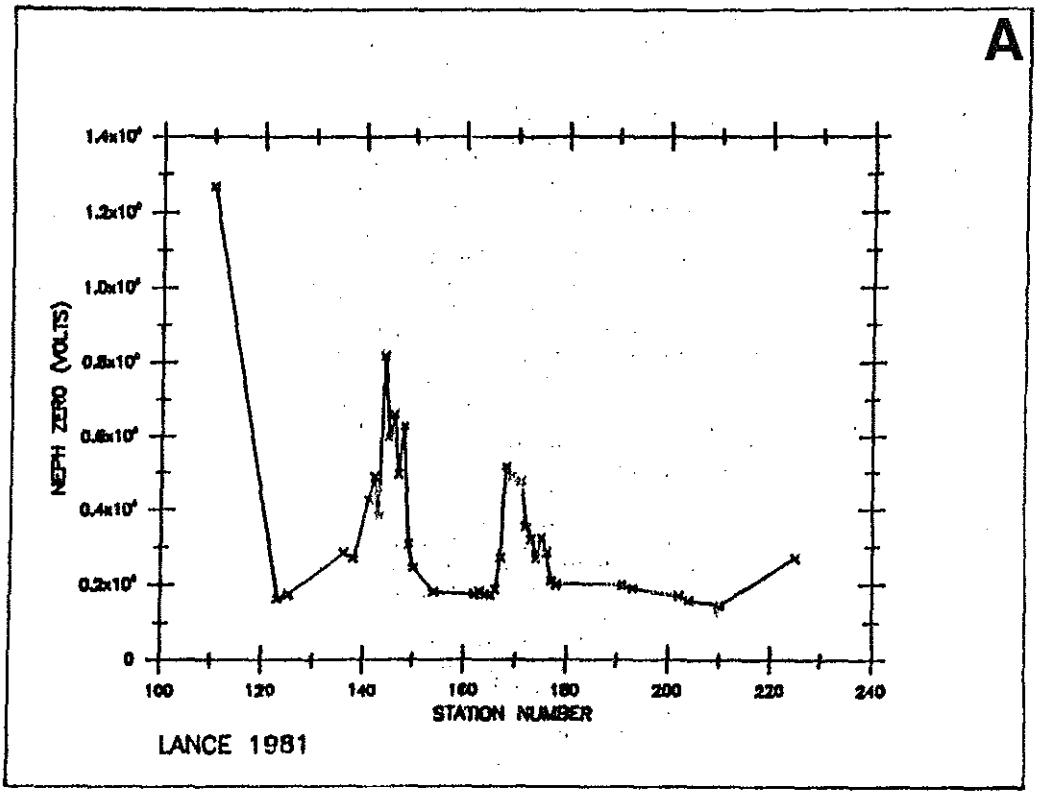
A
NEPH ZERO (VOLTS)
1.4x10⁵
1.2x10⁵
1.0x10⁵
0.8x10⁵
0.6x10⁵
0.4x10⁵
0.2x10⁵
0
100
120
140
160
180
200
220
240
STATION NUMBER
LANCE 1981

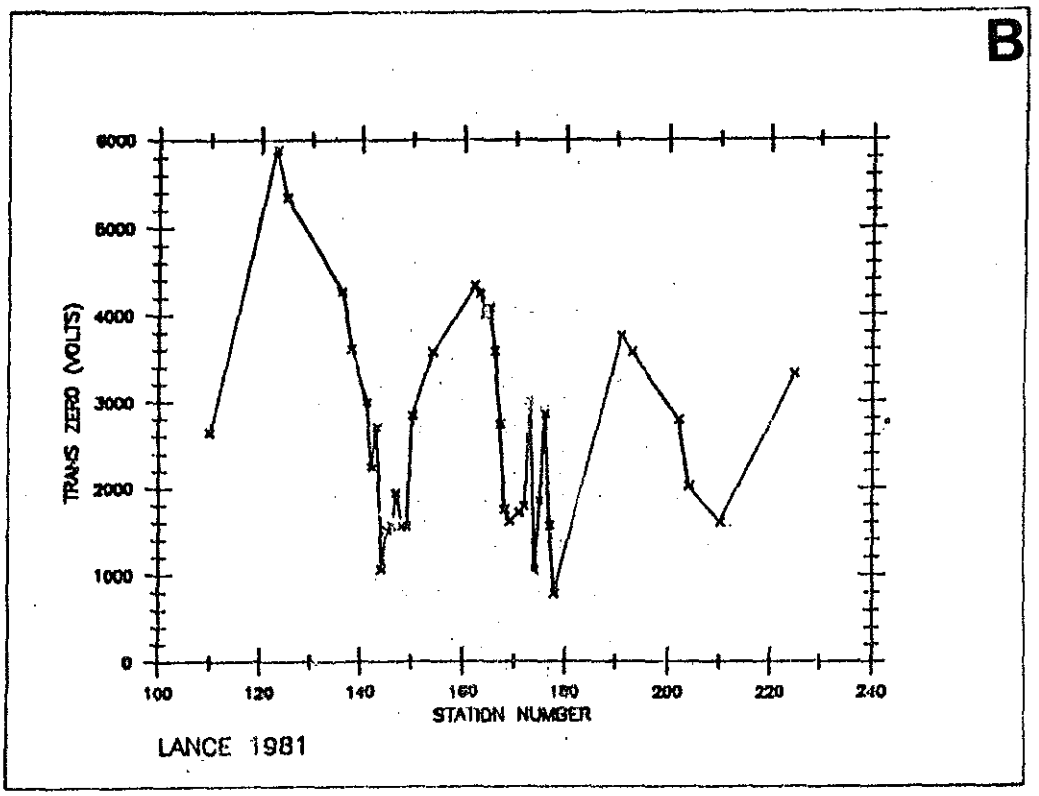
B
TRANS ZERO (VOLTS)
6000
5000
4000
3000
2000
1000
0
100
120
140
160
180
200
220
240
STATION NUMBER
LANCE 1981

Figure 7

Figure 8. 1981 suspended matter calibration data:

A. Light scattering vs. concentration (mg/1)

B. Light attenuation vs. concentration (mg/1)

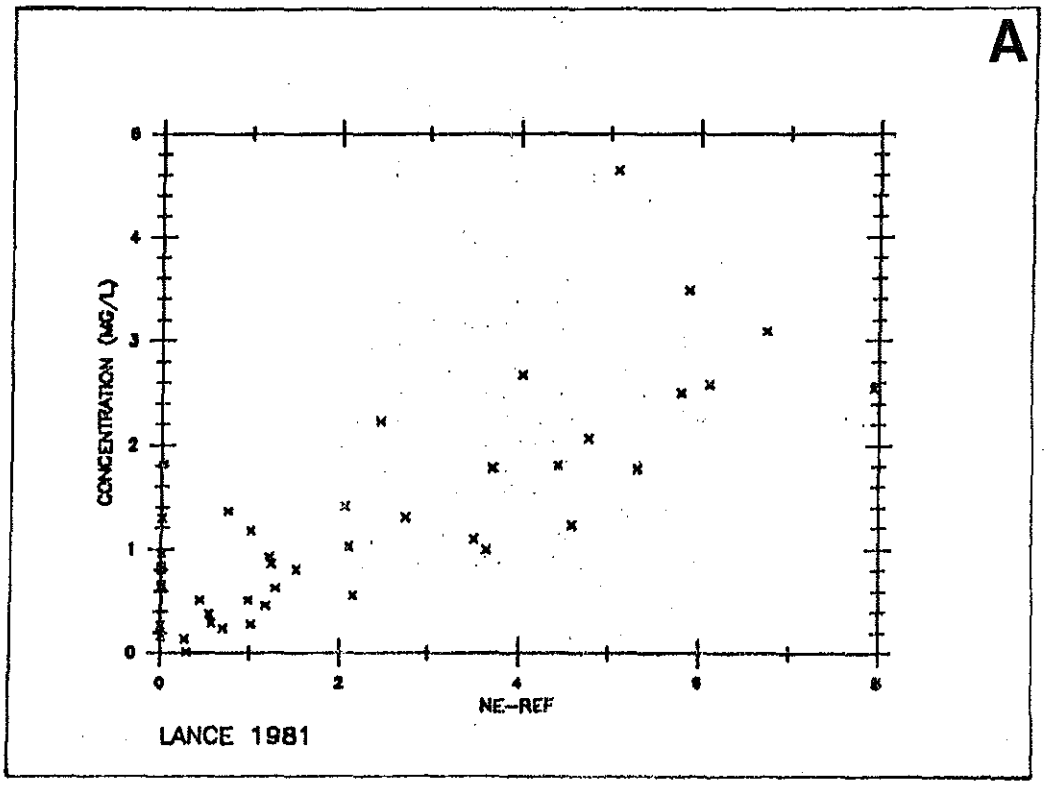
A
CONCENTRATION (MG/L)
0
1
2
3
4
0
2
4
NE-REF
LANCE 1981

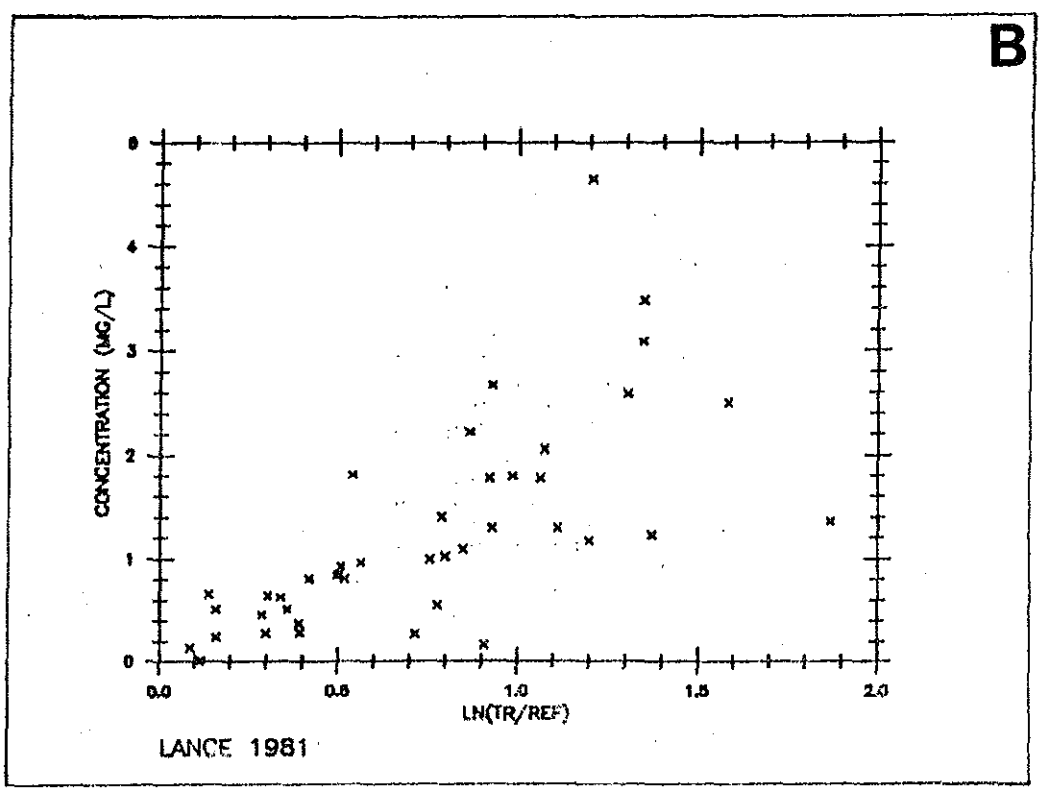
B
CONCENTRATION (MG/L)
0
1
2
3
4
0.0
0.5
1.0
1.5
2.0
LN(TR/REF)
LANCE 1981

Figure 8

Figure 9. Clear water values for 1982.

A. Nephelometer

B. Transmissometer

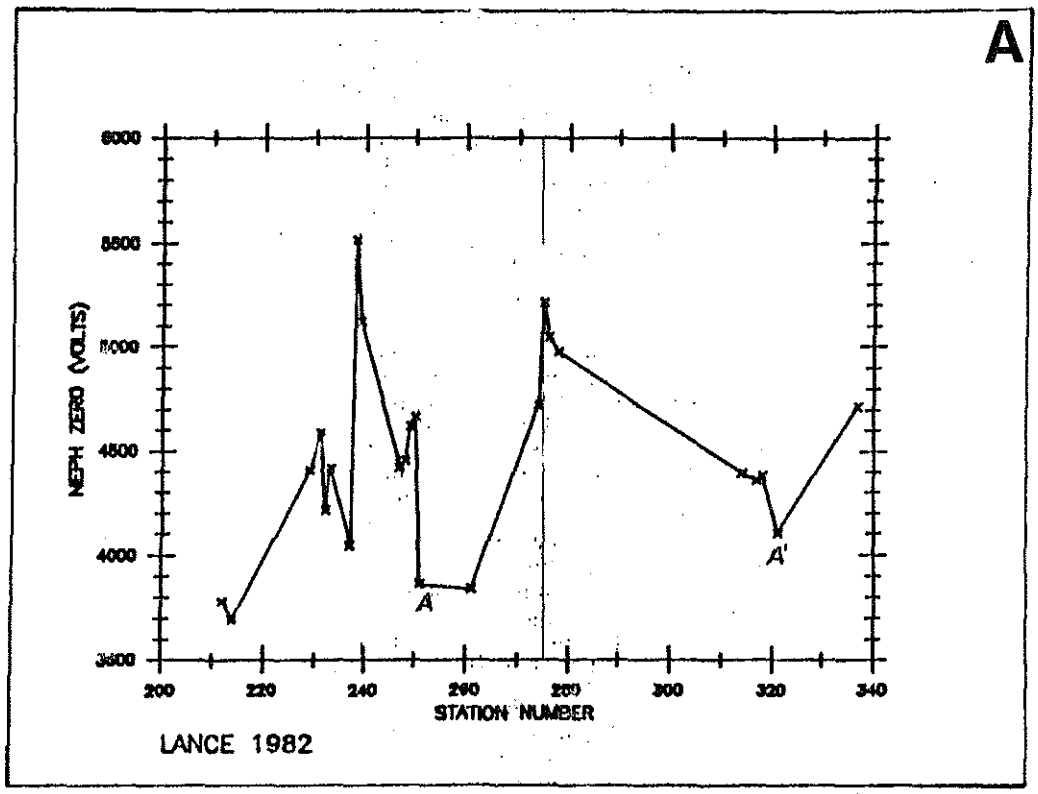
A
6000
5500
5000
4500
4000
3500
NEPH ZERO (VOLTS)
200
220
240
260
280
300
320
340
STATION NUMBER
A
A'
LANCE 1982

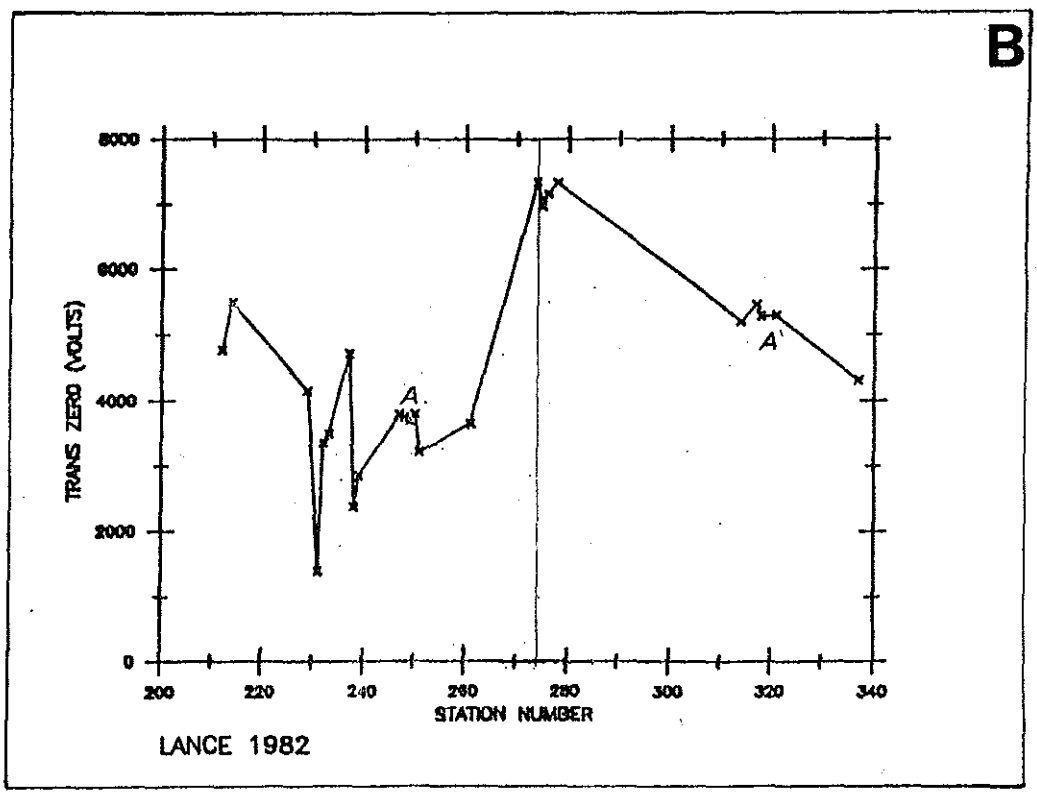
B
8000
6000
4000
2000
0
TRANS ZERO (VOLTS)
200
220
240
260
280
300
320
340
STATION NUMBER
A
A'
LANCE 1982

Figure 9

Figure 10. 1982 suspended matter calibration data:

A. Light scattering vs. concentration (mg/l)

B. Light attenuation vs. concentration (mg/l)

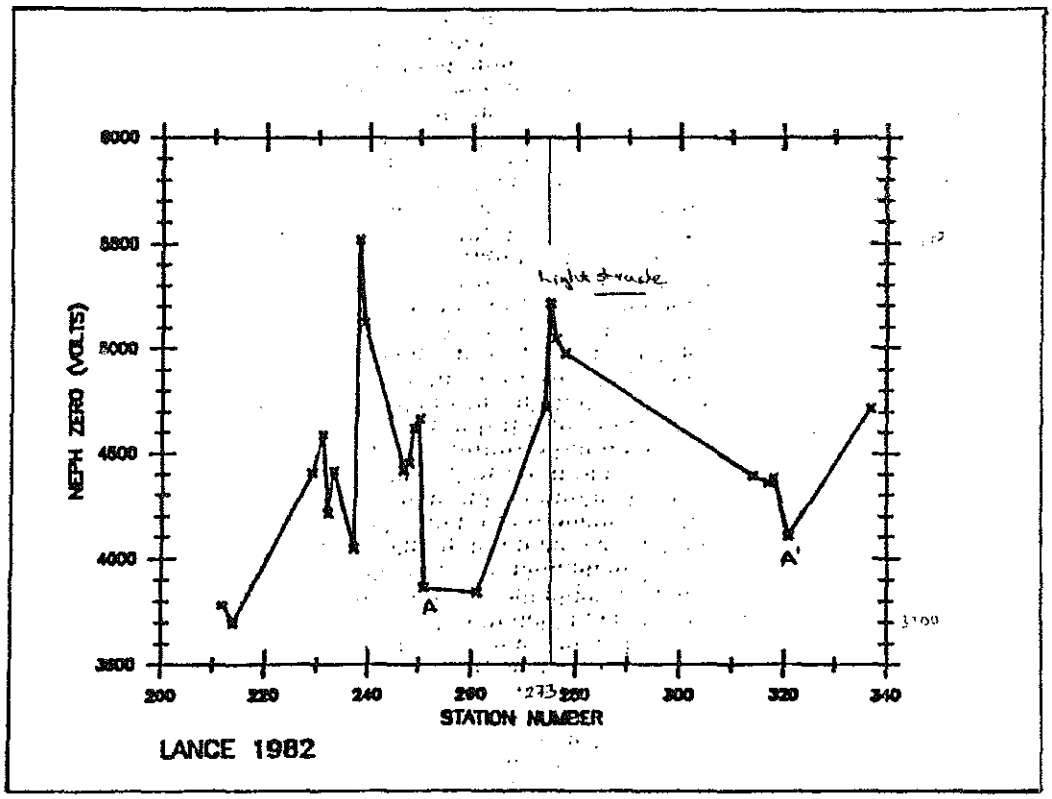
NEPH ZERO (VOLTS)
8000
6000
4000
3800
200
220
240
260
280
300
320
340
STATION NUMBER
A
A'
LANCE 1982

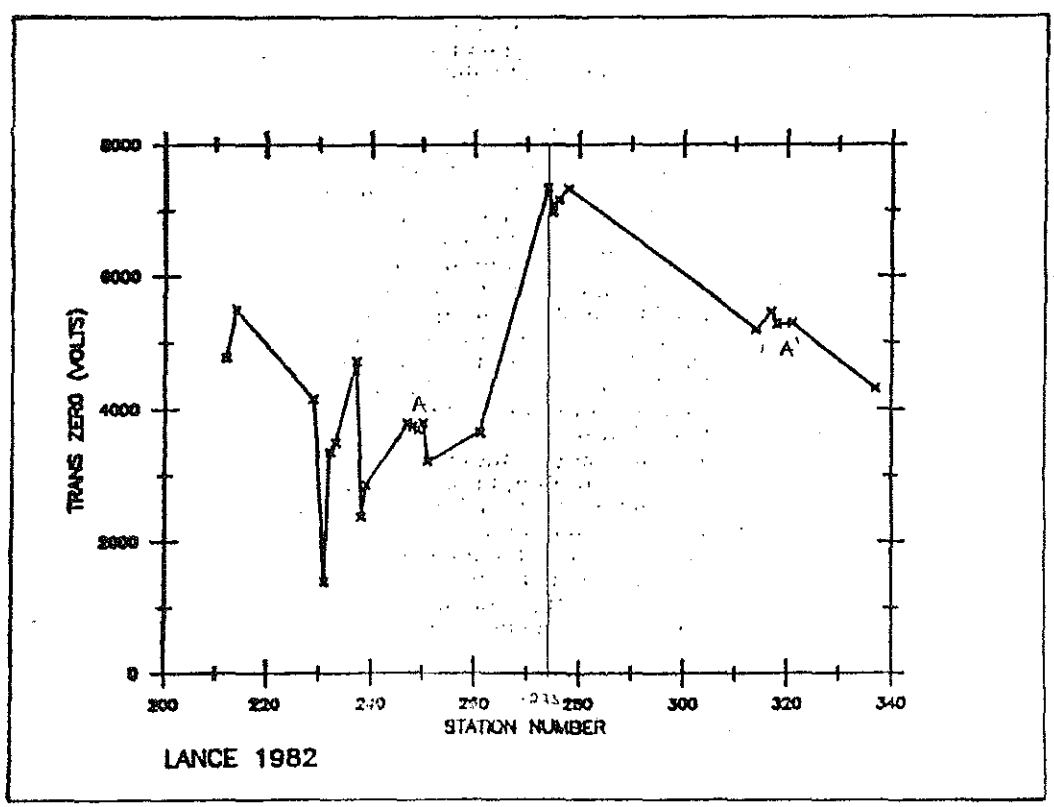
TRANS ZERO (VOLTS)
8000
6000
4000
2000
0
200
220
240
260
280
300
320
340
STATION NUMBER
A
A'
LANCE 1982

Figure 10

at suspended matter "concentrations", not excess turbidity, a reference value must be obtained for background Barents Sea water (tr_{ref}):

$$a = -\ln(tr/tr_{ref})$$

Clear water values were examined, and straight lines were fit to the background voltage values (figures 6, 8, 10). Actual values used were:

Year	Stations	Calibration	fac
1980	DNR		0.4
	58- 86	tr_{ref} = (sta#-58)0.066-13.780	
	89-118	tr_{ref} = (sta#-89)0.086-8.502	
	119-136	tr_{ref} = (sta#-119)0.195-7.129	
1981	all	tr_{ref} = 5.888+(seq#-98)0.056	0.8
1982	212-273	tr_{ref} = 6.519	1.0
	274-339	tr_{ref} = 7.324	

In order investigate the fit to the actual concentration, f_{tr} was calculated:

$$f_{tr} = (-\ln(tr/tr_{ref}) / C_{ws}$$

This value should not vary between the cruises, but it is observed to do so, by a factor of 2. Samples were obtained throughout the Barents Sea in 1980 while in 1981 and 1982 they were obtained mostly close to a Nordaustlandet, in shallow water and close to a source for coarse-grained sediment. The variation could be due to an average grain size change, as mentioned above. Based on the trends observed, that would mean that samples close to the glacier were in general finer-grained than throughout the Barents Sea, which at first seems contradictory. However, the fine-grained component could not be estimated in the optical measurement of the grain size distribution

and it is possible that it is actually more important in this region, than further offshore. Another explanation may be that the optical properties of the water masses are different. Most 1980 samples were obtained in the deep nepheloid layer, within Atlantic Water, while 1981 and 1982 samples were obtained in shallow Arctic or Coastal Water, which is generally "dirtier" than Atlantic Water (Aas 1979). If this is true, then rather than multiplying by f_{tr}, a different reference value should be used.

In 1981, the nephelometer reference level remained constant, while a linear drift was removed from the transmissometer value for 43 stations (figure 7). Since the maximum level decreased throughout the cruise, the trend can easily be explained by corrosion of the transmissometer mirror. For 1981, the variation in t_{ref} was 5.888 - 2.752 volts for the entire cruise, or (after taking the natural log) 1.773 - 1.012, a range of 0.761 (0.609mg/l if f_{tr} is applied). For stations 141 - 178 which are of interest in chapter 4 the values are 5.496 - 3.816 volts, or (taking the natural log) 1.704 - 1.339 with a range of 0.365 (0.292mg/l if f_{tr} of 0.8 is applied). These numbers are large, but are justified because the base level on the nephelometer does not change while a marked trend is observed in the transmissometer. Although there is a lot of scatter in the correlation between light scattering and concentration, and between light attenuation and concentration, a definite correlation does exist (figure 8).

In 1982 only 30 samples were available. A constant reference level also removed from the the nephelometer data (figure 9). Two different constants 6.519 and 7.324 (after ln = 1.875 and 1.991 a

range of 0.116 (0.116mg/1)) were removed from the transmission data because the gain was altered between stations 173 and 174 (figure 9). These constant values were obtained by matching stations A and A' which are located in the same vicinity. The correlations between light scattering and concentration, and between light attenuation and scattering are not well-defined for this year (figure 10).

The most extensive regional sampling program was in 1980 (33 stations), and this year both the nephelometer and transmissometer drifted (figure 5). Drift may have occured because 1) the sensor was found to be corroding at station 89, so screws were tightened, possibly reorientating the nephelometer and transmissometer mirrors slightly, and 2) the light source was replaced at station 118. Straight lines were fit to the clear water minimum to obtain reference values. For 1980, the variation in ne_{ref} is from 0.335 - 0.753, or a range of 0.418 volts. When this is multiplied by a f_{ne} of 0.8, a maximum variation of 0.334mg/1 is subtracted thoughout the study area. Although this number is large, the ne_{ref} values are only used to obtain an estimate of the gain factor (f_{ne}). Varying the scattering data by 0.4 volts will not substantially alter this estimate (figure 7). Ranges in t_{ref} in 1980 are from 13.790 - 3.140 volts for the whole cruise (2.589 and 1.144, range of 1.445 or 0.578mg/1), however only stations 65-81 have been examined in detail (chapter 4). T_{ref} for these stations varies from 13.318 - 12.262, or when the natural log is taken: 2.589 - 2.507 which is a variation of 0.082 (0.033mg/1 if f_{tr} of 0.4 is applied), and is below the contour interval for that discussion (chapter 4).

REFERENCES

Aas, E. (1979) Light scatterance and flourescence observations in the Barents Sea. Inst. for Geof., Un. of Oslo. Institute report series No. 39. 48pp.

Baker, E.T. and J.W. Lavelle (in press) The effect of particle size on the light attenuation coefficient of natural suspensions. J.G.R. 37pp.

Moody, J.A. and B. Butman (in prep.) Light attenuation and scattering as a function of particle size.

Spinrad, R.W., J.R.V. Zaneveld, J.C. Kitchen (1983) A study of the optical characteristics of the suspended particles in the benthic nepheloid layer of the Scotian Rise. J. Geophys. Res. 88:7641-7645.

Optical Measurements

Explanation of table presented below:

yr = year

no = station number

st = nepheloid layer "strength" (maximum near-bottom scattering divided by clear water minimum value). 0.99 means no near-bottom maximum

cd = depth to clear water minimum (m)

mx = depth to near-bottom light scattering maximum (m)

cd = cast depth (m)

wd = water depth (m)

t = (mx-cw) nepheloid layer thickness (m)

sd = sample depth (m)

co = concentration (mg/l)

yr	no	st	cw	mx	cd	wd	t	sd	co	sd	co	sd	co	sd	co
80	003							400	0.78	025	0.05	005	0.22		
80	009	1.82	164	250	250										
80	011	1.22	92	132	132	125	033								
80	017	1.51	236	250	264	280	044								
80	018	2.26	186	236	240	250	064								
80	019	1.59	176	220	220	230	054								
80	021	1.12	68	90	094	100	032	109	0.25	040	0.25	020	0.31		
80	022	1.21	88	98	106	106	018								
80	023	1.58	118	138	140	160	042	157	0.27	030	0.25	010	0.13		
80	028?							279	0.02	025	0.20	010	0.16		
80	030	2.86	130	226	226	330	200	229	0.69						
80	032							134	0.14	115	1.98	075	0.45	035	0.41
								015	0.26						
80	034							021	2.22	003	1.94				
80	035	1.41	48	58	58										
80	036	1.81	94	120	122	122	028	124	0.32						
80	038	1.18	88	110	110	120	032	119	0.21	018	0.93	003	0.28		
80	051							215	0.14	005	0.15				
80	052	1.94	124	182	186	200	076	199	0.15	030	0.10	005	0.14		
80	053							130	0.16	050	0.26	025	0.33	005	0.23
80	054	1.12	122	204	206	206	084	217	0.32	040	0.27				
80	058	1.11	124	268	268	330	206	329	0.48	030	0.29				
80	059	0.99			104	305									

yr	no	st	cw	mx	cd	wd	t	sd	co	sd	co	sd	co	sd	co
80	060	1.54	162	238	238	345	183	244	0.18	145	1.95				
80	061	0.99			118	130									
80	062	1.09	120	204	206	206	86	224	0.22	175	0.02	100	0.23		
80	063	0.99			40	40									
80	064	1.98	128	200	200	320	192	225	0.52	160	0.06	030	0.24		
80	065	0.99			84	85		087	2.28	050	2.76	003	1.51		
80	066	0.99			74	80									
80	067	0.99			88	80		089	0.68	050	1.65	003	1.86		
80	069	1.10	116	122	122	135	19	134	0.16	050	0.77	003	0.58		
80	070	1.30	114	152	152	154	40								
80	071	1.63	110	170	170	178	68	177	0.42	050	0.14	002	0.30		
80	072	?.25	120	142	142	152	32								
80	073	1.12	112	138	138	150	38	149	0.41		0.13	050	0.10		
80	074	1.35	50	60	70	85	35	086	2.56	050	1.58	003	1.89		
80	075	1.82	56	86	86	90	34	100	0.83	050	0.48	003	1.11		
80	078	1.35	132	170	170	180	48								
80	079	1.56	142	202	206	212	70	214	0.40	161	0.22	020	0.56		
80	080	1.28	126	154	154	162	36								
80	081	0.99			94	100		099	0.22	050	1.44	003	0.15		
80	082	0.99			58	60									
80	083	1.03	82	119	118	118	36	121	0.21	072	0.43	020	1.01		
80	086	1.28	118	142	142	142	34	141	0.19	090	0.25	030	0.50		
80	089	1.15	80	160	162	275	195	179	0.21	130	0.74	030	0.54		
80	090	1.26	90	204	210	225	135								
80	091							264	0.32	065	0.22	005	0.32		
80	092	1.24	66	120	120	150	84								
80	093	1.06	112	162	164	140	28								
80	094	0.99			16	20									
80	095	2.41	88	164	164	175	87								
80	096	1.16	98	112	116	119	21	132	1.00	070	1.91	020	0.82		
80	097	0.99			22	32									
80	098	1.15	48	84	84	98	50								
80	100	1.38	66	116	120	125	32								
80	101	1.48	84	156	156	170	86	164	0.61	030	1.02				
80	102	1.24	66	150	158	170	104								
80	103	1.06	80	106	164	164	84	?							
80	104	1.31	106	154	156	180	74								
80	105	1.12	78	142	142	149	71								
80	106	1.70	80	140	156	165	85								
80	107	1.25	116	176	176	185	69								
80	109	1.28	202	226	242	242	40								
80	110	1.06	86	112	122	140	54								
80	111	1.29	126	208	208	215	89								
80	112	1.15	106	188	192	197	91								
80	113	1.32	128	178	184	214	86	213	0.60	150	0.20	030	0.50		
80	114	1.08	224	280	280	340	116								
80	115	1.46	200	280	282	300	100	299	0.42	030	0.13				
80	116	1.43	142	246	248	248	106								
80	117	1.27	100	206	208	215	115								
80	118	1.36	150	266	266	280	130	299	0.43	130	0.24	030	0.95		

yr	no	st	cw	mx	cd	wd	t	sd	co	sd	co	sd	co	sd	co
80	119	1.50	146	284	284	307	161								
80	120	1.18	198	274	278	300	102	299	1.03	250	0.24	020	0.57		
80	121	1.12	138	156	162	175	37	193	0.30	100	0.32	030	0.45		
80	124	1.28	142	278	278	330	188	325	0.31	270	1.55	030	0.29		
80	125	1.23	150	258	268	330	180								
80	126	1.31	118	230	274	285	167	284	0.15	235	0.10	030	0.40		
80	127	1.60	94	112	120	130	36								
80	128	1.46	100	238	254	265	165	275	0.12	200	0.12	030	0.47		
80	129	1.72	140	240	252	252	112								
80	130	1.63	92	108	108	125	33	106	0.52	055	0.47	020	0.59		
80	131	0.99			104	115									
80	133	1.16	108	156	156	168	60	187	0.28	140	0.04	030	0.13		
80	134	1.10	116	136	152	165	49								
80	135							191	0.16	140	0.11	030	0.54		
80	136	1.08	128	146	146	160	32								
81	122							080	0.17	065	0.10	020	0.34		
81	123	1.44	108	138	138	155	47	134	0.24	050	0.20	020	0.43		
81	124							239	0.29	075	0.26	025	0.44		
81	125	1.12	192	326	334	373	181	348	0.51	110	0.20	035	0.41	020	0.70
81	126							085	0.31	025	0.64	001	0.80		
81	128							090	0.71	020	0.59	001	1.22		
81	129							114	0.35	020	0.98	002	0.26		
81	130							060	0.48	020	0.90	002	0.28		
81	131							030	0.74	020	0.63	002	0.38		
81	132							041	0.41	020	1.42	002	0.35		
81	133							074	0.50	060	0.50	021	1.24	002	0.21
81	134	0.99			68	81									
81	135	0.99			46	55									
81	136	1.14	84	92	96	109	25	098	0.51	088	0.46	020	0.50	001	0.29
81	138	1.13	70	92	94	107	37								
81	141	1.42	62	68	82	94	32	079	0.99	070	1.80	020	1.18	001	1.46
81	142	1.36	46	56	64	73	27								
81	143	1.59	50	62	64	77	27								
81	144	1.26	44	72	72	82	38	020	2.99	00128.46					
81	145	2.12	74	84	84	94	20								
81	146	2.05	20	68	76	89	69								
81	147	2.41	20	56	58	43	?								
81	148	1.24	46	58	64	73	27	060	2.59	050	4.64	020	3.33		
81	149	2.05	42	82	82	91	49								
81	150	1.85	42	92	92	102	60	090	2.22	080	1.52	020	3.47	001	2.89
81	151							085	2.06	075	1.09	020	0.89	001	0.69
81	152							110	0.81	100	0.93	020	3.92	001	0.48
81	153							170	1.86	160	0.86	020	1.17	001	0.31
81	154	1.66	136	208	210	227	91	200	0.38	190	0.29	020	0.31	001	0.00
81	155							155	0.28	145	0.19	020	0.26	001	0.27
81	156							110	0.53	100	0.25	020	0.72	001	0.58
81	157							060	0.33	050	0.35	020	0.48	001	0.55
81	158							055	0.46	045	0.40	020	0.67	001	1.27
81	159							090	0.13	080	0.19	020	0.37	001	0.30

yr	no	st	cw	mx	cd	wd	t		sd	co	sd	co	sd	co	sd	co
81	160	0.99			56	76										
81	161	0.99			92	93		?	060	0.33	050	0.38	020	0.50	001	0.49
81	162	1.10	84	96	96	116	32		086	0.13						
81	163	1.08	88	126	126	146	58		124	0.17	114	0.09	019	0.32	001	3.12
81	164	1.29	134	184	184	210	76		201	0.12						
81	165	1.72	82	252	254	267	185		239	0.63	228	0.28	099	0.01	019	0.33
									002	0.31						
81	166	2.32	122	142	142	151	29		184	0.26						
81	167	1.48	60	90	90	96	36									
81	168	1.09	30	64	66	76	46		065	1.78	050	1.78	020	1.34	001	1.08
81	169	1.16	44	60	60	68	24									
81	170	0.99			50	62			045	3.49	035	3.09	020	2.38	001	3.97
81	171	1.72	40	70	78	85	45		060	2.67	016	2.78	000	3.37		
81	172	2.15	28	46	52	61	33		055	4.47	045	2.30	020	3.36	000	4.47
81	173	1.32	38	52	52	56	18	?	054	1.29	045	0.55	020	0.81	000	0.64
81	174	2.24	76	98	98	107	31		100	1.23	090	1.02	010	11.80	005	10.67
									001	12.33	000	7.92				
81	175	1.45	88	116	118	125	37									
81	176	4.79	96	118	118	129	33		110	2.55	010	2.78	000	0.65		
81	177	1.69	106	122	122	125	22		115	1.17	010	14.96	000	12.20		
81	178	1.26	70	72	80	113	43		075	1.36	065	1.47	010	5.88	000	8.15
81	191	1.18	50	54	62	73	23									
81	193	1.06	114	154	156	268	154									
81	194	1.51	246	298	306	326	80									
81	199	1.01	104	158	158	190	86	?								
81	208								100	0.00	080	0.30				
81	209								155	0.06	145	0.06	020	0.16	001	0.27
81	202	1.30	54	256	260	276	122									
81	204	1.07	74	190	208	230	156	?								
81	206	0.99			74	84										
81	210	1.71	78	134	134	190	112		105	0.45	095	0.15	020	0.22	001	0.18
81	211								045	0.33	020	0.51	001	0.84		
81	215								085	0.66	075	0.37				
81	222	0.99			36	38										
81	225	1.69	74	130	130	140	66									
81	226	0.99			116	127										
82	212	1.08	42	48	48	54	12		047	0.51	040	0.38	017	1.03		
82	213								063	0.31	010	0.65				
82	214	0.99			132	220			137	0.27	130	0.34	010	0.29		
82	215								076	2.03	033	0.57	000	2.50		
82	228								009	0.82	007	0.93	000	0.57		
82	229	1.01	32	46	46	55	23		042	0.56	032	0.38	020	0.80	000	2.23
82	231	1.05	58	72	74	83	25		072	0.57	062	0.39	020	0.34	020	0.46
									000	0.97						
82	232	1.47	40	70	76	82	42		072	1.97	062	1.22	020	0.47	000	0.65
82	233	1.27	44	88	90	101	57		088	0.47	020	0.67	000	1.14		
82	234								077	1.11	020	0.83	000	1.83		
82	236								087	0.70	077	0.55	020	0.29	000	0.41
82	237	1.02	80	104	104	105	25		102	0.38	089	0.32	020	0.29	000	0.81
82	238	1.74	30	68	68	83	53		067	1.91	057	1.39	020	1.34	000	1.27

yr	no	st	cw	mx	cd	wd	t	sd	co	sd	co	sd	co	sd	co
82	239	1.10	36	64	72	87	51								
82	243	0.99			68	79		068	0.87	000	1.02				
82	244							025	0.44	000	0.34				
82	245	0.99			60	69									
82	246							068	0.53	000	1.51				
82	247	1.22	54	112	114	124	70	109	0.74	000	1.06				
82	248	1.11	78	112	114	123	45	109	0.43	000	1.02				
82	249	1.07	80	112	112	123	43	109	0.37	000	0.91				
82	250	1.08	88	112	112	123	35	109	0.67	000	2.60				
82	251	1.06	52	112	108	119	67 ?	109	0.46	000	0.97				
82	252							109	0.54	000	1.35				
82	261	1.69	40	46	46	48	8								
82	272	0.99				366									
82	273	0.99				368									
82	274	0.99			82	362									
82	275	0.99			98	369									
82	276	0.99													
82	278	0.99													
82	279	0.99													
82	281	0.99				330									
82	314	0.99			106	112		100	0.32	020	0.55	000	0.79		
82	317	0.99			122	142		127	0.33	030	0.83	000	0.43		
82	318							190	0.65	020	0.62	000	0.58		
82	320	1.50	108	114	122	207	99								
82	321	1.01	90	104	104	99	9 ?								
82	337	1.04	78	82	104			130	0.94	010	1.07	000	1.30		
82	338							298	0.53	010	0.43	000	1.58		